DESY 12-107 ISSN 0418-9833
June 2012

Inclusive Deep Inelastic Scattering at High Q^2 with Longitudinally Polarised Lepton Beams at HERA

H1 Collaboration

Abstract

Inclusive $e^{\pm}p$ single and double differential cross sections for neutral and charged current deep inelastic scattering processes are measured with the H1 detector at HERA. The data were taken at a centre-of-mass energy of $\sqrt{s} = 319\,\mathrm{GeV}$ with a total integrated luminosity of $333.7\,\mathrm{pb}^{-1}$ shared between two lepton beam charges and two longitudinal lepton polarisation modes. The differential cross sections are measured in the range of negative four-momentum transfer squared, Q^2, between 60 and $50\,000\,\mathrm{GeV}^2$, and Bjorken x between 0.0008 and 0.65. The measurements are combined with earlier published unpolarised H1 data to improve statistical precision and used to determine the structure function $xF_3^{\gamma Z}$. A measurement of the neutral current parity violating structure function $F_2^{\gamma Z}$ is presented for the first time. The polarisation dependence of the charged current total cross section is also measured. The new measurements are well described by a next-to-leading order QCD fit based on all published H1 inclusive cross section data which are used to extract the parton distribution functions of the proton.

Published in JHEP09(2012)061

F.D. Aaron[5,45], C. Alexa[5], V. Andreev[25], S. Backovic[30], A. Baghdasaryan[38], S. Baghdasaryan[38], E. Barrelet[29], W. Bartel[11], K. Begzsuren[35], A. Belousov[25], P. Belov[11], J.C. Bizot[27], V. Boudry[28], I. Bozovic-Jelisavcic[2], J. Bracinik[3], G. Brandt[11], M. Brinkmann[11], V. Brisson[27], D. Britzger[11], D. Bruncko[16], A. Bunyatyan[13,38], A. Bylinkin[24], L. Bystritskaya[24], A.J. Campbell[11], K.B. Cantun Avila[22], F. Ceccopieri[4], K. Cerny[32], V. Cerny[16], V. Chekelian[26], J.G. Contreras[22], J.A. Coughlan[6], J. Cvach[31], J.B. Dainton[18], K. Daum[37,42], B. Delcourt[27], J. Delvax[4], E.A. De Wolf[4], C. Diaconu[21], M. Dobre[12,47,48], V. Dodonov[13], A. Dossanov[12,26], A. Dubak[30], G. Eckerlin[11], S. Egli[36], A. Eliseev[25], E. Elsen[11], L. Favart[4], A. Fedotov[24], R. Felst[11], J. Feltesse[10], J. Ferencei[16], D.-J. Fischer[11], M. Fleischer[11], A. Fomenko[25], E. Gabathuler[18], J. Gayler[11], S. Ghazaryan[11], A. Glazov[11], L. Goerlich[7], N. Gogitidze[25], M. Gouzevitch[11,43], C. Grab[40], A. Grebenyuk[11], T. Greenshaw[18], G. Grindhammer[26], S. Habib[11], D. Haidt[11], R.C.W. Henderson[17], E. Hennekemper[15], H. Henschel[39], M. Herbst[15], G. Herrera[23], M. Hildebrandt[36], K.H. Hiller[39], J. Hladký[31], D. Hoffmann[21], R. Horisberger[36], T. Hreus[4], F. Huber[14], M. Jacquet[27], X. Janssen[4], L. Jönsson[20], H. Jung[11,4], M. Kapichine[9], I.R. Kenyon[3], C. Kiesling[26], M. Klein[18], C. Kleinwort[11], R. Kogler[12], P. Kostka[39], M. Krämer[11], J. Kretzschmar[18], K. Krüger[15], M.P.J. Landon[19], W. Lange[39], G. Laštovička-Medin[30], P. Laycock[18], A. Lebedev[25], V. Lendermann[15], S. Levonian[11], G. Li[27,51], K. Lipka[11,47], B. List[11], J. List[11], B. Lobodzinski[11], R. Lopez-Fernandez[23], V. Lubimov[24], E. Malinovski[25], H.-U. Martyn[1], S.J. Maxfield[18], A. Mehta[18], A.B. Meyer[11], H. Meyer[37], J. Meyer[11], S. Mikocki[7], I. Milcewicz-Mika[7], F. Moreau[28], A. Morozov[9], J.V. Morris[6], K. Müller[41], Th. Naumann[39], P.R. Newman[3], C. Niebuhr[11], A. Nikiforov[11,52], D. Nikitin[9], G. Nowak[7], K. Nowak[12], J.E. Olsson[11], D. Ozerov[11], P. Pahl[11], V. Palichik[9], M. Pandurovic[2], C. Pascaud[27], G.D. Patel[18], E. Perez[10,44], A. Petrukhin[11], I. Picuric[30], H. Pirumov[14], D. Pitzl[11], R. Plačakytė[11], B. Pokorny[32], R. Polifka[32,49], B. Povh[13], V. Radescu[11], N. Raicevic[30], T. Ravdandorj[35], P. Reimer[31], E. Rizvi[19], P. Robmann[41], R. Roosen[4], A. Rostovtsev[24], M. Rotaru[5], J.E. Ruiz Tabasco[22], S. Rusakov[25], D. Šálek[32], D.P.C. Sankey[6], M. Sauter[14], E. Sauvan[21,50], S. Schmitt[11], L. Schoeffel[10], A. Schöning[14], H.-C. Schultz-Coulon[15], F. Sefkow[11], L.N. Shtarkov[25], S. Shushkevich[11], T. Sloan[17], Y. Soloviev[11,25], P. Sopicki[7], D. South[11], V. Spaskov[9], A. Specka[28], Z. Staykova[4], M. Steder[11], B. Stella[33], G. Stoicea[5], U. Straumann[41], T. Sykora[4,32], P.D. Thompson[3], T.H. Tran[27], D. Traynor[19], P. Truöl[41], I. Tsakov[34], B. Tseepeldorj[35,46], J. Turnau[7], A. Valkárová[32], C. Vallée[21], P. Van Mechelen[4], Y. Vazdik[25], D. Wegener[8], E. Wünsch[11], J. Žáček[32], J. Zálešák[31], Z. Zhang[27], A. Zhokin[24], R. Žlebčík[32], H. Zohrabyan[38], and F. Zomer[27]

[1] *I. Physikalisches Institut der RWTH, Aachen, Germany*
[2] *Vinca Institute of Nuclear Sciences, University of Belgrade, 1100 Belgrade, Serbia*
[3] *School of Physics and Astronomy, University of Birmingham, Birmingham, UK*[b]
[4] *Inter-University Institute for High Energies ULB-VUB, Brussels and Universiteit Antwerpen, Antwerpen, Belgium*[c]
[5] *National Institute for Physics and Nuclear Engineering (NIPNE) , Bucharest, Romania*[k]
[6] *STFC, Rutherford Appleton Laboratory, Didcot, Oxfordshire, UK*[b]
[7] *Institute for Nuclear Physics, Cracow, Poland*[d]
[8] *Institut für Physik, TU Dortmund, Dortmund, Germany*[a]
[9] *Joint Institute for Nuclear Research, Dubna, Russia*
[10] *CEA, DSM/Irfu, CE-Saclay, Gif-sur-Yvette, France*
[11] *DESY, Hamburg, Germany*

[12] *Institut für Experimentalphysik, Universität Hamburg, Hamburg, Germany*[a]
[13] *Max-Planck-Institut für Kernphysik, Heidelberg, Germany*
[14] *Physikalisches Institut, Universität Heidelberg, Heidelberg, Germany*[a]
[15] *Kirchhoff-Institut für Physik, Universität Heidelberg, Heidelberg, Germany*[a]
[16] *Institute of Experimental Physics, Slovak Academy of Sciences, Košice, Slovak Republic*[e]
[17] *Department of Physics, University of Lancaster, Lancaster, UK*[b]
[18] *Department of Physics, University of Liverpool, Liverpool, UK*[b]
[19] *School of Physics and Astronomy, Queen Mary, University of London, London, UK*[b]
[20] *Physics Department, University of Lund, Lund, Sweden*[f]
[21] *CPPM, Aix-Marseille Univ, CNRS/IN2P3, 13288 Marseille, France*
[22] *Departamento de Fisica Aplicada, CINVESTAV, Mérida, Yucatán, México*[i]
[23] *Departamento de Fisica, CINVESTAV IPN, México City, México*[i]
[24] *Institute for Theoretical and Experimental Physics, Moscow, Russia*[j]
[25] *Lebedev Physical Institute, Moscow, Russia*
[26] *Max-Planck-Institut für Physik, München, Germany*
[27] *LAL, Université Paris-Sud, CNRS/IN2P3, Orsay, France*
[28] *LLR, Ecole Polytechnique, CNRS/IN2P3, Palaiseau, France*
[29] *LPNHE, Université Pierre et Marie Curie Paris 6, Université Denis Diderot Paris 7, CNRS/IN2P3, Paris, France*
[30] *Faculty of Science, University of Montenegro, Podgorica, Montenegro*[l]
[31] *Institute of Physics, Academy of Sciences of the Czech Republic, Praha, Czech Republic*[g]
[32] *Faculty of Mathematics and Physics, Charles University, Praha, Czech Republic*[g]
[33] *Dipartimento di Fisica Università di Roma Tre and INFN Roma 3, Roma, Italy*
[34] *Institute for Nuclear Research and Nuclear Energy, Sofia, Bulgaria*
[35] *Institute of Physics and Technology of the Mongolian Academy of Sciences, Ulaanbaatar, Mongolia*
[36] *Paul Scherrer Institut, Villigen, Switzerland*
[37] *Fachbereich C, Universität Wuppertal, Wuppertal, Germany*
[38] *Yerevan Physics Institute, Yerevan, Armenia*
[39] *DESY, Zeuthen, Germany*
[40] *Institut für Teilchenphysik, ETH, Zürich, Switzerland*[h]
[41] *Physik-Institut der Universität Zürich, Zürich, Switzerland*[h]

[42] *Also at Rechenzentrum, Universität Wuppertal, Wuppertal, Germany*
[43] *Also at IPNL, Université Claude Bernard Lyon 1, CNRS/IN2P3, Villeurbanne, France*
[44] *Also at CERN, Geneva, Switzerland*
[45] *Also at Faculty of Physics, University of Bucharest, Bucharest, Romania*
[46] *Also at Ulaanbaatar University, Ulaanbaatar, Mongolia*
[47] *Supported by the Initiative and Networking Fund of the Helmholtz Association (HGF) under the contract VH-NG-401.*
[48] *Absent on leave from NIPNE-HH, Bucharest, Romania*
[49] *Also at Department of Physics, University of Toronto, Toronto, Ontario, Canada M5S 1A7*
[50] *Also at LAPP, Université de Savoie, CNRS/IN2P3, Annecy-le-Vieux, France*
[51] *Now at EPC, Institute of High Energy Physics, Beijing, China*
[52] *Now at Humbold Universität Berlin, Berlin, Germany*

[a] *Supported by the Bundesministerium für Bildung und Forschung, FRG, under contract numbers 05H09GUF, 05H09VHC, 05H09VHF, 05H16PEA*
[b] *Supported by the UK Science and Technology Facilities Council, and formerly by the UK Particle Physics and Astronomy Research Council*
[c] *Supported by FNRS-FWO-Vlaanderen, IISN-IIKW and IWT and by Interuniversity Attraction Poles Programme, Belgian Science Policy*
[d] *Partially Supported by Polish Ministry of Science and Higher Education, grant DPN/N168/DESY/2009*
[e] *Supported by VEGA SR grant no. 2/7062/ 27*
[f] *Supported by the Swedish Natural Science Research Council*
[g] *Supported by the Ministry of Education of the Czech Republic under the projects LC527, INGO-LA09042 and MSM0021620859*
[h] *Supported by the Swiss National Science Foundation*
[i] *Supported by CONACYT, México, grant 48778-F*
[j] *Russian Foundation for Basic Research (RFBR), grant no 1329.2008.2 and Rosatom*
[k] *Supported by the Romanian National Authority for Scientific Research under the contract PN 09370101*
[l] *Partially Supported by Ministry of Science of Montenegro, no. 05-1/3-3352*

1 Introduction

Precision measurements of the proton structure in neutral current (NC) and charged current (CC) deep inelastic scattering (DIS) with polarised lepton beams provide important information on the understanding of parton dynamics and quantum chromodynamics (QCD). Previously published measurements at the electron[1]-proton collider HERA [1–16] have already provided strong constraints on the parton distribution functions (PDFs) of the proton [3, 7, 17–22]. With access to values of four momentum transfers $\sqrt{Q^2}$ comparable to the masses of the Z and W bosons, precision DIS measurements also probe the chiral structure of the electroweak interactions. Inclusive neutral current interactions are defined as the process $ep \to eX$ mediated by γ/Z bosons, whereas inclusive charged current interactions are defined as $ep \to \nu X$ and are purely weak processes mediated by W bosons.

In this paper precise measurements of the inclusive neutral and charged current ep cross sections at high Q^2 are presented utilising the complete HERA II[2] data set of $333.7\,\mathrm{pb}^{-1}$ recorded by the H1 detector at a centre-of-mass energy of $\sqrt{s} = 319\,\mathrm{GeV}$ with longitudinally polarised electron and positron beams. The inclusive NC and CC polarised single differential cross sections, $\mathrm{d}\sigma/\mathrm{d}Q^2$ and the double differential reduced cross sections $\tilde{\sigma}(x, Q^2)$ are presented for e^+p and e^-p scattering. The data were taken with an incident lepton beam energy E_e of $27.6\,\mathrm{GeV}$, whilst the energy of the unpolarised proton beam, E_p, was $920\,\mathrm{GeV}$. The longitudinal polarisation of the lepton beam was $\pm 35\%$ on average.

The NC data cover the Q^2 range from 60 to $50\,000\,\mathrm{GeV}^2$. Together with previous H1 measurements at lower Q^2, down to $\sim 1\,\mathrm{GeV}^2$ [5, 7], the data cover almost five orders of magnitude in kinematic reach. The high Q^2 NC and CC data presented here give unique constraints on the proton PDFs for Bjorken x in the range $0.0008 \leq x \leq 0.65$ which is of direct relevance to all predictions for pp scattering at the LHC [23]. In particular, production cross sections of new high mass states in the LHC kinematic domain are very sensitive to the high x PDFs constrained by DIS data.

The data extend to very high Q^2 which allows structure functions sensitive to the interference of photon and Z boson exchange to be measured. These "interference structure functions" access the difference of quark and anti-quark distributions, with $xF_3^{\gamma Z}$, and a combination of their sums, with $F_2^{\gamma Z}$. They are measured by using both the charge and polarisation dependence of the NC cross section, providing an improved determination of $xF_3^{\gamma Z}$ and a very first measurement of $F_2^{\gamma Z}$.

The measured inclusive cross sections are combined with previously published unpolarised HERA I measurements to provide a single coherent set of cross sections. The sensitivity and kinematic reach of these data enable a dedicated QCD analysis to be performed on H1 data alone. The fit procedure takes into account all point-to-point correlated systematic uncertainties yielding a new determination of PDFs and their uncertainties, termed H1PDF 2012.

This paper is organised as follows: in section 2 the definitions of the inclusive NC and CC cross sections are given together with their relation to the proton structure functions and PDFs. In

[1] In this paper "electron" refers generically to both electrons and positrons. Where distinction is required the terms e^- and e^+ are used.

[2] HERA operation was split into two phases, HERA I which ran from 1992 to 2000, and HERA II which ran from 2003 to 2007.

section 3 the H1 detector and trigger system are described as well as the HERA polarimeters. The simulation programmes and Monte Carlo models used in the analysis are discussed in section 4. In section 5 the analysis procedure is given starting with a description of the kinematic reconstruction methods, calibration and alignment of the detector, and followed by the event selection and assessment of the systematic uncertainties of the measurements. The QCD analysis method is explained in section 6 and the results are presented in section 7. The paper is summarised in section 8.

2 Neutral and Charged Current Cross Sections

2.1 Neutral Currents

The differential cross section for $e^{\pm}p$ scattering after correction for QED radiative effects can be expressed in terms of generalised proton structure functions $\tilde{F}$ as

$$\frac{\mathrm{d}^2\sigma^{\pm}_{\mathrm{NC}}}{\mathrm{d}x\mathrm{d}Q^2} = \frac{2\pi\alpha^2}{xQ^4}(Y_+\tilde{F}_2^{\pm} \mp Y_- x\tilde{F}_3^{\pm} - y^2\tilde{F}_L^{\pm})\cdot(1+\Delta^{\mathrm{weak}}_{\mathrm{NC}})\,, \tag{1}$$

where $Y_{\pm} = 1 \pm (1-y)^2$ and y characterises the inelasticity of the interaction. The fine structure constant is defined as $\alpha \equiv \alpha(Q^2=0)$ and the weak radiative corrections[3] $\Delta^{\mathrm{weak}}_{\mathrm{NC}}$ are defined as in [24] in terms of α and the Z and W boson masses which are taken to be $M_Z = 91.187\,\mathrm{GeV}$ and $M_W = 80.410\,\mathrm{GeV}$.

The generalised structure functions, $\tilde{F}_{2,3}$, may be written as linear combinations of the proton structure functions F_2, $F_{2,3}^{\gamma Z}$, and $F_{2,3}^{Z}$ containing information on QCD parton dynamics as well as on the electroweak (EW) couplings of the quarks to the neutral vector bosons [25]. The structure function F_2 is associated to pure photon exchange terms, $F_{2,3}^{\gamma Z}$ correspond to photon-Z interference terms and $F_{2,3}^{Z}$ describe the pure Z exchange terms. In addition the generalised longitudinal structure function $\tilde{F}_L$ may be similarly decomposed, however this is an important contribution only at high y and is expected to be negligible at large x and Q^2. The linear combinations for $\tilde{F}_2$ and $x\tilde{F}_3$ in arbitrarily polarised $e^{\pm}p$ scattering with lepton polarisation P_e are given by

$$\tilde{F}_2^{\pm} = F_2 - (v_e \pm P_e a_e)\kappa\frac{Q^2}{Q^2+M_Z^2}F_2^{\gamma Z} + (a_e^2 + v_e^2 \pm P_e 2v_e a_e)\kappa^2\left[\frac{Q^2}{Q^2+M_Z^2}\right]^2 F_2^Z\,, \tag{2}$$

$$x\tilde{F}_3^{\pm} = -(a_e \pm P_e v_e)\kappa\frac{Q^2}{Q^2+M_Z^2}xF_3^{\gamma Z} + (2a_e v_e \pm P_e[v_e^2 + a_e^2])\kappa^2\left[\frac{Q^2}{Q^2+M_Z^2}\right]^2 xF_3^Z\,, \tag{3}$$

with $\kappa^{-1} = 4\frac{M_W^2}{M_Z^2}(1-\frac{M_W^2}{M_Z^2})$ in the on-mass-shell scheme. The quantities v_e and a_e are the vector and axial-vector couplings of the electron to the Z boson.

[3]The weak corrections are typically smaller than 1% and never more than 3% at the highest Q^2 and are not applied to the measured cross sections.

It can be seen from equations 2 and 3 that different combinations of structure functions may be experimentally determined by scattering longitudinally polarised leptons on unpolarised protons. In particular, since v_e is small, a measurement of the polarisation asymmetry for fixed lepton charge allows the parity violating structure function $F_2^{\gamma Z}$ to be measured.

In the quark-parton model (QPM), the hadronic structure functions are related to linear combinations of sums and differences of the quark and anti-quark momentum distributions $xq(x, Q^2)$ and $x\bar{q}(x, Q^2)$. The structure function $\tilde{F}_2$ is determined by the sum of quarks and anti-quark momentum distributions, whereas the structure function $x\tilde{F}_3$ is determined by the difference of quarks and anti-quark momentum distributions and is therefore sensitive to the valence quark distributions:

$$\left[F_2, F_2^{\gamma Z}, F_2^Z\right] = x\sum_q [e_q^2, 2e_q v_q, v_q^2 + a_q^2](q + \bar{q}), \tag{4}$$

$$\left[xF_3^{\gamma Z}, xF_3^Z\right] = 2x\sum_q [e_q a_q, v_q a_q](q - \bar{q}). \tag{5}$$

Here v_q and a_q are the vector and axial-vector couplings of the quarks to the Z boson and e_q is the charge of the quark of flavour q.

The reduced NC cross section is defined by

$$\tilde{\sigma}^{\pm}_{\rm NC}(x, Q^2) \equiv \frac{{\rm d}^2\sigma^{\pm}_{\rm NC}}{{\rm d}x{\rm d}Q^2}\frac{xQ^4}{2\pi\alpha^2}\frac{1}{Y_+} \equiv \left(\tilde{F}_2^{\pm} \mp \frac{Y_-}{Y_+}x\tilde{F}_3^{\pm} - \frac{y^2}{Y_+}\tilde{F}_L^{\pm}\right)(1 + \Delta^{\rm weak}_{\rm NC}). \tag{6}$$

2.2 Charged Currents

The differential CC cross section for $e^{\pm}p$ scattering of polarised leptons with unpolarised protons, corrected for QED radiative effects, can be expressed as

$$\frac{{\rm d}^2\sigma^{\pm}_{\rm CC}}{{\rm d}x{\rm d}Q^2} = (1 \pm P_e)\frac{G_F^2}{4\pi x}\left[\frac{M_W^2}{M_W^2 + Q^2}\right]^2 \left(Y_+ W_2^{\pm} \mp Y_- xW_3^{\pm} - y^2 W_L^{\pm}\right)\cdot(1 + \Delta^{\rm weak}_{\rm CC}), \tag{7}$$

where G_F is the Fermi constant defined using the weak boson masses [24]. Here $W_2^{\pm}$, $xW_3^{\pm}$ and $W_L^{\pm}$ are the structure functions for CC $e^{\pm}p$ scattering, and $\Delta^{\rm CC}_{\rm weak}$ represents the weak radiative corrections for CC interactions. From equation 7 it can be seen that the cross section has a linear dependence on the polarisation of the electron beam P_e. For a fully right handed e^- beam ($P_e = 1$), or a fully left handed e^+ beam ($P_e = -1$) the cross section is identically zero in the Standard Model (SM). In the QPM $W_L^{\pm} \equiv 0$, and the structure functions $W_2^{\pm}$ and $xW_3^{\pm}$ are expressed as the flavour dependent sum and difference of the quark and anti-quark momentum distributions. In the CC case only the positively charged quarks contribute to W^- mediated scattering and conversely only negatively charged quarks couple to the exchanged W^+ boson, thus

$$W_2^- = x(U + \overline{D}), \quad W_2^+ = x(\overline{U} + D), \tag{8}$$

$$xW_3^- = x(U - \overline{D}), \quad xW_3^+ = x(D - \overline{U}), \tag{9}$$

where, below the b quark mass threshold

$$U = u + c\,, \;\; \overline{U} = \bar{u} + \bar{c}\,, \;\; D = d + s\,, \;\; \overline{D} = \bar{d} + \bar{s}\,, \tag{10}$$

where u, d, s, c represent quark densities of each flavour in the standard notation. Here U represents the sum of up-type, and D the sum of down-type quark densities.

The reduced CC cross section is then defined as

$$\tilde{\sigma}_{\rm CC}(x, Q^2) \equiv \frac{4\pi x}{G_F^2} \left[\frac{M_W^2 + Q^2}{M_W^2} \right]^2 \frac{{\rm d}^2\sigma_{\rm CC}}{{\rm d}x{\rm d}Q^2}\,. \tag{11}$$

3 H1 Apparatus, Trigger and Data Samples

3.1 The H1 Detector

A detailed description of the H1 detector can be found elsewhere [26–29]. The coordinate system of H1 is defined such that the positive z axis is in the direction of the proton beam (forward direction) and the nominal interaction point is located at $z = 0$. The polar angle θ is then defined with respect to this axis. The detector components most relevant to this analysis are the Liquid Argon (LAr) calorimeter, which measures the positions and energies of particles over the range $4^\circ < \theta < 154^\circ$, the inner tracking detectors, which measure the angles and momenta of charged particles over the range $7^\circ < \theta < 165^\circ$, and a lead-fibre calorimeter (SpaCal) covering the range $153^\circ < \theta < 177^\circ$.

The LAr calorimeter consists of an inner electromagnetic section with lead absorbers and an outer hadronic section with steel absorbers. The calorimeter is divided into eight wheels along the beam axis, each consisting of eight absorber stacks arranged in an octagonal formation around the beam axis. The electromagnetic and the hadronic sections are highly segmented in the transverse and the longitudinal directions. Electromagnetic shower energies are measured with a resolution of $\delta E/E \simeq 0.11/\sqrt{E/\text{GeV}} \oplus 0.01$ and hadronic energies with $\delta E/E \simeq 0.46/\sqrt{E/\text{GeV}} \oplus 0.03$ as determined using electron and pion test beam data [30, 31].

In the central region, $25^\circ < \theta < 155^\circ$, the central tracking detector (CTD) measures the trajectories of charged particles in two cylindrical drift chambers immersed in a uniform $1.16\,\text{T}$ solenoidal magnetic field. The CTD also contains a further drift chamber (COZ) between the two drift chambers to improve the z coordinate reconstruction, as well as a multi-wire proportional chamber at inner radii (CIP) mainly used for triggering [32]. The CTD measures charged particles with a transverse momentum resolution of $\sigma(p_T)/p_T \simeq 0.2\%\, p_T/\text{GeV} \oplus 1.5\%$. The forward tracking detector (FTD) is used to supplement track reconstruction in the region $7^\circ < \theta < 30^\circ$ [33] and improves the hadronic final state reconstruction of forward going low momentum particles.

The CTD tracks are linked to hits in the vertex detectors: the central silicon tracker (CST) [34, 35], the forward silicon tracker (FST), and the backward silicon tracker (BST). These detectors provide precise spatial track reconstruction and therefore also improve the primary vertex spatial reconstruction. The CST consists of two layers of double-sided silicon strip detectors surrounding the beam pipe covering an angular range of $30^\circ < \theta < 150^\circ$ for tracks passing through both layers. The FST consists of five double wheels of single-sided strip detectors [36] measuring the transverse coordinates of charged particles. The BST design is very similar to the FST and consists of six double wheels of strip detectors [37].

In the backward region the SpaCal provides an energy measurement for hadronic particles, and has a hadronic energy resolution of $\delta E/E \simeq 0.70/\sqrt{E/\mathrm{GeV}} \oplus 0.01$ and a resolution for electromagnetic energy depositions of $\delta E/E \simeq 0.07/\sqrt{E/\mathrm{GeV}} \oplus 0.01$ measured using test beam data [38]. It also provides a trigger used for efficiency estimations which is based on electromagnetic energy and timing information inside the calorimeter.

The ep luminosity is determined online by measuring the event rate for the Bethe-Heitler process of QED bremsstrahlung $ep \rightarrow ep\gamma$. The photons are detected in the photon tagger located at $z = -103\,\mathrm{m}$. An electron tagger is placed at $z = -5.4\,\mathrm{m}$ adjacent to the beam-pipe. It is used to provide information on $ep \rightarrow eX$ events at very low Q^2 (photoproduction) where the electron scatters through a small angle ($\pi - \theta < 5\,\mathrm{mrad}$). The overall normalisation is determined using a precision measurement of the QED Compton process [39].

At HERA transverse polarisation of the lepton beam arises naturally through synchrotron radiation via the Sokolov-Ternov effect [40]. Spin rotators installed in the beam-line on either side of the H1 detector allow transversely polarised leptons to be rotated into longitudinally polarised states and back again. The degree of polarisation is constant around the HERA ring and is continuously measured using two independent polarimeters LPOL [41] and TPOL [42]. The polarimeters are situated in beam-line sections in which the beam leptons have longitudinal and transverse polarisations, respectively. Both measurements rely on an asymmetry in the energy spectrum of left and right handed circularly polarised photons undergoing Compton scattering with the lepton beam. The TPOL measurement uses in addition a spatial asymmetry. The LPOL and TPOL measurements are averaged when both measurements are available, otherwise only one polarimeter measurement is used [43].

3.2 The Trigger

The H1 trigger system is a three level trigger with a first level latency of approximately $2\,\mu$s. NC events at high Q^2 are triggered mainly using information from the LAr calorimeter. The calorimeter has a finely segmented pointing geometry allowing the trigger to select localised energy deposits in the electromagnetic section of the calorimeter pointing to the nominal interaction vertex. For electrons with energy above $11\,\mathrm{GeV}$ this is determined to be 100% efficient using an independently triggered sample of events. At lower energies the triggers based on LAr information are supplemented by using additional information from the tracking detectors. The LAr calorimeter electronics allow scattered leptons to be triggered with energies as low as $5\,\mathrm{GeV}$, the minimum value considered in this analysis. This gives access to the high y kinematic region. For electron energies of $5\,\mathrm{GeV}$, the combined trigger efficiency increases from 87% to 92% during the HERA II run due to several incremental improvements in the trigger set-up.

The characteristic feature of CC events is a large missing transverse momentum, P_T^{miss}, which is identified at the trigger level using the LAr calorimeter vector sum of energy within "trigger towers", i.e. groups of trigger regions with a projective geometry pointing to the nominal interaction vertex. At low $P_T^{\rm miss}$ the efficiency is enhanced by use of an additional trigger requiring hadronic energy in combination with track information from the inner tracking chambers. At $12\,{\rm GeV}$, the minimum $P_T^{\rm miss}$ considered in this analysis, the efficiency is 60%, rising to 90% for $P_T^{\rm miss}$ of $25\,{\rm GeV}$. This is determined from the *pseudo CC* sample. This sample is constructed of NC events in which all information from the scattered lepton is suppressed (see section 5.4). The trigger energy sums are then recalculated for the remaining hadronic final state. This sample also provides a useful high statistics cross check of further aspects of the CC analysis.

3.3 Data Samples

The data sets used in this analysis are subdivided into samples or periods of left handed and right handed polarised lepton beams with polarisation $P_e = (N_R - N_L)/(N_R + N_L)$, where N_R (N_L) is the number of right (left) handed leptons in the beam. The corresponding data sets are termed the R and L data sets respectively. The luminosity and longitudinal lepton beam polarisation for each data set are given in table 1.

	R	L
e^-p	$\mathcal{L} = 47.3\,{\rm pb}^{-1}$ $P_e = (+36.0 \pm 1.0)\%$	$\mathcal{L} = 104.4\,{\rm pb}^{-1}$ $P_e = (-25.8 \pm 0.7)\%$
e^+p	$\mathcal{L} = 101.3\,{\rm pb}^{-1}$ $P_e = (+32.5 \pm 0.7)\%$	$\mathcal{L} = 80.7\,{\rm pb}^{-1}$ $P_e = (-37.0 \pm 0.7)\%$

Table 1: Table of integrated luminosities, $\mathcal{L}$, and luminosity weighted longitudinal lepton beam polarisation, P_e, for the data sets presented here.

4 Simulation Programs

In order to determine acceptance corrections, DIS processes are generated at leading order (LO) QCD using the DJANGOH 1.4 [44] Monte Carlo (MC) simulation program which is based on HERACLES 4.6 [45] for the electroweak interaction and on LEPTO 6.5.1 [46] for the hard matrix element calculation. The colour dipole model (CDM) as implemented in ARIADNE [47] is used to generate higher order QCD dynamics. The JETSET 7.410 program [48] is used to simulate the hadronisation process in the 'string-fragmentation' model. Additional DJANGOH study samples are produced in which the higher order QCD effects are simulated using DGLAP inspired parton showers matched to the hard LO matrix element calculation, known as MEPS. The simulated events are produced with PDFs from a NLO QCD fit (HERAPDF1.0) which includes combined H1 and ZEUS low Q^2 and high Q^2 NC and CC data from HERA I [17]. In order to improve the precision with which the acceptance corrections are determined, the simulated cross sections are reweighted using the PDF set determined in this analysis, H1PDF 2012 (see section 6). All data distributions are compared to the MC expectations using H1PDF 2012.

The dominant ep background contribution to DIS is due to large cross section photoproduction (γp) processes in which energetic $\pi^0 \to \gamma\gamma$ decays or charged hadrons are mis-identified as the scattered electron in the NC channel, or hadronic final states produce large fake missing transverse momentum mimicking a CC interaction. These are simulated using the PYTHIA 6.224 [49] generator with leading order parton distribution functions for the proton and photon taken from [50]. Additional small background contributions arise from elastic and inelastic QED Compton processes generated with the WABGEN program [51]; lepton pair production via two photon interactions simulated by the GRAPE code [52]; prompt photon production in which the photon may be mis-identified as an electron generated by PYTHIA; and real $W^{\pm}/Z$ production samples produced with EPVEC [53].

The detector response to events produced by the various generator programs is simulated in detail using a program based on GEANT3 [54]. The simulation includes detailed time dependent modelling of detector noise conditions, beam optics, polarisation and inefficient channel maps reflecting actual running conditions throughout the HERA II data taking period. These simulated events are then subjected to the same reconstruction, calibration, alignment and analysis chain as the real data.

5 Experimental Procedure

5.1 Kinematic Reconstruction

Precise reconstruction of the event kinematics is crucial for the measurement of DIS cross sections. In the NC channel several different methods are available due to the redundancy arising from the simultaneous reconstruction of the scattered lepton and the hadronic final state. In contrast the CC event kinematics can be reconstructed using only one method based on the measurement of the hadronic final state since the neutrino escapes the detector unobserved. Typically the quantities Q^2 and y are reconstructed and x is obtained via the relation $Q^2 = sxy$.

In NC interactions the properties of the scattered lepton are described in terms of its energy E'_e and polar scattering angle θ_e defined with respect to the proton direction. The hadronic final state (HFS) is characterised using the quantities $P_{T,h} = \sqrt{(\sum_i p_{x,i})^2 + (\sum_i p_{y,i})^2}$ and $\Sigma = \sum_i (E_i - p_{z,i})$ where the summation is performed over all HFS particles i assuming charged particles have the pion mass. Due to the large momentum of the incident proton in the lab frame compared to the electron, the HFS particles are often forward going (positive z) and lead to losses in the forward beam-pipe. The quantities $P_{T,h}$ and Σ are chosen due to their relative insensitivity to these losses. The inclusive hadronic polar angle γ_h, defined by $\tan(\gamma_h/2) = \Sigma/P_{T,h}$, is used in the calibration procedure.

In general the scattered lepton quantities are precisely determined whereas the hadronic quantities have moderate precision due to particle losses and fluctuations in the hadronic shower. Isolated low energy calorimeter deposits are classified as noise originating from electronic sources or back-scattered low energy particles and are excluded from the HFS. The HFS is measured using a sophisticated energy flow algorithm [55, 56] which combines tracks with calorimetric energy measurements in an optimum way avoiding double counting. For each track (assumed to be a charged pion) the measured track uncertainties are compared to the expected calorimetric energy resolution. The track measurement alone is used to reconstruct the particle momentum if it has superior resolution except in cases where an excess of energy in the calorimeter is observed originating from neutral particles. This is then taken into account appropriately. If the expected calorimeter resolution is better, then either the calorimeter information alone is used to define the hadron momentum or, similarly to the previous case, a combination in which the track is used and the calorimeter energy is reduced appropriately. At high Q^2 and high x, corresponding to small γ_h, the HFS is dominated by one or more jets thus the complete HFS can be approximated by the sum of jet four-momenta corresponding to localised calorimetric energy sums above threshold. This technique allows a further suppression of noise in the hadronic reconstruction which is important in this kinematic region.

Several reconstruction methods are used in the analysis for determining the kinematics and for providing systematic cross checks. The most precise method for $y \gtrsim 0.1$ is the e-method which relies solely on E'_e and θ_e to reconstruct the kinematic variables Q^2 and y as:

$$Q^2_e = \frac{(E'_e \sin\theta_e)^2}{1-y_e}\,, \quad y_e = 1 - \frac{E'_e}{E_e}\sin^2\left(\frac{\theta_e}{2}\right)\,. \tag{12}$$

This method is used in the NC analysis region $y > 0.19$.

The resolution of the e-method degrades at low y and is also susceptible to large QED radiative corrections at the highest and lowest y. In the Σ-method [57] y is reconstructed as $\Sigma/(\Sigma + E'_e(1-\cos\theta_e))$ and is therefore less sensitive to QED radiative effects. The $e\Sigma$-method [58] is an optimum combination of the two and maintains good resolution throughout the kinematic range of the NC measurement with acceptably small QED radiative corrections. The kinematics are determined using

$$Q^2_{e\Sigma} = Q^2_e = \frac{(E'_e \sin\theta_e)^2}{1-y_e}\,, \quad y_{e\Sigma} = 2E_e\frac{\Sigma}{[\Sigma + E'_e(1-\cos\theta_e)]^2}\,. \tag{13}$$

The $e\Sigma$-method is employed to reconstruct the event kinematics for $y \leq 0.19$. In this phase space region the HFS is partially lost in the forward beam-pipe and the influence of noise on the HFS becomes large. In order to limit this effect the $e\Sigma$-method is modified such that the summation in the calculation of the quantity Σ is performed only over hadronic jets. A longitudinally invariant k_T jet algorithm [59, 60] is used and further details are given in section 5.3.

The double angle method (DA-method) [61, 62] provides a useful technique for calibrating the electromagnetic (EM) and hadronic calorimeters using θ_e and γ_h as input. Where the HFS is well contained within the detector ($y \gtrsim 0.3$) the DA-method has good resolution and is to first order independent of the calorimeter energy scales. The following formulae are used to determine the kinematics:

$$Q^2_{DA} = \frac{4E^2_e \sin\gamma_h(1+\cos\theta_e)}{\sin\gamma_h + \sin\theta_e - \sin(\theta_e+\gamma_h)}\,, \quad y_{DA} = \frac{\sin\theta_e(1-\cos\gamma_h)}{\sin\gamma_h + \sin\theta_e - \sin(\theta_e+\gamma_h)}\,. \tag{14}$$

Finally for CC interactions the event kinematics may only be reconstructed by the h-method [63] which can be systematically studied using the NC sample. The h-method kinematic variables are reconstructed using the relations

$$Q^2_h = \frac{P^2_{T,h}}{1-y_h}\,, \qquad y_h = \frac{\Sigma}{2\,E_e}\,. \tag{15}$$

5.2 Polar Angle Measurement and Energy Calibration

In neutral current interactions the polar angle of the scattered lepton, θ_e, is determined using the position of its energy deposit (cluster) in the LAr calorimeter, and the event vertex reconstructed with tracks from charged particles. The relative alignment of the calorimeter and tracking chambers is determined using a sample of events with a well measured lepton track [64] in which the COZ chambers provide an accurate z spatial reconstruction of the particle trajectory. The lepton track is helically extrapolated to an octagonal surface with inner radius $r = 105\,\mathrm{cm}$ positioned axially along the beam line. The shape describes the inner surface of the LAr calorimeter. The z position of the intersection of the track trajectory and this surface defines the quantity z_{imp}. The electron cluster barycentre is extrapolated to the same surface along a straight line from the interaction vertex. The distance between the extrapolated track and cluster is then minimised with respect to the six alignment parameters for LAr (three shifts and three rotations about the coordinate axes) keeping the CTD position fixed. Four additional parameters are introduced to allow independent shifts in z for each LAr wheel. The procedure is performed on data and checked on MC simulation to ensure that no spurious misalignments from the method appear. The alignment parameters are obtained for each of four periods when the detector was moved between data taking periods. The residual discrepancy in $\Delta\theta = \theta_{\mathrm{track}} - \theta_{\mathrm{clus}}$ between data and simulation determines the systematic uncertainty on the measurement of θ_e and is shown in figure 1. The uncertainty is taken to be $1\,\mathrm{mrad}$.

Cross checks are performed using the alternative $\Delta\phi$ alignment method [65] in which the difference in azimuthal angle between track and cluster is studied as a function of ϕ_{track}. Minimisation of this difference constrains three rotations of the calorimeter about the tracker and two translations in x and y. The z translation is constrained by minimising the distribution of $\Delta\theta$. This method is found to agree well with the default alignment procedure.

An *in situ* energy calibration of the electromagnetic part of the LAr calorimeter is performed using the method described in [65] for both data and simulation. Briefly, a sample of NC events in which the HFS is well contained in the detector is used with the DA-method to predict the scattered lepton energy which is then compared to the measured electromagnetic energy response allowing local calibration factors to be determined in a finely segmented grid in z and ϕ. The events used in the calibration are required to have $E'_e > 14\,\mathrm{GeV}$; $44\,\mathrm{GeV} < E - P_z < 66\,\mathrm{GeV}$ to limit radiative effects, where $E - P_z = \Sigma + E'_e(1 - \cos\theta_e)$; $\gamma_h > 10°$ to ensure good containment of the HFS and $y_\Sigma < 0.3$ for $z_{\mathrm{imp}} \leq 20\,\mathrm{cm}$ or $y_\Sigma < 0.5$ for $20\,\mathrm{cm} < z_{\mathrm{imp}} \leq 100\,\mathrm{cm}$ in order to obtain a good estimate of E_{DA}, the predicted scattered lepton energy from the DA-method. In each calibration region the calibration factor is taken as the mean value of E_{DA}/E'_e. The calibration is applied octant-wise for each wheel of the LAr calorimeter. In a second step, the calibration is applied in fine z_{imp} regions which become coarser with increasing z_{imp} as statistical precision decreases. The influence of non-Gaussian tails is limited by determining the calibration factors from events where E_{DA}/E'_e deviates by less than $\pm 15\%$ of the mean. The procedure is then iterated where the window is narrowed to $\pm 10\%$. The calibration is performed for each period of data taking separately.

The electromagnetic calibration performs well except in regions close to z and ϕ cracks in the detector. These local detector regions are removed from the analysis in order to limit the size of the corrections. Figure 2(a) shows the residual mismatch between E_{DA} and E'_e after performing the calibration step. The residual mis-calibrations are within $\simeq 0.3\%$. In the region of large z, which corresponds to large Q^2 and large x, the sample size becomes small and the bin size in z is increased. For the very largest z the data from all run periods are combined to provide a single calibration factor. The uncorrelated systematic uncertainty on the electromagnetic energy scale is estimated from the relative deviation of E'_e/E_{DA} between data and simulation and is found to vary from 0.3% in the central part of the calorimeter to 1% in the forward region where statistics are limited.

The calibration is validated with independent data samples not used in the calibration procedure which allow checks of the calibration linearity at low energy. These are performed using $J/\psi \rightarrow ee$ decays and QED Compton interactions $ep \rightarrow e\gamma p$ with E'_e of $3-8\,\mathrm{GeV}$ in which the lepton track momentum P_{track} is compared to the measured energy E'_e of the cluster as shown in figure 2(b). The simulation on average describes the data well in this low energy region. Differences in the material description lead to differences in the radiative tails of the P_{track} spectrum and are not of direct relevance in this analysis.

The hadronic response of the detector is calibrated by requiring a transverse momentum balance between the predicted P_T in the DA-method ($P_{T,DA}$) and the measured hadronic final state using a tight selection of well reconstructed events with a single jet where the $P_{T,DA}$ measurement is reliable to within 0.3% as verified in the simulation [66]. The tracks require no correction as validated by the reconstruction of particle decays. The calorimeter calibration constants are then determined in a minimisation procedure across the detector acceptance separately for HFS objects inside and outside jets and for electromagnetic and hadronic contributions to the HFS. Calorimeter energy deposits are classified as those originating from electromagnetic interactions and from hadronic interactions with the help of several neural networks. The procedure is described in detail in [66] and for SpaCal in [67].

Detailed studies of the hadronic response of the calorimeter lead to an improved understanding of the hadronic energy measurement. The calibration procedure is verified on a sample of two-jet events, and on a sample in which more hadronic activity outside of the jet is allowed. Further checks are performed by requiring longitudinal momentum conservation of $E - P_z$ of the hadronic final state and the scattered lepton, instead of transverse momentum conservation. In addition the reference scale may be taken from the scattered lepton rather than the DA-method prediction. These studies allow the systematic uncertainty of the hadronic scale to be reduced with respect to previous measurements [3]. The uncorrelated part of the hadronic scale uncertainty is reduced to 1% from 1.7% previously. Figure 3 demonstrates the quality of the hadronic calibration showing the level of agreement between data and simulation after the calibration procedure. In figure 3(a) the mean transverse momentum balance between the hadronic final state and the scattered lepton versus the lepton $P_{T,e}$ is shown for the complete HERA II data set. The simulation provides an accurate modelling of the data behaviour to within 1% precision. In figure 3(b) the quantity y_h is compared to the DA-method prediction, y_{DA}, as a function of the inclusive hadronic angle, γ_h, for the full HERA II data sample. Since y_h is related to the longitudinal energy flow (see equation 15) this provides an alternative check of the calibration. The simulation models the data well.

In this analysis it is the relative difference between data and simulation that is relevant, and good agreement is found to within 1%. In addition a 0.3% correlated uncertainty is considered and accounts for a possible bias in the P_T reconstruction in the DA-method reference scale used in the calibration of the electron and HFS energy. This is determined by varying θ_e and γ_h by the angular measurement uncertainty.

5.3 Neutral Current Measurement Procedure

Inelastic ep interactions are required to have a well reconstructed interaction vertex to suppress beam induced background events. High Q^2 neutral current events are selected by requiring each event to have a compact and isolated cluster in the electromagnetic part of the LAr calorimeter[4]. The scattered lepton is identified as the cluster of highest transverse momentum. In the central detector region, $\theta \geq 30°$, the cluster must be associated to a CTD track. Forward going leptons with $\theta < 30°$ traverse the region between the FTD and CTD where an increased amount of dead material causes electrons to shower. Since in this kinematic region the scattered lepton has high energy and the contribution from photoproduction background is very small, no tracker information is required to be associated with the lepton for $\theta < 30°$.

Energy-momentum conservation requires the variable $E - P_z$ summed over all final state particles (including the electron) to be approximately equal to twice the initial electron beam energy. Restricting $E - P_z$ to be greater than 35 GeV considerably reduces the photoproduction background and the radiative processes in which the scattered lepton or bremsstrahlung photons escape undetected in the lepton beam direction.

The photoproduction background increases rapidly with decreasing electron energy, therefore the analysis is separated into two distinct regions: the *nominal* analysis ($y_e \leq 0.63$ for $Q^2_e \leq 890\,\mathrm{GeV}^2$ and $y_e < 0.93$ for $Q^2_e > 890\,\mathrm{GeV}^2$) for which the minimum electron energy is $11\,\mathrm{GeV}$ and the *high y* analysis ($0.63 < y_e < 0.9$ and $56 < Q^2_e < 890\,\mathrm{GeV}^2$) for which the minimum electron energy is $5\,\mathrm{GeV}$. The techniques employed to contend with background in each analysis are described below.

5.3.1 Nominal Analysis

For the *nominal* analysis the small photoproduction contribution is statistically subtracted using the background simulation. The overall normalisation of the background simulation is checked using a sample of data events in which the true scattered lepton is observed in the electron tagger which, however, has limited acceptance.

The comparison of the e^-p data and the simulation is shown in figure 4(a) for the scattered lepton energy spectrum and polar angle, and the distribution of $E - P_z$, which are all used in the kinematic reconstruction of x and Q^2 using the $e\Sigma$-method. The corresponding distributions for e^+p data and simulation are shown in figure 4(b). In the figure the R and L data are combined and the simulation is normalised to the luminosity of the data, as is also done for all later performance figures. All distributions are described well by the simulation aside from a small difference in normalisation which is discussed in section 7.2 where the data are compared to the NLO QCD fit.

[4] Small local detector regions are disregarded in the analysis where the cluster of the scattered electron is not fully contained e.g. intermediate space between stacks, or where the trigger is not fully efficient.

For the NC analysis in the region $y < 0.19$ the noise component has an increasing influence in the transverse momentum balance $P_{T,h}/P_{T,e}$ through its effect on $P_{T,h}$. The event kinematics reconstructed with the $e\Sigma$-method in which the HFS is formed from hadronic jets only, limits the noise contribution and substantially improves the $P_{T,h}/P_{T,e}$ description. The jets are found with the longitudinally invariant k_T jet algorithm [59, 60] as implemented in FastJet [68, 69] with radius parameter $R = 1.0$ and are required to have transverse momenta $P_{T,\mathrm{jet}} > 2\,\mathrm{GeV}$. In figure 5(a) the quality of the simulation and its description of the e^-p data for $y_e < 0.19$ can be seen for the distributions of the $P_{T,h}/P_{T,e}$, γ_h, and $E - P_z$ where all HFS quantities are obtained using the vector sum of jet four-momenta. Distributions for the e^+p sample are also shown in figure 5(b). Overall both sets of distributions are well described in shape by the simulation.

At low y, the forward going hadronic final state particles can undergo interactions with material of the beam pipe. In some cases the products of these secondary interactions are incorrectly assigned as originating from the primary vertex, producing a bias in the determination of the primary interaction vertex position. Such cases are recognised and corrected by considering a vertex position calculated using a stand alone reconstruction of the track associated with the electron cluster [65, 67].

For the nominal analysis the photoproduction contribution is low, and this allows the electron candidate track verification in the region $\theta \geq 30°$ to be supplemented with an alternative method which increases efficiency. For NC events with no CTD track associated to the electron cluster, the track verification is achieved by searching for hits in the CIP located on the line from the interaction vertex to the electron cluster.

This optimised treatment of the vertex determination and verification of the electron cluster with the tracker information improves the reliability of the vertex position determination and increases the efficiency of the procedure to 99.5%.

5.3.2 High y Analysis

In the *high y* region the neutral current analysis is extended to lower energies of the scattered electron, $E'_e > 5\,\mathrm{GeV}$. At low energies photoproduction background contributions arise due to $\pi^0 \to \gamma\gamma$ decays and charged hadrons being mis-identified as electron candidates. Part of this background is suppressed by requiring a well measured track linked to the calorimeter cluster. The track is furthermore required to have the same charge as the beam lepton. The remaining background in the correctly charged sample is estimated from the number of data events in which the detected lepton has opposite charge to the beam lepton. A charge asymmetry can arise due to the different detector response to particles compared to anti-particles, in particular p and $\bar{p}$ [70, 75]. By taking into account the charge asymmetry between negative and positive background, the background estimate is statistically subtracted from the correctly charged sample. The charge asymmetry between fake lepton candidates in the e^+p and e^-p data sets is determined by measuring the ratio of wrongly charged fake scattered lepton candidates in e^+p and e^-p scattering, taking into account the difference in luminosity. The asymmetry is found to be 1.03 ± 0.05. This is cross checked using a sample of photoproduction events in which the scattered electron is detected in the electron tagger. Further details are given in [67, 71].

The e-method using scattered lepton variables alone has the highest precision in this region of phase space and is used to reconstruct the event kinematics.

Figure 6(a) shows the scattered lepton energy spectrum, the polar angle distribution and the $E - P_z$ spectrum of the *high y* sample for the e^-p data before background subtraction and the simulation to which the background, obtained from wrongly charged lepton candidates in the data, is added. The corresponding distributions for the e^+p data can be seen in figure 6(b). The shapes of the E'_e and θ_e distributions are strongly affected by the selections used in the trigger which vary with E'_e and z_{imp}. The NC simulation provides a good description of these distributions. The difference between data and simulation in the $E - P_z$ spectrum is well within the systematic uncertainty of the hadronic calibration which at high y depends largely on the SpaCal (see table 2).

5.4 Charged Current Measurement Procedure

The selection of charged current events requires a large missing transverse momentum, $P_T^{\rm miss} \equiv P_{T,h} \geq 12\,\text{GeV}$, assumed to be carried by an undetected neutrino. The event must also have a well defined reconstructed vertex. The kinematic variables y and Q^2 are determined using the h-method. In order to restrict the measurement to a region with good kinematic resolution the events are required to have $y_h < 0.85$. In addition the measurement is confined to the region with sufficiently high trigger efficiency by demanding $y_h > 0.03$. This criterion also restricts the measurement to the region where any bias in the interaction vertex position due to forward going hadronic final state particles is limited and well modelled.

The ep background is dominated by photoproduction and is suppressed by exploiting the correlation between $P_{T,h}$ and the ratio V_{ap}/V_p of transverse energy flow anti-parallel and parallel to the hadronic final state transverse momentum vector $\vec{P}_{T,h}$ [64, 72]. They are determined from the transverse momentum vectors $\vec{P}_{T,i}$ of all the particles i which belong to the hadronic final state according to

$$V_p = \sum_i \frac{\vec{P}_{T,h} \cdot \vec{P}_{T,i}}{P_{T,h}} \qquad \text{for} \qquad \vec{P}_{T,h} \cdot \vec{P}_{T,i} > 0 \tag{16}$$

$$V_{ap} = -\sum_i \frac{\vec{P}_{T,h} \cdot \vec{P}_{T,i}}{P_{T,h}} \qquad \text{for} \qquad \vec{P}_{T,h} \cdot \vec{P}_{T,i} < 0\,. \tag{17}$$

This variable provides good discrimination between the CC signal which lies at small V_{ap}/V_p and large $P_{T,h}$, and the background which lies at large V_{ap}/V_p and small $P_{T,h}$. For $P_{T,h} > 25\,\text{GeV}$, $V_{ap}/V_p < 0.25$ is required. For smaller transverse momenta the maximum allowed ratio is reduced as a parabolic function of $P_{T,h}$ such that at $12\,\text{GeV}$ values down to $V_{ap}/V_p = 0.10 - 0.12$ are accepted depending on the different data sets since the relative photoproduction contributions differ for the four R/L $e^{\pm}p$ samples. The residual ep background is negligible for most of the measured kinematic domain, though it reaches 15% at the lowest Q^2 and the highest y. The simulation is used to estimate this contribution which is subtracted statistically from the CC data sample. A systematic uncertainty of 30% is attributed to the photoproduction background. The non-ep background is rejected as described in [3, 72] by removing events with topologies typical of cosmic ray and beam-gas interaction background as well as events with timing inconsistent with the HERA bunch crossing intervals.

All efficiencies in the CC analysis can be reliably determined from the *pseudo CC* data samples of NC events, free from background contamination, in which all information associated to the scattered electron is suppressed. The production of the samples involves the identification of the scattered lepton and subsequent deletion of all calorimetric energies associated to the cluster. All trigger related energy sums are recalculated after removal of the trigger towers associated with the electron. Finally all CTD hits in a road around the electron trajectory are deleted. After removal of this information the events are passed through the standard H1 software chain to fully reconstruct the event including all particle trajectories and the interaction vertex. The *pseudo CC* samples are then reweighted to the CC cross section employing the original $e\Sigma$ kinematic quantities using H1PDF 2012. The *pseudo CC* samples are produced for each data taking period to accurately describe running conditions as closely as possible. A potential bias in the method is studied by comparing *pseudo CC* data with *pseudo CC* simulation using NC DJANGOH samples which are processed in the same way. In all cases the *pseudo CC* data and *pseudo CC* MC are found to provide adequate descriptions of each measured efficiency and also compare well to standard DJANGOH CC simulation after the application of additional adjustment factors as described below. Any remaining discrepancies are accounted for in the systematic uncertainties as described in section 5.6.

The *pseudo CC* data are used to give a precise measure of the CC trigger efficiency for each data taking period separately. The efficiency is measured in each x, Q^2 bin and the simulation is reweighted to describe the observed behaviour. The efficiency is found to be 79% at $Q^2 = 300\,\mathrm{GeV}^2$ and reaches 98% at $Q^2 \geq 3\,000\,\mathrm{GeV}^2$.

The e^+p and e^-p distributions for P_T^{miss} and $E - P_z$ are shown for data and simulation in figure 7. The spectra are well described by the simulation.

5.5 Cross Section Measurement

For both the NC and CC analyses the selected event samples are corrected for detector acceptance, efficiencies and migrations using the simulation and converted to QED corrected cross sections. The quality of the simulation, in which all selection efficiency effects are included, is shown in figures 1-7 and gives a reliable determination of detector acceptance. The accessible kinematic ranges of the measurements depend on the resolution of the reconstructed kinematics and are determined by requiring the purity and stability of any measurement bin to be larger than 30% as determined from signal MC. The purity is defined as the fraction of events generated and reconstructed in a measurement bin (N^{g+r}) from the total number of events reconstructed in the bin (N^r). The stability is the ratio of the number of events generated and reconstructed in a bin to the number of events generated in that bin (N^g). The detector acceptance, $\mathcal{A} = N^r/N^g$, is obtained from the ratio of stability divided by purity and corrects the measured signal event yields for detector effects including resolution smearing and selection efficiency.

The measured differential cross sections $\sigma(x, Q^2)$ are then determined using the relation

$$\sigma(x, Q^2) = \frac{N - B}{\mathcal{L} \cdot \mathcal{A}} \cdot \mathcal{C} \cdot \left(1 + \Delta^{\mathrm{QED}}\right) , \tag{18}$$

where N and B are the selected number of data events and the estimated number of background events respectively, $\mathcal{L}$ is the integrated luminosity, $\mathcal{C}$ is the bin centre correction, and $(1+\Delta^{\mathrm{QED}})$ are the QED radiative corrections.

The bin centre correction $\mathcal{C}(x_c, Q_c^2)$ is a factor obtained from NLO QCD expectation using H1PDF 2012, σ^{th}, and scales the bin integrated cross section to a differential cross section at the kinematic point x_c, Q_c^2 defined as

$$\mathcal{C}(x_c, Q_c^2) = \frac{\sigma^{th}(x_c, Q_c^2)}{\iint_{bin} \mathrm{d}x\mathrm{d}Q^2 \;\; \sigma^{th}(x, Q^2)} \,. \tag{19}$$

The single differential cross sections are obtained using the obvious extensions to the formulae given above.

The DIS cross sections σ can be factorised as

$$\sigma = \sigma^{\mathrm{Born}}(1 + \Delta^{\mathrm{QED}})(1 + \Delta^{\mathrm{weak}})\,, \tag{20}$$

where σ^{Born} is the Born cross section and Δ^{QED} are the QED radiative corrections. The measured cross sections presented in section 7, in which the effects of QED radiation have been corrected for, correspond to the differential cross sections $\mathrm{d}^2\sigma/\mathrm{d}x\mathrm{d}Q^2$ defined in equations 1 and 7. The QED radiative corrections are defined in [1, 3] and are calculated to first order in α using the program HERACLES [45] as implemented in DJANGOH [44] and verified with the numerical analysis programs HECTOR [24] and EPRC [73]. In order to retain sensitivity to higher order EW effects in the measured cross sections, no Δ^{weak} corrections are applied to the measurements.

New measurements of the unpolarised cross sections are also performed. The L and R data sets for e^+p and e^-p scattering are merged and the cross sections are measured with a resulting small residual polarisation of $+1.7\%$ in e^+p and -6.6% in e^-p data. This remaining polarisation is corrected for using the H1PDF 2012 fit to yield HERA II cross sections with $P_e = 0$.

5.6 Systematic Uncertainties

The uncertainties on the measurement lead to systematic errors on the cross sections, which can be split into bin-to-bin correlated and uncorrelated parts. All the correlated systematic errors are found to be symmetric to a good approximation and are assumed so in the following. The total systematic error is formed by adding the individual errors in quadrature.

The size of each systematic uncertainty source and its region of applicability are given in table 2. Further details can be found elsewhere [64–67,72]. The influence of the systematic uncertainties on the NC and CC cross section measurements are given in tables 13-24, and their origin and method of estimation are discussed below.

Electron Energy Uncertainty: The calibration of the electromagnetic part of the LAr calorimeter is performed using a subset of NC data. Uncertainties arise from the particular choice of calibration samples, the linearity correction uncertainty, and at very high Q^2 from the limited statistics due to the sharply decreasing NC cross section. The uncertainty varies for each wheel of the LAr calorimeter and values are listed in table 2. The correlated part of the uncertainty comes from the residual global shift between data and MC in the kinematic peak of the E_e' distribution (shown in figure 4) after the calibration procedure and is determined to be 0.3%. It results in a correlated systematic error on the NC cross section which is up to 2% at low y and $Q^2 \lesssim 1\,000\,\mathrm{GeV}^2$, increasing to $\sim 4\%$ at larger Q^2.

Source		Uncertainty
Electron energy scale	$z_{\text{imp}} \leq -150\,\text{cm}$	0.5% unc. $\oplus$ 0.3% corr.
	$-150 < z_{\text{imp}} \leq -60\,\text{cm}$	0.3% unc. $\oplus$ 0.3% corr.
	$-60 < z_{\text{imp}} \leq +20\,\text{cm}$	0.5% unc. $\oplus$ 0.3% corr.
	$+20 < z_{\text{imp}} \leq +110\,\text{cm}$	0.5% unc. $\oplus$ 0.3% corr.
	$z_{\text{imp}} > +110\,\text{cm}$	1.0% unc. $\oplus$ 0.3% corr.
Electron scale linearity	$E'_e < 11\,\text{GeV}$	0.5%
Hadronic energy scale	LAr & Tracks	1.0% unc. $\oplus$ 0.3% corr.
	SpaCal	5.0% unc. $\oplus$ 0.3% corr.
Polar angle	θ_e	$1\,\text{mrad}$ corr.
Noise	NC $y < 0.19$	5% energy not in jets , corr.
	NC $y > 0.19$	20% corr.
	CC	20% corr.
NC trigger efficiency	e^+p 2003-2004	0.5%
	e^-p 2004-2005	0.6%
	e^-p 2006	0.5%
	e^+p 2006-2007	0.3%
	NC *high* y	$0.5 - 1.2\%$
Electron track and vertex efficiency	$\theta_e > 50^\circ$	0.2%
	$\theta_e < 50^\circ$, NC *high* y	1.0%
Electron charge determination	NC *high* y	0.5%
Electron ID efficiency	$z_{\text{imp}} < 20\,\text{cm}$ ($\geq 20\,\text{cm}$)	0.2% (1.0%)
Background	NC, CC: γp	30% corr.
	CC: NC (others)	10% (20%) corr.
Background γp charge asymmetry	NC *high* y	1.03 ± 0.05 corr.
CC trigger efficiency (ϵ)		$15\% \cdot (1-\epsilon) \oplus 0.2\%$
CC vertex efficiency	$y \geq 0.15$ (< 0.15)	1.5% (3.0%)
CC background finder efficiency	$y \geq 0.08$ (< 0.08)	1.0% (2.0%)
CC V_{ap}/V_p bg suppression cut		± 0.02 corr.
QED radiative corrections	NC $x < 0.1$, $0.1 \leq x < 0.3$, $x \geq 0.3$	$0.3/1.0/2.0\%$
	NC *high* y	1.0%
	CC kinematics dependent	$\sim 1.0 - 2.0\%$
Acceptance corrections	NC $e^\pm p$: $Q^2 \leq 5000$ (> 5000) GeV^2	0.2% (1.0%)
	CC e^-p: $Q^2 \leq 5000$ (> 5000) GeV^2	0.2% (1.0%)
	CC e^+p: $Q^2 \leq 5000$ (> 5000) GeV^2	0.5% (3.0%)
Polarisation	LPOL (TPOL)	2.0% (1.9%)
Luminosity		2.3% corr. $\oplus$ 1.5% unc.

Table 2: Table of applied systematic uncertainties and regions of applicability. Uncertainties which are considered point-to-point correlated are labelled corr. and correspond to the sources listed in table 4. All other sources are considered uncorrelated. The effect of these uncertainties on the cross section measurements are given in the tables of section 7.

Hadronic Calibration Uncertainty: An uncorrelated uncertainty of 1% is obtained for the hadronic energy measurement. The uncertainty is determined by quantifying the agreement between data and simulation in the mean of the $P_{T,h}/P_{T,DA}$ distribution in each x, Q^2 measurement bin by means of pull distributions. The pull is defined as the difference in the mean values divided by the uncertainty which includes the uncorrelated hadronic calibration component. An uncertainty of 1% yields a pull distribution which is Gaussian distributed, centred on zero, and with unit standard deviation. A 0.3% correlated component to the uncertainty is considered which originates from the calibration method due to the uncertainty of the reference scale [66]. The resulting correlated systematic error is typically below 1% for NC and CC cross sections, and the uncorrelated component is up to 5% at large x.

Polar Angle Uncertainty: A correlated $1\,\mathrm{mrad}$ uncertainty on the determination of the electron polar angle is considered, accounting for any remaining discrepancy in the measurements of θ_{clus} and θ_{track} after the alignment procedure described in section 5.2. The uncertainty accommodates differences between periods due to changes in the tracking capability of the detector for example when the FST or the CST were not fully operational during data taking. This leads to a typical uncertainty on the NC reduced cross section of less than 1%, increasing at high x.

Noise Subtraction Uncertainty: Energy classified as noise in the LAr calorimeter is excluded from the HFS. For $y < 0.19$ in the NC analysis the calorimetric energy not contained within hadronic jets is classified as noise. The uncertainty on the subtracted noise is estimated to be 5% of the noise contribution. This variation encompasses all observed differences between data and simulation in the ratio of $P_{T,h}/P_{T,e}$ in each x, Q^2 measurement bin in this kinematic region. Changing the jet algorithm to the SIScone method [74], varying the minimum jet transverse momentum $p_{T,jet}$ by 50%, and varying the jet radius parameter by 25% all have a minor effect on the resulting distribution of $P_{T,h}/P_{T,e}$ and deviations are contained within the 5% scaling of hadronic energy not associated with a jet. For the CC analysis and for $y > 0.19$ in the NC analysis the noise contribution is defined as the sum of isolated low energy calorimetric depositions. In this kinematic region the contribution is small and a conservative uncertainty of 20% of the noise is assigned to accommodate differences between data and simulation. As a cross check this same noise definition is used for $y < 0.19$ and it is verified that a 20% noise variation also encompasses any difference between data and simulation. The check results in larger event migrations outside the measured region compared to using the default jet method in this kinematic region. This source of systematic uncertainty gives rise to a correlated systematic error at low y comparable to or smaller than the correlated electron energy scale uncertainty except for $x \geq 0.4$ and $Q^2 \lesssim 5\,000\,\mathrm{GeV}^2$ in the NC measurements where the uncertainty due to noise rises to $5 - 10\%$.

NC Trigger Efficiency Uncertainty: The uncertainty on the trigger efficiency in the NC *nominal* analysis is determined separately for each data taking period to account for changing trigger and beam conditions (using several dedicated monitor triggers). Three trigger requirements are employed: the global timing, the event timing and the calorimeter energy. The efficiency of global timing criteria to suppress out of time beam related background was continuously monitored with high precision and found to be 99% initially rising to 100% at the end of the HERA II running period. The efficiency of the calorimeter energy trigger requirements is determined in a fine grid in z_{imp} and ϕ_e, the azimuthal angle of the scattered lepton. Time dependent local regions of the calorimeter with efficiencies of less than 99% are rejected in the analysis [65]. Finally the event timing trigger requirements were also continuously monitored in the data. After rejection of local inefficient regions the overall trigger efficiency is close to 100% and the uncertainty is listed in table 2.

NC *high y* Trigger Efficiency Uncertainty: The trigger efficiency estimate for the *high y* analysis involves several strategies due to the complex nature of the trigger designed to record low energy electrons in a high hadronic background environment. All efficiencies are measured individually in each data taking period. The efficiency of the electron calorimeter energy requirement is estimated using events triggered by the HFS in the SpaCal. This method allows the trigger energy threshold to be accurately measured and any potential bias is controlled by comparing this efficiency with that determined from events triggered by the HFS in the LAr. The same global timing and event timing conditions as mentioned above are used in the *high y* triggers. Finally the triggers place conditions on the charged particle multiplicity. The efficiency of these track requirements is measured with a variety of independent control samples and the uncertainty is determined from the level of agreement between them [67]. Taking all contributions to the trigger condition into account leads to an error of between 0.5 to 1.2% on the high y cross sections.

Electron Track-Vertex Efficiency Uncertainty: In the NC analysis the efficiency for reconstructing a track associated to the scattered lepton and for reconstructing the interaction vertex are determined simultaneously. The efficiency measurement is performed using a control selection of clean NC events with $45 < E - P_z < 65\,\mathrm{GeV}$ and additional topological algorithms are employed to remove non-ep and QED Compton backgrounds. Three algorithms are used to determine the interaction vertex and the MC and data are compared in the efficiency for each contributing algorithm. The kinematic dependence for the efficiency of each algorithm is well reproduced by the simulation after the application of a single small adjustment to the MC of -0.3%. The combined efficiency in the NC *nominal* analysis is found to be 99.5% in the data [67]. The residual differences between data and simulation define the uncorrelated systematic uncertainty which is 0.2% for $\theta_e > 50^\circ$ and 1% for $\theta_e \leq 50^\circ$ and is considered to be uncorrelated since a number of different vertex reconstruction algorithms are employed. In the *high y* analysis the efficiency is checked using a sample of QED Compton events which is limited in statistical precision and a 1% uncertainty is adopted [67].

Electron Charge Identification Efficiency Uncertainty: In the NC *high y* analysis the efficiency for correct charge identification of the scattered lepton is measured in the region $15 < E'_e < 25\,\mathrm{GeV}$. The simulation describes efficiency of the data with an overall difference of 0.5%, and no significant time dependence. Therefore the measured cross section is corrected for this difference by increasing the measured values by $2 \times 0.5\%$ and a final uncertainty of $2 \times 0.25\%$ is used. The factor of two accounts for the fact that charge mis-identification has a dual influence on the measurement by causing a loss of signal events and also an increase of the subtracted background [67].

Electron Identification Uncertainty: A calorimetric algorithm based on longitudinal and transverse shower shape quantities is used to identify electrons in the NC analysis. The efficiency of this selection can be estimated using a simple track based electron finder which searches for an isolated high p_T track associated to an electromagnetic energy deposition. The efficiency is measured in the *high y* and *nominal* analysis regions and is found to be well described by the simulation and shows little time variation. Thus the complete

HERA II data sample is combined to estimate the efficiency at large z_{imp} in order to reduce statistical fluctuations. The efficiency is found to be 98.6% overall and is described by the MC to within 0.2% for $z_{\mathrm{imp}} < 20\,\mathrm{cm}$ and 1.0% for $z_{\mathrm{imp}} > 20\,\mathrm{cm}$ [67].

Background Subtraction Uncertainty: In the CC and the NC *nominal* analysis the photoproduction background is estimated from simulation and a 30% uncertainty on the subtracted photoproduction background is assigned. A background dominated control sample is used to determine the size of this uncertainty. For both analyses the control samples consist of events passing the complete CC or *nominal* NC analysis selections in addition to the requirement of an energetic electron observed upstream in the electron tagger. Such events arise from photoproduction interactions in which the HFS observed in the main detector gives rise to a fake electron signature or fake missing transverse momentum in the NC and CC analyses respectively. Due to the restricted acceptance of the electron tagger the background samples have limited statistical precision but simulation provides a reasonable description of the data within the estimated uncertainty. For the CC analysis the region of $V_{ap}/V_p > 0.3$ is exclusively populated by photoproduction background. The data distribution is well described in shape and normalisation within the quoted uncertainty. In the *high y* analysis, simulation is not used to estimate the background contribution, nevertheless the tagged sample electron energy spectrum is well described in shape by the simulation within an overall normalisation uncertainty of 30%. This source results in a correlated systematic error of typically $\lesssim 1\%$ for the NC *nominal* analysis and CC cross sections.

In the CC analysis a background contribution of NC events arises in which the scattered lepton is poorly measured in the detector close to uninstrumented regions. Such contributions are suppressed by a set of topological algorithms to identify such events. The algorithms search for single isolated CTD tracks not recognised as from the scattered electron and opposite to the HFS [72], or search for low energy electromagnetic clusters associated to a CTD track with low calorimetric activity around the cluster and well separated from the remaining HFS [64]. These background contributions are well simulated and subtracted using simulation. A 10% uncertainty on the amount subtracted is considered.

NC *high y* Background Subtraction Uncertainty: In the NC *high y* analysis the photoproduction background is estimated from wrongly charged fake lepton candidates directly from the data as described in section 5.3. The asymmetry in the charge of fake leptons is measured to be $N^-/N^+ = 1.03 \pm 0.05$ where N^- is the number of fake e^- candidates and N^+ is the number of fake e^+ candidates. The ratio is measured independently for L and R data samples and also for two different energy regions of the fake lepton. All results are consistent within the large statistical uncertainties and are combined. The resulting uncertainty on the measured cross sections is found to be less than 1% [67].

CC Trigger Efficiency Uncertainty: For the CC analysis the efficiency is determined using the *pseudo CC* data samples and the CC simulation is corrected in each x, Q^2 measurement bin. In an alternative approach the efficiency is measured and parameterised as a function of P_T^{miss} and γ_h determined using calorimetric information only to mimic the trigger algorithms; the resulting differences agree within 15% of the inefficiency which is taken as the systematic uncertainty. Whilst the *pseudo CC* sample benefits from the excellent kinematic resolution from the suppressed electron and high statistics from the large NC cross section, at high Q^2 approaching the EW scale (where the efficiency is close to 100%) the NC and CC cross sections are of similar magnitude and therefore the *pseudo CC* sample has similar statistical uncertainty as the CC sample itself. Thus for $P_T^{\rm miss} > 25\,{\rm GeV}$ the complete HERA II data are combined to estimate the efficiency in this region after first checking for consistency between the periods. An uncertainty of 0.2% is included to accommodate any remaining influence from the lack of statistical precision.

CC Vertex Efficiency Uncertainty: The CC vertex finding efficiency is estimated using the *pseudo CC* data and MC samples and is compared to the efficiency estimate from the CC simulation within the range $-35 < z_{\rm vtx} < +35\,{\rm cm}$ where $z_{\rm vtx}$ is the z position of the reconstructed event vertex. The comparison is performed for each data taking period to account for changing detector configurations. Small adjustment factors are applied to the CC simulation so that the efficiency agrees with the *pseudo CC* data samples. Residual differences between the simulation and the *pseudo CC* samples are used to determine the size of this uncertainty which is 1.5% for $y_h \geq 0.15$ and 3% for $y_h < 0.15$.

CC Background Finder Uncertainty: The use of topological and timing algorithms in the CC analysis to suppress non-ep interactions can lead to a signal inefficiency. The *pseudo CC* data yield a lower efficiency than the simulation by $\approx 2 - 3\%$ [64]. The simulation is therefore weighted to provide a better description. After the adjustment all samples agree to within 1% for $y_h \geq 0.08$ and 2% for $y_h < 0.08$.

CC V_{ap}/V_p Background Rejection Uncertainty: The correlated error due to the uncertainty of the efficiency of the anti-photoproduction cut in the CC analysis is estimated by varying the quantity V_{ap}/V_p by ± 0.02 in the simulation. The size of the variation is determined by comparing different methods to calculate V_{ap}/V_p, e.g. using individual calorimeter cells or hadronic clusters, as well as using Monte Carlo samples with different hadronisation models (CDM versus MEPS) which affect the shape of the V_{ap}/V_p distribution [64]. This leads to a maximum error at low $P_{T,h}$ of up to 6% in the single differential cross section ${\rm d}^2\sigma_{CC}/{\rm d}x{\rm d}Q^2$. This is the dominant contribution to the correlated uncertainty of the CC double differential cross section for $x \leq 0.032$.

QED Radiative Corrections Uncertainty: An error on the NC and CC cross sections originating from the QED radiative corrections is taken into account. This is determined by comparing the predicted radiative corrections from the programs HERACLES (as implemented in DJANGOH), HECTOR, and EPRC [73]. The radiative corrections due to the exchange of two or more photons between the lepton and the quark lines, which are not included in DJANGOH, vary with the polarity of the lepton beam. This variation (estimated using EPRC) is expected to be small compared to the quoted errors and is neglected [67].

Acceptance Correction Uncertainty: The MC simulation is used to determine acceptance corrections to the data and relies on a specific choice of PDF. Changing the PDF used influences the acceptance which for NC $e^{\pm}p$ and CC e^-p changes by 0.2% for $Q^2 < 5\,000\,{\rm GeV}^2$, and by 1.0% for $Q^2 > 5\,000\,{\rm GeV}^2$. For CC e^+p the changes are 0.5% for $Q^2 < 5\,000\,{\rm GeV}^2$ and 3.0% for $Q^2 > 5\,000\,{\rm GeV}^2$.

Polarisation Uncertainty: The independent polarisation measurements from the TPOL and LPOL have a relative uncertainty $\delta P/P = 1.9\%$ and 2.0% respectively. In general the polarimeter measurements agree to within 1.5% although variations with time are observed and folded into the final quoted polarisation uncertainties on the measured cross sections presented here. In three run periods the disagreement rises to $5 - 10\%$ affecting approximately $16\,\mathrm{pb}^{-1}$ of the luminosity. In these periods the uncertainty is enlarged [43].

Luminosity Uncertainty: The luminosity is measured using elastic QED Compton events [39] with an uncertainty of 2.3%, of which 1.1% is from the uncertainty in the theoretical calculation of the elastic QED Compton process. In addition, there is a 1.5% normalisation uncertainty on each data taking period, originating from time-dependent corrections when extrapolating the QED Compton analysis to smaller datasets.

In summary the typical total systematic error is substantially reduced compared to previous H1 publications [1–4] to about 1.5% for the NC double differential cross sections, and 4% for the CC double differential cross sections. For the $\mathrm{d}\sigma_{\mathrm{NC(CC)}}/\mathrm{d}Q^2$ measurements, the error is typically 1.3% (NC) and 3% (CC). This reduction is achieved through a better understanding of the response of the detector and in particular for the hadronic and EM calibrations, as well as the reconstruction of polar angles. Further detailed studies also allow reductions in the systematic uncertainties of the electron identification and the trigger efficiency.

6 QCD Analysis

To assess the impact of the H1 NC and CC cross sections at high Q^2 measured with the longitudinally polarised lepton beams on the determination of PDFs, a new QCD analysis (H1PDF 2012) is performed. In addition to the new HERA II data presented here, the previously published unpolarised HERA I data at high Q^2 [1–3] and at low Q^2 [75], as well as the H1 measurements at lower proton beam energies [75] are used, as shown in table 3. This analysis supersedes the previous H1PDF 2009 fit [7].

6.1 Analysis Framework and Settings

The present QCD analysis uses the HERAFITTER framework [7, 17], an open source software package based on the QCD evolution code QCDNUM (v17.04) [76].

The fit strategy follows closely the one adopted for the determination of the HERAPDF1.0 sets [17]. The QCD predictions for the differential cross sections are obtained by solving the DGLAP evolution equations [77–81] at NLO in the $\overline{\mathrm{MS}}$ scheme with the renormalisation and factorisation scales chosen to be Q. The heavy quark coefficient functions are calculated in the RT general-mass variable-flavour-number scheme [82]. The result is cross checked against the ACOT scheme variant [83] that takes full account of quark masses. The heavy quark masses for charm, $m_c = 1.4\,\mathrm{GeV}$ and beauty, $m_b = 4.75\,\mathrm{GeV}$ are chosen following [84]. The strong coupling constant is fixed to $\alpha_s(M_Z^2) = 0.1176$ [85], as used for the HERAPDF1.0 NLO sets.

Data set	$x_{\min}$	$x_{\max}$	$Q^2_{\min}$ (GeV^2)	$Q^2_{\max}$ (GeV^2)	$\delta\mathcal{L}$ (%)	Ref.	Comment
e^+ Combined low Q^2	0.00004	0.20	0.5	150	0.5	[75]	$\sqrt{s} = 301, 319$ GeV
e^+ Combined low E_p	0.00003	0.003	1.5	90	0.5	[75]	$\sqrt{s} = 225, 252$ GeV
e^+ NC 94-97	0.0032	0.65	150	30 000	$0.5 \oplus 1.4$	[1]	$\sqrt{s} = 301$ GeV
e^+ CC 94-97	0.013	0.40	300	15 000			
e^- NC 98-99	0.0032	0.65	150	30 000	$0.5 \oplus 1.7$	[2]	$\sqrt{s} = 319$ GeV
e^- CC 98-99	0.013	0.40	300	15 000			
e^- NC 98-99 *high y*	0.00131	0.0105	100	800		[3]	$\sqrt{s} = 319$ GeV
e^- NC 99-00	0.0032	0.65	150	30 000	$0.5 \oplus 1.4$		$\sqrt{s} = 319$ GeV; incl. *high y*
e^+ CC 99-00	0.013	0.40	300	15 000			$\sqrt{s} = 319$ GeV
e^+ NC *high y*	0.0008	0.0105	60	800	$2.3 \oplus 1.0 \oplus 1.1$		$\sqrt{s} = 319$ GeV
e^- NC *high y*	0.0008	0.0105	60	800	$2.3 \oplus 1.2 \oplus 0.8$		$\sqrt{s} = 319$ GeV
e^+ NC L	0.002	0.65	120	30 000	$2.3 \oplus 1.5$		$\sqrt{s} = 319$ GeV
e^+ CC L	0.008	0.40	300	15 000			
e^+ NC R	0.002	0.65	120	30 000	$2.3 \oplus 1.5$		
e^+ CC R	0.008	0.40	300	15 000			
e^- NC L	0.002	0.65	120	50 000	$2.3 \oplus 1.5$		$\sqrt{s} = 319$ GeV
e^- CC L	0.008	0.40	300	30 000			
e^- NC R	0.002	0.65	120	30 000	$2.3 \oplus 1.5$		
e^- CC R	0.008	0.40	300	15 000			

Table 3: Table of data sets used in the QCD fit. The normalisation uncertainties of each data set ($\delta\mathcal{L}$) are given as well as the kinematic ranges in x and Q^2. When there are two uncertainties shown, the first one corresponds to the correlated error across the data sets and the second one is the uncertainty of the relevant data sets. The second and third uncertainties of the NC *high y* analyses represent the corresponding uncertainties of the L and R data sets, respectively.

The χ^2 function which is minimised using the MINUIT package [86] is defined similarly to [17] as

$$\chi^2 = \sum_i \frac{\left[\mu_i - m_i\left(1 - \sum_j \gamma^i_j b_j\right)\right]^2}{\delta^2_{i,\mathrm{unc}} m_i^2 + \delta^2_{i,\mathrm{stat}} \mu_i m_i \left(1 - \sum_j \gamma^i_j b_j\right)} + \sum_j b_j^2 + \sum_i \ln \frac{\delta^2_{i,\mathrm{unc}} m_i^2 + \delta^2_{i,\mathrm{stat}} \mu_i m_i}{\delta^2_{i,\mathrm{unc}} \mu_i^2 + \delta^2_{i,\mathrm{stat}} \mu_i^2}, \quad (21)$$

where m_i is the theoretical prediction and μ_i is the measured cross section at point i, (Q^2, x, s) with the relative statistical and uncorrelated systematic uncertainty $\delta_{i,\mathrm{stat}}$, $\delta_{i,\mathrm{unc}}$, respectively. The above χ^2 definition takes into account that the quoted uncertainties are based on measured cross sections, which are subject to statistical fluctuations. Therefore one needs to correct for possible biases by using the expected instead of the observed number of events with the corresponding errors scaled accordingly. The correlations between data points caused by systematic uncertainties are also taken into account in the fit via the χ^2 definition, with γ^i_j denoting the relative correlated systematic uncertainties and b_j their shifts with a penalty term $\sum_j b_j^2$ added. A $\ln$ term is introduced in addition which arises from the likelihood transition to χ^2 when the scaling of the errors is applied.

The systematic uncertainties for the polarised measurements of the high Q^2 HERA II NC *nominal* and *high y* and CC cross sections are described in detail in section 5.6. The correlations among the uncertainty sources across the data sets are summarised in table 4. The new measurements reported here have a common normalisation uncertainty of 2.3% originating from the luminosity measurement based on the QED Compton analysis ($\delta^{\mathcal{L}5}$ in table 4). Each data set has an additional uncorrelated normalisation uncertainty of 1.5% ($\delta^{\mathcal{L}6} - \delta^{\mathcal{L}9}$ in table 4). The uncertainty is correlated for all measurement points within the data set. The uncorrelated normalisation uncertainty for the unpolarised HERA II NC *high y* data is a luminosity weighted average of the left and right handed polarised periods. The combined low Q^2 data set has 47 sources of uncertainty which are assumed to be uncorrelated with those of the high Q^2 data sets and are not listed in table 4 but are described in [75]. The only exception is the common normalisation uncertainty of 0.5% arising from the theoretical uncertainty in the Bethe-Heitler cross section. This is considered to be correlated with all HERA I data sets ($\delta^{\mathcal{L}1}$ in table 4). The combined data with low proton beam energies has nine sources of correlated systematic uncertainty that are treated independently from all other sources except for $\delta^{\mathcal{L}1}$.

For the polarised HERA II data there is an additional source of uncertainty arising from the polarisation measurement as described in section 5.6. This affects the construction of the theoretical differential cross sections and it is accounted for in the QCD fit procedure by allowing the polarisation to vary within its uncertainties as follows:

$$P_e^i = P_e^i \cdot (1 \pm \delta^{Pi}) \;\text{ with }\; \delta^{Pi} = \delta^i_{\text{unc}} \cdot b^i_{\text{unc}} \oplus \gamma^i_{\text{TPOL}} \cdot b_{\text{TPOL}} \oplus \gamma^i_{\text{LPOL}} \cdot b_{\text{LPOL}}, \tag{22}$$

with index i representing the four different data running periods ($\delta^{P1} - \delta^{P4}$ in table 4). The values for δ_{unc}, γ_{TPOL}, and γ_{LPOL} are listed in table 5. They correspond to the uncorrelated uncertainties and to the two uncertainties for the polarisation determination method (LPOL, TPOL) which are correlated across different data sets. Note that the uncorrelated uncertainties δ_{unc} are still correlated for measurements within a data set. The free parameters b^i_{unc}, b_{TPOL} and b_{LPOL} are free parameters of the QCD fit.

The HERA data have a minimum invariant mass of the hadronic system, W, of $15\,\text{GeV}$ and a maximum x of 0.65, such that they are in a kinematic region where there is no sensitivity to target mass effects and large-x higher-twist contributions. A minimum Q^2 cut of $Q^2_{\text{min}} = 3.5\,\text{GeV}^2$ is imposed to remain in the kinematic region where perturbative QCD should be applicable.

6.2 Parameterisations

Fits to determine PDFs require an ansatz for the parametrisation as a function of x at the starting scale Q_0^2 of the evolution, here chosen to be $1.9\ \text{GeV}^2$, below the charm threshold. The parametrised PDFs are chosen to be the valence quark distributions xu_v, xd_v, the u-type and d-type anti-quark distributions $x\overline{U}$ and $x\overline{D}$ and the gluon distribution $xg(x)$, according to the sensitivity of the H1 data to the PDFs. The following functional forms are considered:

$$xf(x) = A_f x^{B_f} (1-x)^{C_f} (1 + D_f x + E_f x^2)\,, \tag{23}$$

$$xg(x) = A_g x^{B_g} (1-x)^{C_g} (1 + D_g x + E_g x^2) - A'_g x^{B'_g} (1-x)^{C'_g}\,, \tag{24}$$

where the A to E are the parameters of the fit specified below. The parametric form for the gluon allows extra flexibility in the low x region, and C'_g is set to 25 to suppress the negative contribution at high x. Relaxing the parameter C'_g does not cause significant changes to the fit results.

Data set	$\delta^{\mathcal{L}}$		δ^{E}	δ^{θ}	δ^{h}	δ^{N}	δ^{B}	δ^{V}	δ^{S}	δ^{pol}
e^+ Combined low Q^2	$\delta^{\mathcal{L}1}$									
e^+ Combined low E_p	$\delta^{\mathcal{L}1}$									
e^+ NC 94-97	$\delta^{\mathcal{L}1}$	$\delta^{\mathcal{L}2}$	δ^{E1}	$\delta^{\theta 1}$	δ^{h1}	δ^{N1}	δ^{B1}	–	–	–
e^+ CC 94-97	$\delta^{\mathcal{L}1}$	$\delta^{\mathcal{L}2}$	–	–	δ^{h1}	δ^{N1}	δ^{B1}	δ^{V1}	–	–
e^- NC 98-99	$\delta^{\mathcal{L}1}$	$\delta^{\mathcal{L}3}$	δ^{E1}	$\delta^{\theta 2}$	δ^{h1}	δ^{N1}	δ^{B1}	–	–	–
e^- NC 98-99 *high* y	$\delta^{\mathcal{L}1}$	$\delta^{\mathcal{L}3}$	δ^{E1}	$\delta^{\theta 2}$	δ^{h1}	δ^{N1}	–	–	δ^{S1}	–
e^- CC 98-99	$\delta^{\mathcal{L}1}$	$\delta^{\mathcal{L}3}$	–	–	δ^{h1}	δ^{N1}	δ^{B1}	δ^{V2}	–	–
e^+ NC 99-00	$\delta^{\mathcal{L}1}$	$\delta^{\mathcal{L}4}$	δ^{E1}	$\delta^{\theta 2}$	δ^{h1}	δ^{N1}	δ^{B1}	–	δ^{S1}	–
e^+ CC 99-00	$\delta^{\mathcal{L}1}$	$\delta^{\mathcal{L}4}$	–	–	δ^{h1}	δ^{N1}	δ^{B1}	δ^{V2}	–	–
e^+ NC *high* y	$\delta^{\mathcal{L}5}$	$\delta^{\mathcal{L}6}$, $\delta^{\mathcal{L}7}$	δ^{E2}	$\delta^{\theta 3}$	δ^{h2}	δ^{N2}	–	–	δ^{S2}	–
e^- NC *high* y	$\delta^{\mathcal{L}5}$	$\delta^{\mathcal{L}8}$, $\delta^{\mathcal{L}9}$	δ^{E2}	$\delta^{\theta 3}$	δ^{h2}	δ^{N2}	–	–	δ^{S2}	–
e^+ NC L	$\delta^{\mathcal{L}5}$	$\delta^{\mathcal{L}6}$	δ^{E2}	$\delta^{\theta 3}$	δ^{h2}	δ^{N2}	δ^{B1}	–	–	δ^{P1}
e^+ CC L	$\delta^{\mathcal{L}5}$	$\delta^{\mathcal{L}6}$	–	–	δ^{h2}	δ^{N3}	δ^{B1}	δ^{V3}	–	δ^{P1}
e^+ NC R	$\delta^{\mathcal{L}5}$	$\delta^{\mathcal{L}7}$	δ^{E2}	$\delta^{\theta 3}$	δ^{h2}	δ^{N2}	δ^{B1}	–	–	δ^{P2}
e^+ CC R	$\delta^{\mathcal{L}5}$	$\delta^{\mathcal{L}7}$	–	–	δ^{h2}	δ^{N3}	δ^{B1}	δ^{V3}	–	δ^{P2}
e^- NC L	$\delta^{\mathcal{L}5}$	$\delta^{\mathcal{L}8}$	δ^{E2}	$\delta^{\theta 3}$	δ^{h2}	δ^{N2}	δ^{B1}	–	–	δ^{P3}
e^- CC L	$\delta^{\mathcal{L}5}$	$\delta^{\mathcal{L}8}$	–	–	δ^{h2}	δ^{N3}	δ^{B1}	δ^{V3}	–	δ^{P3}
e^- NC R	$\delta^{\mathcal{L}5}$	$\delta^{\mathcal{L}9}$	δ^{E2}	$\delta^{\theta 3}$	δ^{h2}	δ^{N2}	δ^{B1}	–	–	δ^{P4}
e^- CC R	$\delta^{\mathcal{L}5}$	$\delta^{\mathcal{L}9}$	–	–	δ^{h2}	δ^{N3}	δ^{B1}	δ^{V3}	–	δ^{P4}

Table 4: Correlation of systematic error sources across different data sets. For each of the nine correlated systematic error sources one or more parameters are included in the fit procedure. The sources considered are due to the luminosity uncertainty ($\delta^{\mathcal{L}}$), the electron energy uncertainty (δ^{E}), the electron polar angle measurement (δ^{θ}), the hadronic energy uncertainty (δ^{h}), the uncertainty due to noise subtraction (δ^{N}), the background subtraction error (δ^{B}), the uncertainty in measurement of the ratio V_{ap}/V_p (δ^{V}), the error of the background charge asymmetry (δ^{S}), and the error of the polarisation measurement (δ^{pol}). The table entries indicate the correlation of the error sources across the data sets where each numerical index corresponds to a fit parameter for the given error source. For example, the uncertainty due to the noise subtraction is the same for all data sets in HERA I leading to one common parameter in the fit (δ^{N1}), whereas the V_{ap}/V_p uncertainty has two independently varying parameters (δ^{V1} and δ^{V2}) for the CC HERA I data sets.

δ^{Pi} (Period)	$\delta_{\rm unc}$ (%)	$\gamma_{\rm LPOL}$ (%)	$\gamma_{\rm TPOL}$ (%)
δ^{P1} (e^+L)	1.7	0.34	0.36
δ^{P2} (e^+R)	2.0	0.48	0.37
δ^{P3} (e^-L)	2.6	0.59	0.53
δ^{P4} (e^-R)	2.7	0.55	0.58

Table 5: Uncorrelated and correlated uncertainties of the polarisation measurement for each HERA II running period.

The normalisation parameters, A_{u_v} and A_{d_v}, are constrained by the quark number sum rules and A_g by the momentum sum rule. Since the H1 data have little sensitivity to the light sea flavour decomposition, additional assumptions are imposed. The strange quark distribution is expressed as an x-independent fraction, f_s, of the d-type sea, $f_s = x\overline{s}/x\overline{D}$, at the starting scale, with $f_s = 0.31$ as preferred by neutrino-induced di-muon production [87]. The B parameters $B_{\overline{U}}$ and $B_{\overline{D}}$, responsible for the shape at low x, are set equal, such that there is a single B parameter for the sea distributions. The constraint $A_{\overline{U}} = A_{\overline{D}}(1 - f_s)$ is applied to ensure that $x\overline{u} \to x\overline{d}$ as $x \to 0$.

The optimal parametrisation is found through a scanning procedure which iteratively adds parameters according to the data precision and PDF sensitivity. Starting with a basic parametric form with 9 parameters and all D and E parameters set to zero and without the negative gluon term, a series of 10 parameter fits are performed with all combinations of one extra parameter except for the negative gluon term where two extra parameters are added. The fit resulting in the lowest χ^2 is then chosen as the best 10 parameter fit. The process is continued adding one extra parameter till no significant improvement in χ^2 is obtained. This results in a best fit with 13 parameters which is taken as the central fit. No further significant χ^2 reduction is achieved with 14 parameters.

Due to more precise data from HERA II an enhanced flexibility is allowed for the valence quark parameterisations compared to the H1PDF 2009 fit, with $E_{u_v} \neq 0$ and independent parameters B for the up and down valence quark distributions. The resulting parameterisations at the starting scale Q_0^2 are

$$
\begin{aligned}
xg(x) &= A_g x^{B_g}(1-x)^{C_g} - A'_g x^{B'_g}(1-x)^{25}\,, && (25)\\
xu_v(x) &= A_{u_v} x^{B_{u_v}}(1-x)^{C_{u_v}}\left(1 + E_{u_v}x^2\right)\,, && (26)\\
xd_v(x) &= A_{d_v} x^{B_{d_v}}(1-x)^{C_{d_v}}\,, && (27)\\
x\overline{U}(x) &= A_{\overline{U}} x^{B_{\overline{U}}}(1-x)^{C_{\overline{U}}}\,, && (28)\\
x\overline{D}(x) &= A_{\overline{D}} x^{B_{\overline{D}}}(1-x)^{C_{\overline{D}}}\,. && (29)
\end{aligned}
$$

The uncertainties in the PDF determinations arise from experimental uncertainties as well as from assumptions in the QCD analysis. The PDF experimental uncertainties are estimated using a Monte Carlo technique [88]. The method consists of preparing N replica data sets in which the central values of the cross sections fluctuate within their statistical and systematic uncertainties taking into account all point-to-point correlations. The preparation of the data is repeated $N \simeq 400$ times and for all these replicas complete NLO QCD fits are performed to extract 400 different PDF sets. The one standard deviation band of the experimental PDF uncertainties is estimated using the root-mean-squared of the PDF sets obtained for the replicas. The band is then attributed to the central fit resulting in an asymmetric uncertainty, as the central fit does not necessarily coincide with the mean of the N replicas.

Parametrisation uncertainties correspond to the set of 14 parameter fits considered in the χ^2 optimisation (compared to the 13 parameter central value fit) and to the variations of the starting scale Q_0^2. The uncertainties are constructed as an envelope built from the maximal deviation at each x value from the central fit. The variations of Q_0^2 mostly increase the PDF uncertainties of the sea and gluon at small x.

Model uncertainties are evaluated by varying the input assumptions and follow the variations adopted in HERAPDF1.0 [17]. The variation of input values chosen for the central fit is specified in table 6. The strange quark fraction is varied between 0.23 and 0.38 [19]. However, recent results from the ATLAS collaboration [89] hint at an unsuppressed strange quark sea distribution with $f_s = 0.5$ that exceeds the variation range for f_s, as given above. This value of f_s is also studied.

The difference between the central fit and the fits corresponding to model variations of f_s, $Q^2_{\rm min}$, the charm quark mass m_c and the beauty quark mass m_b are added in quadrature, separately for positive and negative deviations, and represent the model uncertainty of the H1PDF 2012 fit.

Parameter	Central Value	Lower Limit	Upper Limit
f_s	0.31	0.23	0.38
m_c (GeV)	1.4	1.35 (for $Q_0^2 = 1.8$ GeV)	1.65
m_b (GeV)	4.75	4.3	5.0
$Q^2_{\rm min}$ (GeV^2)	3.5	2.5	5.0
Q_0^2 (GeV^2)	1.9	1.5 ($f_s = 0.29$)	2.5 ($m_c = 1.6$, $f_s = 0.34$)

Table 6: Central values of input parameters to the QCD fit and their variations.

The total PDF uncertainty is obtained by adding in quadrature the experimental, model and parametrisation uncertainties.

7 Results

7.1 NC and CC Double Differential Cross Sections

7.1.1 Measurements with Polarised Lepton Beams

The reduced cross sections $\tilde{\sigma}_{\rm NC,CC}(x, Q^2)$ measured in the kinematic range $120 \leq Q^2 \leq 50\,000$ GeV^2 and $0.002 \leq x \leq 0.65$ for NC, and $300 \leq Q^2 \leq 30\,000$ GeV^2 and $0.008 \leq x \leq 0.4$ for CC are shown in figures 8-11 and given in tables 13-20. The NC cross sections corresponding to the left and right handed polarised lepton beams $e^{\pm}$ (figures 8 and 9) are found to agree at low Q^2 ($\lesssim 1\,000\,\mathrm{GeV}^2$). At higher Q^2 and at high y, deviations are observed between the measured cross sections of the L and R data sets as expected from the parity violation of Z boson exchange at high Q^2. The CC reduced cross sections for the L and R data sets are very different for all Q^2 (figures 10 and 11) as parity violation is maximal with W boson exchange. These cross sections agree well with the H1PDF 2012 fit, which is also shown. Both the statistical and systematic precision have substantially improved with respect to the corresponding measurements from HERA I with the unpolarised lepton beams.

The NC reduced cross sections for $e^{\pm}p$ collisions in the phase-space of $0.19 < y < 0.63$ and $90 \leq Q^2 \leq 800\,\mathrm{GeV}^2$ are also measured in y and Q^2 bins for $P_e = 0$ by combining the left and right handed polarised data sets and correcting for small residual polarisation effects. These cross sections are presented in tables 21 and 22. However, these cross sections are redundant with those presented in tables 13-16 and therefore they should not be used together in a fit.

The *high y* measurement is restricted to the Q^2 range $60 \leq Q^2 \leq 800\,\mathrm{GeV}^2$ where the sensitivity to the beam polarisation is small. Therefore the left and right handed polarised data sets are combined for the measurements shown in figure 12 and given in tables 23 and 24. Within the experimental uncertainties, the two sets of measurements are in agreement. The *high y* data are also well described by H1PDF 2012. The error bands correspond to the total uncertainty of the fit. The asymmetry of the uncertainty is due to the effect of the assumptions and the experimental uncertainty of the QCD analysis, as described in section 6.1.

The L and R data sets are combined accounting for the small residual polarisation to provide unpolarised ($P_e = 0$) cross section measurements presented in tables 25-28. These are then used in the combination with HERA I measurements. It should be noted that these tables are given for completeness and they should not be used in any fit together with the corresponding polarised cross sections, as they are redundant.

7.1.2 Combination with Previous H1 Measurements

The new unpolarised HERA II cross section measurements are combined with previously published unpolarised H1 measurements from HERA I [1–3]. The combination is performed taking into account correlated systematic uncertainties represented as nuisance parameters [5,90]. The correlation of uncertainties across different data sets is given in table 4 and follows the prescription given in [3]. The HERA II systematic uncertainties are in general considered uncorrelated with those from HERA I apart from the photoproduction background uncertainty. This assumption is motivated by improvements in the calibration procedures which lead to better determined central values for the HERA II result. This approach leads to a conservative estimate of the uncertainties for the combined sample. In the years $1994 - 1997$ the data were taken at the lower centre of mass energy of $\sqrt{s} = 301\,\mathrm{GeV}$ whilst the other data samples are taken at $\sqrt{s} = 319\,\mathrm{GeV}$. To take this into account the data at $\sqrt{s} = 301\,\mathrm{GeV}$ are corrected to $\sqrt{s} = 319\,\mathrm{GeV}$ using the H1PDF 2012 parametrisation. This correction and the combination are only performed for data points at $y < 0.35$ as at larger y the contribution of the longitudinal structure F_L is sizable, and therefore the uncertainty of this correction is minimised. The correction is typically $0.5 - 2.5\%$ for $y < 0.35$ and never more than 3.8%.

A total of 854 data points are averaged to 413 cross section measurements. The data show good consistency with a total χ^2 per degree of freedom (ndf) of $\chi^2/\mathrm{ndf} = 412.1/441$. Out of

Source	Shift in units of standard deviation	Shift in % of cross section
$\delta^{\mathcal{L}1}$ (BH Theory)	-0.39	-0.19
$\delta^{\mathcal{L}2}$ (e^+ 94-97)	-0.46	-0.66
$\delta^{\mathcal{L}3}$ (e^- 98-99)	-0.69	-1.20
$\delta^{\mathcal{L}4}$ (e^+ 99-00)	-0.07	-0.10
$\delta^{\mathcal{L}5}$ (QEDC)	0.81	1.70
$\delta^{\mathcal{L}6}, \delta^{\mathcal{L}7}$ (e^+L+R)	0.84	0.80
$\delta^{\mathcal{L}8}, \delta^{\mathcal{L}9}$ (e^-L+R)	0.84	0.89

Table 7: Shifts of the normalisation parameters $\delta^{\mathcal{L}}$ (see table 4) both for the luminosity measurements of HERA I (BH Theory) and HERA II (QEDC) and for the individual normalisation of each data set after combination of HERA I and HERA II measurements. The shifts are expressed in units of standard deviations of the parameters as well as the fractional change in the cross sections.

22 nuisance parameters corresponding to the correlated systematic error sources none develop a significant deviation from zero. The values of the nuisance parameters for the global normalisations are given in table 7 which represents the values as fractions of the normalisation uncertainty and as absolute shifts in per cent. The adjustments of the relative normalisations are small. The normalisation of the data collected in the years $1999 - 2000$ stays constant and the other HERA I data samples shift down by maximally 1.2%, while the HERA II samples shift up by maximally 1.7%.

The combined HERA I+II NC and CC cross sections are shown in figures 13-16 and given in tables 29-32. The H1PDF 2012 fit is found to give a good description of the x, Q^2 behaviour of the data. The NC data exhibits a strong rise with decreasing x which can be interpreted as being due to the high density of low x quarks in the proton. The e^-p data are in good agreement with the e^+p measurements for $Q^2 \lesssim 1\,000\,\mathrm{GeV}^2$. At larger values of Q^2 the e^-p data are generally higher than the e^+p data, as is expected from the effects of Z boson exchange. The difference is used to extract the $xF_3^{\gamma Z}$ structure function as described in section 7.5.

In figures 15 and 16, the quark contributions from $x(u+c)$ and $(1-y)^2 x(d+s)$ are indicated for e^-p and e^+p data, respectively, illustrating that the CC data can be used to separate the up- and down-type quark distributions in the proton.

7.2 Fit Results

The data in the full phase space are well described by the fit with a χ^2 per degree of freedom $1569.6/1461$. The central fit satisfies the criteria that structure functions are positive and $xd_v > x\overline{d}$ at large x. The PDF parameters obtained from the QCD analysis are presented in table 8. Since the measured polarisation values are allowed to vary in the fit procedure within their uncertainties, the corresponding shift parameters are minimised together with the PDF parameters and are shown in table 9. They are found to have little correlation with the PDF parameters.

Parameter	Central value
B_g	0.020
C_g	6.4
A'_g	0.30
B'_g	-0.27
B_{u_v}	0.70
C_{u_v}	4.9
E_{u_v}	12
B_{d_v}	0.97
C_{d_v}	5.2
$C_{\bar{U}}$	3.4
$A_{\bar{D}}$	0.17
$B_{\bar{D}}$	-0.15
$C_{\bar{D}}$	9.7

Table 8: Parameters of the central fit.

Parameter	Central value
$b_{\rm unc}^{1(e^+pL)}$	0.16
$b_{\rm unc}^{2(e^+pR)}$	0.19
$b_{\rm unc}^{3(e^-pL)}$	-0.32
$b_{\rm unc}^{4(e^-pR)}$	0.50
$b_{\rm TPOL}$	0.11
$b_{\rm LPOL}$	0.11

Table 9: Parameters corresponding to the polarisation shifts.

Table 10 summarises the partial χ^2 values corresponding to both the statistical and uncorrelated systematic uncertainties for each data set used in the fit. The total correlated χ^2 value (not included in the table) amounts to 67.4 units. The systematic shifts allowed by the Hessian method to account for the correlations are generally small (less than one standard deviation). Table 11 presents the optimised normalisation shifts obtained by the fit. The values are shown separately for each data period. The fit results in shifting the global normalisation of the HERA I data points by -0.7% and that of the HERA II data points by 2.9% corresponding to 1.3 standard devations. The shift values are consistent with those from the combination obtained in section 7.1.2 although the numerical values are different due to the additional low Q^2 and low E_p data sets used in the fit.

It has been observed previously that the heavy flavour scheme used here results in a rather large χ^2 value in fits for the low Q^2 data [75]. In this analysis, the corresponding partial χ^2 contributions are also large. The overall quality of the fit is improved if the ACOT scheme is used, due to a considerably better agreement with the low Q^2 data ($\simeq$ 30 units improvement in χ^2). For the high Q^2 measurements, however, which are the focus of this paper, using the ACOT scheme is slightly worse than using the RT prescription [82].

The H1PDF 2012 fit results are summarised in figures 17-19, shown at the starting scale $Q_0^2 =$

Data Set	Number of data points	χ^2 (unc. err.)
e^+ Combined low Q^2	171	196
e^+ Combined low E_p	124	132
e^+ NC 94-97	130	92
e^+ CC 94-97	25	22
e^- NC 98-99	126	113
e^- NC 98-99 *high* y	13	5.4
e^- CC 98-99	28	19
e^+ NC 99-00	147	144
e^+ CC 99-00	28	29
e^+ NC *high* y	11	5.6
e^- NC *high* y	11	7.7
e^+ NC L	137	124
e^+ CC L	28	46
e^+ NC R	138	138
e^+ CC R	29	40
e^- NC L	139	174
e^- CC L	29	27
e^- NC R	138	142
e^- CC R	28	16

Table 10: Results of the H1PDF 2012 fit. For each data set the number of data points are given, along with the χ^2 contribution determined using uncorrelated errors (unc. err.) of the data points.

Data Period	Global Normalisation	Per Period Normalisation	Total Normalisation
e^+ Combined low Q^2	0.993	–	0.993
e^+ Combined low E_p	0.993	–	0.993
HERA I e^+ 94-97	0.993	0.999	0.992
HERA I e^- 98-99	0.993	1.003	0.996
HERA I e^+ 99-00	0.993	1.005	0.998
HERA II e^+ L	1.029	0.991	1.020
HERA II e^+ R	1.029	1.013	1.042
HERA II e^- L	1.029	1.010	1.039
HERA II e^- R	1.029	1.014	1.043

Table 11: Factors corresponding to the global luminosity normalisations ($\mathcal{L}1$, $\mathcal{L}5$), the normalisation for each data period ($\mathcal{L}2$, $\mathcal{L}3$, $\mathcal{L}4$ for HERA I and $\mathcal{L}6$, $\mathcal{L}7$, $\mathcal{L}8$, $\mathcal{L}9$ for HERA II), and the overall combined normalisation of the data sets as determined by the QCD fit.

$1.9\,\mathrm{GeV}^2$, evolved to $Q^2 = 10\,\mathrm{GeV}^2$ and to $Q^2 = M_W^2$. The fit result when using $f_s = 0.5$ lies well within the uncertainty band of the H1PDF 2012 set.

The consistency of results is checked by comparing with PDF fits determined from the combined unpolarised HERA I and II measurements presented in section 7.1.2. The resulting PDFs and shifts of the correlated sources are in good agreement when using the separate data sets or when using the combined unpolarised data.

In order to assess the impact of the new HERA II data, the QCD fit is repeated under the same conditions with the new measurements excluded. For this comparison replica data sets are generated from the expected cross sections by using the corresponding experimental uncertainties, thereby resulting in symmetrical error bands. As shown in figure 20, the new high Q^2 data have a visible impact on all distributions, especially in the xD distribution.

7.3 NC and CC Cross Sections $\mathrm{d}\sigma/\mathrm{d}Q^2$

The single differential NC cross sections $\mathrm{d}\sigma_{\rm NC}/\mathrm{d}Q^2$ measured for $y < 0.9$ with both e^-p and e^+p data are shown in figure 21 (upper plots) and given in tables 33-36. The data are measured in the range $Q^2 \geq 200\,\mathrm{GeV}^2$ up to $50\,000\,\mathrm{GeV}^2$ over which the cross sections fall by more than six orders of magnitude with increasing Q^2. The cross sections are well described by the SM expectations based on the H1PDF 2012 fit. The lower panel of figure 21 shows the ratios of the measurements to the corresponding SM values determined from the H1PDF 2012 fit. The asymmetric uncertainty represents the effect of the assumptions and the experimental uncertainty of the QCD analysis and is explained in section 6.2. Note that in this lower figure the H1 data are scaled by the normalisation shifts imposed by the QCD fit given in table 11.

The Q^2 dependence of the CC cross sections $\mathrm{d}\sigma_{\rm CC}/\mathrm{d}Q^2$ for $y < 0.9$ is shown in figure 22. In the upper figure, the strong polarisation dependence is clearly visible. In the lower figure, the same normalisation shifts as for the NC data are applied. The CC cross sections together with the kinematic correction factors are given in tables 37-40.

Combining the left and right handed polarisation data sets and correcting for the residual polarisation effects, the resulting unpolarised NC and CC cross section measurements from HERA II are listed in tables 41-44. These cross sections are combined with the corresponding measurements from HERA I using the same procedure as for the combination of the double differential sections, described in section 7.1.2. The results are shown in tables 45-48.

The Q^2 dependence of the combined HERA I+II NC and CC cross sections for $P_e = 0$ is shown in figure 23. The NC cross sections exceed the CC cross sections at $Q^2 \simeq 200$ GeV^2 by more than two orders of magnitude. The steep decrease of the NC cross section with increasing Q^2 is due to the dominating photon exchange cross section which is proportional to $1/Q^4$. In contrast the CC cross section is proportional to $\left[M_W^2/(Q^2 + M_W^2)\right]^2$ and approaches a constant value at $Q^2 \simeq 300$ GeV^2. The NC and CC cross sections are of comparable size at $Q^2 \sim 10^4$ GeV^2, where the photon and Z exchange contributions to the NC process are of similar size to those of $W^{\pm}$ exchange to the CC process. These measurements thus illustrate the unified behaviour of the electromagnetic and the weak interactions in DIS.

7.4 NC Polarisation Asymmetry and $F_2^{\gamma Z}$

The SM predicts a difference in the NC cross section for leptons with different helicity states arising from the chiral structure of the neutral electroweak exchange. With longitudinally polarised lepton beams in HERA II such polarisation effects can be tested, providing a direct measure of electroweak effects in the NC cross sections. The polarisation asymmetry, $A^\pm$, is defined as

$$A^\pm = \frac{2}{P_L^\pm - P_R^\pm} \cdot \frac{\sigma^\pm(P_L^\pm) - \sigma^\pm(P_R^\pm)}{\sigma^\pm(P_L^\pm) + \sigma^\pm(P_R^\pm)} \ , \tag{30}$$

where $P_L^\pm$ and $P_R^\pm$ are the longitudinal lepton beam polarisation in the $e^\pm p$ R and L data sets. To a very good approximation $A^\pm$ measures the structure function ratio $A^\pm \simeq \mp\kappa a_e Q^2/(Q^2 + M_Z^2) F_2^{\gamma Z}/\tilde{F}_2$, which is proportional to the product $a_e v_q$ and thus is a direct measure of parity violation. In e^+ scattering A^+ is expected to be positive and about equal to $-A^-$ in e^- scattering. At large x the asymmetry measures the d/u ratio of the valence quark distributions according to

$$A^\pm \propto \pm\kappa \frac{1 + d_v/u_v}{4 + d_v/u_v} \, . \tag{31}$$

The polarised single differential cross sections $\mathrm{d}\sigma_{\mathrm{NC}}/\mathrm{d}Q^2$ are used to construct the asymmetry where it is assumed that the correlated uncertainties of each measurement cancel. The asymmetry is shown in figure 24 compared to the H1PDF 2012 fit. The magnitude of the asymmetry is observed to increase with increasing Q^2 and is positive in e^+p and negative in e^-p scattering. The data are in good agreement with the SM using H1PDF 2012 and confirm the parity violation effects of electroweak interactions at large Q^2.

For a given lepton charge the difference in the left and right polarised NC cross sections is sensitive to $F_2^{\gamma Z}$ as well as $xF_3^{\gamma Z}$ and xF_3^Z as given by

$$\frac{\sigma^\pm(P_L^\pm) - \sigma^\pm(P_R^\pm)}{P_L^\pm - P_R^\pm} = \frac{\kappa Q^2}{Q^2 + M_Z^2} \left[\mp a_e F_2^{\gamma Z} + \frac{Y_-}{Y_+} v_e x F_3^{\gamma Z} - \frac{Y_-}{Y_+} \frac{\kappa Q^2}{Q^2 + M_Z^2} (v_e^2 + a_e^2) x F_3^Z \right] . \tag{32}$$

By taking the difference of equation 32 for the e^+p and e^-p data, the terms proportional to $xF_3^{\gamma Z}$ and xF_3^Z cancel and $F_2^{\gamma Z}$ can be directly extracted using the measured cross sections. The measurement is performed for $Q^2 \geq 200~\mathrm{GeV}^2$. It is shown in figure 25 and listed in table 49. Only a weak Q^2 dependence is expected and therefore the measurements are transformed to a common Q^2 value of $1\,500~\mathrm{GeV}^2$ using the H1PDF 2012 fit and are averaged in each x bin. The average is calculated as a weighted mean using the quadratic sum of statistical and uncorrelated systematic uncertainties. The result is displayed in figure 26 in comparison to the H1PDF 2012 fit and listed in table 50. The correlated uncertainties of the $F_2^{\gamma Z}$ measurement consist of contributions from the point-to-point correlated sources of uncertainties. The dominant contribution at low Q^2 and low y is the normalisation uncertainty of 1.5% of each data set. The global luminosity uncertainty of 2.3% is not included.

7.5 Measurement of $xF_3^{\gamma Z}$

The new combined HERA I+II NC unpolarised cross section measurements for e^+p and e^-p scattering are used to update the previous measurement of the structure function $xF_3^{\gamma Z}$ [2, 3]. Only data taken at $E_p = 920$ GeV are used for this determination. The structure function $x\tilde{F}_3$ is obtained in a simultaneous fit with $x\tilde{F}_3$, $\tilde{\sigma}_0^\pm \equiv \tilde{F}_2^\pm - y^2/Y_+ \tilde{F}_L^\pm$ and nuisance parameters for the systematics shifts b_j being free minimisation parameters. The χ^2 function for the minimisation is

$$\chi^2\left(\tilde{\sigma}_0^{\pm}, x\tilde{F}_3^{\pm}, b\right) = \sum_i \frac{\left[\left(\tilde{\sigma}_{0,i}^{\pm} \mp \frac{Y_-}{Y_+} x\tilde{F}_{3,i}^{\pm}\right) - \sum_j \Gamma_{i,j} b_j - \mu_i^{\pm}\right]^2}{\Delta_i^2} + \sum_j b_j^2 \,. \quad (33)$$

Here $\mu_i^{\pm}$ is the measured central value of the reduced $e^{\pm}p$ cross section at an x, Q^2 point i with a combined statistical and uncorrelated systematic uncertainty $\Delta_i = \sqrt{(\Delta_{i,\mathrm{stat}}^2 + \Delta_{i,\mathrm{syst}}^2)}$. The effect of correlated error sources j on the cross section measurements is given by the systematic error matrix $\Gamma_{i,j}$. The χ^2 function depends quadratically on $\tilde{\sigma}_{0,i}^{\pm}$ and $x\tilde{F}_{3,i}^{\pm}$. The minimisation of the χ^2 function with respect to these variables leads to a system of linear equations which is solved analytically, similar to [75]. This procedure gives results equivalent to a determination of $x\tilde{F}_3$ in which the systematic uncertainties are treated by varying the measurements by each systematic error and adding the resulting deviations in quadrature.

The dominant contribution to $x\tilde{F}_3$ arises from γZ interference, which allows the extraction of $xF_3^{\gamma Z}$ according to $xF_3^{\gamma Z} \simeq -x\tilde{F}_3(Q^2 + M_Z^2)/(\kappa a_e Q^2)$ where the pure Z boson exchange term is neglected. This is justified since the contribution of xF_3^Z is suppressed by the small coupling v_e and an additional factor $\kappa Q^2/(Q^2 + M_Z^2)$ (see eq. 3). The resulting structure function for $Q^2 > 1\,000\ \mathrm{GeV}^2$ is presented in table 51 and shown in figure 27 together with the expectations determined from the H1PDF 2012 fit. Since at high x and low Q^2 the expected sensitivity to $x\tilde{F}_3$ is smaller than the luminosity uncertainty, the measurement is not performed in this region.

This non-singlet structure function exhibits only a weak dependence on Q^2 and therefore the measurements can be first transformed to $Q^2 = 1500\ \mathrm{GeV}^2$ using H1PDF 2012 and then averaged for fixed x values. The averaged $xF_3^{\gamma Z}$ is given in table 52 and shown in figure 28 in comparison with the H1PDF 2012 fit. The calculation from the H1PDF 2012 fit gives a good description of the $xF_3^{\gamma Z}$ measurement. The structure function $xF_3^{\gamma Z}$ determines both the shape and magnitude of the valence distribution $2u_v + d_v$ assuming the quark and anti-quark sea distributions are the same. The integral of this structure function is analogous to the GLS sum rule in neutrino scattering [91] which is in LO predicted to be $5/3$ and acquires $\mathcal{O}(\alpha_s/\pi)$ QCD corrections [92]. The measured value using all HERA I+II data is

$$\int_{0.016}^{0.725} \mathrm{d}x\ F_3^{\gamma Z}(x, Q^2 = 1\,500\ \mathrm{GeV}^2) = 1.22 \pm 0.09(\mathrm{stat}) \pm 0.07(\mathrm{syst})\ , \quad (34)$$

which can be compared to the H1PDF 2012 fit in the same region $\int_{0.016}^{0.725} F_3^{\gamma Z}\,\mathrm{d}x = 1.16^{+0.02}_{-0.03}$ including the total estimated uncertainty. The extrapolation of the measurement to the full kinematic region in x by applying a scale factor determined from the H1PDF 2012 fit, yields $\int_0^1 \mathrm{d}x\ F_3^{\gamma Z} = 1.69 \pm 0.12(\mathrm{stat}) \pm 0.10(\mathrm{syst})$. No additional uncertainty due to the scale factor is considered. This value agrees with the integral evaluated using the H1PDF 2012 fit over the full x range at $Q^2 = 1\,500\ \mathrm{GeV}^2$ which is determined to be $\int_0^1 F_3^{\gamma Z}\,\mathrm{d}x = 1.595$. The quark number sum rules are imposed as constraints in the QCD fit and therefore this measurement validates the sum rules.

7.6 Total CC Cross Sections σ_{CC}^{tot}

The total CC cross sections for $Q^2 > 400\ \mathrm{GeV}^2$ and $y < 0.9$ are listed in table 12 for the e^- and e^+ data and for the different longitudinal lepton beam polarisations. Corrections ($k_{\mathrm{cor}}^{\pm}$) from the analysis phase space $Q^2 > 400\,\mathrm{GeV}^2$, $p_{T,h} > 12\,\mathrm{GeV}$ and $0.03 < y < 0.85$ are applied using the SM expectation based on H1PDF2012 and are found to be $k^-_{\mathrm{cor}} = 1.070$ for e^-p and $k^+_{\mathrm{cor}} = 1.063$ for e^+p scattering. The corresponding cross sections [4] using the unpolarised HERA I data and the same kinematic corrections are also shown in table 12.

	P_e (%)	$\sigma^{\mathrm{tot}}_{\mathrm{CC}}$ (pb)
e^-p	-25.8 ± 0.7	$66.5 \pm 1.0_{\mathrm{stat}} \pm 1.8_{\mathrm{syst}} \pm 1.8_{\mathrm{lumi}}$
	0	$57.0 \pm 2.2_{\mathrm{stat}} \pm 0.9_{\mathrm{syst}} \pm 1.0_{\mathrm{lumi}}$
	$+36.0 \pm 1.0$	$33.7 \pm 1.1_{\mathrm{stat}} \pm 0.9_{\mathrm{syst}} \pm 0.9_{\mathrm{lumi}}$
e^+p	-37.0 ± 0.7	$17.3 \pm 0.6_{\mathrm{stat}} \pm 0.6_{\mathrm{syst}} \pm 0.5_{\mathrm{lumi}}$
	0	$28.4 \pm 0.8_{\mathrm{stat}} \pm 0.8_{\mathrm{syst}} \pm 0.4_{\mathrm{lumi}}$
	$+32.5 \pm 0.7$	$36.6 \pm 0.8_{\mathrm{stat}} \pm 1.2_{\mathrm{syst}} \pm 1.0_{\mathrm{lumi}}$

Table 12: The total CC cross section $\sigma^{\mathrm{tot}}_{\mathrm{CC}}$ for $Q^2 > 400\,\mathrm{GeV}^2$ and $y < 0.9$. The uncertainties correspond to the statistical, experimental systematic and luminosity uncertainties.

The cross sections are shown in figure 29 and compared to the SM expectations using the H1PDF 2012 fit. They agree within one standard deviation if the normalisation factors as determined from the QCD fit are applied. A linear fit to the polarisation dependence of the measured cross sections is performed taking into account the correlated systematic uncertainties between the measurements and is also shown in figure 29. The fit is performed simultaneously to e^-p and e^+p data and yields a $\chi^2 = 2.0$ for two degrees of freedom. The result of the fit extrapolated to the point $P_e = +1$ for e^-p and $P_e = -1$ for e^+p scattering results in

$$\sigma^{\mathrm{tot}}_{\mathrm{CC}}(P_e = +1, e^-p) = -1.3 \pm 2.4_{\mathrm{exp}} \pm 1.5_{\mathrm{lumi}} \pm 1.2_{\mathrm{pol}}\,\mathrm{pb}\,,$$
$$\sigma^{\mathrm{tot}}_{\mathrm{CC}}(P_e = -1, e^+p) = -0.5 \pm 1.3_{\mathrm{exp}} \pm 0.7_{\mathrm{lumi}} \pm 0.4_{\mathrm{pol}}\,\mathrm{pb}\,,$$

where the quoted errors correspond to the experimental, luminosity and polarisation related uncertainties. These extrapolated cross sections are consistent with the SM prediction of a vanishing cross section and correspond to an upper limit on $\sigma^{\mathrm{tot}}_{\mathrm{CC}}(P_e = +1, e^-p)$ and $\sigma^{\mathrm{tot}}_{\mathrm{CC}}(P_e = -1, e^+p)$ of 4.8 pb and 2.6 pb at 95% confidence level (CL), respectively, as derived according to [93]. This result excludes the existence of charged currents involving right handed fermions mediated by a boson of mass M^R_W below 214 and $194\,\mathrm{GeV}$ at 95% CL respectively, assuming SM couplings and a light right handed ν_e. These limits are comparable with those derived earlier by H1 [4] and ZEUS [94].

8 Conclusions

The inclusive DIS cross section for $e^{\pm}p$ interactions at $\sqrt{s} = 319\,\mathrm{GeV}$ are measured using $333.7\,\mathrm{pb}^{-1}$ of integrated luminosity. The e^-p data analysed here corresponds to an almost ten-fold increase in luminosity over the HERA I data set. Moreover the operation of the HERA collider with left and right handed longitudinally polarised electron and positron beams allows measurements in the neutral and charged current channels with four distinct initial states. The NC and CC cross sections cover the region $Q^2 \gtrsim 100\,\mathrm{GeV}^2$ and Bjorken $x \gtrsim 10^{-3}$. The cross sections are measured differentially in Q^2 and double differentially in x and Q^2. The systematic uncertainties of the measurements are substantially reduced compared to previous publications. In the NC channel a precision of 1.5% is attained for the systematic uncertainty in the kinematic region $Q^2 < 1\,000\,\mathrm{GeV}^2$ and $y > 0.1$, compared to a statistical accuracy of about $1 - 3\%$. The high inelasticity region of $0.63 \leq y \leq 0.90$ for $60 \leq Q^2 \leq 800\,\mathrm{GeV}^2$ is measured in the NC analysis for unpolarised $e^{\pm}p$ scattering. This phase space region is sensitive to the F_L structure function.

A NLO QCD analysis of the data is performed for $Q^2 \geq 3.5\,\mathrm{GeV}^2$ including all previously published H1 NC and CC cross section measurements. The data are well described by the QCD fit over the full phase space. The new data at high Q^2 provide better constraints on the partonic structure of the proton. In particular the CC e^+p data enable an improved flavour separation at high x.

The NC lepton polarisation asymmetry $A^{\pm}$, sensitive to parity violation, is determined separately for e^+p and e^-p scattering. The asymmetry is found to increase in magnitude with Q^2 in agreement with the expectation of the Standard Model. The structure function $F_2^{\gamma Z}$ is measured for the first time using the polarisation dependence of the $e^{\pm}p$ NC cross section. The structure function is reported differentially in x, Q^2 and the result is also averaged at $Q^2 = 1\,500\,\mathrm{GeV}^2$.

At high Q^2 the structure function $xF_3^{\gamma Z}$ is determined using unpolarised NC cross sections obtained from the complete HERA I and HERA II data sets. The $xF_3^{\gamma Z}$ results are averaged at $Q^2 = 1\,500\,\mathrm{GeV}^2$ and cover the range $0.013 \leq x \leq 0.65$. The measurement integrated over x validates a sum rule for charged lepton scattering.

The polarisation dependence of the CC total cross section for $Q^2 > 400\,\mathrm{GeV}^2$ and $y < 0.9$ is measured and compared to the unpolarised HERA I measurements. The data exhibit a linear scaling of the cross sections with P_e which is positive for e^+p and negative for e^-p scattering. The data are consistent with the absence of right handed weak currents.

The analysis reported here completes the measurements of inclusive NC and CC cross sections with the HERA I and HERA II data samples at $\sqrt{s} = 319\,\mathrm{GeV}$ with the H1 detector.

Acknowledgements

We are grateful to the HERA machine group whose outstanding efforts made this experiment possible. We thank the engineers and technicians for their work in the construction and maintenance of the H1 detector, our funding agencies for financial support, the DESY technical staff for continual assistance and the DESY directorate for the hospitality which they extend to the non-DESY members of the collaboration.

References

[1] C. Adloff *et al.* [H1 Collaboration], Eur. Phys. J. **C13** (2000) 609 [hep-ex/9908059].

[2] C. Adloff *et al.* [H1 Collaboration], Eur. Phys. J. **C19** (2001) 269 [hep-ex/0012052].

[3] C. Adloff *et al.* [H1 Collaboration], Eur. Phys. J. **C30** (2003) 1 [hep-ex/0304003].

[4] A. Aktas *et al.* [H1 Collaboration], Phys. Lett. **B634** (2006) 173 [hep-ex/0512060].

[5] F. D. Aaron *et al.* [H1 Collaboration], Eur. Phys. J. **C63** (2009) 625 [arXiv:0904.0929].

[6] F. D. Aaron *et al.* [H1 Collaboration], Phys. Lett. **B665** (2008) 139 [arXiv:0805.2809].

[7] F. D. Aaron *et al.* [H1 Collaboration], Eur. Phys. J. **C64** (2009) 561 [arXiv:0904.3513].

[8] J. Breitweg *et al.* [ZEUS Collaboration], Phys. Lett. **B407** (1997) 432 [hep-ex/9707025].

[9] J. Breitweg *et al.* [ZEUS Collaboration], Phys. Lett. **B487** (2000) 53 [hep-ex/0005018].

[10] J. Breitweg *et al.* [ZEUS Collaboration], Eur. Phys. J. **C7** (1999) 609 [hep-ex/9809005].

[11] S. Chekanov *et al.* [ZEUS Collaboration], Eur. Phys. J. **C21** (2001) 443 [hep-ex/0105090].

[12] J. Breitweg *et al.* [ZEUS Collaboration], Eur. Phys. J. **C12** (2000) 411 [hep-ex/9907010]; Erratum-ibid. C27 (2003) 305.

[13] S. Chekanov *et al.* [ZEUS Collaboration], Eur. Phys. J. **C28** (2003) 175 [hep-ex/0208040].

[14] S. Chekanov *et al.* [ZEUS Collaboration], Phys. Lett. **B539** (2002) 197 [hep-ex/0205091]; Erratum-ibid. B552 (2003) 308.

[15] S. Chekanov *et al.* [ZEUS Collaboration], Phys. Rev. **D70** (2004) 052001 [hep-ex/0401003].

[16] S. Chekanov *et al.* [ZEUS Collaboration], Eur. Phys. J. **C32** (2003) 1 [hep-ex/0307043].

[17] F. D. Aaron *et al.* [H1 and ZEUS Collaborations], JHEP **01** (2010) 109 [arXiv:0911.0884].

[18] P. M. Nadolsky *et al.*, Phys. Rev. **D78** (2008) 013004 [arXiv:0802.0007].

[19] A. D. Martin, W. J. Stirling, R. S. Thorne and G. Watt, Eur. Phys. J. **C63** (2009) 189 [arXiv:0901.0002].

[20] R. D. Ball *et al.*, Nucl. Phys. **B838** (2010) 136 [arXiv:1002.4407].

[21] M. Glück, P. Jimenez-Delgado and E. Reya, Eur. Phys. J. **C53** (2008) 355 [arXiv:0709.0614].

[22] S. Alekhin, J. Blümlein, S. Klein and S. Moch, Phys. Rev. **D81** (2010) 014032 [arXiv:0908.2766].

[23] J. M. Campbell, J. W. Huston and W. J. Stirling, Rep. Prog. Phys. **70** (2007) 89.

[24] A. Arbuzov *et al.*, Comput. Phys. Commun. **94** (1996) 128 [hep-ph/9511434].

[25] M. Klein and T. Riemann, Z. Phys. **C24** (1984) 151.

[26] I. Abt *et al.* [H1 Collaboration], Nucl. Instrum. Meth. **A386** (1997) 310.

[27] I. Abt *et al.* [H1 Collaboration], Nucl. Instrum. Meth. **A386** (1997) 348.

[28] B. Andrieu *et al.* [H1 Calorimeter Group], Nucl. Instrum. Meth. **A336** (1993) 460.

[29] R. D. Appuhn *et al.* [H1 SpaCal Group], Nucl. Instrum. Meth. **A386** (1997) 397.

[30] B. Andrieu *et al.* [H1 Calorimeter Group], Nucl. Instrum. Meth. **A336** (1993) 499.

[31] B. Andrieu *et al.* [H1 Calorimeter Group], Nucl. Instrum. Meth. **A350** (1994) 57.

[32] J. Becker *et al.*, Nucl. Instrum. Meth. **A586** (2008) 190 [physics/0701002].

[33] P. J. Laycock *et al.*, submitted to JINST, [arXiv:1206.4068].

[34] D. Pitzl *et al.*, Nucl. Instrum. Meth. **A454** (2000) 334 [hep-ex/0002044].

[35] B. List, Nucl. Instrum. Meth. **A501** (2001) 49.

[36] I. Glushkov, *D* meson production in deep inelastic electron-proton scattering with the forward and backward silicon trackers of the H1 experiment at HERA*, PhD thesis, Humboldt University, Berlin, 2007, (available at http://www-h1.desy.de/publications/theses_list.html).

[37] J. Kretzschmar, *A precision measurement of the proton structure function F2 with the H1 experiment*, PhD thesis, Humboldt University, Berlin, 2008, (available at http://www-h1.desy.de/publications/theses_list.html).

[38] T. Nicholls *et al.* [H1 SpaCal Group], Nucl. Instrum. Meth. **A374** (1996) 149.

[39] F. Aaron *et al.* [H1 Collaboration], DESY-12-062, submitted to Eur. Phys. J. **C**, [arXiv:1205.2448].

[40] A. A. Sokolov and I. M. Ternov, Sov. Phys. Dokl. **8** (1964) 1203.

[41] M. Beckmann *et al.*, Nucl. Instrum. Meth. **A479** (2002) 334 [physics/0009047].

[42] D. P. Barber *et al.*, Nucl. Instrum. Meth. **A338** (1994) 166.

[43] B. Sobloher *et al.*, *Polarisation at HERA - Reanalysis of the HERA II Polarimeter Data*, DESY 11-259 [arXiv:1201.2894].

[44] G. A. Schuler and H. Spiesberger, DJANGO, Proceedings of "Physics at HERA", eds., W. Buchmüller and G. Ingelman, (1991) 1419.

[45] A. Kwiatkowski, H. Spiesberger and H. J. Mohring, Comput. Phys. Commun. **69** (1992) 155.

[46] G. Ingelman, LEPTO 6.1, Proceedings of “Physics at HERA”, eds., W. Buchmüller and G. Ingelman, (1991) 1366.

[47] L. Lönnblad, Comput. Phys .Commun. **71** (1992) 15.

[48] T. Sjöstrand and M. Bengtsson, Comput. Phys. Commun. **43** (1987) 367.

[49] T. Sjöstrand, L. Lönnblad and S. Mrenna, *PYTHIA 6.2: Physics and manual* [hep-ph/0108264].

[50] M. Glück, E. Reya and A. Vogt, Phys. Rev. **D45** (1992) 3986.

[51] C. Berger and P. Kandel, Proceedings of “Monte Carlo generators for HERA physics”, eds., A. Doyle, G. Grindhammer, G. Ingelman and H. Jung, (1999) 596.

[52] T. Abe *et al.*, GRAPE-Dilepton 1.0, Proceedings of “Monte Carlo generators for HERA physics”, eds., A. Doyle, G. Grindhammer, G. Ingelman and H. Jung,(1999) 566.

[53] U. Baur, J. A. M. Vermaseren and D. Zeppenfeld, Nucl. Phys. **B375** (1991) 3.

[54] R. Brun, *et.al.*, GEANT3, Technical Report CERN-DD-81-1 (1987).

[55] M. Peez, *Recherche de deviations au Model Standard dans les processus de grande energie transverse sur le collisionneur electron - proton*, PhD thesis, Univ. Lyon, 2003, DESY-THESIS-2003-023, (available at http://www-h1.desy.de/publications/theses_list.html).

[56] S. Hellwig, *Untersuchung der $D^* - \pi_{\rm slow}$ Double Tagging Methode in Charmanalysen*, Dipl thesis, Univ. Hamburg, 2004, (available at http://www-h1.desy.de/publications/theses_list.html).

[57] U. Bassler and G. Bernardi, Nucl. Instrum. Meth. **A361** (1995) 197 [hep-ex/9412004].

[58] U. Bassler and G. Bernardi, Nucl. Instrum. Meth. **A426** (1999) 583 [hep-ex/9801017].

[59] S. Catani, Y. L. Dokshitzer, M. H. Seymour and B. R. Webber, Nucl. Phys. **B406** (1993) 187.

[60] S. D. Ellis and D. E. Soper, Phys. Rev. **D48** (1993) 3160 [hep-ph/9305266].

[61] S. Bentvelsen *et al.*, Proceedings of “Physics at HERA”, eds., W. Buchmüller and G. Ingelman, (1991) 23.

[62] K. Hoeger, Proceedings of “Physics at HERA”, eds., W. Buchmüller and G. Ingelman, (1991) 43.

[63] A. Blondel and F. Jacquet, Proceedings of “Study of an ep Facility for Europe”, ed., U. Amaldi, (1979) 391.

[64] T. H. Tran, *Precision measurement of cross sections of charged and neutral current processes at high Q^2 at HERA*, PhD thesis, Univ. Paris-Sud 11, 2010, DESY-THESIS-2011-009, (available at http://www-h1.desy.de/publications/theses_list.html).

[65] A. Nikiforov, *Measurements of the neutral current $e^{\pm}p$ cross sections using longitudinally polarised lepton beams at HERA II*, PhD thesis, Ludwig-Maximilians-Univ., München, 2007, (available at http://www-h1.desy.de/publications/theses_list.html).

[66] R. Kogler, *Measurement of jet production in deep-inelastic ep scattering at HERA*, PhD thesis, Hamburg University, 2011, DESY-THESIS-2011-003, MPP-2010-175, (available at http://www-h1.desy.de/publications/theses_list.html).

[67] S. Shushkevich, *Measurement of neutral current cross sections with longitudinally polarised leptons at HERA*, PhD thesis, Ludwig-Maximilians-Univ., München, 2011.

[68] M. Cacciari, G. P. Salam and G. Soyez, CERN-PH-TH/2011-297 (2011) [arXiv:1111.6097].

[69] M. Cacciari and G. P. Salam, Phys. Lett. **B641** (2006) 57 [hep-ph/0512210].

[70] C. Adloff *et al.* [H1 Collaboration], Eur. Phys. J. **C21** (2001) 33 [hep-ex/0012053].

[71] S. Z. Habib, *Unpolarized neutral current $e^{\pm}p$ cross section measurements at the H1 experiment, HERA*, PhD thesis, Hamburg University, 2009, DESY-THESIS-2009-039, (available at http://www-h1.desy.de/publications/theses_list.html).

[72] R. Placakyte, *First measurement of charged current cross sections with longitudinally polarised positrons at HERA*, PhD thesis, Ludwig-Maximilians-Univ., München, 2006, (available at http://www-h1.desy.de/publications/theses_list.html).

[73] H. Spiesberger, EPRC, Proceedings of "Future Physics at HERA", eds., G. Ingelman, A. De Roeck and R. Klanner, (1996) 227.

[74] G. P. Salam and G. Soyez, JHEP **0705** (2007) 086 [arXiv:0704.0292].

[75] F. D. Aaron *et al.* [H1 Collaboration], Eur. Phys. J. **C71** (2010) 1579 [arXiv:1012.4355].

[76] M. Botje, Comput. Phys. Commun. **182** (2011) 490 [arXiv:1005.1481].

[77] V. N. Gribov and L. N. Lipatov, Sov. J. Nucl. Phys. **15** (1972) 438.

[78] V. N. Gribov and L. N. Lipatov, Sov. J. Nucl. Phys. **15** (1972) 675.

[79] L. N. Lipatov, Sov. J. Nucl. Phys. **20** (1975) 94.

[80] Y. L. Dokshitzer, Sov. Phys. JETP **46** (1977) 641.

[81] G. Altarelli and G. Parisi, Nucl. Phys. **B126** (1977) 298.

[82] R. S. Thorne and R. G. Roberts, Phys. Rev. **D57** (1998) 6871 [hep-ph/9709442].

[83] M. Aivazis, J. C. Collins, F. I. Olness and W.-K. Tung, Phys. Rev. **D50** (1994) 3102 [hep-ph/9312319].

[84] A. D. Martin, W. J. Stirling, R. S. Thorne and G. Watt, Eur. Phys. J. **C70** (2010) 51 [arXiv:1007.2624].

[85] C. Amsler *et al.*, (Particle Data Group), Phys. Lett. **B667** (2008) 1.

[86] F. James and M. Roos, Comput. Phys. Commun. **10** (1975) 343.

[87] D. Mason *et al.* [NuTeV Collaboration], Phys. Rev. Lett. **99** (2007) 192001.

[88] Z. J. Ajaltouni *et al.*, Proceedings of "HERA and the LHC workshop series on the implications of HERA for LHC physics", eds. H. Jung and A. De Roeck,(2008) 331, [arXiv:0903.3861].

[89] G. Aad *et al.* [ATLAS Collaboration], CERN-PH-EP-2012-030, submitted to Phys. Rev. Lett., [arXiv:1203.4051].

[90] A. Glazov, AIP Conf. Proc. **792** (2005) 237.

[91] D. J. Gross and C. H. Llewellyn Smith, Nucl. Phys. B **14** (1969) 337.

[92] E. Rizvi and T. Sloan, Eur. Phys. J. direct C **3** (2001) N2 [hep-ex/0101007].

[93] G. J. Feldman and R. D. Cousins, Phys. Rev. D **57** (1998) 3873 [physics/9711021].

[94] H. Abramowicz *et al.* [ZEUS Collaboration], Eur. Phys. J. **C70** (2010) 945 [arXiv:1008.3494].

[95] A. Benvenuti *et al.* [BCDMS Collaboration], Phys. Lett. **B223** (1989) 485.

Q^2 (GeV^2)	x	$\tilde{\sigma}_{\mathrm{NC}}$	δ_{tot} (%)	δ_{stat} (%)	δ_{unc} (%)	$\delta^{E}_{\mathrm{unc}}$ (%)	$\delta^{h}_{\mathrm{unc}}$ (%)	δ_{cor} (%)	$\delta^{E^+}_{\mathrm{cor}}$ (%)	$\delta^{\theta^+}_{\mathrm{cor}}$ (%)	$\delta^{h^+}_{\mathrm{cor}}$ (%)	$\delta^{N^+}_{\mathrm{cor}}$ (%)	$\delta^{B^+}_{\mathrm{cor}}$ (%)
120	0.0020	1.312	1.73	0.87	1.02	0.54	0.09	1.09	−0.36	−0.61	0.02	0.18	−0.81
120	0.0032	1.182	1.89	1.24	1.21	0.77	0.05	0.75	−0.35	−0.62	0.02	0.19	−0.16
150	0.0032	1.195	1.43	0.73	0.91	0.43	0.06	0.81	−0.32	−0.59	0.02	0.19	−0.41
150	0.0050	1.071	1.74	0.88	1.20	0.86	0.00	0.90	−0.55	−0.71	0.00	0.04	−0.04
150	0.0080	0.9197	2.54	1.20	1.85	1.24	1.02	1.26	−0.79	−0.80	−0.27	−0.50	−0.08
150	0.0130	0.7984	4.03	1.68	3.09	2.78	0.82	1.96	−1.61	−0.64	−0.28	−0.85	−0.09
200	0.0032	1.222	1.81	1.35	0.94	0.18	0.07	0.75	0.18	−0.50	0.01	0.15	−0.51
200	0.0050	1.079	1.57	0.96	0.99	0.54	0.02	0.75	−0.44	−0.58	0.01	0.14	−0.08
200	0.0080	0.9389	1.93	0.99	1.39	1.10	0.00	0.91	−0.60	−0.69	0.00	0.00	0.00
200	0.0130	0.7669	1.62	1.14	0.89	0.19	0.03	0.72	−0.04	−0.46	−0.02	0.55	0.00
200	0.0200	0.6800	1.81	1.23	1.14	0.68	0.19	0.70	−0.47	−0.39	−0.08	0.32	−0.01
200	0.0320	0.5735	2.21	1.38	1.51	1.07	0.51	0.85	−0.60	−0.56	−0.19	0.09	0.00
200	0.0500	0.5107	2.97	1.63	1.78	1.47	0.02	1.73	−0.89	−0.79	−0.18	1.24	0.00
200	0.0800	0.4341	3.41	1.73	2.19	1.90	0.19	1.96	−1.13	−0.86	−0.07	1.35	−0.01
200	0.1300	0.3521	3.54	2.09	2.21	1.36	1.09	1.81	−0.80	−1.02	−0.27	−1.23	0.00
200	0.1800	0.2987	4.40	2.71	2.82	1.17	1.97	2.01	−0.83	−1.23	−0.49	−1.26	0.00
250	0.0050	1.096	1.56	1.12	0.89	0.30	0.06	0.60	−0.29	−0.42	0.02	0.18	−0.27
250	0.0080	0.9512	1.67	1.10	1.01	0.55	0.00	0.76	−0.50	−0.57	0.00	0.04	0.00
250	0.0130	0.8042	2.08	1.20	1.25	0.89	0.18	1.15	0.50	−0.66	0.03	0.79	−0.02
250	0.0200	0.6806	2.10	1.23	1.31	0.93	0.26	1.10	0.35	−0.57	0.07	0.87	0.00
250	0.0320	0.5813	2.19	1.30	1.42	1.10	0.11	1.06	0.52	−0.63	−0.08	0.67	0.00
250	0.0500	0.4968	2.44	1.48	1.46	1.12	0.16	1.27	0.45	−0.57	−0.12	1.03	−0.01
250	0.0800	0.4166	2.94	1.52	1.11	0.41	0.34	2.26	0.18	−0.45	−0.02	2.21	0.00
250	0.1300	0.3560	2.55	1.54	1.82	1.08	0.76	0.92	0.51	−0.56	−0.22	−0.46	0.00
250	0.1800	0.3035	4.11	2.11	2.69	1.59	1.59	2.28	1.02	−0.80	−0.38	−1.84	0.00
300	0.0050	1.110	2.23	1.89	1.00	0.17	0.08	0.63	−0.17	−0.46	0.03	0.15	−0.38
300	0.0080	0.9626	1.71	1.28	0.92	0.35	0.02	0.65	−0.35	−0.53	0.01	0.10	−0.08
300	0.0130	0.8029	1.97	1.28	1.18	0.80	0.00	0.93	−0.79	−0.50	0.00	0.00	0.00
300	0.0200	0.6884	2.00	1.42	1.07	0.57	0.17	0.91	0.43	−0.53	0.03	0.61	−0.02
300	0.0320	0.5748	2.15	1.50	1.20	0.79	0.03	0.97	0.46	−0.55	−0.03	0.65	0.00
300	0.0500	0.4892	2.57	1.62	1.45	1.10	0.18	1.38	0.60	−0.66	−0.10	1.05	0.00
300	0.0800	0.4164	3.12	1.72	1.48	1.09	0.18	2.14	0.47	−0.69	−0.06	1.97	−0.01
300	0.1300	0.3547	2.76	1.71	1.89	1.35	0.42	1.07	0.66	−0.69	−0.17	0.45	0.00
300	0.1800	0.2961	4.67	2.26	3.02	2.14	1.53	2.76	1.31	−0.88	−0.36	−2.23	0.00
300	0.4000	0.1439	6.67	2.75	3.63	2.38	1.99	4.88	1.39	−1.03	−0.41	−4.55	0.00
400	0.0080	1.025	1.91	1.54	0.96	0.38	0.04	0.59	−0.33	−0.41	0.01	0.16	−0.22
400	0.0130	0.8439	1.93	1.50	0.97	0.42	0.00	0.72	−0.41	−0.59	0.00	0.03	−0.02
400	0.0200	0.7106	2.25	1.54	1.28	0.91	0.00	1.03	−0.90	−0.50	0.00	0.00	0.00
400	0.0320	0.5984	2.15	1.63	1.02	0.46	0.09	0.95	0.45	−0.48	−0.02	0.69	−0.01
400	0.0500	0.4846	2.32	1.84	1.12	0.51	0.34	0.85	0.50	−0.36	−0.13	0.58	−0.01
400	0.0800	0.4188	2.74	1.91	1.05	0.27	0.23	1.67	0.22	−0.33	0.05	1.62	0.00
400	0.1300	0.3598	2.65	1.93	1.42	0.64	0.16	1.12	0.55	−0.49	−0.10	0.85	0.00
400	0.1800	0.2991	4.47	2.43	2.57	1.14	1.78	2.73	1.06	−0.54	−0.48	−2.41	0.00
400	0.4000	0.1438	7.28	3.09	3.24	1.27	2.22	5.74	1.18	−0.56	−0.31	−5.58	0.00
500	0.0080	0.9879	2.83	2.57	1.05	0.16	0.07	0.52	−0.24	−0.39	0.02	0.16	−0.20
500	0.0130	0.8903	2.15	1.85	0.96	0.31	0.03	0.56	−0.25	−0.49	0.00	0.08	−0.06
500	0.0200	0.7270	2.31	1.83	1.15	0.69	0.00	0.80	−0.69	−0.40	0.00	0.00	0.00
500	0.0320	0.6232	2.35	1.87	1.09	0.50	0.25	0.91	0.52	−0.38	−0.03	0.65	0.00
500	0.0500	0.5411	2.44	1.99	1.12	0.56	0.18	0.84	0.56	−0.32	−0.06	0.54	0.00
500	0.0800	0.4169	2.96	2.27	1.17	0.60	0.07	1.49	0.60	−0.52	−0.02	1.26	0.00
500	0.1300	0.3658	3.21	2.54	1.38	0.44	0.07	1.41	0.44	−0.38	−0.11	1.28	0.00
500	0.1800	0.3299	3.63	2.86	1.95	0.90	0.92	1.11	0.90	−0.53	−0.30	−0.18	0.00
500	0.2500	0.2529	5.34	3.32	2.54	0.99	1.69	3.32	0.99	−0.53	−0.44	−3.09	0.00
650	0.0130	0.8832	2.38	2.08	1.06	0.48	0.05	0.49	−0.32	−0.31	0.01	0.14	−0.13
650	0.0200	0.7582	2.48	2.14	1.06	0.41	0.00	0.70	−0.47	−0.52	0.00	0.03	0.00
650	0.0320	0.6334	2.84	2.23	1.43	1.01	0.00	1.04	−0.94	−0.45	0.00	0.00	0.00
650	0.0500	0.5229	2.82	2.35	1.24	0.68	0.15	0.94	0.75	−0.43	−0.12	0.34	0.00
650	0.0800	0.4300	3.14	2.66	1.16	0.41	0.08	1.22	0.47	−0.30	0.07	1.08	0.00
650	0.1300	0.3599	3.64	2.94	1.55	0.70	0.21	1.48	0.72	−0.51	−0.06	1.19	0.00
650	0.1800	0.3140	3.77	3.18	1.78	0.79	0.46	0.93	0.82	−0.37	−0.17	0.17	0.00
650	0.2500	0.2471	5.56	4.13	2.44	1.09	1.40	2.82	1.06	−0.44	−0.34	−2.55	0.00
650	0.4000	0.1222	8.53	6.14	3.78	1.65	2.42	4.56	1.67	−0.71	−0.63	−4.13	0.00

Table 13: The NC e^-p reduced cross section $\tilde{\sigma}_{\mathrm{NC}}(x, Q^2)$ with lepton beam polarisation $P_e = -25.8\%$ with statistical (δ_{stat}), total (δ_{tot}), total uncorrelated systematic (δ_{unc}) errors, two of its contributions from the electron energy error (δ^{E}_{unc}) and the hadronic energy error ($\delta^{h}_{\mathrm{unc}}$). The effect of the other uncorrelated systematic errors is included in δ_{unc}. In addition the correlated systematic (δ_{cor}) and its contributions from a positive variation of one standard deviation of the electron energy error ($\delta^{E^+}_{cor}$), of the polar electron angle error ($\delta^{\theta^+}_{\mathrm{cor}}$), of the hadronic energy error ($\delta^{h^+}_{\mathrm{cor}}$), of the error due to noise subtraction ($\delta^{N^+}_{\mathrm{cor}}$) and of the error due to background subtraction ($\delta^{B^+}_{\mathrm{cor}}$) are given. The normalisation and polarisation uncertainties are not included in the errors. The table continues on the next page.

Q^2 (GeV^2)	x	$\tilde{\sigma}_{\rm NC}$	$\delta_{\rm tot}$ (%)	$\delta_{\rm stat}$ (%)	$\delta_{\rm unc}$ (%)	$\delta_{\rm unc}^{E}$ (%)	$\delta_{\rm unc}^{h}$ (%)	$\delta_{\rm cor}$ (%)	$\delta_{\rm cor}^{E+}$ (%)	$\delta_{\rm cor}^{\theta+}$ (%)	$\delta_{\rm cor}^{h+}$ (%)	$\delta_{\rm cor}^{N+}$ (%)	$\delta_{\rm cor}^{B+}$ (%)
800	0.0130	0.9026	3.72	3.50	1.21	0.16	0.08	0.41	0.11	−0.33	0.03	0.19	−0.10
800	0.0200	0.7206	2.78	2.51	1.11	0.46	0.01	0.45	−0.25	−0.36	0.00	0.08	−0.06
800	0.0320	0.6195	3.12	2.67	1.40	0.90	0.00	0.80	−0.59	−0.53	0.00	0.00	0.00
800	0.0500	0.5387	3.04	2.74	1.14	0.26	0.08	0.63	0.38	−0.26	−0.06	0.42	−0.02
800	0.0800	0.4321	3.48	3.04	1.29	0.45	0.28	1.09	0.62	−0.46	−0.05	0.77	0.00
800	0.1300	0.3392	4.15	3.58	1.55	0.43	0.26	1.42	0.63	−0.37	−0.07	1.21	0.00
800	0.1800	0.3127	4.27	3.75	1.84	0.59	0.64	0.87	0.75	−0.37	−0.18	0.16	0.00
800	0.2500	0.2409	5.39	4.63	2.17	0.59	1.05	1.72	0.77	−0.30	−0.23	−1.48	0.00
800	0.4000	0.1340	9.10	5.93	4.25	1.68	2.96	5.44	1.78	−0.71	−0.76	−5.03	0.00
1000	0.0130	0.8430	4.06	3.45	1.68	0.27	0.22	1.34	−0.03	−0.20	0.05	0.19	−1.31
1000	0.0200	0.7686	3.10	2.87	1.07	0.32	0.06	0.45	−0.18	−0.37	0.01	0.11	−0.12
1000	0.0320	0.6579	3.10	2.82	1.17	0.57	0.00	0.50	−0.26	−0.43	0.00	0.01	0.00
1000	0.0500	0.5030	3.67	3.15	1.59	1.17	0.00	0.99	−0.71	−0.68	0.00	0.00	0.00
1000	0.0800	0.4311	3.71	3.43	1.14	0.05	0.18	0.84	0.17	−0.23	0.05	0.78	0.00
1000	0.1300	0.3308	4.65	4.21	1.52	0.29	0.28	1.26	0.40	−0.33	−0.17	1.14	0.00
1000	0.1800	0.3587	4.48	3.98	1.82	0.72	0.53	0.96	0.73	−0.43	−0.25	0.37	0.00
1000	0.2500	0.2591	5.40	4.61	2.25	0.90	1.12	1.68	1.01	−0.45	−0.34	−1.22	0.00
1000	0.4000	0.1266	9.18	6.56	4.16	1.84	2.83	4.89	1.55	−0.48	−0.56	−4.58	0.00
1200	0.0130	0.9167	6.04	5.43	2.21	0.21	0.27	1.48	0.35	0.22	0.05	0.22	−1.41
1200	0.0200	0.7663	3.83	3.60	1.22	0.29	0.09	0.46	−0.19	−0.26	0.02	0.12	−0.31
1200	0.0320	0.6765	3.45	3.27	0.98	0.27	0.03	0.52	−0.21	−0.47	0.00	0.06	−0.01
1200	0.0500	0.5310	3.76	3.48	1.27	0.82	0.00	0.62	−0.45	−0.42	0.00	0.00	0.00
1200	0.0800	0.4462	4.05	3.73	1.38	0.93	0.19	0.77	0.58	−0.27	−0.15	0.40	0.00
1200	0.1300	0.3503	5.66	5.38	1.51	0.73	0.09	0.90	0.43	−0.14	−0.02	0.78	0.00
1200	0.1800	0.3217	5.03	4.65	1.71	0.83	0.34	0.87	0.63	−0.35	−0.15	0.47	0.00
1200	0.2500	0.2147	6.06	5.58	2.16	1.27	0.74	0.93	0.82	−0.27	−0.19	−0.29	0.00
1200	0.4000	0.1230	9.42	7.08	4.36	2.61	2.68	4.42	1.58	−0.33	−0.62	−4.06	0.00
1500	0.0200	0.8069	4.76	4.26	1.78	0.09	0.16	1.18	0.18	−0.24	0.04	0.15	−1.13
1500	0.0320	0.6724	4.24	4.06	1.12	0.40	0.06	0.48	−0.38	−0.25	0.01	0.13	−0.06
1500	0.0500	0.5470	4.25	4.02	1.25	0.74	0.00	0.54	−0.34	−0.42	0.00	0.01	0.00
1500	0.0800	0.4986	4.29	4.05	1.23	0.64	0.13	0.70	0.42	−0.17	−0.01	0.53	0.00
1500	0.1300	0.3514	5.63	5.25	1.79	1.12	0.18	0.92	0.72	−0.27	−0.13	0.49	0.00
1500	0.1800	0.3066	5.83	5.42	1.89	1.13	0.23	1.01	0.60	−0.11	−0.05	0.80	0.00
1500	0.2500	0.2297	6.52	6.05	2.24	1.29	0.85	0.90	0.68	−0.18	−0.25	−0.51	0.00
1500	0.4000	0.1353	10.32	8.82	4.02	2.35	2.33	3.54	1.51	−0.30	−0.61	−3.13	0.00
1500	0.6500	0.01469	19.63	14.78	6.93	4.41	4.39	10.90	3.27	−0.40	−0.95	−10.34	0.00
2000	0.0219	0.8967	7.26	6.58	2.49	0.20	0.18	1.79	0.18	−0.20	0.03	0.19	−1.76
2000	0.0320	0.6323	5.13	4.89	1.50	0.20	0.10	0.49	−0.16	−0.41	0.03	0.15	−0.15
2000	0.0500	0.5475	5.03	4.87	1.19	0.43	0.02	0.42	−0.25	−0.33	0.01	0.04	−0.02
2000	0.0800	0.4363	5.28	5.02	1.43	0.84	0.00	0.79	−0.64	−0.46	0.00	0.00	0.00
2000	0.1300	0.3653	6.25	5.98	1.64	0.72	0.06	0.80	0.48	−0.24	0.04	0.59	0.00
2000	0.1800	0.2969	6.95	6.52	2.17	1.45	0.23	1.01	0.79	−0.26	−0.16	0.54	0.00
2000	0.2500	0.2483	7.08	6.68	2.20	1.28	0.56	0.81	0.67	−0.30	−0.13	−0.31	0.00
2000	0.4000	0.1249	9.82	8.56	3.87	2.33	1.97	2.88	1.36	−0.13	−0.55	−2.47	0.00
2000	0.6500	0.01062	23.74	19.67	8.15	5.31	5.23	10.50	2.50	−0.39	−1.12	−10.13	0.00
3000	0.0320	0.7671	4.82	4.41	1.83	0.25	0.11	0.67	−0.14	−0.30	0.02	0.11	−0.57
3000	0.0500	0.5870	4.27	4.01	1.40	0.15	0.05	0.37	−0.11	−0.34	0.02	0.08	−0.05
3000	0.0800	0.4900	4.59	4.37	1.33	0.55	0.00	0.51	−0.33	−0.39	0.00	0.01	0.00
3000	0.1300	0.4137	5.49	5.17	1.72	0.85	0.00	0.61	−0.50	−0.34	0.00	0.00	0.00
3000	0.1800	0.2885	6.48	6.14	1.87	1.02	0.19	0.83	0.55	−0.11	−0.06	0.61	0.00
3000	0.2500	0.2131	6.96	6.55	2.16	1.36	0.40	0.96	0.86	−0.06	−0.15	−0.38	0.00
3000	0.4000	0.1245	8.85	7.49	4.03	2.77	1.83	2.44	1.71	−0.18	−0.40	−1.69	0.00
3000	0.6500	0.01303	18.15	14.62	6.92	4.13	4.71	8.23	2.69	−0.28	−1.38	−7.65	0.00
5000	0.0547	0.6559	6.35	5.98	2.02	0.18	0.14	0.72	0.14	−0.38	0.03	0.13	−0.58
5000	0.0800	0.5540	4.92	4.65	1.57	0.16	0.05	0.35	−0.19	−0.27	0.00	0.06	−0.08
5000	0.1300	0.4827	5.55	5.23	1.80	0.33	0.01	0.46	0.23	−0.39	0.00	0.01	0.00
5000	0.1800	0.3772	6.42	6.13	1.87	0.26	0.00	0.37	−0.11	−0.35	0.00	0.00	0.00
5000	0.2500	0.2235	8.37	8.02	2.25	0.96	0.00	0.79	0.77	−0.19	0.00	0.00	0.00
5000	0.4000	0.1051	10.63	9.88	3.51	1.93	1.48	1.80	1.41	−0.09	−0.54	−0.99	0.00
5000	0.6500	0.01439	18.84	16.48	7.19	4.40	4.59	5.64	2.53	0.24	−1.02	−4.93	0.00
8000	0.0875	0.6428	9.35	8.89	2.72	0.56	0.06	1.01	0.26	−0.33	0.02	0.09	−0.92
8000	0.1300	0.5263	7.49	7.10	2.35	0.27	0.02	0.45	−0.20	−0.31	0.01	0.05	−0.26
8000	0.1800	0.3753	8.33	8.01	2.27	0.17	0.03	0.39	−0.09	−0.38	−0.01	0.02	0.00
8000	0.2500	0.2636	9.47	9.07	2.64	1.14	0.00	0.60	0.60	0.06	0.00	0.00	0.00
8000	0.4000	0.1164	13.53	12.62	4.43	3.21	0.00	2.07	1.98	0.60	0.00	0.00	0.00
8000	0.6500	0.01037	23.03	21.89	6.35	3.71	3.52	3.31	2.15	0.36	−0.82	−2.36	0.00
12000	0.1300	0.7243	16.19	15.45	4.58	0.69	0.15	1.48	0.28	−0.26	0.04	0.13	−1.42
12000	0.1800	0.5335	9.86	9.59	2.25	0.11	0.07	0.39	−0.06	−0.32	0.03	0.09	−0.19
12000	0.2500	0.3098	11.43	11.15	2.49	0.98	0.02	0.52	0.49	−0.15	0.01	0.03	0.00
12000	0.4000	0.2097	13.47	12.42	4.94	4.03	0.00	1.68	1.58	0.58	0.00	0.00	0.00
12000	0.6500	0.01439	28.78	27.80	6.56	4.81	3.13	3.56	2.71	0.51	−0.95	−2.05	0.00
20000	0.2500	0.5939	13.71	13.34	2.94	1.16	0.08	1.17	0.39	−0.17	0.03	0.05	−1.09
20000	0.4000	0.2141	17.21	16.55	4.59	3.54	0.03	1.11	1.09	0.12	0.01	0.03	−0.16
20000	0.6500	0.01850	44.37	40.89	16.39	16.00	0.00	5.30	4.61	2.63	0.00	0.00	0.00
30000	0.4000	0.1671	36.74	36.01	7.03	3.51	0.15	1.93	1.04	−0.15	0.03	0.11	−1.62
30000	0.6500	0.04155	39.86	37.83	11.89	11.21	0.00	3.97	3.49	1.90	0.00	0.01	0.00
50000	0.6500	0.1133	58.72	57.78	10.19	7.43	0.00	2.38	2.03	1.25	0.00	0.00	0.00

Table 13: continued.

Q^2 (GeV^2)	x	$\tilde{\sigma}_{\mathrm{NC}}$	δ_{tot} (%)	δ_{stat} (%)	δ_{unc} (%)	$\delta_{\mathrm{unc}}^{E}$ (%)	$\delta_{\mathrm{unc}}^{h}$ (%)	δ_{cor} (%)	$\delta_{\mathrm{cor}}^{E^+}$ (%)	$\delta_{\mathrm{cor}}^{\theta^+}$ (%)	$\delta_{\mathrm{cor}}^{h^+}$ (%)	$\delta_{\mathrm{cor}}^{N^+}$ (%)	$\delta_{\mathrm{cor}}^{B^+}$ (%)
120	0.0020	1.316	1.92	1.29	0.95	0.38	0.09	1.05	−0.24	−0.67	0.02	0.18	−0.75
120	0.0032	1.190	2.32	1.78	1.24	0.76	0.05	0.83	−0.40	−0.68	0.02	0.22	−0.16
150	0.0032	1.185	1.62	1.09	0.89	0.37	0.07	0.80	−0.30	−0.58	0.02	0.20	−0.41
150	0.0050	1.083	2.08	1.29	1.30	0.99	0.01	0.98	−0.56	−0.81	0.00	0.05	−0.03
150	0.0080	0.9357	2.88	1.78	1.85	1.35	0.86	1.31	−0.86	−0.86	−0.30	−0.38	−0.06
150	0.0130	0.7694	4.23	2.42	2.90	2.48	1.06	1.90	−1.43	−0.96	−0.33	−0.74	−0.10
200	0.0032	1.166	2.38	2.06	0.95	0.14	0.07	0.72	−0.14	−0.52	0.02	0.16	−0.46
200	0.0050	1.071	1.91	1.46	0.96	0.48	0.02	0.77	−0.39	−0.65	0.00	0.12	−0.09
200	0.0080	0.9308	2.19	1.44	1.34	1.03	0.00	0.97	−0.65	−0.72	0.00	0.00	0.00
200	0.0130	0.7788	2.04	1.67	0.89	0.08	0.05	0.76	−0.09	−0.41	−0.07	0.62	−0.03
200	0.0200	0.6780	2.22	1.81	1.05	0.52	0.04	0.75	−0.43	−0.46	−0.04	0.40	−0.01
200	0.0320	0.5524	2.72	2.12	1.36	0.79	0.57	1.01	−0.39	−0.91	−0.18	−0.12	−0.01
200	0.0500	0.5222	3.39	2.48	1.78	1.44	0.08	1.47	−0.81	−0.48	−0.10	1.13	0.00
200	0.0800	0.4227	3.94	2.51	2.30	2.01	0.20	1.99	−1.18	−0.53	−0.12	1.50	0.00
200	0.1300	0.3548	3.91	2.84	2.21	1.32	1.14	1.52	−0.84	−0.88	−0.30	−0.86	0.00
200	0.1800	0.3054	5.42	4.12	2.83	1.44	1.77	2.10	−0.96	−0.75	−0.31	−1.69	0.00
250	0.0050	1.079	2.03	1.69	0.94	0.39	0.07	0.62	−0.39	−0.34	0.01	0.17	−0.28
250	0.0080	0.9100	2.15	1.64	1.09	0.68	0.00	0.86	−0.66	−0.55	0.00	0.02	−0.03
250	0.0130	0.7825	2.51	1.80	1.32	0.94	0.26	1.15	0.47	−0.65	0.04	0.83	−0.03
250	0.0200	0.6562	2.44	1.86	1.25	0.85	0.18	0.98	0.30	−0.46	0.05	0.81	−0.03
250	0.0320	0.5549	2.57	1.95	1.34	0.99	0.08	0.98	0.43	−0.56	−0.12	0.66	0.00
250	0.0500	0.4587	2.90	2.20	1.25	0.82	0.05	1.41	0.29	−0.44	−0.02	1.31	0.00
250	0.0800	0.4222	3.32	2.24	1.33	0.88	0.09	2.06	0.44	−0.65	−0.07	1.90	0.00
250	0.1300	0.3639	3.03	2.29	1.74	1.09	0.48	0.95	0.53	−0.65	−0.23	0.39	0.00
250	0.1800	0.2977	5.03	3.24	2.85	1.90	1.51	2.57	1.11	−0.67	−0.29	−2.20	0.00
300	0.0050	1.140	3.03	2.77	1.03	0.24	0.07	0.70	−0.27	−0.54	0.02	0.18	−0.30
300	0.0080	0.9564	2.18	1.89	0.88	0.20	0.02	0.63	−0.20	−0.58	0.01	0.11	−0.05
300	0.0130	0.7934	2.35	1.92	1.05	0.57	0.00	0.87	−0.56	−0.67	0.00	0.00	0.00
300	0.0200	0.6795	2.61	2.10	1.15	0.69	0.14	1.03	0.55	−0.61	0.01	0.61	0.00
300	0.0320	0.5821	2.74	2.18	1.29	0.90	0.07	1.07	0.55	−0.58	−0.11	0.70	0.00
300	0.0500	0.4916	3.12	2.46	1.52	1.17	0.13	1.17	0.61	−0.67	−0.07	0.73	0.00
300	0.0800	0.4185	3.69	2.56	1.40	0.91	0.37	2.26	0.29	−0.60	−0.04	2.15	−0.01
300	0.1300	0.3461	3.43	2.61	1.89	1.33	0.42	1.17	0.73	−0.60	−0.17	0.67	0.00
300	0.1800	0.2791	5.61	3.47	3.26	2.22	1.87	2.96	1.40	−0.95	−0.42	−2.40	0.00
300	0.4000	0.1494	7.25	3.91	3.41	2.10	1.91	5.07	1.16	−0.76	−0.31	−4.86	0.00
400	0.0080	0.9779	2.67	2.41	0.97	0.36	0.05	0.61	−0.33	−0.46	0.01	0.15	−0.18
400	0.0130	0.8148	2.57	2.24	1.04	0.55	0.00	0.70	−0.55	−0.44	0.00	0.02	−0.01
400	0.0200	0.6607	2.89	2.36	1.31	0.93	0.00	1.04	−0.93	−0.47	0.00	0.00	0.00
400	0.0320	0.5791	2.80	2.46	1.07	0.50	0.18	0.82	0.49	−0.44	−0.08	0.48	0.00
400	0.0500	0.4854	3.05	2.70	1.20	0.52	0.48	0.79	0.51	−0.44	−0.11	0.41	0.00
400	0.0800	0.3915	3.85	3.05	1.18	0.27	0.55	2.02	0.24	−0.35	0.07	1.98	0.00
400	0.1300	0.3593	3.59	2.96	1.53	0.75	0.39	1.33	0.69	−0.59	−0.21	0.95	0.00
400	0.1800	0.3012	5.07	3.45	2.34	0.96	1.53	2.88	0.90	−0.44	−0.31	−2.68	0.00
400	0.4000	0.1452	8.22	4.99	3.43	1.51	2.33	5.55	1.43	−0.89	−0.44	−5.27	0.00
500	0.0080	0.9388	4.11	3.93	1.11	0.22	0.08	0.48	−0.20	−0.37	0.02	0.15	−0.17
500	0.0130	0.8057	3.02	2.80	1.00	0.37	0.02	0.55	−0.30	−0.45	0.00	0.09	−0.06
500	0.0200	0.6732	3.18	2.80	1.19	0.73	0.00	0.92	−0.73	−0.57	0.00	0.00	−0.01
500	0.0320	0.5728	3.24	2.89	1.11	0.49	0.28	0.95	0.49	−0.35	0.16	0.71	0.00
500	0.0500	0.5054	3.43	3.01	1.30	0.77	0.35	1.00	0.78	−0.50	−0.23	0.32	0.00
500	0.0800	0.4245	3.86	3.28	1.15	0.34	0.37	1.68	0.34	−0.35	0.04	1.60	0.00
500	0.1300	0.3611	4.68	4.14	1.56	0.80	0.20	1.52	0.80	−0.54	−0.11	1.17	0.00
500	0.1800	0.3152	4.60	4.06	1.84	0.78	0.72	1.12	0.78	−0.69	−0.30	−0.29	0.00
500	0.2500	0.2397	6.88	5.05	2.74	1.22	1.82	3.79	1.22	−0.60	−0.36	−3.51	0.00
650	0.0130	0.8564	3.31	3.13	1.00	0.25	0.06	0.38	−0.11	−0.31	0.02	0.14	−0.12
650	0.0200	0.7176	3.55	3.26	1.20	0.65	0.01	0.74	−0.54	−0.52	0.00	0.02	−0.01
650	0.0320	0.6245	3.76	3.33	1.37	0.89	0.00	1.07	−0.87	−0.62	0.00	0.00	0.00
650	0.0500	0.5392	3.74	3.46	1.14	0.42	0.10	0.83	0.50	−0.26	0.07	0.61	0.00
650	0.0800	0.4014	4.36	4.01	1.29	0.62	0.20	1.12	0.64	−0.36	−0.12	0.84	0.00
650	0.1300	0.3282	5.40	4.99	1.50	0.47	0.22	1.43	0.52	−0.25	−0.13	1.30	0.00
650	0.1800	0.3253	5.04	4.67	1.70	0.61	0.26	0.83	0.63	−0.38	−0.13	−0.38	0.00
650	0.2500	0.2467	6.96	5.55	2.90	1.44	1.83	3.04	1.42	−0.56	−0.51	−2.58	0.00
650	0.4000	0.1106	9.89	8.49	3.44	1.47	1.94	3.71	1.46	−0.74	−0.33	−3.31	0.00

Table 14: The NC e^-p reduced cross section $\tilde{\sigma}_{\mathrm{NC}}(x,Q^2)$ with lepton beam polarisation $P_e = +36.0\%$ with statistical (δ_{stat}), total (δ_{tot}), total uncorrelated systematic (δ_{unc}) errors, two of its contributions from the electron energy error (δ_{unc}^{E}) and the hadronic energy error ($\delta_{\mathrm{unc}}^{h}$). The effect of the other uncorrelated systematic errors is included in δ_{unc}. In addition the correlated systematic (δ_{cor}) and its contributions from a positive variation of one standard deviation of the electron energy error ($\delta_{cor}^{E^+}$), of the polar electron angle error ($\delta_{\mathrm{cor}}^{\theta^+}$), of the hadronic energy error ($\delta_{\mathrm{cor}}^{h^+}$), of the error due to noise subtraction ($\delta_{\mathrm{cor}}^{N^+}$) and of the error due to background subtraction ($\delta_{\mathrm{cor}}^{B^+}$) are given. The normalisation and polarisation uncertainties are not included in the errors. The table continues on the next page.

Q^2 (GeV^2)	x	$\tilde{\sigma}_{NC}$	δ_{tot} (%)	δ_{stat} (%)	δ_{unc} (%)	δ_{unc}^{E} (%)	δ_{unc}^{h} (%)	δ_{cor} (%)	$\delta_{cor}^{E^+}$ (%)	$\delta_{cor}^{\theta^+}$ (%)	$\delta_{cor}^{h^+}$ (%)	$\delta_{cor}^{N^+}$ (%)	$\delta_{cor}^{B^+}$ (%)
800	0.0130	0.8156	5.41	5.20	1.42	0.68	0.08	0.56	−0.34	−0.38	0.01	0.16	−0.16
800	0.0200	0.6970	3.96	3.76	1.16	0.52	0.03	0.44	−0.33	−0.27	0.00	0.08	−0.02
800	0.0320	0.5977	4.18	3.87	1.38	0.84	0.00	0.74	−0.67	−0.32	0.00	0.00	0.00
800	0.0500	0.5348	4.27	4.04	1.17	0.24	0.17	0.73	0.48	−0.35	0.06	0.41	−0.01
800	0.0800	0.3757	5.10	4.83	1.26	0.31	0.07	1.06	0.53	−0.44	−0.06	0.81	0.00
800	0.1300	0.3512	6.24	5.90	1.57	0.19	0.34	1.27	0.45	−0.40	−0.03	1.12	−0.02
800	0.1800	0.3117	6.72	6.28	2.02	0.86	0.74	1.28	1.02	−0.47	−0.28	−0.55	0.00
800	0.2500	0.2222	7.37	6.66	2.48	0.99	1.32	1.95	1.20	−0.40	−0.26	−1.46	0.00
800	0.4000	0.1183	11.91	9.46	4.15	1.43	2.88	5.92	1.54	−0.56	−0.85	−5.63	0.00
1000	0.0130	0.8198	5.57	5.19	1.71	0.28	0.22	1.08	0.05	−0.20	0.06	0.18	−1.05
1000	0.0200	0.6965	4.63	4.48	1.10	0.37	0.05	0.43	−0.20	−0.35	0.02	0.10	−0.08
1000	0.0320	0.6199	4.84	4.66	1.20	0.58	0.00	0.58	−0.34	−0.47	0.00	0.01	0.00
1000	0.0500	0.4908	5.01	4.74	1.42	0.90	0.00	0.77	−0.47	−0.61	0.00	0.00	0.00
1000	0.0800	0.4084	5.43	5.21	1.30	0.57	0.16	0.85	0.41	−0.32	0.11	0.66	0.00
1000	0.1300	0.3811	6.19	5.82	1.52	0.19	0.32	1.45	0.46	−0.26	−0.02	1.35	0.00
1000	0.1800	0.2933	6.70	6.43	1.79	0.49	0.59	0.63	0.41	−0.33	−0.12	−0.32	0.00
1000	0.2500	0.2710	7.06	6.71	2.01	0.64	0.64	0.96	0.75	−0.24	−0.25	0.48	0.00
1000	0.4000	0.1238	12.66	9.92	4.75	2.23	3.36	6.28	1.75	−0.65	−0.72	−5.95	0.00
1200	0.0130	0.7581	9.74	9.00	2.85	0.18	0.22	2.39	−0.20	−0.13	0.04	0.15	−2.37
1200	0.0200	0.7496	5.51	5.37	1.17	0.10	0.07	0.42	0.09	−0.32	0.02	0.10	−0.24
1200	0.0320	0.6278	5.19	5.03	1.13	0.56	0.01	0.55	−0.38	−0.39	0.00	0.05	−0.01
1200	0.0500	0.5154	5.39	5.22	1.24	0.75	0.00	0.56	−0.34	−0.44	0.00	0.00	0.00
1200	0.0800	0.4535	5.77	5.53	1.41	0.93	0.24	0.83	0.62	−0.27	−0.09	0.47	0.00
1200	0.1300	0.3312	7.25	7.00	1.57	0.81	0.04	1.07	0.60	−0.25	−0.04	0.85	0.00
1200	0.1800	0.2648	7.86	7.60	1.93	1.15	0.48	0.65	0.57	−0.12	−0.10	0.27	0.00
1200	0.2500	0.2152	8.51	8.26	1.92	0.89	0.59	0.71	0.58	−0.29	−0.18	0.22	0.00
1200	0.4000	0.1305	12.00	10.01	4.37	2.59	2.70	4.96	1.87	−0.33	−0.84	−4.51	0.00
1500	0.0200	0.7118	6.93	6.68	1.77	0.38	0.17	0.60	−0.13	−0.31	0.02	0.16	−0.47
1500	0.0320	0.6266	6.33	6.22	1.10	0.23	0.03	0.46	−0.32	−0.31	0.01	0.10	−0.04
1500	0.0500	0.5367	6.19	6.00	1.37	0.90	0.00	0.66	−0.51	−0.42	0.00	0.01	0.00
1500	0.0800	0.4479	6.51	6.35	1.32	0.76	0.07	0.52	0.33	−0.16	0.02	0.37	0.00
1500	0.1300	0.3257	10.30	10.17	1.48	0.41	0.14	0.81	0.41	0.12	0.06	0.69	0.00
1500	0.1800	0.2626	9.05	8.79	1.91	1.11	0.21	1.04	0.70	−0.35	−0.31	0.61	0.00
1500	0.2500	0.2490	9.06	8.68	2.43	1.48	0.98	0.89	0.82	0.11	0.21	−0.26	0.00
1500	0.4000	0.09081	14.08	13.16	3.83	2.26	2.00	3.25	1.26	−0.38	−0.53	−2.92	0.00
1500	0.6500	0.01231	27.10	23.63	7.54	4.91	4.80	10.93	2.61	−0.52	−1.01	−10.55	0.00
2000	0.0219	0.7395	10.99	10.62	2.48	0.48	0.22	1.37	−0.27	−0.20	0.06	0.21	−1.31
2000	0.0320	0.6267	7.47	7.29	1.58	0.27	0.10	0.49	0.06	−0.33	0.04	0.11	−0.33
2000	0.0500	0.5035	7.69	7.57	1.25	0.49	0.01	0.49	−0.40	−0.28	0.00	0.03	0.00
2000	0.0800	0.4419	7.52	7.37	1.38	0.70	0.00	0.52	−0.32	−0.41	0.00	0.00	0.00
2000	0.1300	0.3075	9.88	9.69	1.71	0.73	0.34	0.85	0.17	−0.18	0.15	0.80	0.00
2000	0.1800	0.2856	10.11	9.83	2.18	1.38	0.43	0.94	0.80	−0.25	−0.08	0.42	0.00
2000	0.2500	0.2258	10.72	10.39	2.42	1.46	0.84	1.04	0.96	−0.24	−0.28	−0.16	0.00
2000	0.4000	0.1182	13.61	12.93	3.47	1.96	1.54	2.46	1.25	−0.05	−0.40	−2.08	0.00
2000	0.6500	0.007810	35.78	33.44	7.79	4.64	5.28	10.04	2.98	−0.66	−0.96	−9.52	0.00
3000	0.0320	0.5900	7.76	7.46	1.90	0.09	0.12	0.93	0.10	−0.26	0.03	0.13	−0.88
3000	0.0500	0.5803	6.14	5.96	1.44	0.28	0.06	0.40	−0.15	−0.35	0.03	0.09	−0.08
3000	0.0800	0.4753	6.78	6.63	1.31	0.40	0.00	0.52	−0.28	−0.44	0.00	0.01	−0.02
3000	0.1300	0.3423	8.65	8.44	1.76	0.87	0.00	0.66	−0.52	−0.41	0.00	0.00	0.00
3000	0.1800	0.3003	9.27	9.00	2.05	1.27	0.21	0.89	0.78	−0.09	−0.09	0.41	0.00
3000	0.2500	0.2826	8.95	8.59	2.32	1.56	0.37	0.95	0.86	−0.09	0.06	0.38	0.00
3000	0.4000	0.08914	13.50	12.93	3.43	2.12	1.39	1.76	1.28	−0.19	−0.44	−1.10	0.00
3000	0.6500	0.005010	37.74	35.57	8.46	5.69	5.45	9.35	3.03	−0.13	−1.35	−8.74	0.00
5000	0.0547	0.5599	9.80	9.54	2.13	0.37	0.10	0.68	−0.18	−0.32	0.03	0.10	−0.56
5000	0.0800	0.4362	7.86	7.68	1.62	0.25	0.06	0.42	−0.22	−0.29	0.01	0.08	−0.19
5000	0.1300	0.3964	8.70	8.49	1.85	0.43	0.02	0.44	0.25	−0.37	0.00	0.02	−0.04
5000	0.1800	0.3454	9.67	9.47	1.91	0.29	0.00	0.43	−0.30	−0.31	0.00	0.00	0.00
5000	0.2500	0.2430	17.03	16.81	2.56	1.47	0.00	0.94	0.93	−0.10	0.00	0.00	0.00
5000	0.4000	0.1382	13.32	12.82	3.38	1.76	1.27	1.30	1.08	−0.11	−0.27	−0.67	0.00
5000	0.6500	0.01280	27.43	25.88	6.77	3.48	4.66	6.05	2.25	0.35	−1.49	−5.40	0.00
8000	0.0875	0.5903	14.27	13.94	2.79	0.22	0.16	1.32	0.13	−0.41	0.04	0.16	−1.23
8000	0.1300	0.4711	11.39	11.13	2.40	0.29	0.08	0.39	−0.19	−0.25	0.02	0.09	−0.20
8000	0.1800	0.3787	11.97	11.74	2.31	0.17	0.00	0.34	0.13	−0.31	0.00	0.02	0.00
8000	0.2500	0.2430	14.27	14.04	2.56	0.80	0.00	0.34	0.31	0.12	0.00	0.00	0.00
8000	0.4000	0.1130	19.80	18.93	5.29	4.26	0.00	2.41	2.38	0.36	0.00	0.00	0.00
8000	0.6500	0.01617	28.34	26.77	8.04	5.47	4.37	4.62	3.03	−0.35	−0.99	−3.34	0.00
12000	0.1300	0.6871	23.67	23.42	3.21	1.04	0.09	1.28	0.50	−0.41	0.03	0.08	−1.10
12000	0.1800	0.3882	16.90	16.73	2.34	0.50	0.09	0.39	−0.15	−0.29	0.03	0.10	−0.19
12000	0.2500	0.3008	16.92	16.72	2.60	1.20	0.01	0.46	0.45	0.12	0.01	0.03	0.00
12000	0.4000	0.1494	22.50	21.86	4.91	3.98	0.00	2.06	1.96	0.65	0.00	0.00	0.00
12000	0.6500	0.01225	45.33	44.83	6.13	4.35	2.88	2.67	2.19	0.30	−0.58	−1.38	0.00
20000	0.2500	0.1984	34.22	34.11	2.68	1.19	0.08	0.57	0.53	−0.18	0.02	0.08	−0.07
20000	0.4000	0.2224	24.77	24.30	4.72	3.73	0.02	0.82	0.81	0.10	0.01	0.02	0.00
20000	0.6500	0.01299	72.61	70.89	14.87	14.40	0.00	4.95	4.11	2.76	0.00	0.00	0.00
30000	0.4000	0.2553	43.91	43.40	6.07	3.07	0.11	2.69	1.09	−0.53	0.02	0.06	−2.40
30000	0.6500	0.03854	58.87	57.81	10.51	9.70	0.00	3.70	3.26	1.74	0.00	0.00	0.00

Table 14: continued.

Q^2 (GeV^2)	x	$\tilde{\sigma}_{\mathrm{NC}}$	δ_{tot} (%)	δ_{stat} (%)	δ_{unc} (%)	$\delta_{\mathrm{unc}}^{E}$ (%)	$\delta_{\mathrm{unc}}^{h}$ (%)	δ_{cor} (%)	$\delta_{\mathrm{cor}}^{E^+}$ (%)	$\delta_{\mathrm{cor}}^{\theta^+}$ (%)	$\delta_{\mathrm{cor}}^{h^+}$ (%)	$\delta_{\mathrm{cor}}^{N^+}$ (%)	$\delta_{\mathrm{cor}}^{B^+}$ (%)
120	0.0020	1.342	1.71	0.97	0.93	0.55	0.09	1.05	−0.31	−0.58	0.02	0.17	−0.79
120	0.0032	1.226	1.89	1.38	0.98	0.50	0.03	0.84	−0.28	−0.76	0.00	0.20	−0.07
150	0.0032	1.225	1.42	0.82	0.83	0.48	0.06	0.80	−0.34	−0.54	0.01	0.19	−0.45
150	0.0050	1.076	1.82	1.00	1.22	0.98	0.00	0.92	−0.66	−0.64	0.00	0.04	−0.02
150	0.0080	0.9295	2.64	1.36	1.89	1.34	1.05	1.24	−0.84	−0.56	−0.31	−0.66	−0.05
150	0.0130	0.8072	4.12	1.92	2.85	2.47	1.00	2.28	−1.54	−1.30	−0.32	−1.02	−0.01
200	0.0032	1.240	1.97	1.55	0.84	0.13	0.08	0.88	−0.14	−0.64	0.02	0.18	−0.56
200	0.0050	1.101	1.58	1.08	0.87	0.50	0.02	0.75	−0.41	−0.62	0.00	0.11	−0.07
200	0.0080	0.9486	1.98	1.09	1.32	1.10	0.00	0.98	−0.59	−0.78	0.00	0.00	−0.01
200	0.0130	0.7920	1.63	1.24	0.77	0.10	0.03	0.72	0.06	−0.45	0.01	0.55	−0.01
200	0.0200	0.6872	1.89	1.38	1.05	0.69	0.06	0.75	−0.35	−0.55	−0.15	0.33	−0.02
200	0.0320	0.5807	2.33	1.61	1.47	1.10	0.47	0.85	−0.62	−0.54	−0.17	0.10	0.00
200	0.0500	0.5212	3.20	1.79	2.00	1.78	0.06	1.73	−1.22	−0.69	−0.05	1.02	0.00
200	0.0800	0.4303	3.50	1.99	2.07	1.81	0.08	2.00	−1.04	−0.86	−0.20	1.46	0.00
200	0.1300	0.3652	3.67	2.25	2.30	1.56	1.08	1.78	−1.05	−0.92	−0.21	−1.09	0.00
200	0.1800	0.3205	4.68	2.97	3.01	1.73	1.85	1.99	−0.99	−0.81	−0.35	−1.49	0.00
250	0.0050	1.106	1.59	1.25	0.78	0.29	0.06	0.59	−0.27	−0.43	0.01	0.16	−0.26
250	0.0080	0.9476	1.73	1.24	0.93	0.58	0.00	0.76	−0.50	−0.57	0.00	0.03	−0.03
250	0.0130	0.7931	2.09	1.38	1.17	0.87	0.17	1.04	0.45	−0.60	−0.06	0.72	−0.01
250	0.0200	0.6765	2.23	1.40	1.35	1.07	0.28	1.08	0.48	−0.65	−0.03	0.72	−0.01
250	0.0320	0.5679	2.17	1.46	1.29	1.01	0.16	0.95	0.39	−0.46	0.04	0.74	0.00
250	0.0500	0.4983	2.56	1.57	1.23	0.90	0.14	1.61	0.42	−0.56	−0.12	1.44	0.00
250	0.0800	0.4353	2.96	1.71	1.07	0.53	0.29	2.17	0.30	−0.43	0.03	2.10	−0.01
250	0.1300	0.3763	2.79	1.81	1.84	1.13	0.84	1.05	0.56	−0.60	−0.31	−0.58	0.00
250	0.1800	0.2954	4.13	2.39	2.49	1.51	1.36	2.27	0.84	−0.68	−0.24	−1.98	0.00
300	0.0050	1.113	2.42	2.13	0.94	0.25	0.08	0.68	−0.25	−0.39	0.02	0.16	−0.47
300	0.0080	0.9562	1.80	1.45	0.83	0.38	0.02	0.68	−0.38	−0.55	0.00	0.10	−0.05
300	0.0130	0.8024	1.95	1.45	0.97	0.61	0.00	0.85	−0.60	−0.61	0.00	0.00	−0.01
300	0.0200	0.6950	2.05	1.60	0.92	0.45	0.17	0.89	0.31	−0.44	−0.04	0.71	−0.02
300	0.0320	0.5811	2.36	1.69	1.25	0.96	0.11	1.07	0.53	−0.64	−0.03	0.68	−0.02
300	0.0500	0.4956	2.63	1.82	1.37	1.05	0.24	1.32	0.62	−0.63	−0.10	0.97	0.00
300	0.0800	0.4375	3.31	1.85	1.44	1.06	0.39	2.33	0.47	−0.61	−0.08	2.20	−0.01
300	0.1300	0.3645	2.93	1.93	1.84	1.32	0.46	1.20	0.66	−0.73	−0.21	−0.66	0.00
300	0.1800	0.3022	4.79	2.52	2.97	2.01	1.65	2.80	1.03	−0.67	−0.34	−2.49	0.00
300	0.4000	0.1520	7.17	3.06	3.84	2.51	2.25	5.22	1.39	−0.94	−0.41	−4.93	0.00
400	0.0080	1.005	2.03	1.77	0.83	0.28	0.06	0.57	−0.29	−0.42	0.01	0.14	−0.20
400	0.0130	0.8181	2.05	1.71	0.91	0.49	0.01	0.69	−0.48	−0.48	0.00	0.03	−0.01
400	0.0200	0.6991	2.35	1.77	1.15	0.83	0.00	1.03	−0.83	−0.61	0.00	0.00	0.00
400	0.0320	0.5960	2.31	1.91	0.95	0.48	0.08	0.90	0.48	−0.43	−0.05	0.62	0.00
400	0.0500	0.4920	2.51	2.05	1.08	0.62	0.26	0.97	0.59	−0.53	−0.09	0.55	0.00
400	0.0800	0.4180	3.26	2.15	1.03	0.28	0.42	2.23	0.24	−0.27	0.14	2.20	0.00
400	0.1300	0.3590	2.88	2.11	1.48	0.77	0.37	1.28	0.71	−0.65	−0.24	0.81	0.00
400	0.1800	0.3005	4.89	2.76	2.57	1.25	1.74	3.11	1.18	−0.64	−0.41	−2.77	0.00
400	0.4000	0.1541	7.61	3.56	3.27	1.33	2.25	5.88	1.25	−0.76	−0.36	−5.69	0.00
500	0.0080	0.9664	3.15	2.93	1.03	0.31	0.07	0.55	−0.16	−0.37	0.01	0.15	−0.34
500	0.0130	0.8628	2.37	2.10	0.91	0.41	0.02	0.61	−0.38	−0.47	0.01	0.10	−0.04
500	0.0200	0.7297	2.46	2.09	1.00	0.57	0.00	0.81	−0.55	−0.59	0.00	0.00	0.00
500	0.0320	0.5975	2.68	2.28	1.02	0.44	0.37	0.98	0.45	−0.39	−0.07	0.77	−0.01
500	0.0500	0.5146	2.70	2.29	1.08	0.59	0.23	0.94	0.59	−0.48	−0.12	0.53	0.00
500	0.0800	0.4219	3.11	2.48	1.01	0.35	0.18	1.58	0.35	−0.28	−0.03	1.52	0.00
500	0.1300	0.3936	3.62	2.93	1.36	0.54	0.06	1.64	0.54	−0.43	−0.10	1.48	0.00
500	0.1800	0.3095	3.70	3.13	1.78	0.73	0.79	0.88	0.73	−0.41	−0.24	−0.13	0.00
500	0.2500	0.2451	6.29	3.83	2.82	1.19	2.00	4.12	1.19	−0.56	−0.34	−3.89	0.00
650	0.0130	0.8608	2.56	2.35	0.90	0.29	0.04	0.47	−0.26	−0.38	0.01	0.09	−0.08
650	0.0200	0.7302	2.82	2.47	1.15	0.73	0.00	0.76	−0.56	−0.51	0.00	0.02	−0.02
650	0.0320	0.6111	2.95	2.56	1.16	0.70	0.00	0.90	−0.66	−0.61	0.00	0.00	0.00
650	0.0500	0.4995	3.15	2.74	1.22	0.74	0.20	0.99	0.78	−0.42	−0.12	0.42	−0.01
650	0.0800	0.3952	3.58	3.04	1.16	0.54	0.18	1.50	0.59	−0.62	0.05	1.24	0.00
650	0.1300	0.3548	3.94	3.30	1.40	0.45	0.02	1.65	0.51	−0.10	−0.10	1.56	0.00
650	0.1800	0.3200	4.16	3.57	1.80	0.80	0.61	1.16	0.82	−0.58	−0.23	−0.53	0.00
650	0.2500	0.2397	6.24	4.65	2.49	1.10	1.51	3.32	1.14	−0.48	−0.35	−3.06	0.00
650	0.4000	0.1337	8.49	6.70	3.67	1.57	2.32	3.70	1.59	−0.51	−0.54	−3.26	0.00

Table 15: The NC e^+p reduced cross section $\tilde{\sigma}_{\mathrm{NC}}(x, Q^2)$ with lepton beam polarisation $P_e = -37.0\%$ with statistical (δ_{stat}), total (δ_{tot}), total uncorrelated systematic (δ_{unc}) errors, two of its contributions from the electron energy error (δ_{unc}^{E}) and the hadronic energy error ($\delta_{\mathrm{unc}}^{h}$). The effect of the other uncorrelated systematic errors is included in δ_{unc}. In addition the correlated systematic (δ_{cor}) and its contributions from a positive variation of one standard deviation of the electron energy error ($\delta_{cor}^{E^+}$), of the polar electron angle error ($\delta_{\mathrm{cor}}^{\theta^+}$), of the hadronic energy error ($\delta_{\mathrm{cor}}^{h^+}$), of the error due to noise subtraction ($\delta_{\mathrm{cor}}^{N^+}$) and of the error due to background subtraction ($\delta_{\mathrm{cor}}^{B^+}$) are given. The normalisation and polarisation uncertainties are not included in the errors. The table continues on the next page.

Q^2 (GeV^2)	x	$\tilde{\sigma}_{\mathrm{NC}}$	δ_{tot} (%)	δ_{stat} (%)	δ_{unc} (%)	$\delta^{E}_{\mathrm{unc}}$ (%)	$\delta^{h}_{\mathrm{unc}}$ (%)	δ_{cor} (%)	$\delta^{E+}_{\mathrm{cor}}$ (%)	$\delta^{\theta+}_{\mathrm{cor}}$ (%)	$\delta^{h+}_{\mathrm{cor}}$ (%)	$\delta^{N+}_{\mathrm{cor}}$ (%)	$\delta^{B+}_{\mathrm{cor}}$ (%)
800	0.0130	0.7821	4.13	3.94	1.15	0.17	0.08	0.44	−0.26	−0.29	0.03	0.13	−0.14
800	0.0200	0.6885	3.07	2.84	1.06	0.50	0.02	0.49	−0.31	−0.37	0.00	0.05	−0.06
800	0.0320	0.5827	3.37	3.09	1.20	0.67	0.00	0.61	−0.51	−0.33	0.00	0.00	0.00
800	0.0500	0.5163	3.40	3.14	1.09	0.27	0.22	0.70	0.46	−0.30	−0.12	0.42	0.00
800	0.0800	0.4596	3.78	3.35	1.28	0.56	0.25	1.19	0.74	−0.55	−0.17	0.73	−0.01
800	0.1300	0.3435	4.73	4.04	1.57	0.33	0.51	1.90	0.58	−0.61	−0.03	1.71	0.00
800	0.1800	0.3167	4.64	4.18	1.85	0.60	0.74	0.80	0.64	−0.44	−0.16	0.09	0.00
800	0.2500	0.2177	6.15	5.17	2.49	1.17	1.27	2.24	1.22	−0.55	−0.41	−1.75	0.00
800	0.4000	0.1220	10.23	7.21	4.57	2.36	2.94	5.64	2.31	−0.64	−0.69	−5.06	0.00
1000	0.0130	0.8145	4.35	3.89	1.58	0.14	0.26	1.13	−0.13	−0.35	0.05	0.20	−1.05
1000	0.0200	0.7280	3.45	3.28	0.99	0.34	0.04	0.43	−0.21	−0.35	0.01	0.10	−0.10
1000	0.0320	0.5753	3.60	3.38	1.10	0.59	0.00	0.60	−0.34	−0.50	0.00	0.01	−0.02
1000	0.0500	0.4892	4.11	3.58	1.70	1.37	0.00	1.09	−1.02	−0.40	0.00	0.00	0.00
1000	0.0800	0.4180	4.17	3.88	1.28	0.66	0.34	0.78	0.56	−0.25	−0.23	0.43	−0.01
1000	0.1300	0.3302	5.14	4.75	1.46	0.33	0.25	1.31	0.33	−0.28	−0.05	1.24	0.00
1000	0.1800	0.2940	5.24	4.92	1.68	0.43	0.52	0.69	0.42	−0.22	−0.06	0.49	0.00
1000	0.2500	0.2301	6.08	5.56	1.98	0.61	0.78	1.45	0.86	−0.35	−0.22	−1.09	0.00
1000	0.4000	0.1182	9.76	7.75	3.92	1.42	2.74	4.46	1.27	−0.28	−0.62	−4.22	0.00
1200	0.0130	0.7796	7.54	6.75	2.51	0.05	0.29	2.23	−0.16	−0.35	0.04	0.22	−2.19
1200	0.0200	0.6598	4.48	4.32	1.09	0.15	0.09	0.48	0.17	−0.35	0.02	0.13	−0.24
1200	0.0320	0.6262	3.91	3.76	0.96	0.48	0.02	0.47	−0.27	−0.38	0.01	0.06	0.00
1200	0.0500	0.5134	4.22	3.95	1.28	0.95	0.00	0.74	−0.52	−0.53	0.00	0.00	0.00
1200	0.0800	0.4159	4.54	4.33	1.11	0.64	0.03	0.75	0.46	−0.26	−0.05	0.53	0.00
1200	0.1300	0.3167	5.68	5.38	1.62	0.99	0.26	0.86	0.53	−0.24	−0.05	0.63	0.00
1200	0.1800	0.2902	5.80	5.47	1.54	0.64	0.18	1.14	0.55	−0.32	−0.19	0.93	0.00
1200	0.2500	0.2617	6.17	5.62	2.28	1.37	1.01	1.09	0.89	−0.30	−0.31	−0.44	0.00
1200	0.4000	0.1060	10.52	8.59	4.01	2.31	2.41	4.55	1.41	−0.53	−0.41	−4.28	0.00
1500	0.0200	0.6541	5.65	5.31	1.75	0.19	0.19	0.83	0.24	−0.20	0.04	0.20	−0.74
1500	0.0320	0.5841	5.32	5.22	0.95	0.07	0.04	0.35	−0.14	−0.30	0.01	0.11	−0.05
1500	0.0500	0.5171	4.72	4.55	1.10	0.61	0.00	0.59	−0.21	−0.55	0.00	0.01	0.00
1500	0.0800	0.4591	5.38	5.12	1.49	1.13	0.11	0.72	0.61	−0.19	−0.09	0.32	0.00
1500	0.1300	0.2984	6.60	6.35	1.54	0.76	0.12	0.91	0.52	−0.31	−0.09	0.68	0.00
1500	0.1800	0.2857	6.66	6.32	1.75	0.97	0.08	1.13	0.60	−0.17	0.05	0.94	0.00
1500	0.2500	0.2522	6.93	6.39	2.49	1.57	1.13	1.04	0.89	−0.16	−0.28	−0.42	0.00
1500	0.4000	0.1182	10.27	8.89	3.60	2.07	1.88	3.67	1.15	−0.19	−0.52	−3.44	0.00
1500	0.6500	0.01535	20.35	16.04	7.26	4.36	4.95	10.19	3.17	−0.56	−1.15	−9.60	0.00
2000	0.0219	0.6530	9.14	8.55	2.83	0.58	0.21	1.52	0.08	−0.07	0.05	0.19	−1.50
2000	0.0320	0.5371	6.19	5.99	1.46	0.20	0.07	0.59	−0.23	−0.46	0.01	0.10	−0.26
2000	0.0500	0.5043	5.78	5.63	1.22	0.64	0.01	0.40	−0.34	−0.21	0.00	0.05	0.00
2000	0.0800	0.4257	5.74	5.55	1.25	0.63	0.00	0.71	−0.37	−0.61	0.00	0.00	0.00
2000	0.1300	0.3059	7.45	7.22	1.72	0.97	0.05	0.69	0.37	−0.18	−0.09	0.55	0.00
2000	0.1800	0.2879	7.67	7.37	1.72	0.68	0.28	1.27	0.45	−0.26	0.05	1.16	0.00
2000	0.2500	0.2094	8.29	7.85	2.40	1.55	0.82	1.15	1.05	−0.32	−0.28	0.18	0.00
2000	0.4000	0.1157	11.03	9.92	3.69	2.16	1.86	3.12	1.33	−0.20	−0.36	−2.79	0.00
2000	0.6500	0.01290	23.59	19.28	8.15	5.05	5.54	10.87	3.09	−0.42	−1.40	−10.32	0.00
3000	0.0320	0.5739	6.00	5.61	1.92	0.21	0.12	0.92	−0.22	−0.28	0.02	0.12	−0.85
3000	0.0500	0.4657	5.21	5.02	1.34	0.13	0.05	0.35	0.12	−0.31	0.02	0.10	−0.06
3000	0.0800	0.4009	5.54	5.36	1.29	0.58	0.01	0.55	−0.25	−0.49	0.00	0.03	−0.02
3000	0.1300	0.3251	6.63	6.38	1.64	0.75	0.00	0.77	−0.61	−0.48	0.00	0.00	0.00
3000	0.1800	0.2637	7.49	7.11	2.14	1.51	0.09	1.02	0.89	−0.16	−0.03	0.46	0.00
3000	0.2500	0.2157	7.43	7.07	2.08	1.33	0.17	0.97	0.76	−0.13	−0.10	0.58	0.00
3000	0.4000	0.1236	9.46	8.29	3.88	2.60	1.79	2.39	1.54	−0.07	−0.48	−1.77	0.00
3000	0.6500	0.01266	21.18	16.94	8.41	5.43	5.69	9.53	3.46	−0.23	−1.22	−8.79	0.00
5000	0.0547	0.4226	8.31	7.86	2.36	0.23	0.08	1.32	0.11	−0.19	0.03	0.09	−1.30
5000	0.0800	0.3438	6.58	6.38	1.57	0.04	0.06	0.38	0.03	−0.32	−0.02	0.07	−0.19
5000	0.1300	0.3067	7.57	7.32	1.83	0.35	0.00	0.55	0.24	−0.49	0.00	0.01	0.00
5000	0.1800	0.2572	8.45	8.19	1.98	0.69	0.00	0.71	−0.49	−0.51	0.00	0.00	0.00
5000	0.2500	0.2211	9.24	8.92	2.30	1.06	0.00	0.72	0.71	−0.06	0.00	0.00	0.00
5000	0.4000	0.09421	12.41	11.65	3.85	2.29	1.77	1.83	1.42	0.17	−0.59	−0.98	0.00
5000	0.6500	0.006800	29.05	27.87	6.12	3.32	3.81	5.48	1.57	0.18	−0.94	−5.17	0.00
8000	0.0875	0.2513	16.23	15.58	3.61	0.36	0.12	2.80	−0.07	−0.23	0.09	0.08	−2.79
8000	0.1300	0.2539	11.45	11.14	2.57	0.57	0.06	0.62	0.35	−0.47	0.03	0.04	−0.20
8000	0.1800	0.2290	11.56	11.31	2.40	0.22	0.01	0.32	0.28	−0.14	0.00	0.02	0.00
8000	0.2500	0.2172	11.35	11.01	2.71	1.07	0.00	0.65	−0.42	−0.50	0.00	0.00	0.00
8000	0.4000	0.1002	15.96	15.10	4.67	3.42	0.00	2.21	2.18	0.40	0.00	0.00	0.00
8000	0.6500	0.01154	26.40	25.07	7.14	4.69	3.58	4.23	2.92	−0.16	−1.15	−2.84	0.00
12000	0.1300	0.2029	29.92	28.52	9.03	0.10	0.10	0.78	−0.60	−0.21	0.03	0.09	−0.44
12000	0.1800	0.2060	17.86	17.53	3.05	0.76	0.07	1.53	0.18	−0.41	0.02	0.07	−1.46
12000	0.2500	0.1398	18.87	18.70	2.49	0.91	0.02	0.57	0.48	−0.30	0.00	0.04	0.00
12000	0.4000	0.07077	24.82	24.35	4.53	3.49	0.00	1.56	1.52	0.34	0.00	0.00	0.00
12000	0.6500	0.007830	45.47	44.93	6.39	4.77	2.77	2.84	2.39	0.29	−0.64	−1.37	0.00
20000	0.2500	0.1059	33.02	32.86	3.23	1.72	0.09	0.70	0.56	−0.35	0.01	0.09	−0.22
20000	0.4000	0.07575	32.17	31.82	4.62	3.56	0.03	1.17	1.16	0.12	0.01	0.03	0.00
20000	0.6500	0.01318	59.92	57.87	14.88	14.39	0.00	4.56	4.12	1.95	0.00	0.00	0.00

Table 15: continued.

Q^2 (GeV^2)	x	$\tilde{\sigma}_{\mathrm{NC}}$	δ_{tot} (%)	δ_{stat} (%)	δ_{unc} (%)	$\delta^{E}_{\mathrm{unc}}$ (%)	$\delta^{h}_{\mathrm{unc}}$ (%)	δ_{cor} (%)	$\delta^{E^+}_{\mathrm{cor}}$ (%)	$\delta^{\theta^+}_{\mathrm{cor}}$ (%)	$\delta^{h^+}_{\mathrm{cor}}$ (%)	$\delta^{N^+}_{\mathrm{cor}}$ (%)	$\delta^{B^+}_{\mathrm{cor}}$ (%)
120	0.0020	1.327	1.63	0.87	0.82	0.33	0.08	1.11	−0.22	−0.70	0.02	0.19	−0.81
120	0.0032	1.169	1.98	1.27	1.24	0.91	0.04	0.88	−0.60	−0.61	0.01	0.16	−0.12
150	0.0032	1.200	1.36	0.74	0.84	0.49	0.06	0.77	−0.38	−0.53	0.01	0.16	−0.38
150	0.0050	1.075	1.59	0.88	1.06	0.78	0.00	0.79	−0.43	−0.66	0.00	0.03	−0.03
150	0.0080	0.9349	2.67	1.22	2.00	1.68	0.70	1.29	−1.12	−0.56	−0.19	−0.26	−0.04
150	0.0130	0.7687	3.92	1.71	2.72	2.32	1.01	2.24	−1.38	−1.43	−0.41	−0.94	−0.01
200	0.0032	1.201	1.86	1.40	0.85	0.12	0.08	0.88	−0.11	−0.62	0.02	0.17	−0.60
200	0.0050	1.073	1.51	0.97	0.89	0.55	0.04	0.74	−0.39	−0.61	0.01	0.12	−0.07
200	0.0080	0.9326	1.87	0.98	1.25	1.01	0.00	1.00	−0.58	−0.82	0.00	0.00	0.00
200	0.0130	0.7830	1.54	1.11	0.76	0.03	0.05	0.75	−0.11	−0.36	−0.07	0.64	−0.01
200	0.0200	0.6755	1.81	1.22	1.09	0.75	0.04	0.76	−0.46	−0.44	−0.04	0.42	0.00
200	0.0320	0.5719	2.14	1.40	1.37	0.91	0.59	0.85	−0.61	−0.56	−0.17	0.14	0.00
200	0.0500	0.4925	2.99	1.62	1.81	1.56	0.10	1.75	−0.92	−0.89	−0.11	1.18	0.00
200	0.0800	0.4300	3.38	1.77	2.07	1.80	0.24	2.00	−1.30	−0.64	−0.12	1.37	0.00
200	0.1300	0.3489	3.50	1.96	2.34	1.75	0.87	1.70	−0.91	−0.89	−0.32	−1.08	0.00
200	0.1800	0.2994	4.43	2.68	2.95	1.52	1.94	1.93	−0.80	−1.21	−0.34	−1.23	0.00
250	0.0050	1.102	1.53	1.13	0.78	0.29	0.06	0.67	−0.28	−0.47	0.01	0.16	−0.34
250	0.0080	0.9413	1.63	1.10	0.97	0.64	0.01	0.72	−0.56	−0.45	0.00	0.03	−0.01
250	0.0130	0.7973	2.07	1.22	1.24	0.94	0.25	1.13	0.50	−0.60	0.03	0.81	−0.02
250	0.0200	0.6883	2.11	1.25	1.33	1.08	0.12	1.06	0.51	−0.67	−0.05	0.65	−0.01
250	0.0320	0.5715	2.05	1.31	1.13	0.81	0.13	1.09	0.35	−0.50	−0.01	0.91	0.00
250	0.0500	0.4919	2.42	1.45	1.21	0.88	0.15	1.51	0.36	−0.58	−0.06	1.34	0.00
250	0.0800	0.4249	2.91	1.46	1.07	0.58	0.13	2.28	0.39	−0.57	−0.08	2.17	0.00
250	0.1300	0.3516	2.52	1.60	1.72	1.12	0.56	0.93	0.48	−0.54	−0.17	−0.55	0.00
250	0.1800	0.2913	4.40	2.20	2.99	1.90	1.81	2.36	1.18	−0.86	−0.41	−1.80	0.00
300	0.0050	1.117	2.27	1.94	0.95	0.31	0.06	0.69	−0.31	−0.36	0.02	0.14	−0.48
300	0.0080	0.9592	1.64	1.29	0.77	0.24	0.02	0.67	−0.24	−0.62	0.00	0.09	−0.05
300	0.0130	0.7840	1.85	1.31	0.99	0.64	0.00	0.84	−0.64	−0.54	0.00	0.00	−0.01
300	0.0200	0.7024	1.94	1.44	0.98	0.59	0.08	0.85	0.39	−0.47	0.01	0.58	−0.01
300	0.0320	0.5671	2.05	1.51	1.09	0.72	0.13	0.86	0.35	−0.49	−0.02	0.62	0.00
300	0.0500	0.4836	2.42	1.66	1.25	0.92	0.16	1.23	0.38	−0.48	−0.02	1.07	0.00
300	0.0800	0.4296	3.13	1.71	1.44	1.10	0.23	2.20	0.54	−0.75	−0.12	1.99	−0.01
300	0.1300	0.3649	2.92	1.75	1.96	1.46	0.54	1.26	0.70	−0.74	−0.19	0.72	0.00
300	0.1800	0.3024	4.73	2.26	2.92	2.00	1.57	2.96	1.10	−0.68	−0.26	−2.65	0.00
300	0.4000	0.1446	6.55	2.95	3.64	2.32	2.11	4.58	1.31	−1.09	−0.49	−4.22	0.00
400	0.0080	0.9652	1.89	1.60	0.81	0.24	0.06	0.58	−0.25	−0.45	0.01	0.14	−0.23
400	0.0130	0.8484	1.85	1.49	0.88	0.43	0.01	0.65	−0.42	−0.50	0.00	0.03	−0.01
400	0.0200	0.6976	2.23	1.57	1.19	0.88	0.00	1.05	−0.88	−0.57	0.00	0.00	0.00
400	0.0320	0.5786	2.19	1.68	0.98	0.50	0.21	1.00	0.49	−0.52	0.04	0.69	−0.01
400	0.0500	0.4884	2.40	1.85	1.15	0.70	0.36	1.01	0.68	−0.46	−0.09	0.58	0.00
400	0.0800	0.4249	2.87	2.00	0.99	0.23	0.35	1.81	0.20	−0.32	−0.08	1.76	0.00
400	0.1300	0.3464	2.61	1.94	1.38	0.53	0.42	1.06	0.49	−0.34	−0.09	0.88	0.00
400	0.1800	0.3011	4.54	2.51	2.37	0.99	1.62	2.95	0.93	−0.50	−0.36	−2.73	0.00
400	0.4000	0.1405	6.94	3.13	3.34	1.40	2.31	5.22	1.31	−0.80	−0.53	−4.96	0.00
500	0.0080	0.9649	2.94	2.69	1.02	0.31	0.10	0.59	−0.15	−0.47	0.01	0.16	−0.30
500	0.0130	0.8436	2.08	1.85	0.83	0.19	0.01	0.47	−0.13	−0.45	0.01	0.08	−0.04
500	0.0200	0.7286	2.35	1.89	1.09	0.71	0.00	0.86	−0.70	−0.49	0.00	0.00	0.00
500	0.0320	0.5997	2.34	1.95	1.00	0.40	0.35	0.84	0.39	−0.35	0.08	0.65	−0.02
500	0.0500	0.5235	2.59	2.06	1.21	0.75	0.36	1.01	0.75	−0.49	−0.19	0.41	0.00
500	0.0800	0.4414	2.96	2.21	1.04	0.34	0.35	1.67	0.34	−0.37	0.10	1.59	0.00
500	0.1300	0.3658	3.33	2.49	1.46	0.74	0.10	1.66	0.74	−0.61	0.08	1.36	0.00
500	0.1800	0.3056	3.61	2.91	1.88	0.82	0.92	1.04	0.82	−0.43	−0.20	−0.44	0.00
500	0.2500	0.2453	6.36	3.60	2.87	1.24	2.04	4.38	1.24	−0.54	−0.48	−4.14	0.00
650	0.0130	0.8253	2.35	2.14	0.86	0.10	0.06	0.44	−0.15	−0.36	0.01	0.14	−0.14
650	0.0200	0.7135	2.51	2.21	1.00	0.47	0.01	0.62	−0.30	−0.55	0.00	0.03	−0.02
650	0.0320	0.6530	2.88	2.28	1.37	1.00	0.00	1.10	−0.95	−0.56	0.00	0.00	0.00
650	0.0500	0.5198	2.77	2.38	1.09	0.54	0.11	0.88	0.61	−0.31	0.05	0.55	0.00
650	0.0800	0.4273	3.24	2.68	1.10	0.43	0.06	1.44	0.44	−0.42	0.06	1.30	0.00
650	0.1300	0.3794	3.85	3.20	1.51	0.70	0.08	1.54	0.74	−0.34	−0.11	1.29	0.00
650	0.1800	0.3399	3.58	3.07	1.63	0.52	0.41	0.87	0.55	−0.38	−0.26	0.49	0.00
650	0.2500	0.2335	5.75	3.85	2.74	1.46	1.63	3.27	1.46	−0.59	−0.40	−2.84	0.00
650	0.4000	0.1321	8.83	5.35	3.95	1.34	2.84	5.80	1.36	−0.64	−0.64	−5.57	0.00

Table 16: The NC e^+p reduced cross section $\tilde{\sigma}_{\mathrm{NC}}(x, Q^2)$ with lepton beam polarisation $P_e = +32.5\%$ with statistical (δ_{stat}), total (δ_{tot}), total uncorrelated systematic (δ_{unc}) errors, two of its contributions from the electron energy error (δ^{E}_{unc}) and the hadronic energy error ($\delta^{h}_{\mathrm{unc}}$). The effect of the other uncorrelated systematic errors is included in δ_{unc}. In addition the correlated systematic (δ_{cor}) and its contributions from a positive variation of one standard deviation of the electron energy error ($\delta^{E^+}_{cor}$), of the polar electron angle error ($\delta^{\theta^+}_{\mathrm{cor}}$), of the hadronic energy error ($\delta^{h^+}_{\mathrm{cor}}$), of the error due to noise subtraction ($\delta^{N^+}_{\mathrm{cor}}$) and of the error due to background subtraction ($\delta^{B^+}_{\mathrm{cor}}$) are given. The normalisation and polarisation uncertainties are not included in the errors. The table continues on the next page.

Q^2 (GeV^2)	x	$\tilde{\sigma}_{NC}$	δ_{tot} (%)	δ_{stat} (%)	δ_{unc} (%)	δ^{E}_{unc} (%)	δ^{h}_{unc} (%)	δ_{cor} (%)	$\delta^{E^+}_{cor}$ (%)	$\delta^{\theta^+}_{cor}$ (%)	$\delta^{h^+}_{cor}$ (%)	$\delta^{N^+}_{cor}$ (%)	$\delta^{B^+}_{cor}$ (%)
800	0.0130	0.8259	3.73	3.47	1.24	0.16	0.09	0.60	−0.32	−0.41	0.03	0.16	−0.26
800	0.0200	0.6916	2.75	2.52	1.00	0.38	0.01	0.45	−0.28	−0.34	0.01	0.09	−0.04
800	0.0320	0.6241	2.99	2.60	1.26	0.77	0.00	0.78	−0.52	−0.59	0.00	0.00	0.00
800	0.0500	0.5204	3.22	2.90	1.11	0.20	0.34	0.84	0.30	−0.28	0.16	0.71	0.00
800	0.0800	0.4397	3.47	3.06	1.24	0.43	0.30	1.09	0.73	−0.34	−0.09	0.73	0.00
800	0.1300	0.3576	4.12	3.54	1.54	0.53	0.05	1.43	0.68	−0.45	−0.18	1.17	0.00
800	0.1800	0.3237	4.19	3.68	1.73	0.56	0.36	1.04	0.75	−0.50	−0.12	0.51	0.00
800	0.2500	0.2512	5.24	4.23	2.39	0.80	1.38	1.96	0.92	−0.36	−0.45	−1.63	0.00
800	0.4000	0.1186	9.66	6.45	3.98	1.76	2.44	5.99	1.72	−0.50	−0.58	−5.68	0.00
1000	0.0130	0.7638	4.22	3.64	1.68	0.20	0.22	1.33	−0.09	−0.25	0.04	0.21	−1.29
1000	0.0200	0.7122	3.17	2.97	0.99	0.29	0.06	0.52	−0.22	−0.43	0.01	0.15	−0.14
1000	0.0320	0.6310	3.14	2.86	1.16	0.70	0.00	0.56	−0.47	−0.32	0.00	0.02	0.00
1000	0.0500	0.5286	3.51	3.09	1.51	1.13	0.00	0.70	−0.44	−0.54	0.00	0.00	0.00
1000	0.0800	0.4441	3.64	3.40	1.15	0.38	0.25	0.55	0.24	−0.20	−0.06	0.44	0.00
1000	0.1300	0.3397	4.88	4.49	1.44	0.28	0.20	1.26	0.28	0.09	0.14	1.22	0.00
1000	0.1800	0.2968	4.73	4.35	1.59	0.25	0.29	0.98	0.50	−0.42	−0.30	0.67	0.00
1000	0.2500	0.2495	5.49	4.74	2.35	1.00	1.26	1.48	1.06	−0.48	−0.21	−0.89	0.00
1000	0.4000	0.1348	10.49	8.52	3.77	1.36	2.54	4.81	1.50	−0.50	−0.65	−4.49	0.00
1200	0.0130	0.8534	6.63	5.78	2.56	0.20	0.30	1.98	−0.13	−0.12	0.07	0.24	−1.96
1200	0.0200	0.7304	3.83	3.64	1.12	0.23	0.07	0.42	−0.21	−0.25	0.02	0.12	−0.23
1200	0.0320	0.5777	3.65	3.51	0.93	0.40	0.02	0.45	−0.23	−0.39	0.00	0.07	−0.01
1200	0.0500	0.5028	3.84	3.52	1.33	1.00	0.00	0.74	−0.61	−0.42	0.00	0.00	−0.01
1200	0.0800	0.4340	4.08	3.76	1.35	0.91	0.20	0.82	0.62	−0.33	−0.12	0.40	0.00
1200	0.1300	0.3561	4.93	4.55	1.63	1.03	0.05	0.95	0.63	−0.33	−0.04	0.64	0.00
1200	0.1800	0.3359	5.64	5.25	1.60	0.76	0.23	1.28	0.51	−0.28	−0.11	1.13	−0.02
1200	0.2500	0.2341	6.45	5.97	2.26	1.39	0.93	0.94	0.77	−0.26	−0.25	−0.38	0.00
1200	0.4000	0.1074	10.58	7.57	4.67	2.83	2.99	5.72	1.85	−0.52	−0.69	−5.34	0.00
1500	0.0200	0.6877	5.07	4.63	1.84	0.25	0.22	0.95	0.22	−0.32	0.06	0.20	−0.83
1500	0.0320	0.5893	4.45	4.29	1.05	0.46	0.05	0.54	−0.34	−0.40	0.02	0.12	−0.02
1500	0.0500	0.5262	4.18	4.00	1.11	0.63	0.00	0.49	−0.35	−0.33	0.00	0.02	0.00
1500	0.0800	0.4314	4.55	4.31	1.26	0.80	0.14	0.75	0.58	−0.20	−0.11	0.42	0.00
1500	0.1300	0.3534	5.50	5.16	1.71	0.94	0.15	0.82	0.50	−0.20	0.11	0.61	0.00
1500	0.1800	0.3074	5.71	5.38	1.60	0.67	0.13	1.04	0.48	−0.21	0.09	0.89	0.00
1500	0.2500	0.2088	6.79	6.22	2.47	1.56	1.09	1.11	0.98	−0.22	−0.44	−0.21	0.00
1500	0.4000	0.1242	9.25	7.55	3.84	2.20	2.17	3.71	1.26	−0.28	−0.50	−3.45	0.00
1500	0.6500	0.01439	19.87	14.78	7.35	4.62	4.82	11.06	2.53	−0.14	−0.88	−10.73	0.00
2000	0.0219	0.7131	8.25	7.48	3.03	0.74	0.22	1.71	0.36	−0.20	0.06	0.22	−1.64
2000	0.0320	0.5443	5.46	5.24	1.47	0.26	0.10	0.44	−0.14	−0.37	0.03	0.12	−0.16
2000	0.0500	0.5434	4.99	4.83	1.21	0.25	0.01	0.36	−0.18	−0.31	0.01	0.03	0.00
2000	0.0800	0.4166	5.32	5.03	1.54	1.09	0.00	0.79	−0.53	−0.58	0.00	0.00	0.00
2000	0.1300	0.3708	6.98	6.71	1.77	1.02	0.13	0.78	0.55	−0.26	−0.08	0.48	0.00
2000	0.1800	0.3058	6.68	6.34	1.68	0.51	0.36	1.28	0.41	−0.28	0.33	1.12	0.00
2000	0.2500	0.2529	7.05	6.45	2.60	1.75	0.98	1.15	1.09	−0.27	−0.19	−0.16	0.00
2000	0.4000	0.1326	9.81	8.15	4.34	2.87	2.26	3.33	1.81	−0.31	−0.80	−2.66	0.00
2000	0.6500	0.01436	21.57	17.19	7.30	4.45	4.75	10.80	2.64	0.23	−0.78	−10.44	0.00
3000	0.0320	0.5957	5.43	5.01	1.86	0.25	0.14	0.96	0.15	−0.26	0.04	0.13	−0.90
3000	0.0500	0.5259	4.47	4.22	1.42	0.46	0.08	0.41	−0.21	−0.34	0.01	0.08	−0.06
3000	0.0800	0.4568	4.65	4.45	1.25	0.49	0.01	0.57	−0.38	−0.42	0.00	0.02	0.00
3000	0.1300	0.3442	5.80	5.53	1.62	0.72	0.00	0.57	−0.43	−0.37	0.00	0.00	0.00
3000	0.1800	0.3252	7.51	7.17	2.03	1.34	0.11	0.92	0.69	−0.14	0.05	0.58	0.00
3000	0.2500	0.2280	6.61	6.20	2.07	1.31	0.22	0.96	0.76	−0.08	−0.10	0.58	0.00
3000	0.4000	0.1160	9.03	7.64	4.01	2.65	2.00	2.65	1.49	−0.13	−0.52	−2.13	0.00
3000	0.6500	0.01250	19.52	15.66	7.85	5.15	5.08	8.63	3.17	−0.28	−1.52	−7.87	0.00
5000	0.0547	0.4956	7.11	6.66	2.23	0.73	0.13	1.11	0.19	−0.43	0.07	0.11	−0.99
5000	0.0800	0.4546	5.24	4.98	1.59	0.28	0.05	0.40	−0.19	−0.33	0.02	0.07	−0.12
5000	0.1300	0.3598	6.29	5.99	1.85	0.49	0.00	0.53	0.30	−0.44	0.00	0.02	0.00
5000	0.1800	0.3183	6.91	6.59	1.99	0.71	0.00	0.49	−0.35	−0.34	0.00	0.00	0.00
5000	0.2500	0.2062	8.71	8.44	2.11	0.46	0.00	0.44	0.42	−0.12	0.00	0.00	0.00
5000	0.4000	0.1106	10.37	9.78	3.26	1.61	1.17	1.18	1.03	0.04	−0.31	−0.48	0.00
5000	0.6500	0.01196	21.05	18.62	7.25	4.45	4.58	6.62	2.40	−0.25	−1.37	−6.01	0.00
8000	0.0875	0.4227	11.07	10.53	3.08	0.73	0.09	1.49	0.25	−0.25	0.03	0.09	−1.45
8000	0.1300	0.3113	9.37	9.01	2.53	0.30	0.06	0.39	−0.16	−0.24	0.01	0.09	−0.25
8000	0.1800	0.2841	9.36	9.01	2.42	0.34	0.00	0.68	0.22	−0.64	0.00	0.01	0.00
8000	0.2500	0.2178	13.40	13.15	2.50	0.22	0.00	0.52	0.45	−0.26	0.00	0.00	0.00
8000	0.4000	0.09797	14.43	13.63	4.43	3.07	0.00	1.67	1.61	0.43	0.00	0.00	0.00
8000	0.6500	0.01497	21.32	19.28	7.87	5.03	4.54	4.58	2.51	0.39	−1.13	−3.64	0.00
12000	0.1300	0.2111	28.35	27.73	5.32	1.04	0.10	2.49	−1.16	−0.65	−0.02	0.09	−2.10
12000	0.1800	0.2186	15.26	15.03	2.52	0.67	0.07	0.70	0.41	−0.49	0.02	0.08	−0.28
12000	0.2500	0.1659	15.54	15.33	2.47	0.86	0.03	0.49	0.36	−0.34	0.00	0.03	0.00
12000	0.4000	0.1208	17.61	16.94	4.56	3.55	0.00	1.56	1.51	0.40	0.00	0.00	0.00
12000	0.6500	0.02165	25.59	24.29	7.16	5.55	3.22	3.62	3.05	0.24	−0.82	−1.75	0.00
20000	0.2500	0.1446	25.36	25.06	3.73	2.53	0.10	1.10	0.98	0.36	0.06	0.11	−0.30
20000	0.4000	0.1094	24.06	23.67	4.25	3.08	0.02	0.79	0.77	−0.19	0.01	0.03	0.00
20000	0.6500	0.006690	72.84	71.00	15.42	14.93	0.00	5.22	4.59	2.49	0.00	0.00	0.00
30000	0.4000	0.08055	51.57	51.28	5.30	3.09	0.08	1.15	0.99	−0.54	0.02	0.06	−0.23
30000	0.6500	0.01363	71.77	70.94	10.44	9.27	0.00	3.06	2.79	1.26	0.00	0.00	0.00

Table 16: continued.

Q^2 (GeV^2)	x	y	$\mathrm{d}^2\sigma_{\mathrm{CC}}/\mathrm{d}x\mathrm{d}Q^2$ ($\mathrm{pb}/\mathrm{GeV}^2$)	δ_{tot} (%)	δ_{stat} (%)	δ_{unc} (%)	δ^h_{unc} (%)	δ_{cor} (%)	$\delta^{V^+}_{\mathrm{cor}}$ (%)	$\delta^{h^+}_{\mathrm{cor}}$ (%)	$\delta^{N^+}_{\mathrm{cor}}$ (%)	$\delta^{B^+}_{\mathrm{cor}}$ (%)
300	0.008	0.369	2.01	49.9	40.7	23.4	1.6	17.0	15.5	0.3	−1.0	−5.8
300	0.013	0.227	0.923	20.6	14.4	10.8	2.7	9.8	9.4	−0.9	−0.3	−1.2
300	0.032	0.092	0.305	15.9	14.0	5.3	2.0	5.5	4.7	−0.4	0.4	−2.4
300	0.080	0.037	$0.776 \cdot 10^{-1}$	15.4	13.5	5.1	2.8	5.3	1.4	−0.4	−4.3	−1.9
500	0.013	0.379	0.790	14.9	9.8	7.1	2.3	8.7	8.5	−0.4	−0.6	−0.5
500	0.032	0.154	0.250	9.3	8.1	3.2	1.5	3.2	2.9	−0.7	0.1	−0.2
500	0.080	0.062	$0.621 \cdot 10^{-1}$	10.4	9.3	4.2	2.4	1.7	0.8	−0.6	−0.2	−0.1
500	0.130	0.038	$0.345 \cdot 10^{-1}$	25.4	21.4	5.3	0.8	12.7	0.1	0.6	−12.3	0.0
1000	0.013	0.757	0.476	14.1	10.2	5.7	1.7	7.9	7.7	−0.8	0.1	−0.5
1000	0.032	0.308	0.230	7.2	6.2	2.8	1.8	2.2	1.9	−0.4	0.3	−0.1
1000	0.080	0.123	$0.710 \cdot 10^{-1}$	7.2	6.4	2.9	1.1	1.4	0.4	−0.4	0.9	−0.1
1000	0.130	0.076	$0.336 \cdot 10^{-1}$	12.3	10.9	3.8	1.5	4.1	0.0	−0.1	−3.7	0.0
2000	0.032	0.615	0.148	6.8	5.8	2.6	1.0	2.2	1.9	−0.4	−0.4	0.0
2000	0.080	0.246	$0.573 \cdot 10^{-1}$	5.8	5.2	2.1	0.5	1.1	0.1	−0.1	0.7	0.0
2000	0.130	0.152	$0.290 \cdot 10^{-1}$	8.1	7.4	3.1	0.9	1.2	−0.0	−0.4	−0.3	0.0
2000	0.250	0.079	$0.105 \cdot 10^{-1}$	17.8	14.6	4.0	0.6	9.3	0.0	0.4	−9.1	0.0
3000	0.080	0.369	$0.397 \cdot 10^{-1}$	5.7	5.2	2.0	0.2	1.2	−0.1	0.2	0.9	0.0
3000	0.130	0.227	$0.234 \cdot 10^{-1}$	6.6	6.1	2.1	0.3	1.3	−0.0	−0.1	0.8	0.0
3000	0.250	0.118	$0.858 \cdot 10^{-2}$	9.9	9.2	2.9	0.5	2.5	0.0	0.2	−2.1	−0.2
5000	0.080	0.615	$0.261 \cdot 10^{-1}$	7.2	6.6	2.4	0.9	1.5	0.1	0.3	1.1	0.0
5000	0.130	0.379	$0.156 \cdot 10^{-1}$	6.4	5.8	2.1	0.2	1.2	−0.0	0.1	0.7	0.0
5000	0.250	0.197	$0.603 \cdot 10^{-2}$	7.7	7.1	2.5	1.5	1.2	−0.0	0.4	0.4	−0.1
5000	0.400	0.123	$0.183 \cdot 10^{-2}$	21.5	19.2	5.2	4.5	8.0	0.0	0.9	−7.4	0.0
8000	0.130	0.606	$0.105 \cdot 10^{-1}$	8.4	7.1	3.6	2.7	2.3	−0.1	1.0	1.8	0.0
8000	0.250	0.315	$0.320 \cdot 10^{-2}$	8.1	7.3	3.0	2.1	1.7	−0.0	0.6	1.2	0.0
8000	0.400	0.197	$0.131 \cdot 10^{-2}$	14.8	13.4	5.5	5.1	2.7	0.0	1.4	−0.8	0.0
15000	0.250	0.591	$0.192 \cdot 10^{-2}$	10.4	8.4	5.4	4.7	2.8	0.0	1.2	2.1	0.0
15000	0.400	0.369	$0.481 \cdot 10^{-3}$	13.1	11.1	6.2	5.7	2.9	0.0	1.9	1.5	0.0
30000	0.400	0.738	$0.200 \cdot 10^{-3}$	20.9	17.2	10.2	9.7	5.8	0.0	3.2	3.9	0.0

Table 17: The CC e^-p cross section $\mathrm{d}^2\sigma_{\mathrm{CC}}/\mathrm{d}x\mathrm{d}Q^2$ for lepton beam polarisation $P_e = -25.8\%$ with statistical (δ_{stat}), total (δ_{tot}), total uncorrelated systematic (δ_{unc}) errors and one of its contributions from the hadronic energy error (δ^h_{unc}). The effect of the other uncorrelated systematic errors is included in δ_{unc}. In addition the correlated systematic (δ_{cor}) and its contributions from a positive variation of one standard deviation of the cuts against photoproduction ($\delta^{V^+}_{\mathrm{cor}}$), of the hadronic energy error ($\delta^{h^+}_{\mathrm{cor}}$), of the error due to noise subtraction ($\delta^{N^+}_{\mathrm{cor}}$) and of the error due to background subtraction ($\delta^{B^+}_{\mathrm{cor}}$) are given. The normalisation and polarisation uncertainties are not included in the errors.

Q^2 (GeV^2)	x	y	$\mathrm{d}^2\sigma_{CC}/\mathrm{d}x\mathrm{d}Q^2$ ($\mathrm{pb}/\mathrm{GeV}^2$)	δ_{tot} (%)	δ_{stat} (%)	δ_{unc} (%)	δ_{unc}^{h} (%)	δ_{cor} (%)	δ_{cor}^{V+} (%)	δ_{cor}^{h+} (%)	δ_{cor}^{N+} (%)	δ_{cor}^{B+} (%)
300	0.008	0.369	1.16	56.6	47.2	26.2	1.7	17.2	15.3	−0.8	−0.9	−0.9
300	0.013	0.227	0.423	38.3	35.0	11.5	1.9	10.6	9.7	−0.4	0.4	−2.5
300	0.032	0.092	0.127	26.0	24.9	5.0	1.4	5.5	4.8	−0.4	0.8	−1.5
300	0.080	0.037	$0.468 \cdot 10^{-1}$	26.1	25.2	4.9	2.0	4.6	1.5	−0.5	−3.0	−2.3
500	0.013	0.379	0.407	23.4	20.5	7.1	2.6	8.6	8.3	−0.8	−0.9	−1.1
500	0.032	0.154	0.141	17.1	16.3	3.7	2.3	3.6	3.3	−0.5	−0.3	−0.6
500	0.080	0.062	$0.364 \cdot 10^{-1}$	19.0	18.4	4.0	1.9	1.9	0.7	−0.4	−0.1	−1.0
500	0.130	0.038	$0.132 \cdot 10^{-1}$	52.4	50.5	6.0	2.1	12.7	0.3	−0.7	−12.3	0.0
1000	0.013	0.757	0.283	22.4	19.9	6.2	2.1	8.2	8.1	−0.7	−0.3	0.0
1000	0.032	0.308	0.115	13.3	12.8	2.5	1.4	2.2	1.8	−0.3	0.6	−0.2
1000	0.080	0.123	$0.441 \cdot 10^{-1}$	12.5	12.0	2.8	0.4	1.6	0.3	−0.2	1.1	−0.3
1000	0.130	0.076	$0.128 \cdot 10^{-1}$	26.8	26.3	3.8	1.4	3.4	0.1	0.1	−2.9	−0.2
2000	0.032	0.615	$0.709 \cdot 10^{-1}$	13.1	12.7	2.6	1.3	2.2	1.8	−0.4	0.1	−0.5
2000	0.080	0.246	$0.232 \cdot 10^{-1}$	12.6	12.4	2.3	1.0	1.1	0.1	−0.3	0.4	0.0
2000	0.130	0.152	$0.128 \cdot 10^{-1}$	16.6	16.3	3.0	0.9	1.2	0.0	−0.3	−0.1	0.0
2000	0.250	0.079	$0.545 \cdot 10^{-2}$	30.3	28.9	3.6	0.3	8.1	0.0	0.3	−7.8	0.0
3000	0.080	0.369	$0.227 \cdot 10^{-1}$	10.4	10.1	2.0	0.2	1.2	−0.0	0.3	0.8	−0.1
3000	0.130	0.227	$0.914 \cdot 10^{-2}$	14.6	14.4	2.1	0.6	1.3	−0.0	−0.4	0.6	0.0
3000	0.250	0.118	$0.381 \cdot 10^{-2}$	20.0	19.6	2.9	0.8	2.2	0.0	0.1	−1.6	0.0
5000	0.080	0.615	$0.135 \cdot 10^{-1}$	13.9	13.6	2.3	0.9	1.5	0.1	0.3	0.9	−0.1
5000	0.130	0.379	$0.838 \cdot 10^{-2}$	12.0	11.7	2.2	0.7	1.5	−0.0	0.3	1.0	0.0
5000	0.250	0.197	$0.280 \cdot 10^{-2}$	15.4	15.1	2.6	1.6	1.4	0.0	0.4	0.5	0.0
5000	0.400	0.123	$0.831 \cdot 10^{-3}$	42.0	40.9	6.3	5.8	7.5	0.0	1.3	−6.7	0.0
8000	0.130	0.606	$0.539 \cdot 10^{-2}$	14.9	14.3	3.3	2.3	1.8	−0.1	0.7	1.1	0.0
8000	0.250	0.315	$0.167 \cdot 10^{-2}$	15.9	15.4	2.9	1.9	1.8	0.0	0.7	1.2	0.0
8000	0.400	0.197	$0.507 \cdot 10^{-3}$	32.2	31.7	5.1	4.6	2.8	0.0	1.4	−0.9	0.0
15000	0.250	0.591	$1.00 \cdot 10^{-3}$	18.8	17.7	5.7	5.0	2.8	−0.0	1.3	2.0	0.0
15000	0.400	0.369	$0.265 \cdot 10^{-3}$	24.3	23.6	5.2	4.6	2.5	0.0	1.1	1.1	0.0

Table 18: The CC e^-p cross section $\mathrm{d}^2\sigma_{CC}/\mathrm{d}x\mathrm{d}Q^2$ for lepton beam polarisation $P_e = +36.0\%$ with statistical (δ_{stat}), total (δ_{tot}), total uncorrelated systematic (δ_{unc}) errors and one of its contributions from the hadronic energy error (δ_{unc}^{h}). The effect of the other uncorrelated systematic errors is included in δ_{unc}. In addition the correlated systematic (δ_{cor}) and its contributions from a positive variation of one standard deviation of the cuts against photoproduction (δ_{cor}^{V+}), of the hadronic energy error (δ_{cor}^{h+}), of the error due to noise subtraction (δ_{cor}^{N+}) and of the error due to background subtraction (δ_{cor}^{B+}) are given. The normalisation and polarisation uncertainties are not included in the errors.

Q^2 (GeV^2)	x	y	$\mathrm{d}^2\sigma_{CC}/\mathrm{d}x\mathrm{d}Q^2$ ($\mathrm{pb/GeV}^2$)	δ_{tot} (%)	δ_{stat} (%)	δ_{unc} (%)	δ^h_{unc} (%)	δ_{cor} (%)	δ^{V+}_{cor} (%)	δ^{h+}_{cor} (%)	δ^{N+}_{cor} (%)	δ^{B+}_{cor} (%)
300	0.008	0.369	1.20	50.7	38.5	26.5	2.7	19.8	16.5	−0.9	−0.7	−7.7
300	0.013	0.227	0.409	32.7	28.4	11.0	2.1	11.9	9.8	−0.7	−0.5	−5.3
300	0.032	0.092	0.101	25.3	23.6	5.4	2.0	7.1	5.1	−0.6	1.3	−4.5
300	0.080	0.037	$0.256 \cdot 10^{-1}$	28.5	27.5	5.2	2.4	5.4	1.7	−0.4	−4.1	−2.6
500	0.013	0.379	0.282	23.6	20.4	7.1	1.8	9.5	9.3	−0.7	0.3	−1.5
500	0.032	0.154	0.104	16.0	15.2	3.1	1.0	3.9	3.6	−0.3	0.7	−0.9
500	0.080	0.062	$0.383 \cdot 10^{-1}$	14.8	14.2	3.7	1.3	2.0	0.9	−0.4	0.7	−1.1
500	0.130	0.038	$0.121 \cdot 10^{-1}$	43.8	41.5	6.1	0.2	12.6	0.1	0.2	−12.3	0.0
1000	0.013	0.757	0.238	21.6	18.4	6.3	0.9	9.5	9.3	−0.3	−0.4	−1.6
1000	0.032	0.308	0.123	10.4	9.9	2.3	0.7	2.3	2.1	−0.2	0.6	−0.2
1000	0.080	0.123	$0.202 \cdot 10^{-1}$	14.2	13.9	2.8	0.6	1.3	0.4	−0.2	0.8	−0.2
1000	0.130	0.076	$0.730 \cdot 10^{-2}$	26.5	26.1	3.8	1.1	2.8	0.0	−0.3	−2.3	0.0
2000	0.032	0.615	$0.531 \cdot 10^{-1}$	11.8	11.3	2.5	0.2	2.4	2.1	−0.1	0.6	−0.3
2000	0.080	0.246	$0.156 \cdot 10^{-1}$	11.8	11.5	2.0	0.2	1.3	0.1	−0.2	0.9	−0.1
2000	0.130	0.152	$0.692 \cdot 10^{-2}$	17.4	17.1	2.9	0.5	1.4	0.0	0.3	0.7	0.0
2000	0.250	0.079	$0.228 \cdot 10^{-2}$	33.3	31.8	3.8	1.2	9.2	0.0	0.6	−8.8	0.0
3000	0.080	0.369	$0.118 \cdot 10^{-1}$	11.7	11.3	2.5	1.5	1.7	−0.0	0.4	1.4	0.0
3000	0.130	0.227	$0.539 \cdot 10^{-2}$	15.2	14.9	2.3	1.0	1.6	−0.0	0.4	1.1	−0.1
3000	0.250	0.118	$0.157 \cdot 10^{-2}$	23.5	23.1	3.7	2.4	2.2	0.0	0.6	−1.4	0.0
5000	0.080	0.615	$0.359 \cdot 10^{-2}$	21.5	21.0	3.5	2.5	2.7	−0.2	0.8	2.2	−0.1
5000	0.130	0.379	$0.305 \cdot 10^{-2}$	16.0	15.6	2.8	1.7	1.9	−0.1	0.3	1.4	0.0
5000	0.250	0.197	$0.808 \cdot 10^{-3}$	22.9	22.5	3.1	2.4	2.0	0.0	0.7	1.0	0.0
5000	0.400	0.123	$0.525 \cdot 10^{-3}$	42.5	40.9	6.7	6.2	9.3	0.0	1.5	−8.3	0.0
8000	0.130	0.606	$0.682 \cdot 10^{-3}$	30.6	29.7	5.7	5.1	3.2	−0.2	1.0	2.3	0.0
8000	0.250	0.315	$0.612 \cdot 10^{-3}$	21.4	20.5	4.7	4.1	2.6	0.0	1.0	1.5	0.0
8000	0.400	0.197	$0.792 \cdot 10^{-4}$	59.1	58.3	8.1	7.8	4.2	0.0	2.1	0.7	0.0
15000	0.250	0.591	$0.721 \cdot 10^{-4}$	46.9	46.0	7.5	6.9	4.8	−0.1	2.6	2.9	0.0
15000	0.400	0.369	$0.311 \cdot 10^{-4}$	45.9	45.0	7.4	7.0	4.2	0.0	2.2	1.3	0.0

Table 19: The CC e^+p cross section $\mathrm{d}^2\sigma_{CC}/\mathrm{d}x\mathrm{d}Q^2$ for lepton beam polarisation $P_e = -37.0\%$ with statistical (δ_{stat}), total (δ_{tot}), total uncorrelated systematic (δ_{unc}) errors and one of its contributions from the hadronic energy error (δ^h_{unc}). The effect of the other uncorrelated systematic errors is included in δ_{unc}. In addition the correlated systematic (δ_{cor}) and its contributions from a positive variation of one standard deviation of the cuts against photoproduction (δ^{V+}_{cor}), of the hadronic energy error (δ^{h+}_{cor}), of the error due to noise subtraction (δ^{N+}_{cor}) and of the error due to background subtraction (δ^{B+}_{cor}) are given. The normalisation and polarisation uncertainties are not included in the errors.

Q^2 (GeV^2)	x	y	$\mathrm{d}^2\sigma_{CC}/\mathrm{d}x\mathrm{d}Q^2$ ($\mathrm{pb/GeV}^2$)	δ_{tot} (%)	δ_{stat} (%)	δ_{unc} (%)	δ_{unc}^{h} (%)	δ_{cor} (%)	δ_{cor}^{V+} (%)	δ_{cor}^{h+} (%)	δ_{cor}^{N+} (%)	δ_{cor}^{B+} (%)
300	0.008	0.369	0.769	58.3	49.3	25.9	2.5	17.3	15.8	−0.7	−0.6	−5.2
300	0.013	0.227	0.586	25.8	20.4	11.5	1.7	11.0	10.3	−0.4	0.3	−2.8
300	0.032	0.092	0.270	14.5	11.9	5.3	1.6	6.2	5.4	−0.3	1.3	−2.5
300	0.080	0.037	$0.514 \cdot 10^{-1}$	18.1	16.8	5.1	2.3	4.2	1.9	−0.3	−2.9	−1.6
500	0.008	0.615	1.56	33.4	23.2	16.2	2.2	17.7	17.5	−0.6	−0.2	−0.5
500	0.013	0.379	0.663	16.4	11.4	7.1	2.0	9.3	9.2	−0.5	−0.3	−0.7
500	0.032	0.154	0.250	9.9	8.5	3.3	1.6	3.6	3.3	−0.6	0.4	−0.5
500	0.080	0.062	$0.597 \cdot 10^{-1}$	10.6	9.8	3.6	0.8	1.5	0.9	−0.2	0.2	−0.1
500	0.130	0.038	$0.266 \cdot 10^{-1}$	27.0	23.7	5.7	1.0	11.6	0.2	−1.0	−11.3	0.0
1000	0.013	0.757	0.387	16.9	12.5	6.1	0.8	9.5	9.4	−0.5	0.6	−0.2
1000	0.032	0.308	0.174	8.1	7.4	2.4	0.9	2.3	2.0	−0.3	0.7	−0.1
1000	0.080	0.123	$0.507 \cdot 10^{-1}$	8.4	7.8	2.8	0.8	1.3	0.4	−0.4	0.7	−0.1
1000	0.130	0.076	$0.265 \cdot 10^{-1}$	12.9	12.1	3.7	0.9	2.8	0.1	−0.3	−2.3	0.0
2000	0.032	0.615	0.103	8.1	7.3	2.4	0.4	2.6	2.2	−0.2	0.9	0.0
2000	0.080	0.246	$0.367 \cdot 10^{-1}$	7.1	6.6	2.0	0.2	1.3	0.1	0.1	1.0	−0.1
2000	0.130	0.152	$0.164 \cdot 10^{-1}$	10.5	9.9	3.0	0.8	1.4	0.0	0.3	0.6	0.0
2000	0.250	0.079	$0.470 \cdot 10^{-2}$	21.3	19.3	3.6	0.6	8.3	0.0	−0.2	−8.0	0.0
3000	0.080	0.369	$0.244 \cdot 10^{-1}$	7.5	6.9	2.4	1.2	1.6	−0.0	0.5	1.2	0.0
3000	0.130	0.227	$0.152 \cdot 10^{-1}$	8.4	8.0	2.1	0.5	1.4	−0.0	0.2	0.9	0.0
3000	0.250	0.118	$0.259 \cdot 10^{-2}$	16.4	15.9	3.4	2.0	2.1	0.0	0.4	−1.2	0.0
5000	0.080	0.615	$0.984 \cdot 10^{-2}$	12.1	10.9	4.0	3.3	3.0	0.1	0.7	2.5	−0.1
5000	0.130	0.379	$0.627 \cdot 10^{-2}$	10.8	9.8	3.4	2.7	2.4	−0.1	0.9	1.9	0.0
5000	0.250	0.197	$0.185 \cdot 10^{-2}$	14.0	13.3	3.4	2.7	1.8	0.0	0.6	0.8	0.0
5000	0.400	0.123	$0.866 \cdot 10^{-3}$	27.7	25.0	7.9	7.5	8.6	0.0	1.5	−7.4	0.0
8000	0.130	0.606	$0.213 \cdot 10^{-2}$	17.0	15.4	5.6	5.0	3.5	−0.2	1.4	2.6	0.0
8000	0.250	0.315	$0.988 \cdot 10^{-3}$	14.8	13.5	4.3	3.6	2.8	0.0	1.2	1.8	0.0
8000	0.400	0.197	$0.295 \cdot 10^{-3}$	29.4	27.8	7.9	7.7	4.5	0.0	2.6	−1.5	0.0
15000	0.250	0.591	$0.306 \cdot 10^{-3}$	21.4	19.0	8.1	7.6	4.5	0.1	2.0	2.9	0.0
15000	0.400	0.369	$0.361 \cdot 10^{-4}$	39.0	38.0	6.8	6.3	4.2	0.0	1.8	1.7	0.0

Table 20: The CC e^+p cross section $\mathrm{d}^2\sigma_{CC}/\mathrm{d}x\mathrm{d}Q^2$ for lepton beam polarisation $P_e = +32.5\%$ with statistical (δ_{stat}), total (δ_{tot}), total uncorrelated systematic (δ_{unc}) errors and one of its contributions from the hadronic energy error (δ_{unc}^{h}). The effect of the other uncorrelated systematic errors is included in δ_{unc}. In addition the correlated systematic (δ_{cor}) and its contributions from a positive variation of one standard deviation of the cuts against photoproduction (δ_{cor}^{V+}), of the hadronic energy error (δ_{cor}^{h+}), of the error due to noise subtraction (δ_{cor}^{N+}) and of the error due to background subtraction (δ_{cor}^{B+}) are given. The normalisation and polarisation uncertainties are not included in the errors.

Q^2 (GeV^2)	x	y	$\tilde{\sigma}_{\mathrm{NC}}$	δ_{tot} (%)	δ_{stat} (%)	δ_{unc} (%)	$\delta^{E}_{\mathrm{unc}}$ (%)	$\delta^{h}_{\mathrm{unc}}$ (%)	δ_{cor} (%)	$\delta^{E^+}_{\mathrm{cor}}$ (%)	$\delta^{\theta^+}_{\mathrm{cor}}$ (%)	$\delta^{h^+}_{\mathrm{cor}}$ (%)	$\delta^{N^+}_{\mathrm{cor}}$ (%)	$\delta^{B^+}_{\mathrm{cor}}$ (%)
90	0.0015	0.595	1.370	2.21	1.21	1.10	0.57	0.12	1.48	−0.06	−0.69	0.02	0.22	−1.29
120	0.0020	0.595	1.293	2.08	1.13	1.05	0.49	0.12	1.40	−0.30	−0.54	0.02	0.20	−1.24
120	0.0022	0.530	1.313	1.78	1.14	0.98	0.37	0.07	0.95	−0.26	−0.67	0.03	0.16	−0.59
120	0.0025	0.475	1.228	1.98	1.32	1.21	0.76	0.06	0.84	−0.40	−0.64	0.02	0.19	−0.32
120	0.0028	0.425	1.254	2.08	1.53	1.13	0.55	0.05	0.85	−0.44	−0.69	0.02	0.20	−0.11
150	0.0025	0.595	1.273	1.93	1.31	0.96	0.24	0.10	1.05	−0.21	−0.43	0.03	0.19	−0.91
150	0.0028	0.530	1.215	1.86	1.30	1.02	0.45	0.07	0.86	−0.39	−0.55	0.01	0.17	−0.52
150	0.0031	0.475	1.210	1.77	1.31	0.96	0.31	0.06	0.71	−0.21	−0.58	0.02	0.20	−0.27
150	0.0035	0.425	1.164	1.79	1.23	1.05	0.56	0.05	0.78	−0.33	−0.65	0.01	0.20	−0.16
150	0.0039	0.375	1.140	1.85	1.14	1.19	0.82	0.01	0.83	−0.50	−0.63	0.00	0.19	−0.06
150	0.0045	0.325	1.107	1.83	1.15	1.13	0.72	0.00	0.86	−0.52	−0.69	0.00	0.00	−0.02
150	0.0060	0.245	1.015	2.01	0.88	1.44	1.18	0.00	1.09	−0.68	−0.85	0.00	0.00	−0.01
200	0.0033	0.595	1.175	2.17	1.69	0.99	0.11	0.08	0.93	0.11	−0.51	0.02	0.14	−0.76
200	0.0037	0.530	1.194	2.03	1.63	0.99	0.28	0.07	0.70	−0.25	−0.53	0.02	0.15	−0.35
200	0.0041	0.475	1.103	2.06	1.71	0.96	0.14	0.05	0.64	−0.17	−0.58	0.01	0.14	−0.15
200	0.0046	0.425	1.093	2.05	1.63	1.02	0.43	0.04	0.71	−0.44	−0.51	0.01	0.21	−0.08
200	0.0052	0.375	1.083	1.98	1.49	1.03	0.48	0.01	0.82	−0.38	−0.70	0.00	0.18	−0.04
200	0.0061	0.325	1.014	2.08	1.38	1.26	0.89	0.00	0.91	−0.64	−0.64	0.00	0.00	−0.03
200	0.0080	0.245	0.9317	1.84	0.81	1.37	1.11	0.00	0.93	−0.65	−0.66	0.00	0.00	0.00
250	0.0041	0.595	1.136	2.42	2.01	1.06	0.25	0.08	0.86	−0.25	−0.39	0.02	0.20	−0.70
250	0.0046	0.530	1.161	2.26	1.92	1.02	0.31	0.07	0.59	−0.31	−0.39	0.01	0.17	−0.26
250	0.0052	0.475	1.048	2.34	2.00	1.05	0.39	0.06	0.59	−0.39	−0.39	0.01	0.16	−0.17
250	0.0058	0.425	1.045	2.15	1.79	1.03	0.41	0.04	0.62	−0.40	−0.44	0.02	0.16	−0.06
250	0.0066	0.375	0.9816	2.09	1.68	1.02	0.45	0.01	0.73	−0.43	−0.56	0.01	0.16	−0.03
250	0.0076	0.325	0.9542	1.98	1.56	1.04	0.52	0.00	0.64	−0.48	−0.43	0.00	0.00	−0.01
250	0.0100	0.245	0.8717	1.75	0.94	1.12	0.77	0.00	0.95	−0.65	−0.69	0.00	0.00	−0.01
300	0.0050	0.595	1.102	2.73	2.37	1.10	0.28	0.07	0.78	−0.27	−0.42	0.02	0.15	−0.58
300	0.0056	0.530	1.110	2.58	2.31	1.02	0.12	0.07	0.53	0.14	−0.43	0.03	0.15	−0.23
300	0.0062	0.475	1.049	2.63	2.28	1.10	0.40	0.06	0.72	−0.40	−0.55	0.02	0.15	−0.19
300	0.0069	0.425	1.007	2.43	2.11	1.02	0.30	0.04	0.65	−0.29	−0.55	0.01	0.18	−0.08
300	0.0079	0.375	0.9664	2.28	1.92	1.03	0.41	0.01	0.69	−0.41	−0.55	0.00	0.12	−0.01
300	0.0091	0.325	0.9142	2.17	1.79	1.01	0.42	0.00	0.67	−0.41	−0.53	0.00	0.00	−0.01
300	0.0121	0.245	0.8206	1.71	1.07	1.03	0.63	0.00	0.84	−0.61	−0.58	0.00	0.00	0.00
400	0.0066	0.595	1.049	3.10	2.77	1.20	0.43	0.08	0.73	−0.33	−0.31	0.02	0.18	−0.54
400	0.0074	0.530	1.049	3.02	2.78	1.08	0.19	0.05	0.47	−0.09	−0.40	0.02	0.12	−0.19
400	0.0083	0.475	0.9833	3.02	2.75	1.11	0.31	0.03	0.57	−0.27	−0.48	0.02	0.14	−0.10
400	0.0093	0.425	0.9605	2.85	2.51	1.11	0.42	0.04	0.77	−0.46	−0.59	0.01	0.18	−0.04
400	0.0105	0.375	0.9145	2.57	2.29	1.03	0.33	0.01	0.54	−0.32	−0.42	0.00	0.13	−0.04
400	0.0121	0.325	0.8656	2.45	2.16	1.01	0.32	0.00	0.58	−0.32	−0.48	0.00	0.00	−0.02
400	0.0161	0.245	0.7548	1.84	1.27	1.03	0.61	0.00	0.83	−0.61	−0.57	0.00	0.00	−0.01
500	0.0083	0.595	0.9427	3.39	3.16	1.12	0.13	0.09	0.52	0.13	−0.38	0.02	0.17	−0.29
500	0.0093	0.530	0.9525	3.40	3.18	1.11	0.11	0.07	0.51	−0.25	−0.42	0.02	0.13	−0.09
500	0.0104	0.475	0.8895	3.65	3.33	1.30	0.62	0.06	0.73	−0.46	−0.51	0.01	0.15	−0.19
500	0.0116	0.425	0.9040	3.20	2.98	1.09	0.16	0.05	0.33	−0.16	−0.25	0.00	0.13	−0.05
500	0.0131	0.375	0.8794	3.12	2.87	1.08	0.26	0.01	0.56	−0.15	−0.53	0.00	0.09	−0.02
500	0.0152	0.325	0.8044	3.04	2.65	1.22	0.69	0.00	0.84	−0.73	−0.42	0.00	0.00	−0.02
500	0.0201	0.245	0.7092	2.02	1.54	1.04	0.60	0.00	0.78	−0.60	−0.50	0.00	0.00	0.00
650	0.0108	0.595	0.9391	3.76	3.52	1.21	0.21	0.06	0.53	−0.14	−0.40	0.02	0.13	−0.30
650	0.0121	0.530	0.8624	3.84	3.60	1.27	0.44	0.08	0.40	−0.23	−0.26	0.03	0.16	−0.12
650	0.0135	0.475	0.8786	3.86	3.64	1.24	0.31	0.06	0.39	−0.30	−0.17	0.02	0.13	−0.11
650	0.0151	0.425	0.8226	3.81	3.49	1.30	0.52	0.03	0.81	−0.54	−0.59	0.01	0.11	0.00
650	0.0171	0.375	0.7808	3.59	3.30	1.26	0.57	0.02	0.63	−0.45	−0.42	0.00	0.14	−0.01
650	0.0197	0.325	0.7520	3.41	3.08	1.27	0.62	0.00	0.74	−0.53	−0.51	0.00	0.00	−0.01
650	0.0261	0.245	0.6866	2.27	1.82	1.13	0.68	0.00	0.78	−0.62	−0.47	0.00	0.00	0.00
800	0.0132	0.595	0.8143	4.52	4.30	1.31	0.21	0.06	0.50	−0.14	−0.42	0.02	0.16	−0.18
800	0.0149	0.530	0.9105	4.49	4.25	1.39	0.48	0.08	0.47	0.35	0.20	0.03	0.18	−0.15
800	0.0166	0.475	0.7637	4.56	4.34	1.32	0.10	0.09	0.53	0.04	−0.49	0.02	0.18	−0.06
800	0.0185	0.425	0.7535	4.31	4.02	1.49	0.80	0.01	0.45	−0.24	−0.35	0.00	0.13	−0.05
800	0.0210	0.375	0.6743	4.22	3.90	1.41	0.71	0.01	0.78	−0.76	−0.14	0.00	0.05	−0.01
800	0.0242	0.325	0.6736	3.86	3.60	1.31	0.57	0.00	0.49	−0.16	−0.46	0.00	0.00	−0.01
800	0.0322	0.245	0.6068	2.68	2.23	1.28	0.85	0.00	0.77	−0.62	−0.44	0.00	0.00	0.00

Table 21: The NC e^-p reduced cross section $\tilde{\sigma}_{\mathrm{NC}}(y, Q^2)$ for $P_e = 0$ with statistical (δ_{stat}), total (δ_{tot}), total uncorrelated systematic (δ_{unc}) errors, two of its contributions from the electron energy error (δ^E_{unc}) and the hadronic energy error (δ^h_{unc}). The effect of the other uncorrelated systematic errors is included in δ_{unc}. In addition the correlated systematic (δ_{cor}) and its contributions from a positive variation of one standard deviation of the electron energy error ($\delta^{E^+}_{cor}$), of the polar electron angle error ($\delta^{\theta^+}_{\mathrm{cor}}$), of the hadronic energy error ($\delta^{h^+}_{\mathrm{cor}}$), of the error due to noise subtraction ($\delta^{N^+}_{\mathrm{cor}}$) and of the error due to background subtraction ($\delta^{B^+}_{\mathrm{cor}}$) are given. The normalisation and polarisation uncertainties are not included in the errors.

Q^2 (GeV^2)	x	y	$\tilde{\sigma}_{\mathrm{NC}}$	δ_{tot} (%)	δ_{stat} (%)	δ_{unc} (%)	$\delta^{E}_{\mathrm{unc}}$ (%)	$\delta^{h}_{\mathrm{unc}}$ (%)	δ_{cor} (%)	$\delta^{E^+}_{\mathrm{cor}}$ (%)	$\delta^{\theta^+}_{\mathrm{cor}}$ (%)	$\delta^{h^+}_{\mathrm{cor}}$ (%)	$\delta^{N^+}_{\mathrm{cor}}$ (%)	$\delta^{B^+}_{\mathrm{cor}}$ (%)
90	0.0015	0.595	1.382	2.20	1.12	1.03	0.62	0.09	1.59	−0.29	−0.64	0.03	0.15	−1.41
120	0.0020	0.595	1.340	1.98	1.02	0.90	0.40	0.10	1.44	−0.29	−0.58	0.02	0.19	−1.28
120	0.0022	0.530	1.312	1.69	1.02	0.96	0.56	0.08	0.95	−0.29	−0.68	0.02	0.18	−0.58
120	0.0025	0.475	1.270	1.79	1.18	1.02	0.62	0.06	0.89	−0.53	−0.66	0.01	0.16	−0.20
120	0.0028	0.425	1.223	1.89	1.42	1.02	0.51	0.04	0.74	−0.29	−0.64	0.01	0.18	−0.12
150	0.0025	0.595	1.240	1.88	1.21	0.83	0.13	0.11	1.17	−0.12	−0.44	0.02	0.18	−1.07
150	0.0028	0.530	1.263	1.59	1.17	0.84	0.30	0.07	0.68	−0.27	−0.47	0.02	0.17	−0.38
150	0.0031	0.475	1.213	1.73	1.19	0.94	0.52	0.04	0.83	−0.48	−0.61	0.01	0.16	−0.26
150	0.0035	0.425	1.209	1.70	1.10	1.06	0.75	0.03	0.74	−0.41	−0.58	0.01	0.16	−0.15
150	0.0039	0.375	1.160	1.62	1.02	0.96	0.62	0.02	0.80	−0.34	−0.70	0.00	0.18	−0.03
150	0.0045	0.325	1.112	1.85	1.04	1.19	0.93	0.00	0.96	−0.66	−0.70	0.00	0.00	−0.03
150	0.0060	0.245	1.015	1.89	0.80	1.37	1.18	0.00	1.03	−0.70	−0.75	0.00	0.00	0.00
200	0.0033	0.595	1.220	2.04	1.55	0.90	0.23	0.09	0.97	−0.22	−0.46	0.02	0.17	−0.81
200	0.0037	0.530	1.177	1.87	1.50	0.86	0.17	0.07	0.72	−0.18	−0.53	0.02	0.17	−0.41
200	0.0041	0.475	1.125	1.90	1.55	0.85	0.12	0.06	0.70	−0.09	−0.64	0.01	0.16	−0.20
200	0.0046	0.425	1.109	1.81	1.44	0.89	0.37	0.05	0.64	−0.29	−0.54	0.01	0.16	−0.08
200	0.0052	0.375	1.059	1.84	1.35	0.94	0.53	0.02	0.82	−0.44	−0.67	0.01	0.17	−0.03
200	0.0061	0.325	1.038	1.81	1.22	1.04	0.71	0.00	0.84	−0.50	−0.68	0.00	0.00	−0.03
200	0.0080	0.245	0.9387	1.77	0.73	1.26	1.07	0.00	1.01	−0.64	−0.79	0.00	0.00	0.00
250	0.0041	0.595	1.139	2.25	1.83	0.94	0.26	0.10	0.90	−0.26	−0.42	0.03	0.17	−0.74
250	0.0046	0.530	1.130	2.04	1.74	0.88	0.16	0.05	0.60	−0.16	−0.46	0.01	0.12	−0.33
250	0.0052	0.475	1.093	2.07	1.75	0.92	0.32	0.06	0.60	−0.32	−0.46	0.01	0.15	−0.14
250	0.0058	0.425	1.089	1.97	1.60	0.93	0.43	0.06	0.68	−0.41	−0.49	0.02	0.18	−0.13
250	0.0066	0.375	1.021	1.83	1.50	0.87	0.36	0.02	0.61	−0.33	−0.49	0.00	0.14	−0.02
250	0.0076	0.325	0.9427	1.96	1.43	1.03	0.68	0.00	0.85	−0.65	−0.54	0.00	0.00	−0.02
250	0.0100	0.245	0.8633	1.60	0.85	1.05	0.80	0.00	0.86	−0.59	−0.62	0.00	0.00	−0.01
300	0.0050	0.595	1.115	2.49	2.15	0.96	0.09	0.08	0.81	−0.08	−0.38	0.01	0.16	−0.70
300	0.0056	0.530	1.093	2.43	2.12	0.95	0.30	0.07	0.71	−0.33	−0.51	0.03	0.15	−0.34
300	0.0062	0.475	1.043	2.32	2.07	0.90	0.07	0.04	0.53	−0.07	−0.50	0.01	0.13	−0.10
300	0.0069	0.425	1.016	2.31	1.93	1.01	0.54	0.04	0.78	−0.54	−0.53	0.01	0.17	−0.10
300	0.0079	0.375	0.9685	2.04	1.74	0.86	0.28	0.00	0.62	−0.28	−0.54	0.00	0.10	−0.02
300	0.0091	0.325	0.8966	2.02	1.65	0.90	0.42	0.00	0.76	−0.42	−0.63	0.00	0.00	−0.01
300	0.0121	0.245	0.8111	1.68	0.98	1.00	0.72	0.00	0.93	−0.72	−0.58	0.00	0.00	−0.01
400	0.0066	0.595	1.021	2.87	2.55	1.03	0.22	0.10	0.82	0.19	−0.59	0.02	0.14	−0.52
400	0.0074	0.530	1.048	2.73	2.46	1.00	0.28	0.07	0.64	−0.29	−0.49	0.01	0.14	−0.25
400	0.0083	0.475	0.9818	2.82	2.50	1.13	0.61	0.05	0.67	−0.61	−0.20	0.00	0.11	−0.14
400	0.0093	0.425	0.9174	2.65	2.33	1.04	0.52	0.04	0.70	−0.52	−0.43	0.01	0.17	−0.08
400	0.0105	0.375	0.8979	2.32	2.09	0.88	0.20	0.01	0.52	−0.20	−0.47	0.00	0.13	−0.02
400	0.0121	0.325	0.8714	2.34	1.91	1.06	0.66	0.00	0.85	−0.66	−0.54	0.00	0.00	−0.01
400	0.0161	0.245	0.7565	1.65	1.15	0.91	0.59	0.00	0.75	−0.58	−0.47	0.00	0.00	0.00
500	0.0083	0.595	0.9509	3.20	2.94	1.10	0.41	0.10	0.60	−0.22	−0.17	0.02	0.17	−0.50
500	0.0093	0.530	0.9256	3.09	2.88	1.02	0.24	0.07	0.40	−0.08	−0.35	0.01	0.11	−0.15
500	0.0104	0.475	0.9175	3.22	2.96	1.10	0.42	0.06	0.63	−0.27	−0.54	0.01	0.17	−0.07
500	0.0116	0.425	0.8560	3.07	2.82	1.01	0.22	0.03	0.67	−0.15	−0.63	0.01	0.16	−0.06
500	0.0131	0.375	0.8663	2.82	2.51	1.04	0.47	0.01	0.75	−0.51	−0.55	0.00	0.09	−0.02
500	0.0152	0.325	0.7935	2.62	2.42	0.91	0.16	0.00	0.44	0.12	−0.42	0.00	0.00	−0.01
500	0.0201	0.245	0.7274	1.95	1.41	1.00	0.68	0.00	0.89	−0.67	−0.58	0.00	0.00	0.00
650	0.0108	0.595	0.8748	3.49	3.25	1.16	0.40	0.06	0.53	−0.39	−0.20	0.01	0.09	−0.27
650	0.0121	0.530	0.8859	3.43	3.20	1.08	0.16	0.06	0.58	−0.20	−0.52	0.02	0.11	−0.13
650	0.0135	0.475	0.7983	3.66	3.42	1.16	0.39	0.04	0.60	−0.27	−0.52	0.00	0.11	−0.06
650	0.0151	0.425	0.8432	3.31	3.12	1.07	0.17	0.05	0.27	−0.11	−0.15	0.02	0.20	−0.01
650	0.0171	0.375	0.7310	3.39	3.09	1.22	0.67	0.01	0.69	−0.48	−0.48	0.00	0.08	−0.05
650	0.0197	0.325	0.7176	3.12	2.86	1.08	0.42	0.00	0.63	−0.46	−0.44	0.00	0.00	−0.01
650	0.0261	0.245	0.6801	2.07	1.68	0.95	0.54	0.00	0.76	−0.47	−0.59	0.00	0.00	0.00
800	0.0132	0.595	0.8173	4.08	3.81	1.32	0.28	0.11	0.66	0.37	−0.44	0.03	0.16	−0.29
800	0.0149	0.530	0.7529	4.10	3.88	1.22	0.29	0.06	0.49	−0.27	−0.35	0.04	0.12	−0.15
800	0.0166	0.475	0.7075	4.27	4.04	1.30	0.47	0.05	0.50	−0.35	−0.30	0.02	0.16	−0.11
800	0.0185	0.425	0.6978	3.97	3.72	1.24	0.49	0.02	0.62	−0.54	−0.27	0.00	0.13	−0.05
800	0.0210	0.375	0.7056	3.81	3.41	1.52	1.05	0.00	0.72	−0.51	−0.50	0.00	0.05	−0.03
800	0.0242	0.325	0.6539	3.63	3.42	1.16	0.39	0.00	0.37	−0.19	−0.32	0.00	0.00	−0.01
800	0.0322	0.245	0.6030	2.37	1.98	1.12	0.74	0.00	0.67	−0.47	−0.48	0.00	0.00	0.00

Table 22: The NC e^+p reduced cross section $\tilde{\sigma}_{\mathrm{NC}}(y, Q^2)$ for $P_e = 0$ with statistical (δ_{stat}), total (δ_{tot}), total uncorrelated systematic (δ_{unc}) errors, two of its contributions from the electron energy error (δ^{E}_{unc}) and the hadronic energy error ($\delta^{h}_{\mathrm{unc}}$). The effect of the other uncorrelated systematic errors is included in δ_{unc}. In addition the correlated systematic (δ_{cor}) and its contributions from a positive variation of one standard deviation of the electron energy error ($\delta^{E^+}_{cor}$), of the polar electron angle error ($\delta^{\theta^+}_{\mathrm{cor}}$), of the hadronic energy error ($\delta^{h^+}_{\mathrm{cor}}$), of the error due to noise subtraction ($\delta^{N^+}_{\mathrm{cor}}$) and of the error due to background subtraction ($\delta^{B^+}_{\mathrm{cor}}$) are given. The normalisation and polarisation uncertainties are not included in the errors.

Q^2 (GeV^2)	x	y	$\tilde{\sigma}_{\mathrm{NC}}$	δ_{tot} (%)	δ_{stat} (%)	δ_{unc} (%)	$\delta_{\mathrm{unc}}^{E}$ (%)	$\delta_{\mathrm{unc}}^{h}$ (%)	δ_{cor} (%)	$\delta_{\mathrm{cor}}^{E^+}$ (%)	$\delta_{\mathrm{cor}}^{\theta^+}$ (%)	$\delta_{\mathrm{cor}}^{h^+}$ (%)	$\delta_{\mathrm{cor}}^{N^+}$ (%)	$\delta_{\mathrm{cor}}^{S^+}$ (%)
60	0.0008	0.75	1.436	2.29	1.02	1.84	0.52	0.28	0.92	−0.19	−0.62	0.05	0.19	−0.62
90	0.0012	0.75	1.437	2.05	0.83	1.71	0.31	0.26	0.77	−0.28	−0.45	0.07	0.20	−0.52
120	0.0016	0.75	1.400	2.15	0.93	1.82	0.48	0.28	0.69	−0.09	−0.40	0.05	0.22	−0.50
150	0.0020	0.75	1.313	2.25	1.05	1.89	0.38	0.27	0.61	−0.19	−0.34	0.06	0.22	−0.41
200	0.0026	0.75	1.252	2.48	1.35	2.00	0.49	0.30	0.56	−0.07	−0.35	0.06	0.24	−0.35
250	0.0033	0.75	1.244	2.56	1.54	1.98	0.31	0.32	0.53	−0.13	−0.29	0.08	0.26	−0.32
300	0.0039	0.75	1.192	2.70	1.79	1.96	0.14	0.31	0.51	−0.12	−0.26	0.06	0.28	−0.31
400	0.0052	0.75	1.122	2.81	1.95	1.96	0.26	0.30	0.50	−0.06	−0.35	0.08	0.25	−0.23
500	0.0066	0.75	1.018	2.90	2.16	1.90	0.13	0.25	0.35	−0.11	−0.15	0.09	0.25	−0.13
650	0.0085	0.75	0.9565	3.13	2.45	1.92	0.21	0.21	0.38	0.07	−0.28	0.06	0.23	−0.08
800	0.0105	0.75	0.9329	3.49	2.85	1.97	0.23	0.21	0.39	−0.22	−0.20	0.06	0.25	−0.04

Table 23: The NC e^-p reduced cross section $\tilde{\sigma}_{\mathrm{NC}}(x, Q^2)$ for $P_e = 0$ with statistical (δ_{stat}), total (δ_{tot}), total uncorrelated systematic (δ_{unc}) errors, two of its contributions from the electron energy error (δ_{unc}^{E}) and the hadronic energy error ($\delta_{\mathrm{unc}}^{h}$). The effect of the other uncorrelated systematic errors is included in δ_{unc}. In addition the correlated systematic (δ_{cor}) and its contributions from a positive variation of one standard deviation of the electron energy error ($\delta_{cor}^{E^+}$), of the polar electron angle error ($\delta_{\mathrm{cor}}^{\theta^+}$), of the hadronic energy error ($\delta_{\mathrm{cor}}^{h^+}$), of the error due to noise subtraction ($\delta_{\mathrm{cor}}^{N^+}$) and of the error due to background subtraction charge asymmetry ($\delta_{\mathrm{cor}}^{S^+}$) are given. The normalisation and polarisation uncertainties are not included in the errors.

Q^2 (GeV^2)	x	y	$\tilde{\sigma}_{\mathrm{NC}}$	δ_{tot} (%)	δ_{stat} (%)	δ_{unc} (%)	$\delta_{\mathrm{unc}}^{E}$ (%)	$\delta_{\mathrm{unc}}^{h}$ (%)	δ_{cor} (%)	$\delta_{\mathrm{cor}}^{E^+}$ (%)	$\delta_{\mathrm{cor}}^{\theta^+}$ (%)	$\delta_{\mathrm{cor}}^{h^+}$ (%)	$\delta_{\mathrm{cor}}^{N^+}$ (%)	$\delta_{\mathrm{cor}}^{S^+}$ (%)
60	0.0008	0.75	1.453	2.21	0.88	1.86	0.70	0.26	0.81	−0.31	−0.48	0.05	0.17	0.54
90	0.0012	0.75	1.460	1.93	0.72	1.64	0.13	0.26	0.73	−0.21	−0.50	0.07	0.21	0.44
120	0.0016	0.75	1.379	2.04	0.84	1.71	0.36	0.28	0.72	0.10	−0.45	0.07	0.23	0.50
150	0.0020	0.75	1.346	2.14	0.96	1.81	0.42	0.25	0.64	−0.24	−0.36	0.07	0.23	0.41
200	0.0026	0.75	1.289	2.38	1.24	1.94	0.59	0.26	0.61	−0.03	−0.45	0.06	0.21	0.35
250	0.0033	0.75	1.263	2.42	1.43	1.88	0.20	0.30	0.50	−0.18	−0.27	0.05	0.23	0.30
300	0.0039	0.75	1.203	2.53	1.63	1.88	0.05	0.34	0.47	−0.17	−0.23	0.08	0.26	0.25
400	0.0052	0.75	1.162	2.60	1.73	1.89	0.35	0.27	0.42	−0.02	−0.27	0.07	0.28	0.14
500	0.0066	0.75	1.038	2.69	1.94	1.83	0.07	0.23	0.41	−0.16	−0.23	0.07	0.25	0.13
650	0.0085	0.75	0.9795	2.93	2.22	1.87	0.23	0.23	0.46	−0.09	−0.34	0.06	0.27	0.09
800	0.0105	0.75	0.9018	3.31	2.65	1.93	0.21	0.24	0.43	0.07	−0.31	0.08	0.28	0.05

Table 24: The NC e^+p reduced cross section $\tilde{\sigma}_{\mathrm{NC}}(x, Q^2)$ for $P_e = 0$ with statistical (δ_{stat}), total (δ_{tot}), total uncorrelated systematic (δ_{unc}) errors, two of its contributions from the electron energy error (δ_{unc}^{E}) and the hadronic energy error ($\delta_{\mathrm{unc}}^{h}$). The effect of the other uncorrelated systematic errors is included in δ_{unc}. In addition the correlated systematic (δ_{cor}) and its contributions from a positive variation of one standard deviation of the electron energy error ($\delta_{cor}^{E^+}$), of the polar electron angle error ($\delta_{\mathrm{cor}}^{\theta^+}$), of the hadronic energy error ($\delta_{\mathrm{cor}}^{h^+}$), of the error due to noise subtraction ($\delta_{\mathrm{cor}}^{N^+}$) and of the error due to background subtraction charge asymmetry ($\delta_{\mathrm{cor}}^{S^+}$) are given. The normalisation and polarisation uncertainties are not included in the errors.

Q^2 (GeV^2)	x	$\tilde{\sigma}_{\rm NC}$	$\delta_{\rm tot}$ (%)	$\delta_{\rm stat}$ (%)	$\delta_{\rm unc}$ (%)	$\delta^{E}_{\rm unc}$ (%)	$\delta^{h}_{\rm unc}$ (%)	$\delta_{\rm cor}$ (%)	$\delta^{E^+}_{\rm cor}$ (%)	$\delta^{\theta^+}_{\rm cor}$ (%)	$\delta^{h^+}_{\rm cor}$ (%)	$\delta^{N^+}_{\rm cor}$ (%)	$\delta^{B^+}_{\rm cor}$ (%)
120	0.0020	1.313	1.61	0.72	0.95	0.49	0.09	1.08	−0.32	−0.63	0.02	0.18	−0.79
120	0.0032	1.184	1.72	1.02	1.15	0.77	0.05	0.78	−0.36	−0.64	0.02	0.20	−0.16
150	0.0032	1.191	1.34	0.61	0.88	0.41	0.06	0.81	−0.32	−0.59	0.02	0.19	−0.41
150	0.0050	1.074	1.69	0.73	1.21	0.90	0.00	0.93	−0.55	−0.74	0.00	0.04	−0.04
150	0.0080	0.9242	2.43	1.00	1.81	1.28	0.96	1.28	−0.82	−0.82	−0.28	−0.46	−0.07
150	0.0130	0.7884	3.81	1.38	2.98	2.68	0.90	1.93	−1.55	−0.74	−0.30	−0.81	−0.10
200	0.0032	1.204	1.60	1.13	0.86	0.14	0.07	0.74	−0.15	−0.51	0.02	0.15	−0.49
200	0.0050	1.075	1.45	0.80	0.95	0.52	0.02	0.75	−0.43	−0.60	0.00	0.13	−0.09
200	0.0080	0.9355	1.82	0.81	1.34	1.07	0.00	0.93	−0.62	−0.70	0.00	0.00	0.00
200	0.0130	0.7699	1.45	0.94	0.83	0.16	0.01	0.73	−0.06	−0.44	−0.04	0.57	−0.01
200	0.0200	0.6787	1.63	1.02	1.05	0.63	0.14	0.71	−0.46	−0.41	−0.06	0.34	−0.01
200	0.0320	0.5663	2.02	1.16	1.41	0.98	0.53	0.88	−0.53	−0.67	−0.19	0.07	0.00
200	0.0500	0.5139	2.74	1.36	1.72	1.46	0.04	1.64	−0.86	−0.69	−0.16	1.20	0.00
200	0.0800	0.4301	3.25	1.42	2.17	1.93	0.19	1.96	−1.15	−0.76	−0.09	1.40	−0.01
200	0.1300	0.3527	3.22	1.68	2.15	1.35	1.10	1.71	−0.82	−0.98	−0.28	−1.11	0.00
200	0.1800	0.3006	4.08	2.27	2.74	1.26	1.90	2.01	−0.87	−1.08	−0.43	−1.40	0.00
250	0.0050	1.089	1.41	0.93	0.86	0.33	0.06	0.61	−0.32	−0.40	0.02	0.18	−0.27
250	0.0080	0.9371	1.57	0.91	1.00	0.59	0.00	0.79	−0.55	−0.56	0.00	0.03	−0.01
250	0.0130	0.7965	1.96	1.00	1.23	0.90	0.20	1.15	0.49	−0.66	0.03	0.80	−0.02
250	0.0200	0.6722	1.93	1.03	1.25	0.91	0.23	1.06	0.33	−0.54	0.06	0.85	−0.01
250	0.0320	0.5724	2.02	1.08	1.35	1.07	0.10	1.03	0.49	−0.61	−0.09	0.67	0.00
250	0.0500	0.4843	2.24	1.23	1.34	1.02	0.11	1.30	0.40	−0.53	−0.09	1.12	0.00
250	0.0800	0.4179	2.75	1.26	1.09	0.56	0.26	2.19	0.27	−0.51	−0.03	2.11	0.00
250	0.1300	0.3581	2.35	1.28	1.75	1.08	0.68	0.93	0.52	−0.59	−0.22	−0.44	0.00
250	0.1800	0.3014	4.00	1.77	2.69	1.69	1.56	2.37	1.05	−0.76	−0.35	−1.95	0.00
300	0.0050	1.117	1.92	1.56	0.91	0.19	0.07	0.65	−0.20	−0.48	0.03	0.16	−0.35
300	0.0080	0.9592	1.51	1.06	0.86	0.31	0.02	0.64	−0.31	−0.55	0.01	0.10	−0.07
300	0.0130	0.7987	1.77	1.06	1.10	0.73	0.00	0.90	−0.72	−0.55	0.00	0.00	0.00
300	0.0200	0.6846	1.84	1.18	1.04	0.61	0.16	0.95	0.47	−0.56	0.02	0.61	−0.02
300	0.0320	0.5763	1.98	1.24	1.18	0.83	0.04	1.00	0.49	−0.56	−0.05	0.66	0.00
300	0.0500	0.4893	2.36	1.35	1.42	1.12	0.16	1.31	0.60	−0.66	−0.08	0.95	0.00
300	0.0800	0.4165	2.95	1.43	1.39	1.03	0.24	2.17	0.42	−0.66	−0.05	2.02	−0.01
300	0.1300	0.3516	2.58	1.43	1.85	1.34	0.42	1.10	0.68	−0.66	−0.17	0.52	0.00
300	0.1800	0.2905	4.57	1.90	3.05	2.16	1.63	2.82	1.34	−0.90	−0.38	−2.28	0.00
300	0.4000	0.1454	6.46	2.25	3.50	2.29	1.97	4.94	1.32	−0.95	−0.38	−4.65	0.00
400	0.0080	1.009	1.70	1.30	0.91	0.38	0.05	0.60	−0.33	−0.43	0.01	0.15	−0.20
400	0.0130	0.8332	1.72	1.25	0.94	0.46	0.00	0.71	−0.45	−0.54	0.00	0.03	−0.02
400	0.0200	0.6936	2.07	1.29	1.24	0.92	0.00	1.03	−0.91	−0.49	0.00	0.00	0.00
400	0.0320	0.5913	1.90	1.36	0.96	0.47	0.03	0.91	0.46	−0.47	−0.04	0.62	0.00
400	0.0500	0.4839	2.04	1.52	1.07	0.51	0.38	0.83	0.50	−0.38	−0.12	0.53	−0.01
400	0.0800	0.4096	2.60	1.62	1.00	0.27	0.33	1.77	0.23	−0.34	0.04	1.73	0.00
400	0.1300	0.3591	2.44	1.62	1.39	0.67	0.20	1.19	0.59	−0.52	−0.13	0.88	0.00
400	0.1800	0.2993	4.20	1.99	2.44	1.08	1.70	2.78	1.01	−0.51	−0.43	−2.50	0.00
400	0.4000	0.1440	7.04	2.64	3.23	1.34	2.25	5.68	1.26	−0.66	−0.35	−5.49	0.00
500	0.0080	0.9703	2.40	2.15	0.95	0.18	0.07	0.51	−0.23	−0.38	0.02	0.15	−0.19
500	0.0130	0.8618	1.87	1.54	0.90	0.33	0.03	0.55	−0.26	−0.48	0.00	0.08	−0.06
500	0.0200	0.7087	2.07	1.53	1.11	0.70	0.00	0.83	−0.70	−0.45	0.00	0.00	0.00
500	0.0320	0.6061	2.09	1.57	1.03	0.50	0.26	0.92	0.51	−0.37	0.06	0.67	0.00
500	0.0500	0.5288	2.18	1.66	1.10	0.62	0.23	0.88	0.63	−0.38	−0.11	0.47	0.00
500	0.0800	0.4184	2.64	1.87	1.06	0.52	0.13	1.53	0.52	−0.47	0.01	1.36	0.00
500	0.1300	0.3636	2.92	2.17	1.33	0.55	0.05	1.43	0.55	−0.43	−0.07	1.25	0.00
500	0.1800	0.3247	3.17	2.34	1.83	0.87	0.86	1.09	0.87	−0.58	−0.30	−0.11	0.00
500	0.2500	0.2483	5.10	2.77	2.52	1.06	1.73	3.46	1.06	−0.55	−0.42	−3.22	0.00
650	0.0130	0.8722	2.03	1.73	0.96	0.41	0.05	0.45	−0.26	−0.31	0.02	0.14	−0.13
650	0.0200	0.7433	2.17	1.79	1.01	0.48	0.01	0.71	−0.49	−0.52	0.00	0.03	−0.01
650	0.0320	0.6288	2.51	1.85	1.34	0.98	0.00	1.04	−0.92	−0.50	0.00	0.00	0.00
650	0.0500	0.5264	2.40	1.95	1.10	0.60	0.08	0.89	0.68	−0.38	−0.07	0.42	0.00
650	0.0800	0.4200	2.73	2.22	1.08	0.47	0.12	1.18	0.52	−0.32	−0.07	1.01	0.00
650	0.1300	0.3491	3.25	2.54	1.42	0.63	0.17	1.46	0.66	−0.43	−0.08	1.23	0.00
650	0.1800	0.3167	3.22	2.63	1.64	0.74	0.40	0.87	0.76	−0.37	−0.15	0.15	0.00
650	0.2500	0.2464	5.05	3.33	2.48	1.20	1.53	2.88	1.17	−0.48	−0.39	−2.56	0.00
650	0.4000	0.1183	7.48	5.00	3.52	1.60	2.28	4.29	1.61	−0.72	−0.54	−3.88	0.00

Table 25: The NC e^-p reduced cross section $\tilde{\sigma}_{\rm NC}(x,Q^2)$ for $P_e = 0$ with statistical ($\delta_{\rm stat}$), total (δ_{tot}), total uncorrelated systematic ($\delta_{\rm unc}$) errors, two of its contributions from the electron energy error (δ^{E}_{unc}) and the hadronic energy error ($\delta^{h}_{\rm unc}$). The effect of the other uncorrelated systematic errors is included in $\delta_{\rm unc}$. In addition the correlated systematic ($\delta_{\rm cor}$) and its contributions from a positive variation of one standard deviation of the electron energy error ($\delta^{E^+}_{cor}$), of the polar electron angle error ($\delta^{\theta^+}_{\rm cor}$), of the hadronic energy error ($\delta^{h^+}_{\rm cor}$), of the error due to noise subtraction ($\delta^{N^+}_{\rm cor}$) and of the error due to background subtraction ($\delta^{B^+}_{\rm cor}$) are given. The normalisation and polarisation uncertainties are not included in the errors. The table continues on the next page.

Q^2 (GeV^2)	x	$\tilde{\sigma}_{\mathrm{NC}}$	δ_{tot} (%)	δ_{stat} (%)	δ_{unc} (%)	$\delta^{E}_{\mathrm{unc}}$ (%)	$\delta^{h}_{\mathrm{unc}}$ (%)	δ_{cor} (%)	$\delta^{E+}_{\mathrm{cor}}$ (%)	$\delta^{\theta+}_{\mathrm{cor}}$ (%)	$\delta^{h+}_{\mathrm{cor}}$ (%)	$\delta^{N+}_{\mathrm{cor}}$ (%)	$\delta^{B+}_{\mathrm{cor}}$ (%)
800	0.0130	0.8721	3.12	2.91	1.05	0.21	0.08	0.42	0.10	−0.35	0.02	0.18	−0.12
800	0.0200	0.7107	2.37	2.09	1.03	0.48	0.02	0.44	−0.27	−0.34	0.00	0.08	−0.05
800	0.0320	0.6105	2.67	2.20	1.30	0.88	0.00	0.77	−0.62	−0.47	0.00	0.00	0.00
800	0.0500	0.5357	2.57	2.27	1.00	0.24	0.11	0.65	0.41	−0.29	−0.02	0.42	−0.02
800	0.0800	0.4131	3.01	2.57	1.12	0.41	0.21	1.08	0.59	−0.45	−0.06	0.78	0.00
800	0.1300	0.3417	3.64	3.08	1.38	0.36	0.21	1.37	0.58	−0.38	−0.04	1.19	0.00
800	0.1800	0.3115	3.81	3.24	1.75	0.67	0.67	0.97	0.83	−0.40	−0.21	0.19	0.00
800	0.2500	0.2344	4.70	3.81	2.10	0.71	1.13	1.78	0.90	−0.33	−0.24	−1.48	0.00
800	0.4000	0.1288	8.54	5.03	4.06	1.61	2.94	5.58	1.71	−0.66	−0.79	−5.21	0.00
1000	0.0130	0.8320	3.50	2.87	1.54	0.27	0.22	1.26	−0.03	−0.20	0.05	0.18	−1.23
1000	0.0200	0.7428	2.64	2.42	0.98	0.33	0.05	0.44	−0.19	−0.37	0.01	0.11	−0.11
1000	0.0320	0.6432	2.70	2.42	1.08	0.57	0.00	0.53	−0.29	−0.44	0.00	0.01	0.00
1000	0.0500	0.4971	3.14	2.63	1.45	1.09	0.00	0.92	−0.64	−0.66	0.00	0.00	0.00
1000	0.0800	0.4223	3.16	2.87	1.02	0.21	0.17	0.83	0.25	−0.26	0.07	0.75	0.00
1000	0.1300	0.3452	3.90	3.41	1.35	0.26	0.23	1.32	0.41	−0.31	−0.12	1.20	0.00
1000	0.1800	0.3367	3.87	3.38	1.67	0.65	0.55	0.85	0.63	−0.40	−0.21	0.35	0.00
1000	0.2500	0.2619	4.54	3.80	2.03	0.82	0.97	1.44	0.93	−0.38	−0.31	−0.97	0.00
1000	0.4000	0.1253	8.71	5.47	4.20	1.96	2.99	5.31	1.61	−0.53	−0.61	−4.99	0.00
1200	0.0130	0.8623	5.36	4.65	2.03	0.09	0.25	1.73	0.23	0.15	0.05	0.20	−1.70
1200	0.0200	0.7572	3.22	2.99	1.11	0.17	0.08	0.43	−0.11	−0.28	0.02	0.11	−0.29
1200	0.0320	0.6579	2.94	2.74	0.94	0.36	0.02	0.52	−0.27	−0.45	0.00	0.06	−0.01
1200	0.0500	0.5236	3.19	2.90	1.19	0.80	0.00	0.60	−0.42	−0.43	0.00	0.00	0.00
1200	0.0800	0.4463	3.45	3.10	1.31	0.93	0.20	0.79	0.59	−0.27	−0.13	0.42	0.00
1200	0.1300	0.3428	4.64	4.31	1.44	0.75	0.06	0.95	0.48	−0.17	−0.03	0.80	0.00
1200	0.1800	0.3026	4.39	3.97	1.69	0.93	0.38	0.80	0.61	−0.28	−0.14	0.41	0.00
1200	0.2500	0.2140	5.10	4.63	1.99	1.15	0.69	0.83	0.75	−0.28	−0.19	−0.17	0.00
1200	0.4000	0.1249	8.54	5.78	4.29	2.60	2.69	4.59	1.67	−0.33	−0.69	−4.20	0.00
1500	0.0200	0.7724	4.08	3.59	1.66	0.10	0.16	0.99	0.14	−0.27	0.03	0.15	−0.93
1500	0.0320	0.6540	3.57	3.40	1.01	0.35	0.05	0.47	−0.36	−0.27	0.01	0.12	−0.05
1500	0.0500	0.5406	3.60	3.34	1.21	0.79	0.00	0.57	−0.39	−0.42	0.00	0.01	0.00
1500	0.0800	0.4800	3.66	3.42	1.16	0.68	0.09	0.65	0.39	−0.17	0.00	0.48	0.00
1500	0.1300	0.3415	5.10	4.77	1.57	0.91	0.17	0.87	0.63	−0.22	−0.07	0.55	0.00
1500	0.1800	0.2914	5.06	4.62	1.80	1.12	0.22	1.00	0.63	−0.18	−0.13	0.74	0.00
1500	0.2500	0.2344	5.50	4.96	2.20	1.35	0.89	0.88	0.72	−0.15	−0.22	−0.43	0.00
1500	0.4000	0.1208	9.06	7.42	3.87	2.32	2.23	3.45	1.43	−0.33	−0.59	−3.06	0.00
1500	0.6500	0.01387	18.01	12.53	6.95	4.57	4.52	10.90	3.07	−0.44	−0.97	−10.41	0.00
2000	0.0219	0.8405	6.23	5.59	2.19	0.25	0.19	1.66	0.16	−0.20	0.04	0.20	−1.63
2000	0.0320	0.6258	4.32	4.06	1.41	0.20	0.10	0.47	−0.10	−0.39	0.03	0.14	−0.21
2000	0.0500	0.5298	4.26	4.10	1.08	0.45	0.02	0.43	−0.30	−0.31	0.01	0.04	−0.02
2000	0.0800	0.4349	4.41	4.15	1.31	0.80	0.00	0.71	−0.55	−0.45	0.00	0.00	0.00
2000	0.1300	0.3449	5.37	5.09	1.53	0.72	0.11	0.80	0.39	−0.22	0.07	0.65	0.00
2000	0.1800	0.2915	5.89	5.43	2.06	1.43	0.29	0.98	0.80	−0.26	−0.13	0.50	0.00
2000	0.2500	0.2398	6.07	5.62	2.14	1.33	0.64	0.86	0.76	−0.28	−0.18	−0.22	0.00
2000	0.4000	0.1221	8.46	7.14	3.63	2.22	1.84	2.75	1.33	−0.11	−0.51	−2.35	0.00
2000	0.6500	0.009670	21.36	16.95	7.85	5.10	5.25	10.35	2.65	−0.48	−1.07	−9.94	0.00
3000	0.0320	0.7040	4.25	3.80	1.74	0.18	0.11	0.74	−0.12	−0.29	0.02	0.11	−0.66
3000	0.0500	0.5792	3.61	3.33	1.34	0.18	0.06	0.37	−0.09	−0.34	0.02	0.08	−0.06
3000	0.0800	0.4805	3.88	3.65	1.23	0.50	0.00	0.51	−0.31	−0.40	0.00	0.01	0.00
3000	0.1300	0.3877	4.75	4.41	1.63	0.86	0.00	0.62	−0.50	−0.36	0.00	0.00	0.00
3000	0.1800	0.2895	5.45	5.07	1.81	1.09	0.19	0.84	0.62	−0.11	−0.07	0.56	0.00
3000	0.2500	0.2321	5.69	5.21	2.11	1.42	0.39	0.91	0.86	−0.07	−0.12	0.26	0.00
3000	0.4000	0.1124	7.82	6.48	3.76	2.58	1.70	2.23	1.58	−0.18	−0.42	−1.51	0.00
3000	0.6500	0.01050	17.55	13.52	7.22	4.58	4.93	8.56	2.79	−0.21	−1.37	−7.97	0.00
5000	0.0547	0.6174	5.46	5.07	1.90	0.12	0.13	0.69	0.05	−0.36	0.03	0.13	−0.57
5000	0.0800	0.5100	4.26	3.98	1.50	0.19	0.05	0.36	−0.20	−0.28	0.01	0.07	−0.11
5000	0.1300	0.4498	4.79	4.46	1.70	0.28	0.01	0.45	0.24	−0.38	0.00	0.01	−0.01
5000	0.1800	0.3628	5.45	5.15	1.75	0.27	0.00	0.38	−0.17	−0.34	0.00	0.00	0.00
5000	0.2500	0.2268	8.07	7.73	2.19	1.11	0.00	0.82	0.81	−0.12	0.00	0.00	0.00
5000	0.4000	0.1141	8.67	7.82	3.34	1.88	1.42	1.66	1.31	−0.04	−0.46	−0.90	0.00
5000	0.6500	0.01375	16.53	13.90	6.85	4.13	4.61	5.75	2.45	0.20	−1.16	−5.07	0.00
8000	0.0875	0.6162	7.97	7.49	2.49	0.39	0.09	1.09	0.22	−0.35	0.02	0.11	−1.00
8000	0.1300	0.5010	6.40	5.98	2.23	0.28	0.03	0.43	−0.19	−0.29	0.01	0.06	−0.25
8000	0.1800	0.3708	6.96	6.61	2.14	0.16	0.02	0.36	−0.05	−0.36	0.01	0.02	0.00
8000	0.2500	0.2533	8.02	7.62	2.46	1.04	0.00	0.52	0.52	0.03	0.00	0.00	0.00
8000	0.4000	0.1138	11.63	10.50	4.51	3.51	0.00	2.16	2.09	0.53	0.00	0.00	0.00
8000	0.6500	0.01193	18.53	16.94	6.54	4.19	3.75	3.66	2.39	0.23	−0.87	−2.63	0.00
12000	0.1300	0.6999	13.48	12.90	3.66	0.51	0.13	1.42	0.34	−0.30	0.04	0.12	−1.34
12000	0.1800	0.4797	8.61	8.32	2.20	0.17	0.08	0.38	−0.03	−0.31	0.03	0.10	−0.19
12000	0.2500	0.3018	9.61	9.27	2.47	1.05	0.02	0.50	0.48	−0.13	0.01	0.03	0.00
12000	0.4000	0.1878	11.98	10.80	4.89	4.02	0.00	1.79	1.68	0.60	0.00	0.00	0.00
12000	0.6500	0.01352	24.68	23.62	6.34	4.68	3.06	3.31	2.56	0.45	−0.84	−1.86	0.00
20000	0.2500	0.4615	12.77	12.42	2.81	1.17	0.08	0.93	0.43	−0.17	0.03	0.06	−0.81
20000	0.4000	0.2125	14.46	13.68	4.57	3.59	0.03	1.03	1.02	0.12	0.01	0.03	−0.11
20000	0.6500	0.01647	39.16	35.42	15.88	15.54	0.00	5.20	4.46	2.67	0.00	0.00	0.00
30000	0.4000	0.1903	28.38	27.72	5.74	3.39	0.14	2.13	1.05	−0.25	0.03	0.09	−1.83
30000	0.6500	0.03988	33.85	31.66	11.35	10.79	0.00	3.90	3.42	1.86	0.00	0.01	0.00
50000	0.6500	0.07518	58.83	57.79	10.56	8.88	0.00	3.06	2.83	1.17	0.00	0.00	0.00

Table 25: continued.

Q^2 (GeV^2)	x	$\tilde{\sigma}_{\mathrm{NC}}$	δ_{tot} (%)	δ_{stat} (%)	δ_{unc} (%)	$\delta_{\mathrm{unc}}^{E}$ (%)	$\delta_{\mathrm{unc}}^{h}$ (%)	δ_{cor} (%)	$\delta_{\mathrm{cor}}^{E^+}$ (%)	$\delta_{\mathrm{cor}}^{\theta^+}$ (%)	$\delta_{\mathrm{cor}}^{h^+}$ (%)	$\delta_{\mathrm{cor}}^{N^+}$ (%)	$\delta_{\mathrm{cor}}^{B^+}$ (%)
120	0.0020	1.334	1.49	0.65	0.80	0.43	0.09	1.08	−0.26	−0.65	0.02	0.18	−0.80
120	0.0032	1.194	1.63	0.94	1.03	0.73	0.03	0.84	−0.46	−0.67	0.01	0.18	−0.10
150	0.0032	1.211	1.25	0.55	0.80	0.49	0.06	0.78	−0.36	−0.53	0.01	0.18	−0.41
150	0.0050	1.075	1.53	0.66	1.09	0.87	0.00	0.84	−0.53	−0.65	0.00	0.04	−0.03
150	0.0080	0.9323	2.44	0.91	1.89	1.53	0.85	1.25	−1.00	−0.56	−0.24	−0.44	−0.05
150	0.0130	0.7854	3.75	1.28	2.72	2.39	1.01	2.25	−1.45	−1.37	−0.37	−0.97	−0.01
200	0.0032	1.218	1.55	1.04	0.74	0.13	0.08	0.88	−0.11	−0.63	0.02	0.18	−0.58
200	0.0050	1.085	1.33	0.72	0.84	0.53	0.03	0.74	−0.40	−0.61	0.01	0.12	−0.07
200	0.0080	0.9394	1.75	0.73	1.24	1.05	0.00	0.99	−0.59	−0.80	0.00	0.00	−0.01
200	0.0130	0.7867	1.30	0.83	0.68	0.02	0.02	0.73	−0.09	−0.40	−0.03	0.60	−0.01
200	0.0200	0.6805	1.55	0.91	1.00	0.72	0.02	0.75	−0.41	−0.49	−0.09	0.38	−0.01
200	0.0320	0.5756	1.91	1.05	1.34	0.99	0.54	0.85	−0.61	−0.55	−0.17	0.13	0.00
200	0.0500	0.5051	2.79	1.20	1.83	1.66	0.04	1.73	−1.05	−0.80	−0.08	1.11	0.00
200	0.0800	0.4300	3.12	1.32	2.00	1.80	0.17	1.99	−1.18	−0.74	−0.15	1.41	0.00
200	0.1300	0.3560	3.20	1.48	2.25	1.67	0.96	1.73	−0.97	−0.90	−0.27	−1.08	0.00
200	0.1800	0.3085	4.00	1.99	2.88	1.61	1.90	1.94	−0.88	−1.04	−0.34	−1.34	0.00
250	0.0050	1.103	1.27	0.84	0.72	0.29	0.06	0.63	−0.28	−0.45	0.01	0.16	−0.30
250	0.0080	0.9437	1.43	0.82	0.91	0.61	0.00	0.73	−0.53	−0.50	0.00	0.03	−0.02
250	0.0130	0.7952	1.83	0.92	1.15	0.91	0.21	1.09	0.48	−0.60	0.03	0.77	−0.02
250	0.0200	0.6829	1.92	0.93	1.29	1.07	0.19	1.07	0.49	−0.66	−0.02	0.68	−0.01
250	0.0320	0.5697	1.82	0.98	1.14	0.90	0.04	1.03	0.36	−0.48	0.01	0.83	0.00
250	0.0500	0.4946	2.21	1.07	1.15	0.89	0.10	1.55	0.39	−0.57	−0.09	1.39	0.00
250	0.0800	0.4294	2.67	1.11	0.98	0.56	0.20	2.22	0.31	−0.51	−0.05	2.14	0.00
250	0.1300	0.3623	2.31	1.20	1.72	1.13	0.68	0.98	0.51	−0.57	−0.23	−0.56	0.00
250	0.1800	0.2930	3.91	1.62	2.71	1.73	1.61	2.31	1.03	−0.78	−0.34	−1.88	0.00
300	0.0050	1.115	1.79	1.44	0.81	0.28	0.07	0.68	−0.28	−0.37	0.02	0.15	−0.48
300	0.0080	0.9575	1.38	0.96	0.73	0.30	0.02	0.67	−0.30	−0.59	0.00	0.10	−0.05
300	0.0130	0.7917	1.59	0.97	0.93	0.63	0.00	0.84	−0.62	−0.57	0.00	0.00	−0.01
300	0.0200	0.6989	1.63	1.07	0.88	0.53	0.12	0.86	0.36	−0.46	−0.01	0.64	−0.02
300	0.0320	0.5730	1.83	1.13	1.09	0.83	0.09	0.95	0.43	−0.55	−0.02	0.64	−0.01
300	0.0500	0.4888	2.15	1.23	1.23	0.98	0.14	1.26	0.49	−0.54	−0.05	1.03	0.00
300	0.0800	0.4330	2.92	1.26	1.37	1.08	0.30	2.25	0.51	−0.69	−0.06	2.08	−0.01
300	0.1300	0.3646	2.58	1.30	1.86	1.40	0.51	1.23	0.68	−0.73	−0.20	0.69	0.00
300	0.1800	0.3022	4.42	1.68	2.89	2.01	1.61	2.89	1.07	−0.68	−0.30	−2.58	0.00
300	0.4000	0.1479	6.45	2.13	3.67	2.40	2.17	4.86	1.34	−1.02	−0.45	−4.53	0.00
400	0.0080	0.9823	1.51	1.19	0.74	0.26	0.06	0.58	−0.27	−0.44	0.01	0.14	−0.22
400	0.0130	0.8346	1.54	1.12	0.82	0.45	0.01	0.67	−0.45	−0.49	0.00	0.03	−0.01
400	0.0200	0.6979	1.92	1.17	1.11	0.86	0.00	1.04	−0.86	−0.58	0.00	0.00	0.00
400	0.0320	0.5861	1.81	1.26	0.88	0.49	0.15	0.95	0.48	−0.48	−0.03	0.66	−0.01
400	0.0500	0.4898	1.99	1.38	1.04	0.67	0.32	0.99	0.64	−0.49	−0.09	0.57	0.00
400	0.0800	0.4217	2.63	1.46	0.90	0.25	0.38	1.99	0.22	−0.30	−0.02	1.96	0.00
400	0.1300	0.3518	2.27	1.43	1.35	0.64	0.40	1.14	0.59	−0.47	−0.16	0.85	0.00
400	0.1800	0.3007	4.28	1.86	2.40	1.11	1.68	3.02	1.04	−0.56	−0.38	−2.75	0.00
400	0.4000	0.1464	6.80	2.35	3.22	1.37	2.28	5.51	1.28	−0.78	−0.46	−5.28	0.00
500	0.0080	0.9650	2.24	1.98	0.87	0.31	0.09	0.57	−0.15	−0.42	0.01	0.16	−0.32
500	0.0130	0.8515	1.67	1.39	0.76	0.29	0.02	0.52	−0.24	−0.46	0.01	0.09	−0.04
500	0.0200	0.7287	1.90	1.40	0.97	0.65	0.00	0.83	−0.64	−0.54	0.00	0.00	0.00
500	0.0320	0.5984	1.96	1.48	0.91	0.41	0.36	0.90	0.42	−0.37	0.07	0.70	−0.01
500	0.0500	0.5193	2.10	1.53	1.06	0.68	0.30	0.97	0.68	−0.49	−0.16	0.46	0.00
500	0.0800	0.4325	2.49	1.65	0.90	0.34	0.28	1.63	0.34	−0.33	0.06	1.56	0.00
500	0.1300	0.3780	2.83	1.90	1.30	0.65	0.04	1.65	0.65	−0.53	−0.07	1.41	0.00
500	0.1800	0.3072	2.91	2.13	1.73	0.78	0.86	0.96	0.78	−0.42	−0.22	−0.30	0.00
500	0.2500	0.2451	5.72	2.63	2.76	1.22	2.02	4.27	1.22	−0.55	−0.42	−4.03	0.00
650	0.0130	0.8403	1.81	1.58	0.76	0.18	0.05	0.43	−0.16	−0.37	0.01	0.12	−0.11
650	0.0200	0.7202	2.02	1.65	0.95	0.58	0.00	0.67	−0.41	−0.53	0.00	0.02	−0.02
650	0.0320	0.6338	2.30	1.70	1.17	0.87	0.00	1.01	−0.82	−0.58	0.00	0.00	0.00
650	0.0500	0.5105	2.26	1.80	1.02	0.63	0.11	0.92	0.69	−0.35	0.06	0.49	0.00
650	0.0800	0.4128	2.67	2.01	0.97	0.48	0.11	1.46	0.50	−0.50	0.06	1.28	0.00
650	0.1300	0.3681	3.08	2.31	1.31	0.59	0.05	1.57	0.64	−0.21	−0.10	1.41	0.00
650	0.1800	0.3309	2.94	2.33	1.56	0.64	0.50	0.89	0.66	−0.46	−0.25	0.28	0.00
650	0.2500	0.2360	5.10	2.97	2.51	1.30	1.58	3.29	1.32	−0.55	−0.38	−2.93	0.00
650	0.4000	0.1328	7.39	4.22	3.65	1.44	2.61	4.84	1.46	−0.58	−0.59	−4.54	0.00

Table 26: The NC e^+p reduced cross section $\tilde{\sigma}_{\mathrm{NC}}(x, Q^2)$ for $P_e = 0$ with statistical (δ_{stat}), total (δ_{tot}), total uncorrelated systematic (δ_{unc}) errors, two of its contributions from the electron energy error (δ_{unc}^{E}) and the hadronic energy error ($\delta_{\mathrm{unc}}^{h}$). The effect of the other uncorrelated systematic errors is included in δ_{unc}. In addition the correlated systematic (δ_{cor}) and its contributions from a positive variation of one standard deviation of the electron energy error ($\delta_{cor}^{E^+}$), of the polar electron angle error ($\delta_{\mathrm{cor}}^{\theta^+}$), of the hadronic energy error ($\delta_{\mathrm{cor}}^{h^+}$), of the error due to noise subtraction ($\delta_{\mathrm{cor}}^{N^+}$) and of the error due to background subtraction ($\delta_{\mathrm{cor}}^{B^+}$) are given. The normalisation and polarisation uncertainties are not included in the errors. The table continues on the next page.

Q^2 (GeV^2)	x	$\tilde{\sigma}_{NC}$	δ_{tot} (%)	δ_{stat} (%)	δ_{unc} (%)	δ^{E}_{unc} (%)	δ^{h}_{unc} (%)	δ_{cor} (%)	$\delta^{E^+}_{cor}$ (%)	$\delta^{\theta^+}_{cor}$ (%)	$\delta^{h^+}_{cor}$ (%)	$\delta^{N^+}_{cor}$ (%)	$\delta^{B^+}_{cor}$ (%)
800	0.0130	0.8056	2.83	2.60	0.96	0.17	0.08	0.53	−0.29	−0.36	0.03	0.14	−0.21
800	0.0200	0.6896	2.14	1.89	0.89	0.43	0.02	0.46	−0.29	−0.35	0.00	0.08	−0.05
800	0.0320	0.6051	2.38	1.99	1.11	0.73	0.00	0.70	−0.51	−0.48	0.00	0.00	0.00
800	0.0500	0.5182	2.44	2.13	0.91	0.23	0.22	0.76	0.37	−0.29	0.13	0.58	0.00
800	0.0800	0.4481	2.74	2.26	1.07	0.48	0.28	1.13	0.73	−0.43	−0.12	0.73	0.00
800	0.1300	0.3511	3.39	2.66	1.33	0.44	0.19	1.63	0.63	−0.52	−0.09	1.40	0.00
800	0.1800	0.3203	3.32	2.76	1.59	0.58	0.53	0.92	0.70	−0.47	−0.14	0.33	0.00
800	0.2500	0.2364	4.48	3.27	2.26	0.96	1.33	2.07	1.04	−0.44	−0.43	−1.68	0.00
800	0.4000	0.1200	8.56	4.81	4.02	2.02	2.66	5.83	1.97	−0.56	−0.63	−5.42	0.00
1000	0.0130	0.7857	3.27	2.66	1.45	0.14	0.24	1.24	−0.10	−0.29	0.04	0.21	−1.18
1000	0.0200	0.7184	2.41	2.20	0.85	0.31	0.05	0.48	−0.22	−0.39	0.01	0.13	−0.12
1000	0.0320	0.6057	2.48	2.18	1.02	0.65	0.00	0.57	−0.41	−0.39	0.00	0.01	−0.01
1000	0.0500	0.5105	2.90	2.34	1.49	1.24	0.00	0.84	−0.69	−0.48	0.00	0.00	0.00
1000	0.0800	0.4320	2.84	2.56	1.04	0.50	0.29	0.64	0.38	−0.22	−0.13	0.44	−0.01
1000	0.1300	0.3352	3.73	3.27	1.26	0.30	0.22	1.27	0.30	0.14	0.09	1.23	0.00
1000	0.1800	0.2953	3.66	3.26	1.44	0.33	0.39	0.84	0.46	−0.33	−0.20	0.59	0.00
1000	0.2500	0.2407	4.38	3.61	2.01	0.83	1.05	1.46	0.98	−0.43	−0.21	−0.98	0.00
1000	0.4000	0.1273	8.40	5.95	3.66	1.38	2.63	4.66	1.40	−0.41	−0.63	−4.37	0.00
1200	0.0130	0.8194	5.30	4.39	2.11	0.13	0.30	2.09	−0.14	−0.22	0.06	0.23	−2.06
1200	0.0200	0.6982	2.98	2.78	0.98	0.13	0.08	0.40	0.08	−0.29	0.02	0.12	−0.23
1200	0.0320	0.5986	2.74	2.56	0.85	0.43	0.02	0.46	−0.24	−0.39	0.00	0.06	−0.01
1200	0.0500	0.5067	3.00	2.63	1.24	0.98	0.00	0.74	−0.57	−0.47	0.00	0.00	−0.01
1200	0.0800	0.4254	3.16	2.84	1.14	0.80	0.11	0.78	0.56	−0.30	−0.09	0.45	0.00
1200	0.1300	0.3382	3.90	3.47	1.52	1.01	0.13	0.91	0.59	−0.29	−0.05	0.63	0.00
1200	0.1800	0.3154	4.28	3.83	1.45	0.71	0.05	1.22	0.53	−0.30	−0.14	1.04	−0.01
1200	0.2500	0.2462	4.77	4.12	2.18	1.38	0.97	1.00	0.83	−0.28	−0.28	−0.41	0.00
1200	0.4000	0.1067	8.83	5.68	4.30	2.61	2.74	5.22	1.66	−0.52	−0.57	−4.88	0.00
1500	0.0200	0.6717	3.95	3.49	1.62	0.13	0.21	0.89	0.23	−0.27	0.05	0.20	−0.79
1500	0.0320	0.5863	3.46	3.33	0.85	0.25	0.05	0.45	−0.25	−0.36	0.02	0.11	−0.03
1500	0.0500	0.5213	3.21	3.00	1.00	0.62	0.00	0.51	−0.29	−0.42	0.00	0.02	0.00
1500	0.0800	0.4430	3.61	3.31	1.25	0.94	0.04	0.74	0.59	−0.19	−0.10	0.38	0.00
1500	0.1300	0.3287	4.36	4.01	1.49	0.86	0.06	0.85	0.51	−0.25	0.06	0.64	0.00
1500	0.1800	0.2974	4.50	4.10	1.53	0.80	0.04	1.07	0.53	−0.20	0.05	0.91	0.00
1500	0.2500	0.2276	5.16	4.46	2.38	1.56	1.11	1.06	0.94	−0.19	−0.37	−0.26	0.00
1500	0.4000	0.1214	7.74	5.75	3.63	2.15	2.05	3.70	1.21	−0.24	−0.51	−3.45	0.00
1500	0.6500	0.01480	16.82	10.87	7.13	4.51	4.88	10.67	2.81	−0.32	−1.00	−10.24	0.00
2000	0.0219	0.6850	6.33	5.63	2.40	0.55	0.21	1.62	0.24	−0.14	0.05	0.20	−1.58
2000	0.0320	0.5398	4.19	3.94	1.33	0.22	0.09	0.50	−0.17	−0.41	0.02	0.11	−0.20
2000	0.0500	0.5250	3.82	3.67	1.01	0.42	0.01	0.37	−0.25	−0.26	0.00	0.04	0.00
2000	0.0800	0.4199	4.01	3.73	1.28	0.89	0.00	0.75	−0.46	−0.60	0.00	0.00	0.00
2000	0.1300	0.3413	5.26	4.96	1.60	1.00	0.10	0.73	0.47	−0.21	−0.09	0.51	0.00
2000	0.1800	0.2973	5.19	4.80	1.50	0.58	0.25	1.26	0.43	−0.28	0.19	1.14	0.00
2000	0.2500	0.2331	5.64	4.98	2.39	1.66	0.91	1.14	1.07	−0.29	−0.23	−0.01	0.00
2000	0.4000	0.1250	8.10	6.30	3.94	2.57	2.09	3.23	1.61	−0.27	−0.62	−2.71	0.00
2000	0.6500	0.01368	18.37	12.83	7.46	4.72	5.11	10.82	2.84	−0.28	−1.06	−10.38	0.00
3000	0.0320	0.5847	4.22	3.74	1.72	0.20	0.13	0.93	0.05	−0.27	0.03	0.13	−0.88
3000	0.0500	0.4979	3.48	3.23	1.26	0.22	0.07	0.35	−0.07	−0.33	0.02	0.09	−0.06
3000	0.0800	0.4309	3.65	3.42	1.15	0.52	0.01	0.56	−0.33	−0.45	0.00	0.02	−0.01
3000	0.1300	0.3349	4.49	4.18	1.50	0.73	0.00	0.65	−0.50	−0.42	0.00	0.00	0.00
3000	0.1800	0.2973	5.61	5.17	1.95	1.41	0.05	0.95	0.78	−0.15	−0.04	0.53	0.00
3000	0.2500	0.2221	5.14	4.66	1.95	1.32	0.20	0.97	0.76	−0.10	−0.10	0.58	0.00
3000	0.4000	0.1191	7.27	5.62	3.86	2.62	1.91	2.54	1.51	−0.10	−0.50	−1.98	0.00
3000	0.6500	0.01256	16.63	11.50	7.93	5.27	5.35	9.02	3.30	−0.26	−1.39	−8.28	0.00
5000	0.0547	0.4615	5.59	5.08	2.01	0.52	0.11	1.18	0.16	−0.33	0.05	0.10	−1.12
5000	0.0800	0.4038	4.20	3.93	1.44	0.15	0.06	0.38	−0.11	−0.33	0.02	0.07	−0.15
5000	0.1300	0.3351	4.96	4.63	1.68	0.36	0.00	0.54	0.27	−0.46	0.00	0.02	0.00
5000	0.1800	0.2902	5.45	5.14	1.75	0.49	0.00	0.50	−0.31	−0.39	0.00	0.00	0.00
5000	0.2500	0.2126	6.47	6.13	1.97	0.71	0.00	0.55	0.54	−0.08	0.00	0.00	0.00
5000	0.4000	0.1030	8.32	7.49	3.32	1.90	1.42	1.45	1.19	0.05	−0.43	−0.69	0.00
5000	0.6500	0.009650	17.88	15.48	6.50	3.98	4.26	6.14	2.06	−0.07	−1.19	−5.66	0.00
8000	0.0875	0.3440	9.35	8.73	2.69	0.33	0.11	2.01	0.13	−0.24	0.05	0.09	−1.99
8000	0.1300	0.2846	7.38	7.00	2.29	0.34	0.06	0.45	−0.20	−0.33	0.02	0.07	−0.23
8000	0.1800	0.2586	7.39	7.05	2.17	0.29	0.01	0.48	0.18	−0.44	0.00	0.02	0.00
8000	0.2500	0.2164	9.14	8.83	2.30	0.56	0.00	0.49	0.43	−0.25	0.00	0.00	0.00
8000	0.4000	0.09858	11.16	10.12	4.30	3.21	0.00	1.89	1.84	0.42	0.00	0.00	0.00
8000	0.6500	0.01341	17.48	15.28	7.24	4.89	4.15	4.42	2.67	0.25	−1.14	−3.32	0.00
12000	0.1300	0.2077	20.59	19.89	5.03	0.64	0.10	1.66	−0.76	−0.46	0.03	0.09	−1.40
12000	0.1800	0.2120	11.71	11.41	2.45	0.63	0.07	0.93	0.31	−0.46	0.02	0.08	−0.75
12000	0.2500	0.1536	12.11	11.86	2.40	0.88	0.02	0.52	0.41	−0.32	0.00	0.04	0.00
12000	0.4000	0.09789	14.69	13.91	4.47	3.53	0.00	1.56	1.51	0.38	0.00	0.00	0.00
12000	0.6500	0.01541	22.64	21.37	6.72	5.23	3.04	3.30	2.78	0.26	−0.75	−1.59	0.00
20000	0.2500	0.1267	20.22	19.92	3.32	2.22	0.09	0.90	0.82	0.22	0.04	0.10	−0.27
20000	0.4000	0.09396	19.49	18.99	4.30	3.27	0.02	0.93	0.92	−0.07	0.01	0.03	0.00
20000	0.6500	0.009430	47.59	44.86	15.10	14.72	0.00	4.96	4.41	2.28	0.00	0.00	0.00
30000	0.4000	0.05285	46.67	46.39	5.08	3.43	0.07	1.04	0.99	−0.21	0.01	0.06	−0.24
30000	0.6500	0.007890	71.87	71.13	9.87	9.04	0.00	3.00	2.73	1.24	0.00	0.00	0.00

Table 26: continued.

Q^2 (GeV^2)	x	y	$\mathrm{d}^2\sigma_{CC}/\mathrm{d}x\mathrm{d}Q^2$ ($\mathrm{pb/GeV}^2$)	δ_{tot} (%)	δ_{stat} (%)	δ_{unc} (%)	δ_{unc}^{h} (%)	δ_{cor} (%)	δ_{cor}^{V+} (%)	δ_{cor}^{h+} (%)	δ_{cor}^{N+} (%)	δ_{cor}^{B+} (%)
300	0.008	0.369	1.64	44.7	33.8	23.9	1.6	16.8	15.5	−0.3	−1.0	−4.9
300	0.013	0.227	0.720	19.9	13.4	10.9	2.6	9.9	9.4	−0.8	−0.3	−1.4
300	0.032	0.092	0.234	14.5	12.4	5.2	1.9	5.4	4.7	−0.4	0.5	−2.2
300	0.080	0.037	$0.640 \cdot 10^{-1}$	13.9	11.9	5.1	2.6	5.0	1.4	−0.4	−4.0	−2.0
500	0.013	0.379	0.629	14.2	8.8	7.1	2.3	8.6	8.5	−0.5	−0.7	−0.6
500	0.032	0.154	0.202	8.6	7.2	3.3	1.7	3.2	3.0	−0.6	0.1	−0.3
500	0.080	0.062	$0.508 \cdot 10^{-1}$	9.4	8.3	4.2	2.3	1.5	0.8	−0.6	−0.2	−0.3
500	0.130	0.038	$0.261 \cdot 10^{-1}$	24.0	19.7	5.4	0.7	12.6	0.1	0.6	−12.3	0.0
1000	0.013	0.757	0.390	13.3	9.1	5.8	1.8	7.9	7.8	−0.8	0.0	−0.4
1000	0.032	0.308	0.182	6.6	5.6	2.8	1.7	2.1	1.9	−0.4	0.3	−0.1
1000	0.080	0.123	$0.588 \cdot 10^{-1}$	6.5	5.7	2.9	0.9	1.4	0.4	−0.3	0.9	−0.1
1000	0.130	0.076	$0.255 \cdot 10^{-1}$	11.5	10.1	3.8	1.5	3.8	0.0	−0.1	−3.6	−0.1
2000	0.032	0.615	0.116	6.3	5.3	2.6	1.1	2.1	1.9	−0.4	−0.3	−0.1
2000	0.080	0.246	$0.438 \cdot 10^{-1}$	5.4	4.8	2.1	0.6	1.0	0.1	−0.1	0.7	0.0
2000	0.130	0.152	$0.225 \cdot 10^{-1}$	7.5	6.8	3.0	0.9	1.1	−0.0	−0.4	−0.3	0.0
2000	0.250	0.079	$0.841 \cdot 10^{-2}$	16.3	13.0	3.9	0.5	9.0	0.0	0.3	−8.8	0.0
3000	0.080	0.369	$0.323 \cdot 10^{-1}$	5.2	4.6	2.0	0.2	1.1	−0.1	0.1	0.9	0.0
3000	0.130	0.227	$0.177 \cdot 10^{-1}$	6.1	5.6	2.1	0.3	1.1	−0.0	−0.1	0.8	0.0
3000	0.250	0.118	$0.665 \cdot 10^{-2}$	9.1	8.3	2.9	0.6	2.3	0.0	0.1	−2.0	−0.2
5000	0.080	0.615	$0.208 \cdot 10^{-1}$	6.6	5.9	2.4	0.9	1.4	0.1	0.2	1.1	0.0
5000	0.130	0.379	$0.125 \cdot 10^{-1}$	5.8	5.2	2.1	0.2	1.1	−0.0	0.1	0.8	0.0
5000	0.250	0.197	$0.471 \cdot 10^{-2}$	7.1	6.4	2.6	1.5	1.1	−0.0	0.4	0.3	−0.1
5000	0.400	0.123	$0.142 \cdot 10^{-2}$	19.8	17.4	5.4	4.7	7.7	0.0	1.0	−7.2	0.0
8000	0.130	0.606	$0.834 \cdot 10^{-2}$	7.7	6.4	3.5	2.6	2.1	−0.1	0.9	1.6	0.0
8000	0.250	0.315	$0.256 \cdot 10^{-2}$	7.5	6.6	3.0	2.1	1.6	−0.0	0.6	1.2	0.0
8000	0.400	0.197	$0.991 \cdot 10^{-3}$	13.7	12.3	5.5	5.0	2.4	0.0	1.4	−0.8	0.0
15000	0.250	0.591	$0.153 \cdot 10^{-2}$	9.8	7.6	5.5	4.8	2.7	−0.0	1.3	2.0	0.0
15000	0.400	0.369	$0.388 \cdot 10^{-3}$	12.1	10.0	6.1	5.6	2.7	0.0	1.7	1.4	0.0
30000	0.400	0.738	$0.149 \cdot 10^{-3}$	19.5	15.6	10.2	9.7	5.4	0.0	3.1	3.8	0.0

Table 27: The CC e^-p cross section $\mathrm{d}^2\sigma_{CC}/\mathrm{d}x\mathrm{d}Q^2$ for lepton beam polarisation $P_e = 0$ with statistical (δ_{stat}), total (δ_{tot}), total uncorrelated systematic (δ_{unc}) errors and one of its contributions from the hadronic energy error (δ_{unc}^{h}). The effect of the other uncorrelated systematic errors is included in δ_{unc}. In addition the correlated systematic (δ_{cor}) and its contributions from a positive variation of one standard deviation of the cuts against photoproduction (δ_{cor}^{V+}), of the hadronic energy error (δ_{cor}^{h+}), of the error due to noise subtraction (δ_{cor}^{N+}) and of the error due to background subtraction (δ_{cor}^{B+}) are given. The normalisation and polarisation uncertainties are not included in the errors.

Q^2 (GeV^2)	x	y	$\mathrm{d}^2\sigma_{CC}/\mathrm{d}x\mathrm{d}Q^2$ ($\mathrm{pb/GeV}^2$)	δ_{tot} (%)	δ_{stat} (%)	δ_{unc} (%)	δ^h_{unc} (%)	δ_{cor} (%)	δ^{V+}_{cor} (%)	δ^{h+}_{cor} (%)	δ^{N+}_{cor} (%)	δ^{B+}_{cor} (%)
300	0.008	0.369	0.938	44.0	30.7	26.0	2.5	17.9	16.0	−0.8	−0.6	−5.9
300	0.013	0.227	0.499	23.0	16.6	11.3	1.8	11.1	10.2	−0.5	−0.3	−3.5
300	0.032	0.092	0.192	13.5	10.7	5.3	1.7	6.4	5.3	−0.4	1.3	−3.1
300	0.080	0.037	$0.393 \cdot 10^{-1}$	15.9	14.4	5.1	2.3	4.4	1.9	−0.3	−3.2	−1.9
500	0.013	0.379	0.486	15.4	10.0	7.1	1.9	9.4	9.2	−0.6	−0.1	−0.9
500	0.032	0.154	0.182	8.9	7.4	3.2	1.5	3.6	3.4	−0.5	0.5	−0.6
500	0.080	0.062	$0.493 \cdot 10^{-1}$	9.0	8.1	3.6	0.9	1.4	0.9	−0.2	0.3	−0.4
500	0.130	0.038	$0.199 \cdot 10^{-1}$	24.4	20.6	5.7	0.7	11.7	0.2	−0.7	−11.5	0.0
1000	0.013	0.757	0.316	15.3	10.3	6.1	0.9	9.5	9.4	−0.5	0.5	−0.6
1000	0.032	0.308	0.149	6.8	5.9	2.3	0.9	2.2	2.0	−0.3	0.6	−0.1
1000	0.080	0.123	$0.366 \cdot 10^{-1}$	7.5	6.8	2.8	0.8	1.2	0.4	−0.3	0.8	−0.1
1000	0.130	0.076	$0.177 \cdot 10^{-1}$	11.9	10.9	3.7	0.9	2.6	0.1	−0.3	−2.3	0.0
2000	0.032	0.615	$0.793 \cdot 10^{-1}$	7.0	6.1	2.4	0.3	2.5	2.2	−0.2	0.8	−0.1
2000	0.080	0.246	$0.269 \cdot 10^{-1}$	6.2	5.8	2.0	0.1	1.2	0.1	−0.0	0.9	−0.1
2000	0.130	0.152	$0.120 \cdot 10^{-1}$	9.2	8.6	3.0	0.8	1.2	0.0	0.3	0.7	0.0
2000	0.250	0.079	$0.356 \cdot 10^{-2}$	18.9	16.5	3.7	0.8	8.4	0.0	0.2	−8.2	0.0
3000	0.080	0.369	$0.185 \cdot 10^{-1}$	6.6	5.9	2.5	1.3	1.5	−0.0	0.5	1.2	0.0
3000	0.130	0.227	$0.107 \cdot 10^{-1}$	7.5	7.1	2.1	0.6	1.3	−0.0	0.2	0.9	0.0
3000	0.250	0.118	$0.210 \cdot 10^{-2}$	13.7	13.1	3.5	2.1	1.8	0.0	0.4	−1.3	0.0
3000	0.400	0.074	$0.236 \cdot 10^{-3}$	73.4	71.0	6.6	5.6	17.6	0.0	0.7	−16.9	0.0
5000	0.080	0.615	$0.696 \cdot 10^{-2}$	10.9	9.7	3.9	3.1	2.8	0.1	0.8	2.4	−0.1
5000	0.130	0.379	$0.476 \cdot 10^{-2}$	9.3	8.3	3.2	2.4	2.1	−0.1	0.7	1.7	0.0
5000	0.250	0.197	$0.136 \cdot 10^{-2}$	12.2	11.4	3.3	2.6	1.6	0.0	0.6	0.8	0.0
5000	0.400	0.123	$0.695 \cdot 10^{-3}$	24.3	21.3	7.7	7.2	8.4	0.0	1.5	−7.6	0.0
8000	0.130	0.606	$0.146 \cdot 10^{-2}$	15.4	13.7	5.6	5.0	3.2	−0.2	1.3	2.5	0.0
8000	0.250	0.315	$0.802 \cdot 10^{-3}$	12.7	11.3	4.4	3.8	2.5	0.0	1.2	1.8	0.0
8000	0.400	0.197	$0.195 \cdot 10^{-3}$	26.8	25.1	8.0	7.7	3.8	0.0	2.5	−1.2	0.0
15000	0.250	0.591	$0.201 \cdot 10^{-3}$	20.0	17.6	7.9	7.4	4.2	−0.1	2.2	2.9	0.0
15000	0.400	0.369	$0.335 \cdot 10^{-4}$	30.2	29.0	7.0	6.5	3.6	0.0	1.9	1.6	0.0

Table 28: The CC e^+p cross section $\mathrm{d}^2\sigma_{CC}/\mathrm{d}x\mathrm{d}Q^2$ for lepton beam polarisation $P_e = 0$ with statistical (δ_{stat}), total (δ_{tot}), total uncorrelated systematic (δ_{unc}) errors and one of its contributions from the hadronic energy error (δ^h_{unc}). The effect of the other uncorrelated systematic errors is included in δ_{unc}. In addition the correlated systematic (δ_{cor}) and its contributions from a positive variation of one standard deviation of the cuts against photoproduction (δ^{V+}_{cor}), of the hadronic energy error (δ^{h+}_{cor}), of the error due to noise subtraction (δ^{N+}_{cor}) and of the error due to background subtraction (δ^{B+}_{cor}) are given. The normalisation and polarisation uncertainties are not included in the errors.

Q^2 (GeV^2)	x	y	$\tilde{\sigma}_{\rm NC}$	F_2	$\delta_{\rm stat}$ (%)	$\delta_{\rm unc}$ (%)	$\delta_{\rm cor}$ (%)	$\delta_{\rm tot}$ (%)	$\sqrt{s}$ (GeV)
60	0.00080	0.750	1.465	—	1.01	1.84	1.65	2.67	319
90	0.00118	0.750	1.468	—	0.82	1.71	1.61	2.49	319
100	0.00131	0.750	1.355	—	4.02	5.50	1.75	7.03	319
100	0.00200	0.494	1.271	1.316	3.43	3.30	1.89	5.12	319
120	0.00158	0.750	1.421	—	0.92	1.71	1.57	2.50	319
120	0.00200	0.593	1.340	—	0.70	0.91	1.73	2.08	319
120	0.00320	0.371	1.205	1.224	0.96	1.08	1.54	2.12	319
150	0.00197	0.750	1.340	—	1.03	1.77	1.54	2.56	319
150	0.00320	0.463	1.215	1.248	0.59	0.85	1.59	1.90	319
150	0.00500	0.296	1.098	1.107	0.71	1.13	1.55	2.04	319
150	0.00800	0.185	0.9412	0.9427	0.97	1.72	1.63	2.56	319
150	0.01300	0.114	0.8045	0.8047	1.37	2.98	1.86	3.77	319
200	0.00263	0.750	1.267	—	1.30	1.85	1.53	2.74	319
200	0.00320	0.618	1.233	—	1.08	0.84	1.60	2.10	319
200	0.00500	0.395	1.097	1.115	0.76	0.91	1.54	1.94	319
200	0.00800	0.247	0.9478	0.9515	0.79	1.24	1.55	2.14	319
200	0.01300	0.152	0.7903	0.7898	0.89	0.81	1.51	1.93	319
200	0.02000	0.099	0.6919	0.6911	0.98	1.02	1.52	2.08	319
200	0.03200	0.062	0.5757	0.5750	1.11	1.37	1.56	2.36	319
200	0.05000	0.040	0.5208	0.5201	1.31	1.67	1.70	2.71	319
200	0.08000	0.025	0.4342	0.4332	1.37	2.10	1.82	3.10	319
200	0.13000	0.015	0.3591	0.3584	1.66	2.15	1.77	3.24	319
200	0.18000	0.011	0.3057	0.3056	2.25	2.74	1.87	4.01	319
250	0.00328	0.750	1.255	—	1.48	1.84	1.53	2.82	319
250	0.00500	0.494	1.113	1.144	0.89	0.83	1.54	1.97	319
250	0.00800	0.309	0.9610	0.9672	0.87	0.97	1.55	2.02	319
250	0.01300	0.190	0.8114	0.8110	0.95	1.18	1.60	2.20	319
250	0.02000	0.124	0.6854	0.6838	0.98	1.18	1.56	2.19	319
250	0.03200	0.077	0.5818	0.5807	1.03	1.28	1.58	2.28	319
250	0.05000	0.049	0.4930	0.4918	1.18	1.25	1.59	2.34	319
250	0.08000	0.031	0.4230	0.4221	1.21	1.04	1.75	2.37	319
250	0.13000	0.019	0.3607	0.3603	1.24	1.66	1.62	2.63	319
250	0.18000	0.014	0.3077	0.3074	1.75	2.69	2.09	3.83	319
250	0.25000	0.010	0.2265	0.2256	7.48	8.60	2.03	11.57	319
250	0.40000	0.006	0.1380	0.1378	9.30	6.80	1.68	11.64	319

Table 29: Combined HERA I+II NC e^-p reduced cross sections for $P_e = 0$. Here F_2 is the dominant electromagnetic structure function and $\delta_{\rm stat}$, $\delta_{\rm unc}$, $\delta_{\rm cor}$ and $\delta_{\rm tot}$ are the relative statistical, total uncorrelated, correlated systematic and total uncertainties, respectively. The table continues on the next pages.

Q^2 (GeV^2)	x	y	$\tilde{\sigma}_{\rm NC}$	F_2	$\delta_{\rm stat}$ (%)	$\delta_{\rm unc}$ (%)	$\delta_{\rm cor}$ (%)	$\delta_{\rm tot}$ (%)	$\sqrt{s}$ (GeV)
300	0.00394	0.750	1.202	—	1.71	1.83	1.52	2.93	319
300	0.00500	0.593	1.143	—	1.49	0.89	1.56	2.33	319
300	0.00800	0.371	0.9817	0.9921	1.01	0.83	1.52	2.01	319
300	0.01300	0.228	0.8203	0.8204	1.01	1.05	1.56	2.14	319
300	0.02000	0.148	0.7002	0.6985	1.12	1.01	1.57	2.18	319
300	0.03200	0.093	0.5882	0.5863	1.18	1.13	1.57	2.26	319
300	0.05000	0.059	0.4981	0.4965	1.28	1.35	1.62	2.47	319
300	0.08000	0.037	0.4196	0.4188	1.37	1.32	1.75	2.59	319
300	0.13000	0.023	0.3559	0.3551	1.37	1.78	1.62	2.77	319
300	0.18000	0.016	0.2962	0.2953	1.88	3.05	2.31	4.26	319
300	0.25000	0.012	0.2806	0.2804	6.86	9.40	2.36	11.87	319
300	0.40000	0.007	0.1484	0.1477	2.21	3.29	2.94	4.93	319
400	0.00525	0.750	1.142	—	1.85	1.83	1.51	3.01	319
400	0.00800	0.494	1.034	1.056	1.24	0.88	1.53	2.16	319
400	0.01300	0.304	0.8532	0.8547	1.19	0.91	1.53	2.14	319
400	0.02000	0.198	0.7108	0.7089	1.23	1.17	1.58	2.32	319
400	0.03200	0.124	0.5992	0.5963	1.30	0.93	1.55	2.23	319
400	0.05000	0.079	0.4951	0.4927	1.44	1.03	1.54	2.35	319
400	0.08000	0.049	0.4179	0.4161	1.54	0.97	1.66	2.47	319
400	0.13000	0.030	0.3643	0.3625	1.54	1.33	1.60	2.59	319
400	0.18000	0.022	0.3066	0.3058	1.97	2.44	2.20	3.83	319
400	0.25000	0.016	0.2400	0.2392	7.60	6.70	1.85	10.30	319
400	0.40000	0.010	0.1479	0.1476	2.56	3.00	3.17	5.06	319
500	0.00656	0.750	1.048	—	2.04	1.79	1.51	3.10	319
500	0.00800	0.618	0.9954	—	2.05	0.93	1.53	2.72	319
500	0.01300	0.380	0.8879	0.8919	1.46	0.88	1.52	2.28	319
500	0.02000	0.247	0.7267	0.7242	1.45	1.07	1.55	2.38	319
500	0.03200	0.154	0.6173	0.6131	1.49	0.99	1.56	2.38	319
500	0.05000	0.099	0.5375	0.5344	1.58	1.06	1.57	2.46	319
500	0.08000	0.062	0.4240	0.4213	1.78	1.06	1.64	2.64	319
500	0.13000	0.038	0.3696	0.3679	2.06	1.27	1.63	2.91	319
500	0.18000	0.027	0.3269	0.3253	2.23	1.76	1.70	3.31	319
500	0.25000	0.020	0.2545	0.2538	2.65	2.41	2.37	4.30	319
500	0.40000	0.012	0.1387	0.1385	15.42	12.00	3.65	19.87	319
500	0.65000	0.008	0.0267	0.0269	19.34	10.50	2.05	22.10	319

Table 29: continued.

Q^2 (GeV^2)	x	y	$\tilde{\sigma}_{NC}$	F_2	δ_{stat} (%)	δ_{unc} (%)	δ_{cor} (%)	δ_{tot} (%)	$\sqrt{s}$ (GeV)
650	0.00853	0.750	0.9854	—	2.32	1.82	1.50	3.31	319
650	0.01300	0.494	0.8981	0.9072	1.65	0.93	1.51	2.42	319
650	0.02000	0.321	0.7604	0.7562	1.71	0.98	1.53	2.50	319
650	0.03200	0.201	0.6454	0.6389	1.75	1.27	1.59	2.69	319
650	0.05000	0.128	0.5368	0.5316	1.85	1.07	1.58	2.66	319
650	0.08000	0.080	0.4291	0.4249	2.10	1.07	1.59	2.84	319
650	0.13000	0.049	0.3538	0.3510	2.42	1.37	1.63	3.23	319
650	0.18000	0.036	0.3240	0.3215	2.50	1.60	1.61	3.38	319
650	0.25000	0.026	0.2524	0.2503	3.17	2.40	2.23	4.56	319
650	0.40000	0.016	0.1185	0.1183	4.85	3.33	2.74	6.50	319
800	0.01050	0.750	0.9536	—	2.69	1.87	1.50	3.61	319
800	0.01300	0.608	0.8883	—	2.77	1.04	1.52	3.33	319
800	0.02000	0.395	0.7309	0.7267	1.99	1.01	1.50	2.69	319
800	0.03200	0.247	0.6300	0.6218	2.08	1.25	1.54	2.88	319
800	0.05000	0.158	0.5504	0.5423	2.15	0.98	1.52	2.81	319
800	0.08000	0.099	0.4280	0.4224	2.42	1.10	1.58	3.09	319
800	0.13000	0.061	0.3526	0.3489	2.92	1.35	1.61	3.60	319
800	0.18000	0.044	0.3164	0.3127	3.09	1.68	1.63	3.88	319
800	0.25000	0.032	0.2380	0.2358	3.64	2.03	1.84	4.55	319
800	0.40000	0.020	0.1311	0.1300	4.84	3.86	3.28	7.00	319
800	0.65000	0.012	0.0149	0.0149	21.85	12.50	3.30	25.39	319
1000	0.01300	0.750	0.8500	—	2.75	1.50	1.91	3.67	319
1000	0.02000	0.494	0.7604	0.7552	2.29	0.96	1.51	2.91	319
1000	0.03200	0.309	0.6503	0.6380	2.31	1.05	1.51	2.96	319
1000	0.05000	0.198	0.5124	0.5017	2.49	1.38	1.56	3.24	319
1000	0.08000	0.124	0.4330	0.4248	2.72	1.01	1.54	3.28	319
1000	0.13000	0.076	0.3621	0.3560	3.21	1.30	1.59	3.81	319
1000	0.18000	0.055	0.3355	0.3310	3.25	1.60	1.57	3.95	319
1000	0.25000	0.040	0.2707	0.2674	3.61	1.97	1.77	4.48	319
1000	0.40000	0.025	0.1283	0.1266	5.26	4.02	3.16	7.33	319
1200	0.01300	0.912	0.8891	—	4.58	2.03	2.23	5.48	319
1200	0.02000	0.593	0.7801	—	2.81	1.06	1.53	3.37	319
1200	0.03200	0.371	0.6749	0.6585	2.60	0.91	1.51	3.14	319
1200	0.05000	0.237	0.5432	0.5282	2.74	1.13	1.51	3.33	319
1200	0.08000	0.148	0.4518	0.4405	2.95	1.23	1.55	3.55	319
1200	0.13000	0.091	0.3533	0.3451	4.04	1.37	1.54	4.54	319
1200	0.18000	0.066	0.3113	0.3048	3.77	1.60	1.57	4.39	319
1200	0.25000	0.047	0.2209	0.2171	4.40	1.90	1.62	5.06	319
1200	0.40000	0.030	0.1272	0.1252	5.58	4.04	2.92	7.48	319

Table 29: continued.

Q^2 (GeV^2)	x	y	$\tilde{\sigma}_{\mathrm{NC}}$	F_2	δ_{stat} (%)	δ_{unc} (%)	δ_{cor} (%)	δ_{tot} (%)	$\sqrt{s}$ (GeV)
1500	0.02000	0.750	0.7971	—	3.41	1.58	1.74	4.14	319
1500	0.03200	0.463	0.6714	0.6482	3.20	0.99	1.51	3.68	319
1500	0.05000	0.296	0.5489	0.5277	3.18	1.15	1.51	3.70	319
1500	0.08000	0.185	0.4925	0.4750	3.23	1.11	1.53	3.74	319
1500	0.13000	0.114	0.3524	0.3409	4.47	1.49	1.56	4.96	319
1500	0.18000	0.082	0.2950	0.2867	4.44	1.70	1.57	5.01	319
1500	0.25000	0.059	0.2368	0.2312	4.76	2.10	1.64	5.45	319
1500	0.40000	0.037	0.1257	0.1235	7.01	3.66	2.48	8.29	319
1500	0.65000	0.023	0.0143	0.0138	11.62	6.34	5.49	14.33	319
2000	0.02190	0.903	0.8634	—	5.51	2.19	2.16	6.31	319
2000	0.03200	0.618	0.6541	—	3.78	1.33	1.52	4.28	319
2000	0.05000	0.395	0.5458	0.5127	3.87	1.05	1.51	4.29	319
2000	0.08000	0.247	0.4551	0.4289	3.89	1.25	1.53	4.36	319
2000	0.13000	0.152	0.3410	0.3241	4.88	1.45	1.53	5.31	319
2000	0.18000	0.110	0.2934	0.2802	5.23	1.96	1.60	5.81	319
2000	0.25000	0.079	0.2413	0.2318	5.40	2.03	1.62	5.99	319
2000	0.40000	0.049	0.1240	0.1202	6.83	3.42	2.21	7.95	319
2000	0.65000	0.030	0.0100	0.0098	16.63	7.84	5.67	19.24	319
3000	0.03200	0.926	0.7216	—	3.75	1.74	1.64	4.45	319
3000	0.05000	0.593	0.5920	—	3.15	1.32	1.51	3.73	319
3000	0.08000	0.371	0.4964	0.4436	3.43	1.19	1.50	3.93	319
3000	0.13000	0.228	0.4036	0.3673	4.11	1.52	1.51	4.64	319
3000	0.18000	0.165	0.3003	0.2761	4.76	1.70	1.57	5.30	319
3000	0.25000	0.119	0.2386	0.2226	4.95	2.01	1.62	5.58	319
3000	0.40000	0.074	0.1162	0.1096	6.17	3.55	2.10	7.42	319
3000	0.65000	0.046	0.0108	0.0105	13.29	7.21	4.95	15.91	319
5000	0.05470	0.903	0.6322	—	5.01	1.90	1.62	5.60	319
5000	0.08000	0.618	0.5384	—	3.69	1.42	1.51	4.23	319
5000	0.13000	0.380	0.4658	0.3819	4.18	1.62	1.51	4.73	319
5000	0.18000	0.274	0.3782	0.3183	4.78	1.66	1.49	5.28	319
5000	0.25000	0.198	0.2451	0.2118	7.02	2.19	1.62	7.53	319
5000	0.40000	0.124	0.1147	0.1027	7.51	3.20	1.87	8.38	319
5000	0.65000	0.076	0.0136	0.0128	13.00	6.38	3.43	14.88	319

Table 29: continued.

Q^2 (GeV^2)	x	y	$\tilde{\sigma}_{\mathrm{NC}}$	F_2	δ_{stat} (%)	δ_{unc} (%)	δ_{cor} (%)	δ_{tot} (%)	$\sqrt{s}$ (GeV)
8000	0.08750	0.903	0.6314	—	7.40	2.49	1.80	8.01	319
8000	0.13000	0.608	0.5309	—	5.55	2.10	1.52	6.12	319
8000	0.18000	0.439	0.3795	0.2781	6.23	2.00	1.50	6.71	319
8000	0.25000	0.316	0.2627	0.2022	7.12	2.33	1.57	7.65	319
8000	0.40000	0.198	0.1231	0.1006	9.69	4.35	2.09	10.83	319
8000	0.65000	0.122	0.0123	0.0103	16.69	6.54	2.85	18.15	319
12000	0.13000	0.912	0.7179	—	12.73	3.66	1.99	13.40	319
12000	0.18000	0.675	0.4894	—	7.88	2.10	1.52	8.30	319
12000	0.25000	0.474	0.3075	0.2042	8.74	2.37	1.53	9.18	319
12000	0.40000	0.296	0.1825	0.1339	10.41	4.73	2.02	11.61	319
12000	0.65000	0.182	0.0139	0.0111	23.27	6.34	2.76	24.27	319
20000	0.25000	0.800	0.4632	—	11.94	2.72	1.71	12.36	319
20000	0.40000	0.494	0.2142	0.1291	12.94	4.32	1.67	13.74	319
20000	0.65000	0.304	0.0162	0.0110	31.41	14.49	3.87	34.81	319
30000	0.40000	0.750	0.2036	—	25.44	5.43	2.24	26.11	319
30000	0.65000	0.456	0.0417	0.0250	30.95	11.34	3.26	33.12	319
50000	0.65000	0.750	0.0780	—	56.70	10.55	2.71	57.74	319

Table 29: continued.

Q^2 (GeV^2)	x	y	$\tilde{\sigma}_{\mathrm{NC}}$	F_2	δ_{stat} (%)	δ_{unc} (%)	δ_{cor} (%)	δ_{tot} (%)	$\sqrt{s}$ (GeV)
60	0.00080	0.750	1.486	—	0.87	1.86	1.21	2.39	319
90	0.00118	0.750	1.491	—	0.71	1.64	1.17	2.14	319
100	0.00131	0.750	1.438	—	1.61	3.50	1.49	4.13	319
100	0.00200	0.494	1.374	1.423	1.41	2.10	1.46	2.92	319
120	0.00158	0.750	1.407	—	0.77	1.45	1.15	2.00	319
120	0.00200	0.593	1.356	—	0.59	0.74	1.35	1.65	319
120	0.00320	0.371	1.218	1.238	0.76	0.90	1.13	1.63	319
150	0.00197	0.750	1.381	—	0.88	1.51	1.13	2.08	319
150	0.00320	0.520	1.229	1.264	1.81	4.90	1.32	5.39	301
150	0.00320	0.463	1.233	1.267	0.50	0.75	1.17	1.48	319
150	0.00500	0.296	1.087	1.097	0.55	0.92	1.09	1.53	319
150	0.00800	0.185	0.9518	0.9545	0.77	1.50	1.16	2.05	319
150	0.01300	0.114	0.7954	0.7953	1.27	2.72	1.68	3.44	319
200	0.00263	0.750	1.306	—	1.09	1.56	1.11	2.21	319
200	0.00320	0.618	1.241	—	0.92	0.71	1.25	1.71	319
200	0.00500	0.443	1.083	1.102	1.82	4.70	1.27	5.20	301
200	0.00500	0.395	1.102	1.122	0.63	0.78	1.11	1.50	319
200	0.00800	0.247	0.9490	0.9539	0.60	1.03	1.11	1.63	319
200	0.01300	0.152	0.8001	0.8009	0.70	0.65	1.08	1.44	319
200	0.02000	0.099	0.6987	0.6989	0.76	0.89	1.08	1.59	319
200	0.03200	0.062	0.5885	0.5886	0.87	1.16	1.10	1.83	319
200	0.05000	0.040	0.5152	0.5146	0.99	1.57	1.36	2.30	319
200	0.08000	0.025	0.4298	0.4296	1.10	1.69	1.40	2.46	319
200	0.13000	0.015	0.3600	0.3597	1.28	1.84	1.34	2.61	319
200	0.18000	0.011	0.3136	0.3137	1.97	2.88	1.47	3.79	319
200	0.25000	0.008	0.2701	0.2697	3.62	4.20	2.61	6.13	319
200	0.40000	0.005	0.1358	0.1359	4.66	4.29	4.83	7.96	319

Table 30: Combined HERA I+II NC e^+p reduced cross sections for $P_e = 0$. Here F_2 is the dominant electromagnetic structure function and δ_{stat}, δ_{unc}, δ_{cor} and δ_{tot} are the relative statistical, total uncorrelated, correlated systematic and total uncertainties, respectively. The table continues on the next pages.

Q^2 (GeV^2)	x	y	$\tilde{\sigma}_{NC}$	F_2	δ_{stat} (%)	δ_{unc} (%)	δ_{cor} (%)	δ_{tot} (%)	$\sqrt{s}$ (GeV)
250	0.00328	0.750	1.278	—	1.24	1.55	1.12	2.27	319
250	0.00500	0.554	1.102	1.136	2.31	4.90	1.31	5.57	301
250	0.00500	0.494	1.124	1.158	0.75	0.69	1.12	1.52	319
250	0.00800	0.309	0.9611	0.9695	0.68	0.82	1.10	1.53	319
250	0.01300	0.190	0.8127	0.8147	0.74	0.99	1.13	1.67	319
250	0.02000	0.124	0.6982	0.6981	0.74	1.08	1.12	1.73	319
250	0.03200	0.077	0.5815	0.5806	0.79	1.02	1.12	1.71	319
250	0.05000	0.049	0.5062	0.5055	0.86	1.01	1.20	1.79	319
250	0.08000	0.031	0.4323	0.4315	0.92	0.90	1.35	1.86	319
250	0.13000	0.019	0.3606	0.3606	0.99	1.45	1.18	2.11	319
250	0.18000	0.014	0.2988	0.2986	1.60	2.71	1.76	3.61	319
250	0.25000	0.010	0.2600	0.2597	2.14	3.68	2.31	4.85	319
250	0.40000	0.006	0.1360	0.1358	3.17	3.97	4.34	6.68	319
300	0.00394	0.750	1.216	—	1.39	1.55	1.10	2.35	319
300	0.00500	0.675	1.146	—	3.39	5.20	1.49	6.38	301
300	0.00500	0.593	1.140	—	1.25	0.81	1.18	1.90	319
300	0.00800	0.416	0.9717	0.9852	2.42	4.90	1.25	5.61	301
300	0.00800	0.371	0.9765	0.9903	0.85	0.71	1.09	1.55	319
300	0.01300	0.228	0.8137	0.8168	0.80	0.84	1.11	1.60	319
300	0.02000	0.148	0.7119	0.7124	0.88	0.82	1.10	1.63	319
300	0.03200	0.093	0.5905	0.5906	0.91	0.97	1.12	1.74	319
300	0.05000	0.059	0.4945	0.4935	0.98	1.09	1.15	1.86	319
300	0.08000	0.037	0.4398	0.4395	1.01	1.19	1.35	2.06	319
300	0.13000	0.023	0.3645	0.3635	1.06	1.59	1.21	2.26	319
300	0.18000	0.016	0.3090	0.3085	1.66	2.89	1.98	3.88	319
300	0.25000	0.012	0.2586	0.2586	2.14	4.45	2.54	5.55	319
300	0.40000	0.007	0.1510	0.1507	1.78	3.03	2.97	4.60	319
400	0.00525	0.750	1.180	—	1.48	1.58	1.08	2.42	319
400	0.00800	0.554	0.9617	0.9883	3.12	4.90	1.29	5.95	301
400	0.00800	0.494	1.005	1.033	1.05	0.73	1.11	1.69	319
400	0.01300	0.304	0.8547	0.8612	0.93	0.77	1.09	1.63	319
400	0.02000	0.198	0.7149	0.7162	0.95	0.98	1.13	1.77	319
400	0.03200	0.124	0.5991	0.5988	1.02	0.82	1.11	1.72	319
400	0.05000	0.079	0.5017	0.5014	1.11	0.96	1.15	1.86	319
400	0.08000	0.049	0.4335	0.4334	1.17	0.85	1.32	1.96	319
400	0.13000	0.030	0.3585	0.3574	1.17	1.17	1.16	2.02	319
400	0.18000	0.022	0.3078	0.3074	1.84	2.40	2.02	3.63	319
400	0.25000	0.016	0.2455	0.2445	2.39	3.23	2.18	4.57	319
400	0.40000	0.010	0.1525	0.1527	2.00	2.45	3.10	4.43	319

Table 30: continued.

Q^2 (GeV^2)	x	y	$\tilde{\sigma}_{NC}$	F_2	δ_{stat} (%)	δ_{unc} (%)	δ_{cor} (%)	δ_{tot} (%)	$\sqrt{s}$ (GeV)
500	0.00656	0.750	1.050	—	1.66	1.55	1.08	2.51	319
500	0.00800	0.675	1.022	—	4.21	5.00	1.31	6.67	301
500	0.00800	0.618	0.9950	—	1.73	0.89	1.12	2.24	319
500	0.01300	0.426	0.8868	0.8984	3.34	5.00	1.25	6.14	301
500	0.01300	0.380	0.8717	0.8832	1.22	0.77	1.09	1.81	319
500	0.02000	0.247	0.7423	0.7447	1.15	0.90	1.11	1.83	319
500	0.03200	0.154	0.6140	0.6141	1.20	0.86	1.11	1.85	319
500	0.05000	0.099	0.5252	0.5245	1.25	0.98	1.17	1.97	319
500	0.08000	0.062	0.4400	0.4393	1.34	0.88	1.19	2.00	319
500	0.13000	0.038	0.3724	0.3712	1.54	1.14	1.25	2.28	319
500	0.18000	0.027	0.3060	0.3053	1.72	1.50	1.24	2.60	319
500	0.25000	0.020	0.2509	0.2504	2.11	2.16	2.39	3.85	319
500	0.40000	0.012	0.1603	0.1596	5.18	5.86	4.75	9.15	319
650	0.00853	0.750	0.9978	—	1.90	1.67	1.07	2.75	319
650	0.01300	0.554	0.8895	0.9110	4.03	3.80	1.39	5.71	301
650	0.01300	0.494	0.8581	0.8792	1.40	0.77	1.08	1.93	319
650	0.02000	0.360	0.7037	0.7094	4.14	3.70	1.23	5.69	301
650	0.02000	0.321	0.7353	0.7406	1.45	0.92	1.09	2.04	319
650	0.03200	0.201	0.6352	0.6360	1.38	1.05	1.12	2.07	319
650	0.05000	0.128	0.5189	0.5187	1.45	0.96	1.14	2.08	319
650	0.08000	0.080	0.4251	0.4242	1.59	0.96	1.19	2.20	319
650	0.13000	0.049	0.3790	0.3780	1.81	1.19	1.24	2.50	319
650	0.18000	0.036	0.3275	0.3261	1.92	1.46	1.23	2.71	319
650	0.25000	0.026	0.2452	0.2442	2.37	2.16	2.10	3.83	319
650	0.40000	0.016	0.1377	0.1375	3.46	3.02	3.02	5.50	319
650	0.65000	0.010	0.0217	0.0219	14.07	7.79	5.62	17.03	319
800	0.01050	0.750	0.9270	—	2.27	1.76	1.08	3.07	319
800	0.01300	0.675	0.9858	—	5.04	4.40	1.46	6.85	301
800	0.01300	0.608	0.8303	—	2.26	1.01	1.11	2.72	319
800	0.02000	0.443	0.7759	0.7864	4.66	4.00	1.38	6.29	301
800	0.02000	0.395	0.7123	0.7216	1.66	0.89	1.08	2.17	319
800	0.03200	0.247	0.6201	0.6222	1.62	1.03	1.08	2.20	319
800	0.05000	0.158	0.5329	0.5331	1.71	0.92	1.09	2.22	319
800	0.08000	0.099	0.4567	0.4563	1.80	1.04	1.16	2.38	319
800	0.13000	0.061	0.3583	0.3570	2.11	1.25	1.23	2.75	319
800	0.18000	0.044	0.3258	0.3249	2.22	1.45	1.17	2.90	319
800	0.25000	0.032	0.2391	0.2381	2.66	1.97	1.68	3.72	319
800	0.40000	0.020	0.1293	0.1284	3.86	3.24	3.13	5.93	319
800	0.65000	0.012	0.0194	0.0189	12.32	7.21	5.46	15.28	319

Table 30: continued.

Q^2 (GeV^2)	x	y	$\tilde{\sigma}_{\mathrm{NC}}$	F_2	δ_{stat} (%)	δ_{unc} (%)	δ_{cor} (%)	δ_{tot} (%)	$\sqrt{s}$ (GeV)
1000	0.01300	0.750	0.8194	—	2.33	1.36	1.53	3.11	319
1000	0.02000	0.554	0.7428	0.7608	5.44	3.70	1.28	6.70	301
1000	0.02000	0.494	0.7340	0.7516	1.92	0.88	1.09	2.38	319
1000	0.03200	0.309	0.6236	0.6286	1.81	0.98	1.09	2.33	319
1000	0.05000	0.198	0.5322	0.5330	1.88	1.26	1.09	2.51	319
1000	0.08000	0.124	0.4424	0.4415	2.03	1.01	1.09	2.52	319
1000	0.13000	0.076	0.3600	0.3589	2.53	1.21	1.19	3.04	319
1000	0.18000	0.055	0.3093	0.3078	2.60	1.30	1.11	3.11	319
1000	0.25000	0.040	0.2487	0.2478	2.89	1.74	1.40	3.65	319
1000	0.40000	0.025	0.1278	0.1273	4.68	3.11	2.71	6.23	319
1000	0.65000	0.015	0.0184	0.0179	14.24	7.75	5.56	17.14	319
1200	0.01300	0.912	0.8416	—	4.33	2.11	2.21	5.30	319
1200	0.02000	0.675	0.7283	—	7.24	3.50	1.27	8.14	301
1200	0.02000	0.593	0.7251	—	2.40	1.00	1.10	2.82	319
1200	0.03200	0.416	0.6335	0.6410	6.46	3.50	1.23	7.45	301
1200	0.03200	0.371	0.6166	0.6248	2.22	0.88	1.08	2.62	319
1200	0.05000	0.237	0.5105	0.5131	2.15	1.07	1.08	2.63	319
1200	0.08000	0.148	0.4411	0.4410	2.25	1.03	1.11	2.71	319
1200	0.13000	0.091	0.3651	0.3639	2.71	1.29	1.13	3.21	319
1200	0.18000	0.066	0.3238	0.3225	3.01	1.29	1.16	3.48	319
1200	0.25000	0.047	0.2549	0.2535	3.26	1.79	1.29	3.94	319
1200	0.40000	0.030	0.1150	0.1142	4.65	3.29	2.87	6.38	319
1200	0.65000	0.018	0.0211	0.0208	15.05	8.72	5.23	18.17	319
1500	0.02000	0.850	0.7975	—	9.15	4.80	1.54	10.45	301
1500	0.02000	0.750	0.6966	—	3.03	1.51	1.29	3.62	319
1500	0.03200	0.520	0.5691	0.5823	8.18	4.00	1.31	9.20	301
1500	0.03200	0.463	0.5977	0.6120	2.88	0.97	1.08	3.22	319
1500	0.05000	0.296	0.5343	0.5389	2.44	0.96	1.06	2.83	319
1500	0.08000	0.185	0.4457	0.4470	2.61	1.11	1.10	3.04	319
1500	0.13000	0.114	0.3424	0.3412	3.14	1.28	1.11	3.57	319
1500	0.18000	0.082	0.3131	0.3115	3.27	1.36	1.16	3.72	319
1500	0.25000	0.059	0.2353	0.2334	3.58	1.91	1.31	4.26	319
1500	0.40000	0.037	0.1195	0.1189	4.84	2.87	2.23	6.06	319
1500	0.65000	0.023	0.0148	0.0149	9.73	5.91	5.31	12.56	319

Table 30: continued.

Q^2 (GeV^2)	x	y	$\tilde{\sigma}_{\mathrm{NC}}$	F_2	δ_{stat} (%)	δ_{unc} (%)	δ_{cor} (%)	δ_{tot} (%)	$\sqrt{s}$ (GeV)
2000	0.02190	0.903	0.7034	—	5.55	2.40	1.85	6.33	319
2000	0.03200	0.675	0.6077	—	9.05	4.00	1.30	9.98	301
2000	0.03200	0.618	0.5687	—	3.35	1.33	1.10	3.77	319
2000	0.05000	0.443	0.5285	0.5406	8.80	4.00	1.26	9.75	301
2000	0.05000	0.395	0.5231	0.5345	3.27	1.07	1.09	3.61	319
2000	0.08000	0.247	0.4225	0.4267	3.02	1.17	1.08	3.41	319
2000	0.13000	0.152	0.3503	0.3500	3.76	1.44	1.12	4.18	319
2000	0.18000	0.110	0.3133	0.3116	3.83	1.37	1.16	4.23	319
2000	0.25000	0.079	0.2381	0.2361	4.01	1.94	1.31	4.64	319
2000	0.40000	0.049	0.1222	0.1206	5.23	3.13	2.16	6.46	319
2000	0.65000	0.030	0.0158	0.0158	10.55	6.09	5.33	13.29	319
3000	0.03200	0.926	0.5990	—	3.69	1.72	1.37	4.30	319
3000	0.05000	0.675	0.5019	—	7.38	3.80	1.32	8.41	301
3000	0.05000	0.593	0.5156	—	2.79	1.25	1.08	3.24	319
3000	0.08000	0.416	0.4504	0.4644	7.76	4.00	1.20	8.82	301
3000	0.08000	0.371	0.4381	0.4520	2.98	1.17	1.09	3.39	319
3000	0.13000	0.228	0.3416	0.3457	3.34	1.36	1.07	3.76	319
3000	0.18000	0.165	0.3078	0.3081	3.90	1.75	1.20	4.44	319
3000	0.25000	0.119	0.2227	0.2212	3.84	1.64	1.21	4.35	319
3000	0.40000	0.074	0.1196	0.1181	4.66	2.94	1.82	5.80	319
3000	0.65000	0.046	0.0127	0.0127	10.00	6.12	4.60	12.59	319
5000	0.05470	0.903	0.4727	—	5.02	2.01	1.52	5.62	319
5000	0.08000	0.675	0.3448	—	10.52	4.40	1.38	11.49	301
5000	0.08000	0.618	0.4131	—	3.41	1.42	1.10	3.86	319
5000	0.13000	0.426	0.3834	0.4061	10.52	4.80	1.29	11.63	301
5000	0.13000	0.380	0.3405	0.3616	4.02	1.61	1.09	4.47	319
5000	0.18000	0.274	0.2806	0.2891	4.24	1.60	1.04	4.65	319
5000	0.25000	0.198	0.2291	0.2301	4.90	2.08	1.17	5.45	319
5000	0.40000	0.124	0.1127	0.1110	5.95	2.71	1.38	6.68	319
5000	0.65000	0.076	0.0100	0.0097	13.32	5.80	3.38	14.91	319
8000	0.08750	0.903	0.3532	—	8.61	2.69	2.15	9.28	319
8000	0.13000	0.675	0.2774	—	16.67	4.70	1.30	17.36	301
8000	0.13000	0.608	0.3025	—	5.88	2.16	1.09	6.36	319
8000	0.18000	0.493	0.2757	0.3100	15.73	6.10	1.43	16.93	301
8000	0.18000	0.439	0.2842	0.3189	5.88	2.17	1.09	6.37	319
8000	0.25000	0.355	0.2688	0.2844	15.22	6.60	1.53	16.66	301
8000	0.25000	0.316	0.2199	0.2326	7.32	2.48	1.18	7.81	319
8000	0.40000	0.198	0.0993	0.0988	8.22	3.69	1.55	9.15	319
8000	0.65000	0.122	0.0147	0.0145	12.92	6.64	2.96	14.82	319

Table 30: continued.

Q^2 (GeV^2)	x	y	$\tilde{\sigma}_{\mathrm{NC}}$	F_2	δ_{stat} (%)	δ_{unc} (%)	δ_{cor} (%)	δ_{tot} (%)	$\sqrt{s}$ (GeV)
12000	0.13000	0.912	0.2126	—	19.65	5.03	1.76	20.36	319
12000	0.18000	0.750	0.1512	—	34.61	3.80	1.50	34.85	301
12000	0.18000	0.675	0.2211	—	9.76	2.16	1.24	10.07	319
12000	0.25000	0.532	0.1239	0.1482	32.50	6.10	1.32	33.09	301
12000	0.25000	0.474	0.1463	0.1744	10.52	2.49	1.11	10.87	319
12000	0.40000	0.296	0.0859	0.0905	11.85	4.07	1.41	12.61	319
12000	0.65000	0.182	0.0160	0.0156	17.95	6.80	2.48	19.35	319
20000	0.25000	0.887	0.0914	—	61.43	5.10	1.79	61.67	301
20000	0.25000	0.800	0.1238	—	17.51	2.77	1.27	17.77	319
20000	0.40000	0.554	0.1371	0.1751	36.34	9.60	1.55	37.62	301
20000	0.40000	0.494	0.0808	0.1035	17.56	4.31	1.26	18.13	319
20000	0.65000	0.304	0.0113	0.0116	33.09	13.65	3.26	35.94	319
30000	0.40000	0.850	0.1817	—	71.96	9.40	1.60	72.59	301
30000	0.40000	0.750	0.0816	—	32.37	5.02	1.25	32.78	319
30000	0.65000	0.456	0.0082	0.0100	69.80	9.86	2.52	70.54	319

Table 30: continued.

Q^2 (GeV^2)	x	y	$\mathrm{d}^2\sigma_{\mathrm{CC}}/\mathrm{d}x\mathrm{d}Q^2$ ($\mathrm{pb/GeV}^2$)	$\tilde{\sigma}_{\mathrm{CC}}$	δ_{stat} (%)	δ_{unc} (%)	δ_{cor} (%)	δ_{tot} (%)	$\sqrt{s}$ (GeV)
300	0.008	0.371	1.88	1.95	31.4	23.7	13.2	41.5	319
300	0.013	0.228	0.731	1.23	12.9	9.6	7.5	17.7	319
300	0.032	0.093	0.269	1.12	10.8	4.5	4.6	12.6	319
300	0.080	0.037	$0.670 \cdot 10^{-1}$	0.696	11.2	4.8	3.4	12.6	319
500	0.013	0.380	0.646	1.16	8.5	6.3	6.6	12.5	319
500	0.032	0.154	0.219	0.963	6.7	3.1	2.8	7.8	319
500	0.080	0.062	$0.551 \cdot 10^{-1}$	0.607	7.7	3.8	1.7	8.7	319
500	0.130	0.038	$0.330 \cdot 10^{-1}$	0.591	15.8	4.5	4.9	17.2	319
1000	0.013	0.760	0.420	0.863	8.7	5.8	6.3	12.2	319
1000	0.032	0.309	0.188	0.952	5.2	2.6	2.1	6.2	319
1000	0.080	0.124	$0.597 \cdot 10^{-1}$	0.755	5.3	2.7	1.6	6.2	319
1000	0.130	0.076	$0.270 \cdot 10^{-1}$	0.555	9.2	3.4	2.1	10.0	319
1000	0.250	0.040	$0.138 \cdot 10^{-1}$	0.546	37.7	10.5	1.6	39.2	319
2000	0.032	0.618	0.122	0.793	5.0	2.5	2.1	5.9	319
2000	0.080	0.247	$0.462 \cdot 10^{-1}$	0.752	4.5	2.0	1.5	5.2	319
2000	0.130	0.152	$0.226 \cdot 10^{-1}$	0.599	6.4	2.8	1.5	7.2	319
2000	0.250	0.079	$0.875 \cdot 10^{-2}$	0.445	11.4	3.5	3.7	12.5	319
3000	0.080	0.371	$0.330 \cdot 10^{-1}$	0.671	4.3	2.1	1.6	5.0	319
3000	0.130	0.228	$0.189 \cdot 10^{-1}$	0.624	5.2	2.1	1.5	5.8	319
3000	0.250	0.119	$0.695 \cdot 10^{-2}$	0.442	7.5	2.7	1.7	8.2	319
3000	0.400	0.074	$0.251 \cdot 10^{-2}$	0.255	35.2	17.1	4.5	39.4	319
5000	0.080	0.618	$0.213 \cdot 10^{-1}$	0.635	5.6	2.5	1.6	6.3	319
5000	0.130	0.380	$0.126 \cdot 10^{-1}$	0.611	4.9	2.2	1.5	5.6	319
5000	0.250	0.198	$0.492 \cdot 10^{-2}$	0.459	5.9	2.4	1.5	6.6	319
5000	0.400	0.124	$0.142 \cdot 10^{-2}$	0.211	15.2	5.1	3.4	16.4	319
8000	0.130	0.608	$0.835 \cdot 10^{-2}$	0.645	6.0	3.5	1.8	7.2	319
8000	0.250	0.316	$0.272 \cdot 10^{-2}$	0.403	6.0	3.0	1.6	6.9	319
8000	0.400	0.198	$0.100 \cdot 10^{-2}$	0.238	11.2	4.9	2.0	12.4	319
15000	0.250	0.593	$0.154 \cdot 10^{-2}$	0.504	7.1	5.4	2.0	9.2	319
15000	0.400	0.371	$0.399 \cdot 10^{-3}$	0.209	9.3	5.6	2.2	11.1	319
30000	0.400	0.741	$0.154 \cdot 10^{-3}$	0.232	15.4	10.6	3.7	19.0	319

Table 31: Combined HERA I+II CC e^-p cross sections for $P_e = 0$. Here δ_{stat}, δ_{unc}, δ_{cor} and δ_{tot} are the relative statistical, total uncorrelated, correlated systematic and total uncertainties, respectively.

Q^2 (GeV^2)	x	y	$\mathrm{d}^2\sigma_{\mathrm{CC}}/\mathrm{d}x\mathrm{d}Q^2$ ($\mathrm{pb}/\mathrm{GeV}^2$)	$\tilde{\sigma}_{\mathrm{CC}}$	δ_{stat} (%)	δ_{unc} (%)	δ_{cor} (%)	δ_{tot} (%)	$\sqrt{s}$ (GeV)
300	0.008	0.371	1.08	1.12	28.5	25.7	13.9	40.8	319
300	0.013	0.228	0.638	1.08	11.1	6.2	6.6	14.3	319
300	0.032	0.093	0.217	0.901	7.8	3.5	3.9	9.4	319
300	0.080	0.037	$0.481 \cdot 10^{-1}$	0.500	10.1	3.6	2.5	11.0	319
500	0.013	0.380	0.550	0.984	7.5	4.5	5.3	10.2	319
500	0.032	0.154	0.190	0.839	5.8	2.4	2.4	6.7	319
500	0.080	0.062	$0.504 \cdot 10^{-1}$	0.555	6.3	2.6	1.3	7.0	319
500	0.130	0.038	$0.222 \cdot 10^{-1}$	0.397	13.5	3.8	3.1	14.4	319
1000	0.013	0.760	0.343	0.705	9.9	6.2	7.5	13.9	319
1000	0.032	0.309	0.145	0.731	4.7	1.9	1.7	5.4	319
1000	0.080	0.124	$0.402 \cdot 10^{-1}$	0.509	5.1	2.1	1.2	5.7	319
1000	0.130	0.076	$0.180 \cdot 10^{-1}$	0.370	8.2	2.9	1.2	8.8	319
1000	0.250	0.040	$0.880 \cdot 10^{-2}$	0.348	18.9	10.8	2.6	21.9	319
2000	0.032	0.618	$0.819 \cdot 10^{-1}$	0.533	4.7	2.0	1.8	5.4	319
2000	0.080	0.247	$0.266 \cdot 10^{-1}$	0.433	4.5	1.7	1.1	5.0	319
2000	0.130	0.152	$0.133 \cdot 10^{-1}$	0.351	6.3	2.4	1.1	6.8	319
2000	0.250	0.079	$0.396 \cdot 10^{-2}$	0.201	10.6	3.3	2.3	11.3	319
3000	0.080	0.371	$0.194 \cdot 10^{-1}$	0.395	4.5	2.0	1.2	5.0	319
3000	0.130	0.228	$0.107 \cdot 10^{-1}$	0.355	5.4	1.8	1.1	5.8	319
3000	0.250	0.119	$0.237 \cdot 10^{-2}$	0.151	9.2	2.9	1.2	9.7	319
3000	0.400	0.074	$0.431 \cdot 10^{-3}$	0.044	32.6	8.7	5.3	34.1	319
5000	0.080	0.618	$0.780 \cdot 10^{-2}$	0.233	7.6	3.2	1.7	8.4	319
5000	0.130	0.380	$0.505 \cdot 10^{-2}$	0.245	6.3	2.5	1.3	6.9	319
5000	0.250	0.198	$0.153 \cdot 10^{-2}$	0.143	8.2	2.6	1.2	8.7	319
5000	0.400	0.124	$0.474 \cdot 10^{-3}$	0.071	17.7	6.0	2.7	18.9	319
8000	0.130	0.608	$0.162 \cdot 10^{-2}$	0.125	10.1	4.6	1.8	11.3	319
8000	0.250	0.316	$0.818 \cdot 10^{-3}$	0.121	8.8	3.8	1.7	9.7	319
8000	0.400	0.198	$0.193 \cdot 10^{-3}$	0.046	19.3	7.8	2.5	20.9	319
15000	0.250	0.593	$0.175 \cdot 10^{-3}$	0.057	14.7	6.1	2.2	16.1	319
15000	0.400	0.371	$0.646 \cdot 10^{-4}$	0.034	17.2	6.5	2.1	18.5	319

Table 32: Combined HERA I+II CC e^+p cross sections for $P_e = 0$. Here δ_{stat}, δ_{unc}, δ_{cor} and δ_{tot} are the relative statistical, total uncorrelated, correlated systematic and total uncertainties, respectively.

Q^2 (GeV^2)	$\mathrm{d}\sigma_{\mathrm{NC}}/\mathrm{d}Q^2$ ($\mathrm{pb}/\mathrm{GeV}^2$)	δ_{stat} (%)	δ_{unc} (%)	δ_{cor} (%)	δ_{tot} (%)	$\delta_{\mathrm{cor}}^{E^+}$ (%)	$\delta_{\mathrm{cor}}^{\theta^+}$ (%)	$\delta_{\mathrm{cor}}^{h^+}$ (%)	$\delta_{\mathrm{cor}}^{N^+}$ (%)	$\delta_{\mathrm{cor}}^{B^+}$ (%)
200	17.91	0.42	0.92	0.62	1.19	−0.22	−0.57	0.00	0.05	−0.06
250	10.61	0.43	1.21	0.67	1.45	0.39	−0.54	0.01	0.05	−0.04
300	6.800	0.51	1.24	0.73	1.53	0.48	−0.55	0.01	0.04	−0.04
400	3.436	0.60	1.06	0.62	1.36	0.46	−0.41	0.01	0.04	−0.03
500	2.038	0.71	1.08	0.62	1.44	0.50	−0.37	0.01	0.04	−0.02
650	1.063	0.86	1.10	0.63	1.53	0.51	−0.35	0.01	0.05	−0.02
800	0.6300	1.05	1.08	0.58	1.61	0.48	−0.31	0.01	0.06	−0.02
1000	0.3640	1.21	1.14	0.60	1.77	0.47	−0.31	0.01	0.05	−0.20
1200	0.2290	1.45	1.28	0.54	2.01	0.46	−0.24	0.01	0.05	−0.15
1500	0.1330	1.72	1.36	0.60	2.27	0.53	−0.21	0.01	0.05	−0.19
2000	$0.6100 \cdot 10^{-1}$	2.09	1.46	0.60	2.62	0.52	−0.24	0.01	0.05	−0.19
3000	$0.2200 \cdot 10^{-1}$	1.96	1.51	0.52	2.52	0.48	−0.16	0.01	0.04	−0.13
5000	$0.5900 \cdot 10^{-2}$	2.46	1.73	0.48	3.05	0.43	−0.15	0.01	0.04	−0.15
8000	$0.1570 \cdot 10^{-2}$	3.81	2.33	0.60	4.51	0.55	−0.06	0.01	0.03	−0.23
12000	$0.5570 \cdot 10^{-3}$	5.73	2.69	0.69	6.36	0.64	0.01	0.02	0.06	−0.25
20000	$0.1180 \cdot 10^{-3}$	9.71	3.92	1.14	10.54	0.92	0.11	0.02	0.04	−0.66
30000	$0.1860 \cdot 10^{-4}$	25.27	6.64	1.98	26.20	1.54	0.32	0.02	0.09	−1.20
50000	$0.2670 \cdot 10^{-5}$	57.78	9.73	1.81	58.62	1.73	0.52	0.00	0.00	0.00

Table 33: The NC e^-p cross section $\mathrm{d}\sigma_{\mathrm{NC}}/\mathrm{d}Q^2$ for lepton beam polarisation $P_e = -25.8\%$ and $y < 0.9$. The statistical (δ_{stat}), uncorrelated systematic (δ_{unc}), correlated systematic (δ_{cor}) and total (δ_{tot}) errors are provided. In addition the correlated systematic error contributions from a positive variation of one standard deviation of the electron energy error ($\delta_{\mathrm{cor}}^{E^+}$), of the polar electron angle error ($\delta_{\mathrm{cor}}^{\theta^+}$), of the hadronic energy error ($\delta_{\mathrm{cor}}^{h^+}$), of the error due to noise subtraction ($\delta_{\mathrm{cor}}^{N^+}$) and of the error due to background subtraction ($\delta_{\mathrm{cor}}^{B^+}$) are given. The normalisation and polarisation uncertainties are not included in the errors.

Q^2 (GeV^2)	$\mathrm{d}\sigma_{\mathrm{NC}}/\mathrm{d}Q^2$ ($\mathrm{pb/GeV}^2$)	δ_{stat} (%)	δ_{unc} (%)	δ_{cor} (%)	δ_{tot} (%)	$\delta_{\mathrm{cor}}^{E^+}$ (%)	$\delta_{\mathrm{cor}}^{\theta^+}$ (%)	$\delta_{\mathrm{cor}}^{h^+}$ (%)	$\delta_{\mathrm{cor}}^{N^+}$ (%)	$\delta_{\mathrm{cor}}^{B^+}$ (%)
200	17.78	0.62	0.91	0.60	1.25	−0.19	−0.56	0.00	0.05	−0.06
250	10.32	0.65	1.22	0.64	1.52	0.38	−0.52	0.00	0.04	−0.05
300	6.781	0.76	1.27	0.77	1.67	0.53	−0.57	0.00	0.05	−0.03
400	3.343	0.91	1.05	0.61	1.52	0.45	−0.41	0.01	0.04	−0.03
500	1.928	1.08	1.09	0.68	1.68	0.53	−0.42	0.01	0.04	−0.02
650	1.030	1.29	1.11	0.63	1.82	0.53	−0.34	0.01	0.05	−0.02
800	0.6080	1.59	1.09	0.55	2.00	0.46	−0.30	0.01	0.05	−0.02
1000	0.3480	1.88	1.17	0.60	2.29	0.48	−0.31	0.01	0.05	−0.18
1200	0.2160	2.18	1.29	0.59	2.60	0.50	−0.23	0.01	0.04	−0.20
1500	0.1210	2.72	1.35	0.54	3.08	0.48	−0.23	0.01	0.05	−0.10
2000	$0.5700 \cdot 10^{-1}$	3.21	1.45	0.57	3.57	0.51	−0.18	0.01	0.05	−0.18
3000	$0.2020 \cdot 10^{-1}$	2.99	1.58	0.60	3.43	0.54	−0.17	0.01	0.05	−0.18
5000	$0.5190 \cdot 10^{-2}$	4.10	1.72	0.42	4.47	0.37	−0.11	0.01	0.05	−0.16
8000	$0.1490 \cdot 10^{-2}$	5.83	2.33	0.63	6.31	0.56	−0.09	0.01	0.06	−0.27
12000	$0.4650 \cdot 10^{-3}$	9.30	2.90	0.79	9.77	0.76	−0.03	0.02	0.05	−0.21
20000	$0.7660 \cdot 10^{-4}$	17.86	3.82	0.81	18.28	0.80	0.11	0.02	0.05	−0.04
30000	$0.2200 \cdot 10^{-4}$	34.74	6.25	2.43	35.38	1.67	0.07	0.01	0.04	−1.77

Table 34: The NC e^-p cross section $\mathrm{d}\sigma_{\mathrm{NC}}/\mathrm{d}Q^2$ for lepton beam polarisation $P_e = +36.0\%$ and $y < 0.9$. The statistical (δ_{stat}), uncorrelated systematic (δ_{unc}), correlated systematic (δ_{cor}) and total (δ_{tot}) errors are provided. In addition the correlated systematic error contributions from a positive variation of one standard deviation of the electron energy error ($\delta_{\mathrm{cor}}^{E^+}$), of the polar electron angle error ($\delta_{\mathrm{cor}}^{\theta^+}$), of the hadronic energy error ($\delta_{\mathrm{cor}}^{h^+}$), of the error due to noise subtraction ($\delta_{\mathrm{cor}}^{N^+}$) and of the error due to background subtraction ($\delta_{\mathrm{cor}}^{B^+}$) are given. The normalisation and polarisation uncertainties are not included in the errors.

Q^2 (GeV^2)	$\mathrm{d}\sigma_{\mathrm{NC}}/\mathrm{d}Q^2$ ($\mathrm{pb/GeV}^2$)	δ_{stat} (%)	δ_{unc} (%)	δ_{cor} (%)	δ_{tot} (%)	$\delta_{\mathrm{cor}}^{E^+}$ (%)	$\delta_{\mathrm{cor}}^{\theta^+}$ (%)	$\delta_{\mathrm{cor}}^{h^+}$ (%)	$\delta_{\mathrm{cor}}^{N^+}$ (%)	$\delta_{\mathrm{cor}}^{B^+}$ (%)
200	18.16	0.47	0.80	0.65	1.14	-0.23	-0.61	0.01	0.05	-0.06
250	10.61	0.49	1.12	0.66	1.39	0.40	-0.52	0.01	0.04	-0.04
300	6.897	0.57	1.15	0.72	1.47	0.47	-0.54	0.01	0.04	-0.04
400	3.419	0.67	0.98	0.63	1.35	0.46	-0.43	0.00	0.04	-0.03
500	1.995	0.81	0.98	0.64	1.43	0.50	-0.40	0.01	0.04	-0.03
650	1.029	0.98	1.02	0.68	1.57	0.55	-0.40	0.01	0.04	-0.02
800	0.6030	1.19	1.06	0.66	1.73	0.55	-0.36	0.01	0.05	-0.02
1000	0.3390	1.41	1.03	0.54	1.83	0.42	-0.27	0.01	0.05	-0.19
1200	0.2130	1.66	1.21	0.63	2.14	0.52	-0.28	0.01	0.05	-0.18
1500	0.1190	2.06	1.39	0.65	2.57	0.59	-0.20	0.01	0.05	-0.17
2000	$0.5470 \cdot 10^{-1}$	2.45	1.39	0.57	2.87	0.49	-0.23	0.01	0.04	-0.17
3000	$0.1830 \cdot 10^{-1}$	2.34	1.60	0.68	2.92	0.64	-0.17	0.01	0.05	-0.18
5000	$0.4070 \cdot 10^{-2}$	3.27	1.75	0.55	3.75	0.46	-0.12	0.01	0.04	-0.28
8000	$0.9380 \cdot 10^{-3}$	5.47	2.49	0.91	6.08	0.76	-0.11	0.02	0.03	-0.49
12000	$0.2170 \cdot 10^{-3}$	10.30	3.20	0.91	10.83	0.76	-0.04	0.01	0.05	-0.49
20000	$0.2920 \cdot 10^{-4}$	21.41	4.38	1.15	21.89	1.14	0.07	0.01	0.05	-0.13

Table 35: The NC e^+p cross section $\mathrm{d}\sigma_{\mathrm{NC}}/\mathrm{d}Q^2$ for lepton beam polarisation $P_e = -37.0\%$ and $y < 0.9$. The statistical (δ_{stat}), uncorrelated systematic (δ_{unc}), correlated systematic (δ_{cor}) and total (δ_{tot}) errors are provided. In addition the correlated systematic error contributions from a positive variation of one standard deviation of the electron energy error ($\delta_{\mathrm{cor}}^{E^+}$), of the polar electron angle error ($\delta_{\mathrm{cor}}^{\theta^+}$), of the hadronic energy error ($\delta_{\mathrm{cor}}^{h^+}$), of the error due to noise subtraction ($\delta_{\mathrm{cor}}^{N^+}$) and of the error due to background subtraction ($\delta_{\mathrm{cor}}^{B^+}$) are given. The normalisation and polarisation uncertainties are not included in the errors.

Q^2 (GeV^2)	$\mathrm{d}\sigma_{\mathrm{NC}}/\mathrm{d}Q^2$ ($\mathrm{pb}/\mathrm{GeV}^2$)	δ_{stat} (%)	δ_{unc} (%)	δ_{cor} (%)	δ_{tot} (%)	$\delta_{\mathrm{cor}}^{E^+}$ (%)	$\delta_{\mathrm{cor}}^{\theta^+}$ (%)	$\delta_{\mathrm{cor}}^{h^+}$ (%)	$\delta_{\mathrm{cor}}^{N^+}$ (%)	$\delta_{\mathrm{cor}}^{B^+}$ (%)
200	17.84	0.42	0.80	0.63	1.10	−0.23	−0.57	0.01	0.05	−0.07
250	10.49	0.44	1.14	0.69	1.40	0.42	−0.55	0.00	0.04	−0.05
300	6.814	0.52	1.15	0.70	1.44	0.46	−0.53	0.00	0.04	−0.04
400	3.392	0.61	0.96	0.61	1.29	0.45	−0.41	0.00	0.04	−0.03
500	2.004	0.72	0.98	0.65	1.38	0.51	−0.40	0.01	0.04	−0.03
650	1.059	0.87	1.03	0.66	1.50	0.54	−0.38	0.01	0.05	−0.03
800	0.6260	1.04	1.03	0.63	1.60	0.53	−0.34	0.01	0.06	−0.03
1000	0.3490	1.26	1.02	0.54	1.71	0.42	−0.28	0.01	0.06	−0.21
1200	0.2180	1.49	1.21	0.57	2.00	0.48	−0.26	0.01	0.05	−0.17
1500	0.1220	1.75	1.28	0.58	2.25	0.52	−0.22	0.01	0.06	−0.14
2000	$0.5850 \cdot 10^{-1}$	2.15	1.43	0.64	2.66	0.57	−0.23	0.01	0.05	−0.16
3000	$0.2020 \cdot 10^{-1}$	2.06	1.54	0.59	2.64	0.54	−0.13	0.01	0.04	−0.17
5000	$0.4920 \cdot 10^{-2}$	2.68	1.76	0.51	3.25	0.44	−0.15	0.01	0.04	−0.20
8000	$0.1140 \cdot 10^{-2}$	4.75	2.39	0.74	5.37	0.68	−0.04	0.01	0.04	−0.28
12000	$0.2750 \cdot 10^{-3}$	8.24	2.91	0.82	8.77	0.74	−0.13	0.01	0.05	−0.33
20000	$0.4080 \cdot 10^{-4}$	16.20	4.65	1.14	16.90	1.08	0.20	0.03	0.06	−0.29
30000	$0.6680 \cdot 10^{-5}$	41.62	6.22	1.46	42.11	1.45	0.05	0.01	0.04	−0.15

Table 36: The NC e^+p cross section $\mathrm{d}\sigma_{\mathrm{NC}}/\mathrm{d}Q^2$ for lepton beam polarisation $P_e = +32.5\%$ and $y < 0.9$. The statistical (δ_{stat}), uncorrelated systematic (δ_{unc}), correlated systematic (δ_{cor}) and total (δ_{tot}) errors are provided. In addition the correlated systematic error contributions from a positive variation of one standard deviation of the electron energy error ($\delta_{\mathrm{cor}}^{E^+}$), of the polar electron angle error ($\delta_{\mathrm{cor}}^{\theta^+}$), of the hadronic energy error ($\delta_{\mathrm{cor}}^{h^+}$), of the error due to noise subtraction ($\delta_{\mathrm{cor}}^{N^+}$) and of the error due to background subtraction ($\delta_{\mathrm{cor}}^{B^+}$) are given. The normalisation and polarisation uncertainties are not included in the errors.

Q^2 (GeV^2)	$\mathrm{d}\sigma_{CC}/\mathrm{d}Q^2$ ($\mathrm{pb/GeV}^2$)	k_{cor}	δ_{stat} (%)	δ_{unc} (%)	δ_{cor} (%)	δ_{tot} (%)	δ_{cor}^{V+} (%)	δ_{cor}^{h+} (%)	δ_{cor}^{N+} (%)	δ_{cor}^{B+} (%)
300	$0.426 \cdot 10^{-1}$	1.493	8.7	7.5	6.4	13.1	5.7	−0.5	−1.3	−2.2
500	$0.282 \cdot 10^{-1}$	1.246	4.9	4.4	4.0	7.8	3.7	−0.6	−0.9	−0.3
1000	$0.203 \cdot 10^{-1}$	1.071	3.8	3.2	2.2	5.5	2.1	−0.4	−0.5	−0.1
2000	$0.118 \cdot 10^{-1}$	1.024	3.3	2.5	1.0	4.3	0.9	−0.2	−0.2	−0.0
3000	$0.713 \cdot 10^{-2}$	1.027	3.4	2.1	0.6	4.1	0.2	−0.0	0.3	−0.1
5000	$0.374 \cdot 10^{-2}$	1.033	3.7	2.3	0.7	4.4	−0.0	0.1	0.4	−0.0
8000	$0.168 \cdot 10^{-2}$	1.049	4.7	3.5	1.6	6.2	−0.0	0.8	1.2	0.0
15000	$0.425 \cdot 10^{-3}$	1.082	6.5	5.9	2.7	9.2	0.0	1.6	1.9	0.0
30000	$0.388 \cdot 10^{-4}$	1.195	14.5	11.4	5.3	19.2	0.0	3.3	3.3	0.0

Table 37: The CC e^-p cross section $\mathrm{d}\sigma_{CC}/\mathrm{d}Q^2$ for lepton beam polarisation $P_e = -25.8\%$ and $y < 0.9$ after correction (k_{cor}) according to the Standard Model expectation for the kinematic cuts $P_{T,h} > 12$ GeV and $0.03 < y < 0.85$. The statistical (δ_{stat}), uncorrelated systematic (δ_{unc}), correlated systematic (δ_{cor}) and total (δ_{tot}) errors are provided. In addition the correlated systematic error contributions from a positive variation of one standard deviation of the cuts against photoproduction (δ_{cor}^{V+}), of the hadronic energy error (δ_{cor}^{h+}), of the error due to noise subtraction (δ_{cor}^{N+}) and of the error due to background subtraction (δ_{cor}^{B+}) are given. The luminosity and polarisation uncertainties are not included in the errors.

Q^2 (GeV^2)	$\mathrm{d}\sigma_{CC}/\mathrm{d}Q^2$ ($\mathrm{pb/GeV}^2$)	k_{cor}	δ_{stat} (%)	δ_{unc} (%)	δ_{cor} (%)	δ_{tot} (%)	δ_{cor}^{V+} (%)	δ_{cor}^{h+} (%)	δ_{cor}^{N+} (%)	δ_{cor}^{B+} (%)
300	$0.207 \cdot 10^{-1}$	1.493	15.1	7.6	6.4	18.1	5.7	−0.5	−0.8	−1.9
500	$0.159 \cdot 10^{-1}$	1.246	10.0	4.6	4.1	11.7	3.8	−0.6	−1.0	−0.8
1000	$0.110 \cdot 10^{-1}$	1.071	7.6	3.0	2.1	8.5	2.0	−0.3	−0.1	−0.2
2000	$0.528 \cdot 10^{-2}$	1.024	7.4	2.5	1.2	7.9	0.8	−0.4	−0.5	−0.2
3000	$0.366 \cdot 10^{-2}$	1.027	7.0	2.2	0.7	7.4	0.2	−0.0	0.3	−0.1
5000	$0.190 \cdot 10^{-2}$	1.033	7.5	2.4	0.9	8.0	−0.0	0.3	0.6	−0.0
8000	$0.838 \cdot 10^{-3}$	1.049	9.8	3.3	1.5	10.5	−0.0	0.8	1.0	0.0
15000	$0.215 \cdot 10^{-3}$	1.082	14.0	5.8	2.7	15.5	−0.0	1.5	2.0	0.0
30000	$0.188 \cdot 10^{-4}$	1.195	28.9	10.8	4.8	31.3	0.0	3.0	2.8	0.0

Table 38: The CC e^-p cross section $\mathrm{d}\sigma_{CC}/\mathrm{d}Q^2$ for lepton beam polarisation $P_e = +36.0\%$ and $y < 0.9$ after correction (k_{cor}) according to the Standard Model expectation for the kinematic cuts $P_{T,h} > 12$ GeV and $0.03 < y < 0.85$. The statistical (δ_{stat}), uncorrelated systematic (δ_{unc}), correlated systematic (δ_{cor}) and total (δ_{tot}) errors are provided. In addition the correlated systematic error contributions from a positive variation of one standard deviation of the cuts against photoproduction (δ_{cor}^{V+}), of the hadronic energy error (δ_{cor}^{h+}), of the error due to noise subtraction (δ_{cor}^{N+}) and of the error due to background subtraction (δ_{cor}^{B+}) are given. The luminosity and polarisation uncertainties are not included in the errors.

Q^2 (GeV^2)	$\mathrm{d}\sigma_{\mathrm{CC}}/\mathrm{d}Q^2$ (pb/GeV^2)	k_{cor}	δ_{stat} (%)	δ_{unc} (%)	δ_{cor} (%)	δ_{tot} (%)	$\delta_{\mathrm{cor}}^{V+}$ (%)	$\delta_{\mathrm{cor}}^{h+}$ (%)	$\delta_{\mathrm{cor}}^{N+}$ (%)	$\delta_{\mathrm{cor}}^{B+}$ (%)
300	$0.157 \cdot 10^{-1}$	1.408	14.2	8.0	8.0	18.2	6.2	−0.6	−0.8	−4.4
500	$0.124 \cdot 10^{-1}$	1.181	8.9	4.3	4.7	11.0	4.3	−0.4	0.2	−1.5
1000	$0.761 \cdot 10^{-2}$	1.043	7.1	3.0	2.4	8.1	2.3	−0.2	−0.1	−0.4
2000	$0.327 \cdot 10^{-2}$	1.026	7.0	2.4	1.2	7.5	1.0	0.0	0.3	−0.1
3000	$0.177 \cdot 10^{-2}$	1.030	7.8	2.6	1.1	8.3	0.3	0.4	0.8	−0.0
5000	$0.600 \cdot 10^{-3}$	1.035	10.6	3.1	1.6	11.3	−0.1	0.6	1.3	−0.0
8000	$0.184 \cdot 10^{-3}$	1.049	15.8	5.7	2.7	17.3	−0.1	1.4	1.9	0.0
15000	$0.198 \cdot 10^{-4}$	1.077	30.7	7.0	3.9	31.9	−0.0	2.4	2.1	0.0

Table 39: The CC e^+p cross section $\mathrm{d}\sigma_{\mathrm{CC}}/\mathrm{d}Q^2$ for lepton beam polarisation $P_e = -37.0\%$ and $y < 0.9$ after correction (k_{cor}) according to the Standard Model expectation for the kinematic cuts $P_{T,h} > 12$ GeV and $0.03 < y < 0.85$. The statistical (δ_{stat}), uncorrelated systematic (δ_{unc}), correlated systematic (δ_{cor}) and total (δ_{tot}) errors are provided. In addition the correlated systematic error contributions from a positive variation of one standard deviation of the cuts against photoproduction ($\delta_{\mathrm{cor}}^{V+}$), of the hadronic energy error ($\delta_{\mathrm{cor}}^{h+}$), of the error due to noise subtraction ($\delta_{\mathrm{cor}}^{N+}$) and of the error due to background subtraction ($\delta_{\mathrm{cor}}^{B+}$) are given. The luminosity and polarisation uncertainties are not included in the errors.

Q^2 (GeV^2)	$\mathrm{d}\sigma_{\mathrm{CC}}/\mathrm{d}Q^2$ (pb/GeV^2)	k_{cor}	δ_{stat} (%)	δ_{unc} (%)	δ_{cor} (%)	δ_{tot} (%)	$\delta_{\mathrm{cor}}^{V+}$ (%)	$\delta_{\mathrm{cor}}^{h+}$ (%)	$\delta_{\mathrm{cor}}^{N+}$ (%)	$\delta_{\mathrm{cor}}^{B+}$ (%)
300	$0.294 \cdot 10^{-1}$	1.408	8.8	8.0	7.1	13.8	6.5	−0.4	−0.5	−2.5
500	$0.259 \cdot 10^{-1}$	1.181	5.3	4.4	4.4	8.2	4.2	−0.4	−0.5	−0.4
1000	$0.145 \cdot 10^{-1}$	1.043	4.5	3.0	2.4	5.9	2.3	−0.4	−0.0	−0.1
2000	$0.707 \cdot 10^{-2}$	1.026	4.2	2.4	1.2	5.0	1.0	0.1	0.4	−0.1
3000	$0.382 \cdot 10^{-2}$	1.030	4.7	2.5	1.1	5.5	0.3	0.4	0.8	0.0
5000	$0.136 \cdot 10^{-2}$	1.035	6.2	3.8	1.9	7.7	−0.0	0.8	1.5	−0.0
8000	$0.438 \cdot 10^{-3}$	1.049	9.1	5.1	2.5	11.1	−0.1	1.4	1.7	0.0
15000	$0.544 \cdot 10^{-4}$	1.077	16.3	7.3	3.6	18.5	0.1	1.8	2.2	0.0

Table 40: The CC e^+p cross section $\mathrm{d}\sigma_{\mathrm{CC}}/\mathrm{d}Q^2$ for lepton beam polarisation $P_e = +32.5\%$ and $y < 0.9$ after correction (k_{cor}) according to the Standard Model expectation for the kinematic cuts $P_{T,h} > 12$ GeV and $0.03 < y < 0.85$. The statistical (δ_{stat}), uncorrelated systematic (δ_{unc}), correlated systematic (δ_{cor}) and total (δ_{tot}) errors are provided. In addition the correlated systematic error contributions from a positive variation of one standard deviation of the cuts against photoproduction ($\delta_{\mathrm{cor}}^{V+}$), of the hadronic energy error ($\delta_{\mathrm{cor}}^{h+}$), of the error due to noise subtraction ($\delta_{\mathrm{cor}}^{N+}$) and of the error due to background subtraction ($\delta_{\mathrm{cor}}^{B+}$) are given. The luminosity and polarisation uncertainties are not included in the errors.

Q^2 (GeV^2)	$\mathrm{d}\sigma_{\mathrm{NC}}/\mathrm{d}Q^2$ (pb/GeV^2)	δ_{stat} (%)	δ_{unc} (%)	δ_{cor} (%)	δ_{tot} (%)	$\delta_{\mathrm{cor}}^{E^+}$ (%)	$\delta_{\mathrm{cor}}^{\theta^+}$ (%)	$\delta_{\mathrm{cor}}^{h^+}$ (%)	$\delta_{\mathrm{cor}}^{N^+}$ (%)	$\delta_{\mathrm{cor}}^{B^+}$ (%)
200	17.85	0.35	0.91	0.61	1.15	−0.21	−0.57	0.00	0.05	−0.06
250	10.50	0.36	1.21	0.66	1.42	0.39	−0.53	0.00	0.04	−0.04
300	6.785	0.42	1.24	0.75	1.51	0.50	−0.55	0.01	0.04	−0.04
400	3.401	0.50	1.05	0.61	1.31	0.45	−0.41	0.01	0.04	−0.03
500	1.999	0.59	1.08	0.64	1.39	0.51	−0.39	0.01	0.04	−0.02
650	1.050	0.72	1.09	0.63	1.45	0.52	−0.35	0.01	0.05	−0.02
800	0.6210	0.87	1.07	0.57	1.49	0.48	−0.31	0.01	0.05	−0.02
1000	0.3580	1.02	1.13	0.60	1.63	0.47	−0.31	0.01	0.05	−0.19
1200	0.2240	1.21	1.27	0.55	1.84	0.47	−0.24	0.01	0.04	−0.16
1500	0.1280	1.45	1.34	0.58	2.06	0.51	−0.21	0.01	0.05	−0.16
2000	$0.5930 \cdot 10^{-1}$	1.75	1.43	0.59	2.34	0.52	−0.22	0.01	0.05	−0.19
3000	$0.2120 \cdot 10^{-1}$	1.64	1.51	0.54	2.29	0.50	−0.16	0.01	0.04	−0.14
5000	$0.5610 \cdot 10^{-2}$	2.11	1.71	0.46	2.76	0.41	−0.14	0.01	0.04	−0.15
8000	$0.1520 \cdot 10^{-2}$	3.19	2.30	0.61	3.98	0.55	−0.07	0.01	0.04	−0.24
12000	$0.5190 \cdot 10^{-3}$	4.88	2.71	0.72	5.63	0.67	0.00	0.02	0.06	−0.24
20000	$0.1030 \cdot 10^{-3}$	8.53	3.86	1.02	9.42	0.89	0.11	0.02	0.04	−0.49
30000	$0.1920 \cdot 10^{-4}$	20.43	6.20	2.10	21.46	1.58	0.25	0.02	0.08	−1.36
50000	$0.1770 \cdot 10^{-5}$	57.80	9.87	2.73	58.70	2.66	0.60	0.00	0.00	0.00

Table 41: The NC e^-p cross section $\mathrm{d}\sigma_{\mathrm{NC}}/\mathrm{d}Q^2$ for $P_e = 0$ and $y < 0.9$. The statistical (δ_{stat}), uncorrelated systematic (δ_{unc}), correlated systematic (δ_{cor}) and total (δ_{tot}) errors are provided. In addition the correlated systematic error contributions from a positive variation of one standard deviation of the electron energy error ($\delta_{\mathrm{cor}}^{E^+}$), of the polar electron angle error ($\delta_{\mathrm{cor}}^{\theta^+}$), of the hadronic energy error ($\delta_{\mathrm{cor}}^{h^+}$), of the error due to noise subtraction ($\delta_{\mathrm{cor}}^{N^+}$) and of the error due to background subtraction ($\delta_{\mathrm{cor}}^{B^+}$) are given. The normalisation and polarisation uncertainties are not included in the errors.

Q^2 (GeV^2)	$\mathrm{d}\sigma_{\mathrm{NC}}/\mathrm{d}Q^2$ (pb/GeV^2)	δ_{stat} (%)	δ_{unc} (%)	δ_{cor} (%)	δ_{tot} (%)	$\delta_{\mathrm{cor}}^{E^+}$ (%)	$\delta_{\mathrm{cor}}^{\theta^+}$ (%)	$\delta_{\mathrm{cor}}^{h^+}$ (%)	$\delta_{\mathrm{cor}}^{N^+}$ (%)	$\delta_{\mathrm{cor}}^{B^+}$ (%)
200	17.98	0.31	0.80	0.64	1.07	−0.23	−0.59	0.01	0.05	−0.07
250	10.54	0.33	1.13	0.68	1.35	0.41	−0.54	0.00	0.04	−0.05
300	6.848	0.38	1.14	0.71	1.40	0.47	−0.53	0.00	0.04	−0.04
400	3.403	0.45	0.96	0.62	1.23	0.46	−0.42	0.00	0.04	−0.03
500	1.999	0.54	0.97	0.65	1.28	0.51	−0.40	0.01	0.04	−0.03
650	1.045	0.65	1.01	0.67	1.38	0.54	−0.39	0.01	0.04	−0.02
800	0.6150	0.79	1.02	0.65	1.44	0.54	−0.35	0.01	0.05	−0.03
1000	0.3440	0.94	1.00	0.54	1.47	0.42	−0.27	0.01	0.05	−0.20
1200	0.2150	1.11	1.19	0.59	1.73	0.50	−0.27	0.01	0.05	−0.17
1500	0.1200	1.34	1.31	0.61	1.97	0.55	−0.22	0.01	0.05	−0.15
2000	$0.5670 \cdot 10^{-1}$	1.62	1.38	0.61	2.21	0.54	−0.23	0.01	0.05	−0.17
3000	$0.1930 \cdot 10^{-1}$	1.55	1.55	0.63	2.28	0.58	−0.15	0.01	0.05	−0.17
5000	$0.4520 \cdot 10^{-2}$	2.07	1.73	0.52	2.75	0.45	−0.14	0.01	0.04	−0.23
8000	$0.1050 \cdot 10^{-2}$	3.60	2.37	0.81	4.38	0.71	−0.07	0.01	0.03	−0.37
12000	$0.2480 \cdot 10^{-3}$	6.43	2.93	0.85	7.12	0.75	−0.09	0.01	0.05	−0.40
20000	$0.3540 \cdot 10^{-4}$	12.92	4.48	1.14	13.72	1.10	0.15	0.02	0.06	−0.23
30000	$0.4190 \cdot 10^{-5}$	38.94	5.92	1.47	39.41	1.44	0.21	0.01	0.04	−0.16

Table 42: The NC e^+p cross section $\mathrm{d}\sigma_{\mathrm{NC}}/\mathrm{d}Q^2$ for $P_e = 0$ and $y < 0.9$. The statistical (δ_{stat}), uncorrelated systematic (δ_{unc}), correlated systematic (δ_{cor}) and total (δ_{tot}) errors are provided. In addition the correlated systematic error contributions from a positive variation of one standard deviation of the electron energy error ($\delta_{\mathrm{cor}}^{E^+}$), of the polar electron angle error ($\delta_{\mathrm{cor}}^{\theta^+}$), of the hadronic energy error ($\delta_{\mathrm{cor}}^{h^+}$), of the error due to noise subtraction ($\delta_{\mathrm{cor}}^{N^+}$) and of the error due to background subtraction ($\delta_{\mathrm{cor}}^{B^+}$) are given. The normalisation and polarisation uncertainties are not included in the errors.

Q^2 (GeV^2)	$\mathrm{d}\sigma_{\mathrm{CC}}/\mathrm{d}Q^2$ ($\mathrm{pb/GeV}^2$)	k_{cor}	δ_{stat} (%)	δ_{unc} (%)	δ_{cor} (%)	δ_{tot} (%)	$\delta_{\mathrm{cor}}^{V+}$ (%)	$\delta_{\mathrm{cor}}^{h+}$ (%)	$\delta_{\mathrm{cor}}^{N+}$ (%)	$\delta_{\mathrm{cor}}^{B+}$ (%)
300	$0.336 \cdot 10^{-1}$	1.493	7.6	7.5	6.4	12.4	5.7	−0.5	−1.2	−2.2
500	$0.229 \cdot 10^{-1}$	1.246	4.4	4.4	4.0	7.4	3.7	−0.6	−0.9	−0.4
1000	$0.163 \cdot 10^{-1}$	1.071	3.4	3.2	2.2	5.2	2.0	−0.4	−0.4	−0.1
2000	$0.917 \cdot 10^{-2}$	1.024	3.0	2.5	1.0	4.1	0.9	−0.2	−0.2	−0.0
3000	$0.568 \cdot 10^{-2}$	1.027	3.0	2.1	0.6	3.8	0.2	−0.0	0.3	−0.1
5000	$0.297 \cdot 10^{-2}$	1.033	3.3	2.3	0.7	4.2	−0.0	0.2	0.4	−0.0
8000	$0.133 \cdot 10^{-2}$	1.049	4.2	3.5	1.5	5.8	−0.0	0.8	1.1	0.0
15000	$0.337 \cdot 10^{-3}$	1.082	5.9	5.9	2.6	8.8	−0.0	1.6	1.9	0.0
30000	$0.305 \cdot 10^{-4}$	1.195	12.9	11.3	5.0	17.9	0.0	3.2	3.2	0.0

Table 43: The CC e^-p cross section $\mathrm{d}\sigma_{\mathrm{CC}}/\mathrm{d}Q^2$ for $P_e = 0$ and $y < 0.9$ after correction (k_{cor}) according to the Standard Model expectation for the kinematic cuts $P_{T,h} > 12$ GeV and $0.03 < y < 0.85$. The statistical (δ_{stat}), uncorrelated systematic (δ_{unc}), correlated systematic (δ_{cor}) and total (δ_{tot}) errors are provided. In addition the correlated systematic error contributions from a positive variation of one standard deviation of the cuts against photoproduction ($\delta_{\mathrm{cor}}^{V+}$), of the hadronic energy error ($\delta_{\mathrm{cor}}^{h+}$), of the error due to noise subtraction ($\delta_{\mathrm{cor}}^{N+}$) and of the error due to background subtraction ($\delta_{\mathrm{cor}}^{B+}$) are given. The luminosity and polarisation uncertainties are not included in the errors.

Q^2 (GeV^2)	$\mathrm{d}\sigma_{\mathrm{CC}}/\mathrm{d}Q^2$ ($\mathrm{pb/GeV}^2$)	k_{cor}	δ_{stat} (%)	δ_{unc} (%)	δ_{cor} (%)	δ_{tot} (%)	$\delta_{\mathrm{cor}}^{V+}$ (%)	$\delta_{\mathrm{cor}}^{h+}$ (%)	$\delta_{\mathrm{cor}}^{N+}$ (%)	$\delta_{\mathrm{cor}}^{B+}$ (%)
300	$0.229 \cdot 10^{-1}$	1.408	7.5	8.0	7.3	13.1	6.4	−0.4	−0.6	−3.0
500	$0.196 \cdot 10^{-1}$	1.181	4.6	4.3	4.4	7.7	4.3	−0.4	−0.4	−0.7
1000	$0.113 \cdot 10^{-1}$	1.043	3.8	3.0	2.3	5.4	2.3	−0.3	−0.1	−0.2
2000	$0.529 \cdot 10^{-2}$	1.026	3.6	2.4	1.2	4.5	1.0	0.0	0.4	−0.1
3000	$0.287 \cdot 10^{-2}$	1.030	4.0	2.6	1.0	4.9	0.3	0.4	0.8	−0.0
5000	$0.101 \cdot 10^{-2}$	1.035	5.3	3.6	1.7	6.9	−0.0	0.7	1.4	−0.0
8000	$0.320 \cdot 10^{-3}$	1.049	7.9	5.2	2.4	10.2	−0.1	1.4	1.8	0.0
15000	$0.384 \cdot 10^{-4}$	1.077	14.4	7.2	3.4	16.7	−0.1	2.0	2.2	0.0

Table 44: The CC e^+p cross section $\mathrm{d}\sigma_{\mathrm{CC}}/\mathrm{d}Q^2$ for $P_e = 0$ and $y < 0.9$ after correction (k_{cor}) according to the Standard Model expectation for the kinematic cuts $P_{T,h} > 12$ GeV and $0.03 < y < 0.85$. The statistical (δ_{stat}), uncorrelated systematic (δ_{unc}), correlated systematic (δ_{cor}) and total (δ_{tot}) errors are provided. In addition the correlated systematic error contributions from a positive variation of one standard deviation of the cuts against photoproduction ($\delta_{\mathrm{cor}}^{V+}$), of the hadronic energy error ($\delta_{\mathrm{cor}}^{h+}$), of the error due to noise subtraction ($\delta_{\mathrm{cor}}^{N+}$) and of the error due to background subtraction ($\delta_{\mathrm{cor}}^{B+}$) are given. The luminosity and polarisation uncertainties are not included in the errors.

Q^2 (GeV^2)	$\mathrm{d}\sigma_{\mathrm{NC}}/\mathrm{d}Q^2$ ($\mathrm{pb}/\mathrm{GeV}^2$)	δ_{stat} (%)	δ_{unc} (%)	δ_{cor} (%)	δ_{tot} (%)
200	18.21	0.34	0.87	1.70	1.94
250	10.72	0.35	1.13	1.69	2.06
300	6.958	0.40	1.17	1.71	2.11
400	3.485	0.48	0.98	1.67	2.00
500	2.047	0.56	1.03	1.71	2.07
650	1.077	0.69	1.04	1.69	2.10
800	0.6402	0.83	1.02	1.67	2.13
1000	0.3670	0.97	1.06	1.68	2.21
1200	0.2310	1.15	1.18	1.66	2.34
1500	0.1314	1.38	1.24	1.67	2.49
2000	$0.6081 \cdot 10^{-1}$	1.66	1.33	1.69	2.72
3000	$0.2201 \cdot 10^{-1}$	1.55	1.38	1.66	2.66
5000	$0.5857 \cdot 10^{-2}$	1.98	1.57	1.65	3.01
8000	$0.1596 \cdot 10^{-2}$	2.98	2.14	1.69	4.04
12000	$0.5190 \cdot 10^{-3}$	4.67	2.53	1.72	5.58
20000	$0.1049 \cdot 10^{-3}$	8.12	3.63	1.83	9.08
30000	$0.1995 \cdot 10^{-4}$	19.00	5.99	2.41	20.06
50000	$0.1839 \cdot 10^{-5}$	56.69	9.87	2.90	57.62

Table 45: Combined HERA I+II NC e^-p cross sections $\mathrm{d}\sigma_{\mathrm{NC}}/\mathrm{d}Q^2$ for $P_e = 0$ and $y < 0.9$. Here δ_{stat}, δ_{unc}, δ_{cor} and δ_{tot} are the relative statistical, total uncorrelated, correlated systematic and total uncertainties, respectively.

Q^2 (GeV^2)	$\mathrm{d}\sigma_{\mathrm{NC}}/\mathrm{d}Q^2$ ($\mathrm{pb/GeV}^2$)	δ_{stat} (%)	δ_{unc} (%)	δ_{cor} (%)	δ_{tot} (%)
200	18.30	0.25	0.68	1.22	1.42
250	10.77	0.27	0.92	1.20	1.54
300	7.008	0.30	0.95	1.22	1.57
400	3.495	0.37	0.79	1.20	1.48
500	2.042	0.43	0.82	1.21	1.53
650	1.067	0.52	0.83	1.23	1.57
800	0.6323	0.64	0.85	1.22	1.61
1000	0.3578	0.75	0.85	1.21	1.65
1200	0.2230	0.89	0.95	1.22	1.78
1500	0.1229	1.08	1.01	1.20	1.90
2000	$0.5794 \cdot 10^{-1}$	1.29	1.11	1.23	2.10
3000	$0.1979 \cdot 10^{-1}$	1.24	1.21	1.22	2.12
5000	$0.4579 \cdot 10^{-2}$	1.69	1.42	1.19	2.51
8000	$0.1109 \cdot 10^{-2}$	2.84	1.99	1.31	3.71
12000	$0.2387 \cdot 10^{-3}$	5.37	2.57	1.29	6.09
20000	$0.3529 \cdot 10^{-4}$	10.62	4.02	1.46	11.45
30000	$0.6517 \cdot 10^{-5}$	25.70	6.07	1.84	26.47

Table 46: Combined HERA I+II NC e^+p cross sections $\mathrm{d}\sigma_{\mathrm{NC}}/\mathrm{d}Q^2$ for $P_e = 0$ and $y < 0.9$. Here δ_{stat}, δ_{unc}, δ_{cor} and δ_{tot} are the relative statistical, total uncorrelated, correlated systematic and total uncertainties, respectively.

Q^2 (GeV^2)	$\mathrm{d}\sigma_{\mathrm{CC}}/\mathrm{d}Q^2$ ($\mathrm{pb/GeV}^2$)	δ_{stat} (%)	δ_{unc} (%)	δ_{cor} (%)	δ_{tot} (%)
300	$0.355 \cdot 10^{-1}$	7.1	6.2	4.9	10.6
500	$0.245 \cdot 10^{-1}$	4.2	3.9	3.3	6.5
1000	$0.166 \cdot 10^{-1}$	3.2	2.8	2.2	4.8
2000	$0.951 \cdot 10^{-2}$	2.8	2.3	1.8	4.0
3000	$0.593 \cdot 10^{-2}$	2.8	2.0	1.6	3.8
5000	$0.301 \cdot 10^{-2}$	3.1	2.2	1.7	4.2
8000	$0.136 \cdot 10^{-2}$	3.9	3.3	2.0	5.5
15000	$0.341 \cdot 10^{-3}$	5.5	5.5	2.7	8.3
30000	$0.291 \cdot 10^{-4}$	12.6	10.3	4.3	16.8

Table 47: Combined HERA I+II CC e^-p cross sections $\mathrm{d}\sigma_{\mathrm{CC}}/\mathrm{d}Q^2$ for $P_e = 0$ and $y < 0.9$. Here δ_{stat}, δ_{unc}, δ_{cor} and δ_{tot} are the relative statistical, total uncorrelated, correlated systematic and total uncertainties, respectively.

Q^2 (GeV^2)	$\mathrm{d}\sigma_{\mathrm{CC}}/\mathrm{d}Q^2$ ($\mathrm{pb}/\mathrm{GeV}^2$)	δ_{stat} (%)	δ_{unc} (%)	δ_{cor} (%)	δ_{tot} (%)
300	$0.266 \cdot 10^{-1}$	5.5	4.8	4.0	8.3
500	$0.200 \cdot 10^{-1}$	3.6	3.0	2.8	5.4
1000	$0.113 \cdot 10^{-1}$	2.9	2.3	1.9	4.2
2000	$0.535 \cdot 10^{-2}$	2.8	2.0	1.4	3.7
3000	$0.295 \cdot 10^{-2}$	3.0	2.1	1.4	3.9
5000	$0.104 \cdot 10^{-2}$	4.1	2.8	1.8	5.3
8000	$0.322 \cdot 10^{-3}$	6.3	4.4	2.5	8.1
15000	$0.424 \cdot 10^{-4}$	11.4	6.5	2.9	13.4

Table 48: Combined HERA I+II CC e^+p cross sections $\mathrm{d}\sigma_{\mathrm{CC}}/\mathrm{d}Q^2$ for $P_e = 0$ and $y < 0.9$. Here δ_{stat}, δ_{unc}, δ_{cor} and δ_{tot} are the relative statistical, total uncorrelated, correlated systematic and total uncertainties, respectively.

Q^2 (GeV^2)	x	$F_2^{\gamma Z}$	Δ_{stat}	Δ_{unc}	Δ_{cor}	Δ_{tot}
200	0.020	−0.412	0.908	0.682	0.946	1.478
200	0.032	0.647	0.873	0.753	0.799	1.403
200	0.050	−1.814	0.922	0.871	0.724	1.460
200	0.080	0.547	0.807	0.861	0.600	1.323
200	0.130	−0.836	0.766	0.742	0.497	1.177
200	0.180	−1.246	0.909	0.819	0.458	1.306
250	0.020	1.373	0.734	0.657	0.755	1.241
250	0.032	1.165	0.649	0.554	0.638	1.066
250	0.050	1.275	0.615	0.470	0.547	0.948
250	0.080	−0.583	0.561	0.365	0.477	0.822
250	0.130	−1.174	0.499	0.480	0.421	0.810
250	0.180	0.087	0.564	0.611	0.341	0.899
300	0.020	0.510	0.720	0.448	0.647	1.067
300	0.032	−0.653	0.633	0.437	0.544	0.942
300	0.050	−0.429	0.593	0.432	0.465	0.869
300	0.080	−0.306	0.532	0.381	0.404	0.769
300	0.130	0.293	0.454	0.422	0.356	0.715
300	0.180	0.568	0.490	0.559	0.276	0.793
300	0.400	−0.399	0.297	0.333	0.153	0.472
400	0.020	1.214	0.601	0.406	0.492	0.876
400	0.032	0.095	0.545	0.281	0.420	0.743
400	0.050	−0.099	0.498	0.263	0.347	0.661
400	0.080	0.835	0.452	0.208	0.301	0.582
400	0.130	−0.265	0.389	0.246	0.258	0.528
400	0.180	−0.041	0.403	0.350	0.215	0.576
400	0.400	−0.339	0.264	0.229	0.109	0.366
500	0.020	1.071	0.595	0.304	0.412	0.785
500	0.032	1.059	0.522	0.243	0.345	0.671
500	0.050	0.882	0.474	0.236	0.301	0.609
500	0.080	0.199	0.427	0.179	0.247	0.525
500	0.130	−0.406	0.443	0.205	0.214	0.533
500	0.180	0.228	0.399	0.226	0.183	0.494
500	0.250	0.271	0.378	0.257	0.142	0.478

Table 49: The measured structure function $F_2^{\gamma Z}$ determined using the polarised HERA II data set. The absolute statistical, uncorrelated, correlated and total uncertainties Δ_{stat}, Δ_{unc}, Δ_{cor} and Δ_{tot} are also given. The luminosity uncertainty of 2.3% is not included in the errors. Table continues on next pages.

Q^2 (GeV^2)	x	$F_2^{\gamma Z}$	Δ_{stat}	Δ_{unc}	Δ_{cor}	Δ_{tot}
650	0.020	0.408	0.563	0.242	0.330	0.696
650	0.032	0.730	0.501	0.254	0.287	0.630
650	0.050	0.027	0.439	0.184	0.235	0.530
650	0.080	0.905	0.390	0.147	0.190	0.458
650	0.130	0.848	0.389	0.159	0.165	0.452
650	0.180	0.102	0.361	0.168	0.164	0.430
650	0.250	−0.081	0.337	0.193	0.110	0.403
650	0.400	0.160	0.249	0.138	0.086	0.297
800	0.020	0.345	0.516	0.189	0.260	0.608
800	0.032	0.767	0.466	0.199	0.229	0.556
800	0.050	0.098	0.428	0.148	0.198	0.494
800	0.080	0.506	0.377	0.134	0.159	0.431
800	0.130	0.007	0.382	0.134	0.131	0.426
800	0.180	0.096	0.363	0.146	0.126	0.411
800	0.250	0.634	0.302	0.137	0.089	0.343
800	0.400	0.165	0.225	0.130	0.047	0.264
1000	0.020	0.620	0.509	0.154	0.222	0.576
1000	0.032	0.936	0.445	0.147	0.190	0.506
1000	0.050	0.504	0.377	0.158	0.154	0.437
1000	0.080	0.492	0.348	0.105	0.131	0.386
1000	0.130	−0.446	0.349	0.105	0.108	0.380
1000	0.180	0.726	0.313	0.111	0.104	0.348
1000	0.250	0.058	0.285	0.111	0.091	0.319
1000	0.400	0.187	0.211	0.107	0.039	0.240
1200	0.020	0.723	0.544	0.146	0.194	0.596
1200	0.032	0.049	0.432	0.110	0.164	0.474
1200	0.050	0.056	0.368	0.114	0.134	0.408
1200	0.080	0.081	0.337	0.101	0.114	0.370
1200	0.130	0.492	0.332	0.092	0.088	0.355
1200	0.180	0.887	0.298	0.089	0.081	0.322
1200	0.250	−0.228	0.255	0.086	0.060	0.276
1200	0.400	−0.057	0.174	0.089	0.031	0.197
1500	0.020	0.938	0.541	0.183	0.163	0.594
1500	0.032	0.379	0.444	0.095	0.133	0.474
1500	0.050	0.139	0.361	0.093	0.114	0.389
1500	0.080	0.196	0.330	0.087	0.099	0.355
1500	0.130	0.560	0.334	0.078	0.073	0.351
1500	0.180	0.475	0.269	0.074	0.063	0.286
1500	0.250	−0.435	0.237	0.081	0.052	0.256
1500	0.400	0.375	0.158	0.065	0.031	0.173
1500	0.650	0.011	0.035	0.015	0.004	0.038

Table 49: continued.

Q^2 (GeV^2)	x	$F_2^{\gamma Z}$	Δ_{stat}	Δ_{unc}	Δ_{cor}	Δ_{tot}
2000	0.022	1.246	0.709	0.227	0.142	0.758
2000	0.032	0.071	0.397	0.100	0.100	0.422
2000	0.050	0.467	0.342	0.072	0.089	0.361
2000	0.080	−0.081	0.286	0.068	0.073	0.302
2000	0.130	0.683	0.280	0.065	0.059	0.293
2000	0.180	0.161	0.252	0.065	0.050	0.265
2000	0.250	0.363	0.209	0.063	0.040	0.222
2000	0.400	0.128	0.138	0.053	0.023	0.150
2000	0.650	0.024	0.027	0.010	0.003	0.029
3000	0.032	0.850	0.294	0.098	0.081	0.320
3000	0.050	0.261	0.219	0.063	0.068	0.238
3000	0.080	0.279	0.200	0.049	0.057	0.214
3000	0.130	0.383	0.190	0.050	0.045	0.201
3000	0.180	0.186	0.181	0.049	0.037	0.191
3000	0.250	−0.254	0.145	0.043	0.031	0.155
3000	0.400	0.124	0.083	0.036	0.016	0.092
3000	0.650	0.034	0.016	0.007	0.003	0.018
5000	0.055	0.491	0.239	0.068	0.049	0.253
5000	0.080	0.661	0.155	0.042	0.041	0.166
5000	0.130	0.408	0.154	0.042	0.035	0.163
5000	0.180	0.263	0.147	0.037	0.029	0.154
5000	0.250	−0.100	0.154	0.030	0.020	0.158
5000	0.400	−0.056	0.075	0.023	0.010	0.079
5000	0.650	0.019	0.015	0.005	0.002	0.016
8000	0.088	0.480	0.265	0.065	0.035	0.275
8000	0.130	0.249	0.172	0.045	0.028	0.180
8000	0.180	0.107	0.147	0.034	0.022	0.152
8000	0.250	0.049	0.125	0.027	0.017	0.129
8000	0.400	0.003	0.074	0.023	0.008	0.078
8000	0.650	−0.006	0.014	0.005	0.001	0.015
12000	0.130	0.086	0.406	0.086	0.033	0.416
12000	0.180	0.304	0.181	0.033	0.022	0.186
12000	0.250	0.063	0.134	0.023	0.014	0.137
12000	0.400	0.204	0.093	0.027	0.009	0.098
12000	0.650	0.028	0.017	0.004	0.002	0.018
20000	0.250	0.698	0.184	0.031	0.023	0.188
20000	0.400	0.035	0.117	0.025	0.008	0.120
20000	0.650	−0.000	0.023	0.007	0.001	0.024

Table 49: continued.

x	$F_2^{\gamma Z}$	$\Delta_{\rm stat}$	$\Delta_{\rm unc}$	$\Delta_{\rm cor}$	$\Delta_{\rm tot}$
0.020	0.751	0.188	0.080	0.326	0.385
0.032	0.546	0.139	0.053	0.213	0.259
0.050	0.299	0.104	0.036	0.139	0.177
0.080	0.398	0.081	0.025	0.098	0.129
0.130	0.286	0.074	0.023	0.074	0.107
0.180	0.264	0.065	0.020	0.055	0.087
0.250	0.051	0.056	0.015	0.032	0.067
0.400	0.068	0.035	0.013	0.017	0.041
0.650	0.019	0.008	0.003	0.002	0.009

Table 50: Averaged structure function $F_2^{\gamma Z}$ for $Q^2 = 1\,500\,\mathrm{GeV}^2$ determined using the polarised HERA II data set. The absolute statistical, uncorrelated, correlated and total uncertainties $\Delta_{\rm stat}$, $\Delta_{\rm unc}$, $\Delta_{\rm cor}$ and $\Delta_{\rm tot}$ are also given. The luminosity uncertainty of 2.3% is not included in the errors.

Q^2 (GeV^2)	x	$xF_3^{\gamma Z}$	$\Delta_{\rm stat}$	$\Delta_{\rm unc}$	$\Delta_{\rm cor}$	$\Delta_{\rm tot}$
1200	0.013	0.256	0.301	0.158	0.086	0.350
1200	0.020	0.410	0.211	0.098	0.098	0.253
1200	0.032	0.726	0.277	0.114	0.140	0.331
1200	0.050	0.666	0.373	0.190	0.184	0.457
1200	0.080	0.339	0.560	0.274	0.259	0.676
1200	0.130	−0.744	0.961	0.507	0.349	1.141
1200	0.180	−1.05	1.22	0.617	0.437	1.433
1200	0.250	−3.87	1.43	0.812	0.458	1.706
1200	0.400	2.13	1.58	1.26	0.394	2.057
1500	0.020	0.512	0.174	0.099	0.066	0.211
1500	0.032	0.595	0.222	0.078	0.088	0.251
1500	0.050	0.184	0.286	0.121	0.123	0.334
1500	0.080	1.03	0.430	0.186	0.177	0.500
1500	0.130	0.348	0.693	0.325	0.221	0.797
1500	0.180	−1.01	0.865	0.419	0.273	0.999
1500	0.250	0.058	1.01	0.583	0.298	1.207
1500	0.400	0.755	1.20	0.825	0.259	1.478
1500	0.650	−0.095	0.433	0.262	0.051	0.508
2000	0.022	0.576	0.221	0.102	0.049	0.248
2000	0.032	0.403	0.146	0.063	0.050	0.167
2000	0.050	0.169	0.206	0.068	0.070	0.228
2000	0.080	0.414	0.275	0.112	0.096	0.312
2000	0.130	−0.222	0.456	0.183	0.129	0.508
2000	0.180	−0.642	0.594	0.260	0.163	0.669
2000	0.250	0.116	0.681	0.351	0.177	0.786
2000	0.400	0.131	0.727	0.462	0.153	0.875
2000	0.650	−0.665	0.278	0.157	0.030	0.321
3000	0.032	0.320	0.091	0.049	0.030	0.108
3000	0.050	0.274	0.084	0.040	0.034	0.099
3000	0.080	0.347	0.127	0.052	0.048	0.145
3000	0.130	0.635	0.200	0.096	0.065	0.232
3000	0.180	−0.116	0.270	0.124	0.076	0.307
3000	0.250	0.325	0.295	0.147	0.081	0.340
3000	0.400	−0.114	0.302	0.209	0.070	0.373
3000	0.650	−0.105	0.108	0.066	0.013	0.127

Table 51: The measured structure function $xF_3^{\gamma Z}$ determined using the complete HERA I+II data set. The absolute statistical, uncorrelated, correlated and total uncertainties $\Delta_{\rm stat}$, $\Delta_{\rm unc}$, $\Delta_{\rm cor}$ and $\Delta_{\rm tot}$ are also given.

Q^2 (GeV^2)	x	$xF_3^{\gamma Z}$	Δ_{stat}	Δ_{unc}	Δ_{cor}	Δ_{tot}
5000	0.055	0.297	0.073	0.033	0.019	0.082
5000	0.080	0.308	0.058	0.026	0.020	0.067
5000	0.130	0.516	0.096	0.045	0.028	0.109
5000	0.180	0.578	0.123	0.055	0.033	0.139
5000	0.250	0.132	0.167	0.081	0.034	0.188
5000	0.400	0.023	0.151	0.078	0.027	0.172
5000	0.650	0.084	0.051	0.025	0.005	0.057
8000	0.088	0.398	0.078	0.029	0.014	0.084
8000	0.130	0.437	0.063	0.028	0.014	0.070
8000	0.180	0.255	0.076	0.030	0.015	0.083
8000	0.250	0.164	0.095	0.035	0.016	0.102
8000	0.400	0.155	0.091	0.047	0.013	0.103
8000	0.650	−0.026	0.031	0.015	0.003	0.034
12000	0.130	0.598	0.113	0.038	0.010	0.119
12000	0.180	0.395	0.063	0.018	0.009	0.066
12000	0.250	0.331	0.061	0.018	0.008	0.064
12000	0.400	0.332	0.070	0.032	0.008	0.078
12000	0.650	−0.012	0.026	0.009	0.002	0.027
20000	0.250	0.361	0.058	0.015	0.006	0.060
20000	0.400	0.219	0.049	0.017	0.004	0.052
20000	0.650	0.014	0.018	0.008	0.001	0.019
30000	0.400	0.122	0.056	0.012	0.003	0.057
30000	0.650	0.055	0.023	0.006	0.001	0.024

Table 51: continued.

x	$xF_3^{\gamma Z}$	Δ_{stat}	Δ_{unc}	Δ_{cor}	Δ_{tot}
0.013	0.258	0.304	0.159	0.086	0.354
0.020	0.470	0.135	0.071	0.080	0.172
0.032	0.393	0.070	0.034	0.048	0.091
0.050	0.266	0.073	0.033	0.050	0.095
0.080	0.327	0.051	0.023	0.031	0.064
0.130	0.489	0.047	0.020	0.022	0.055
0.180	0.360	0.046	0.016	0.018	0.052
0.250	0.330	0.040	0.012	0.012	0.044
0.400	0.227	0.035	0.013	0.008	0.038
0.650	0.018	0.015	0.006	0.002	0.016

Table 52: Averaged structure function $xF_3^{\gamma Z}$ for $Q^2 = 1\,500\,\mathrm{GeV}^2$ determined using the complete HERA I+II data set. The absolute statistical, uncorrelated, correlated and total uncertainties Δ_{stat}, Δ_{unc}, Δ_{cor} and Δ_{tot} are also given.

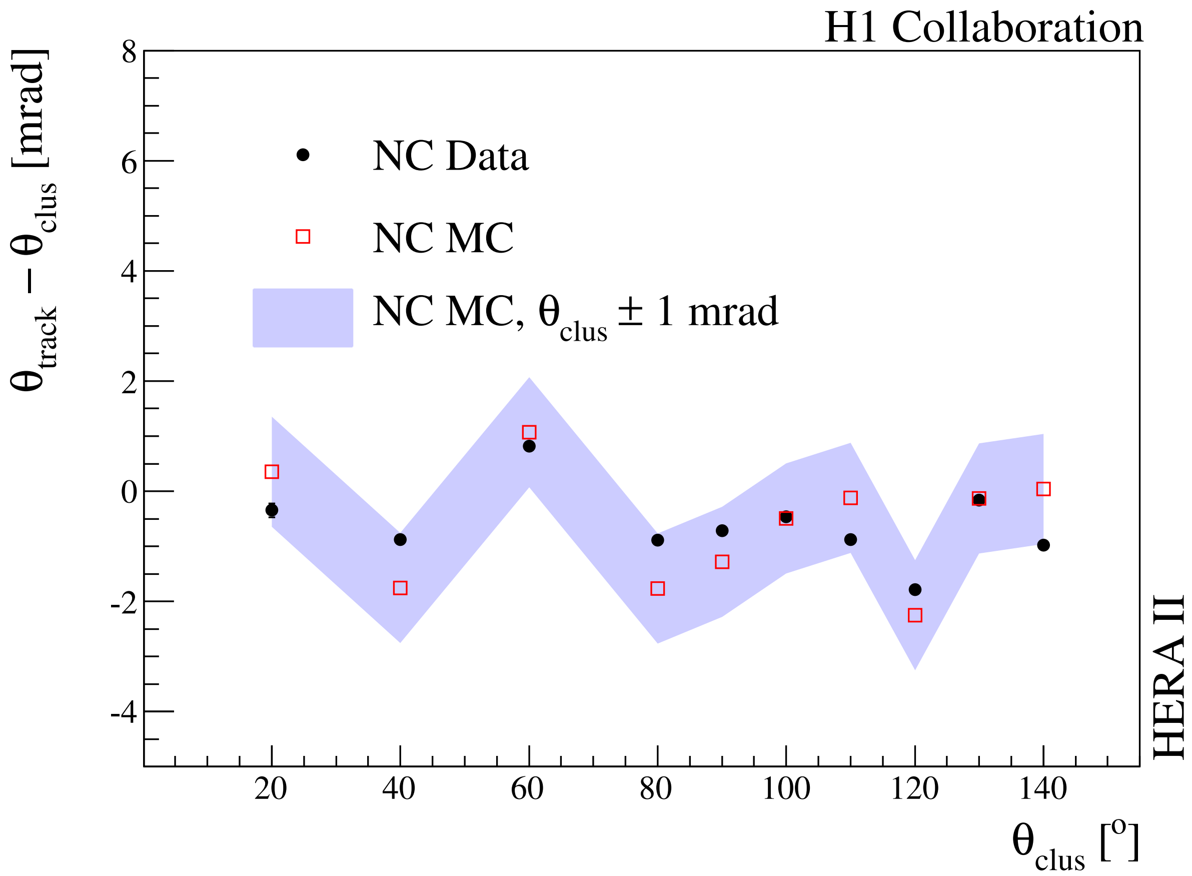

Figure 1: The mean value of $\Delta\theta = \theta_{\text{track}} - \theta_{\text{clus}}$ as a function of the polar angle of the cluster θ_{clus} after alignment for data (solid points) covering the complete HERA II data set and simulation (open squares). The shaded band corresponds to a ± 1 mrad uncertainty.

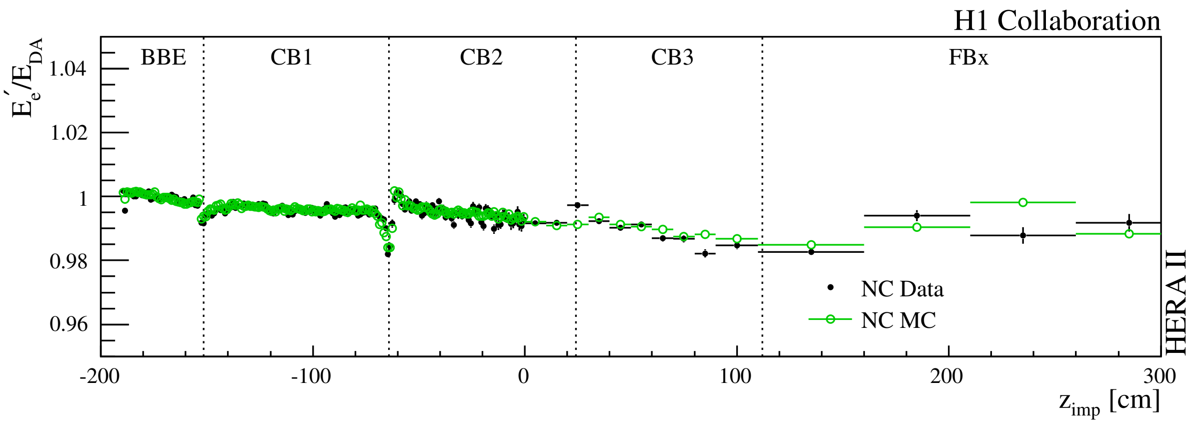

(a)

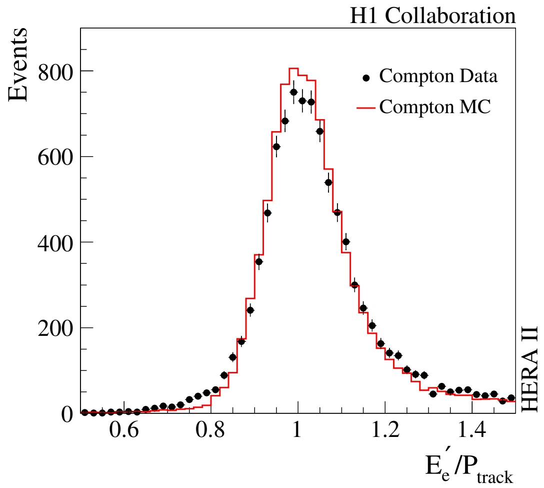

(b)

Figure 2: (a) The mean value of E'_e/E_{DA} as a function of $z_{\rm imp}$ for data (solid points) and simulation (open circles) based on a NC DIS sample for the complete HERA II data sample, where BBE, CB1, CB2, CB3 and FBx stand for Backward Barrel Electromagnetic, Central Barrel and Forward Barrel wheels. (b) The distribution of $E'_e/P_{\rm track}$ with data (solid points) and simulation (histogram), based on a QED Compton selection in the energy range between $3-8\,$GeV for the complete HERA II data set.

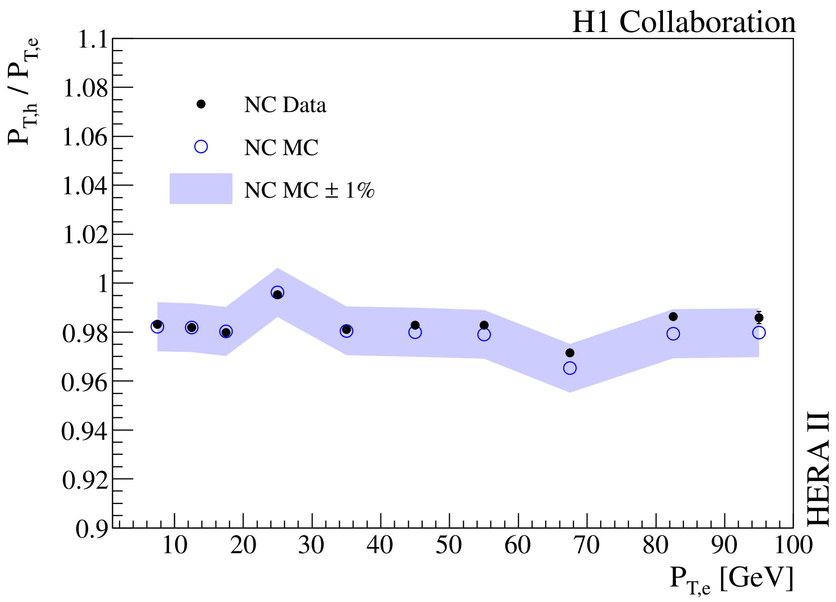

(a)

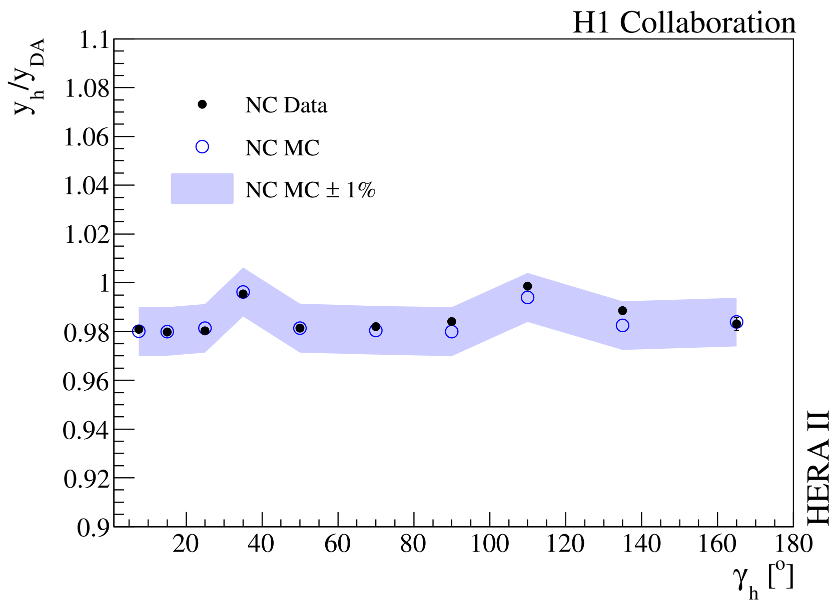

(b)

Figure 3: (a) Mean values of $P_{T,h}/P_{T,e}$ as a function of $P_{T,e}$ and (b) $y_h/y_{\rm DA}$ as a function of γ_h for neutral current data (solid points) and simulation (open circles) for the complete HERA II data set. The shaded bands correspond to a $\pm1\%$ variation around the simulation.

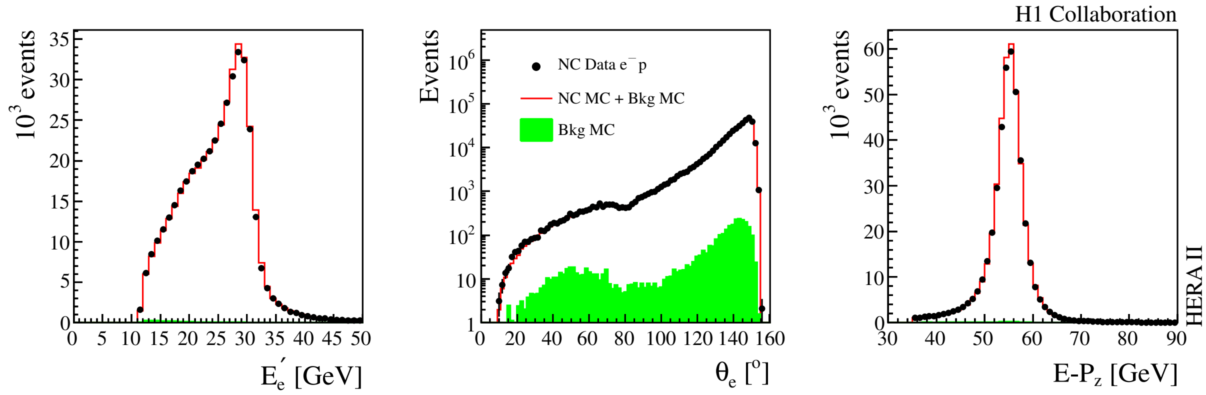

(a)

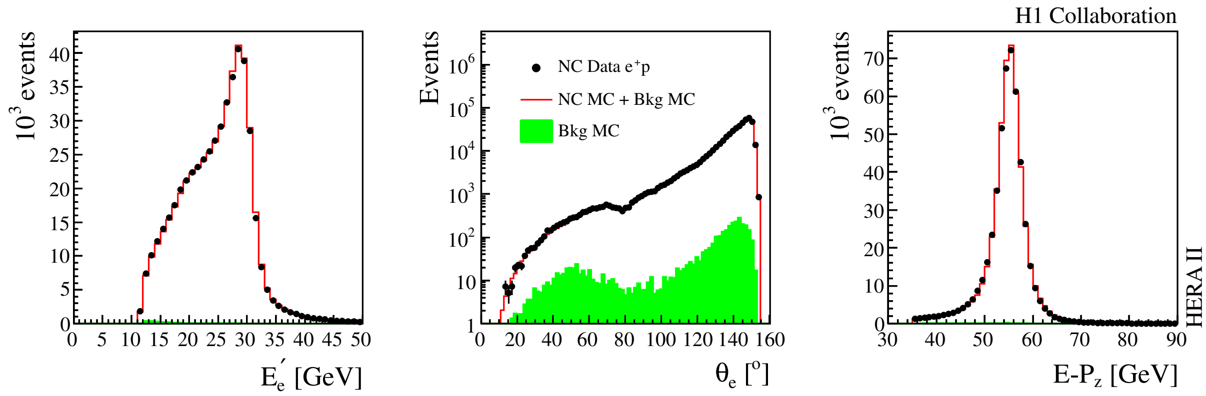

(b)

Figure 4: Distributions of E_e', θ_e and $E - P_z$ for (a) e^-p and (b) e^+p NC data (solid points) and simulation (histograms). The estimated background contribution is shown as the shaded histogram.

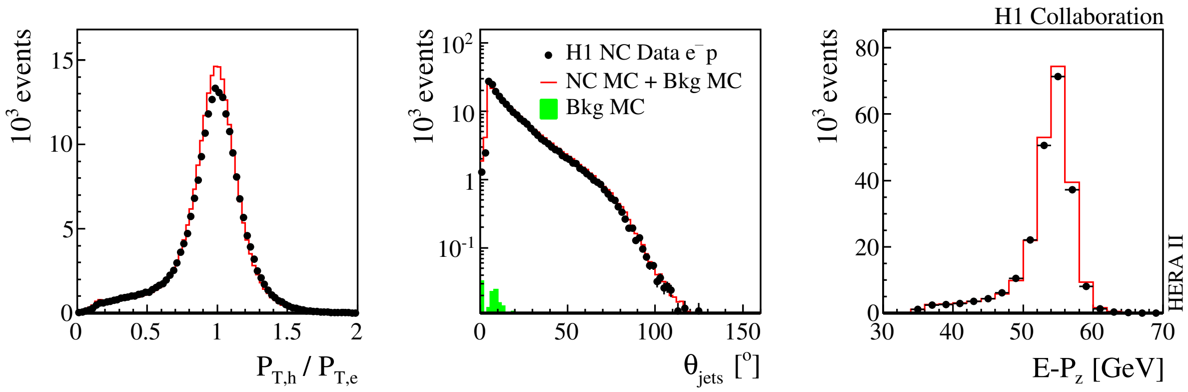

(a)

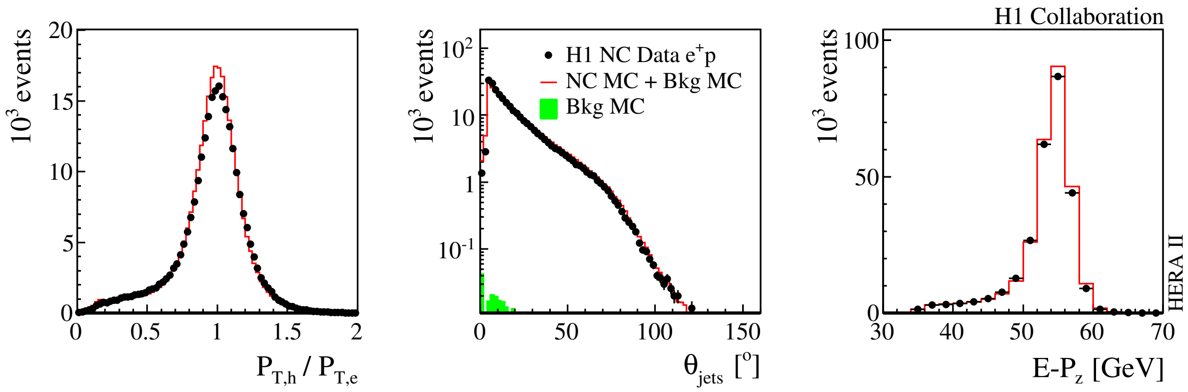

(b)

Figure 5: Distributions of $P_{T,h}/P_{T,e}$, $\theta_{\rm jets}$ and $E-P_z$ in the region $y<0.19$ for (a) e^-p and (b) e^+p data (solid points) and for simulation (histograms). The estimated background contribution is shown as the shaded histograms. The quantities $P_{T,h}$, $\theta_{\rm jets}$ and the hadronic contribution to $E-P_z$ are calculated using energies associated within jets (see text).

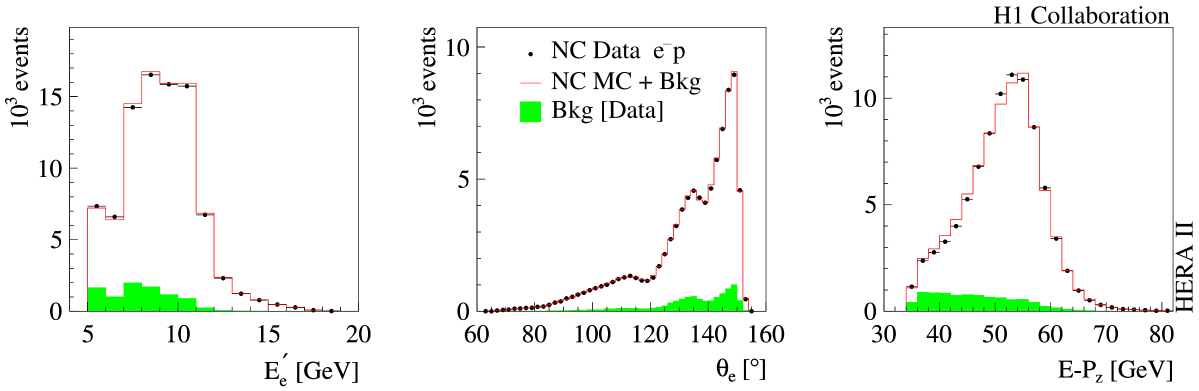

(a)

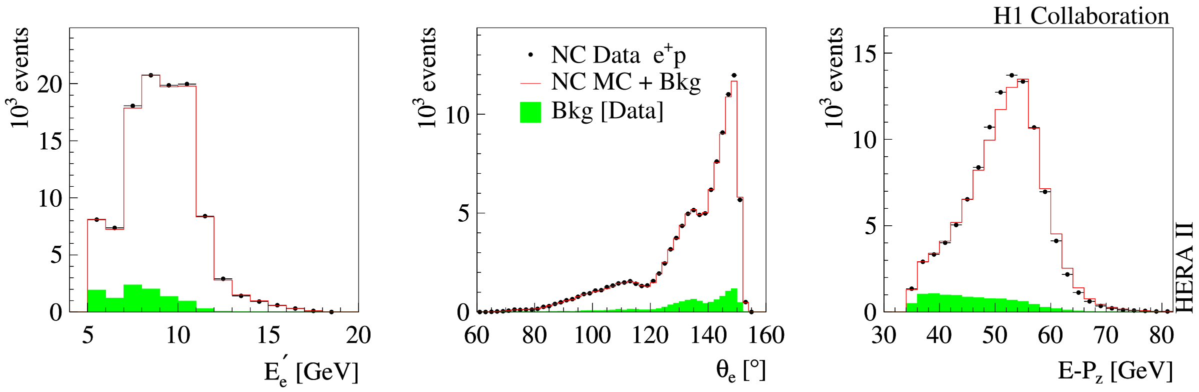

(b)

Figure 6: Distributions of E'_e, θ_e and $E - P_z$ for (a) e^-p and (b) e^+p NC *high* y analysis data. The data is shown as solid points and the histogram represent the MC simulation and the background obtained from data. The background corresponds to the wrongly charged lepton candidates in the data corrected for the charge asymmetry and is shown as the shaded histogram.

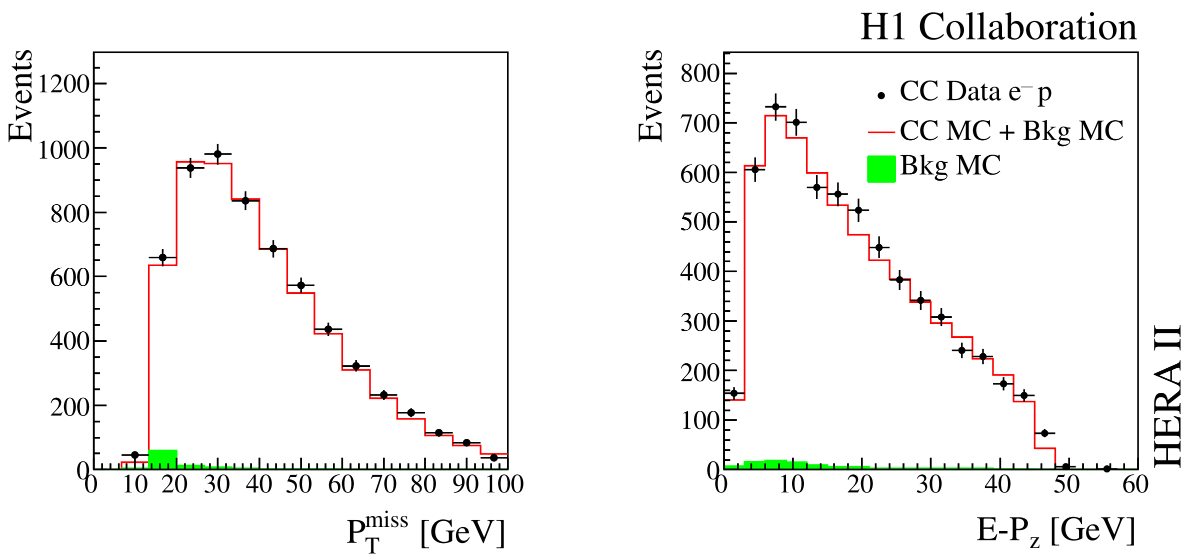

(a)

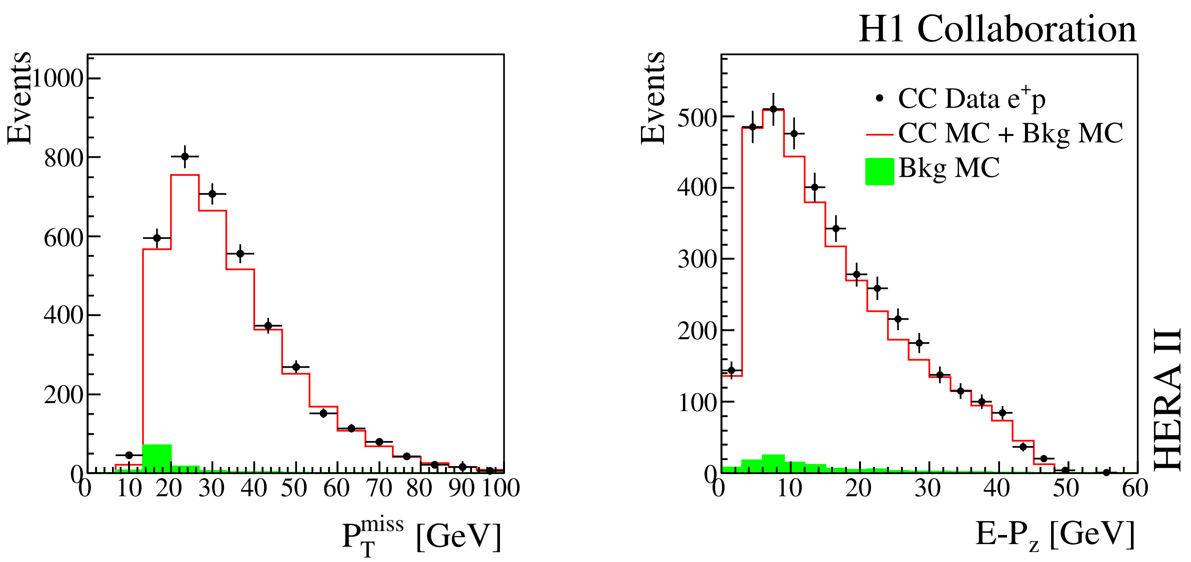

(b)

Figure 7: Distributions of $P_T^{\rm miss}$ and $E - P_z$ for (a) e^-p and (b) e^+p CC data (solid points) and simulation (histograms). The estimated background contribution is shown as the shaded histograms.

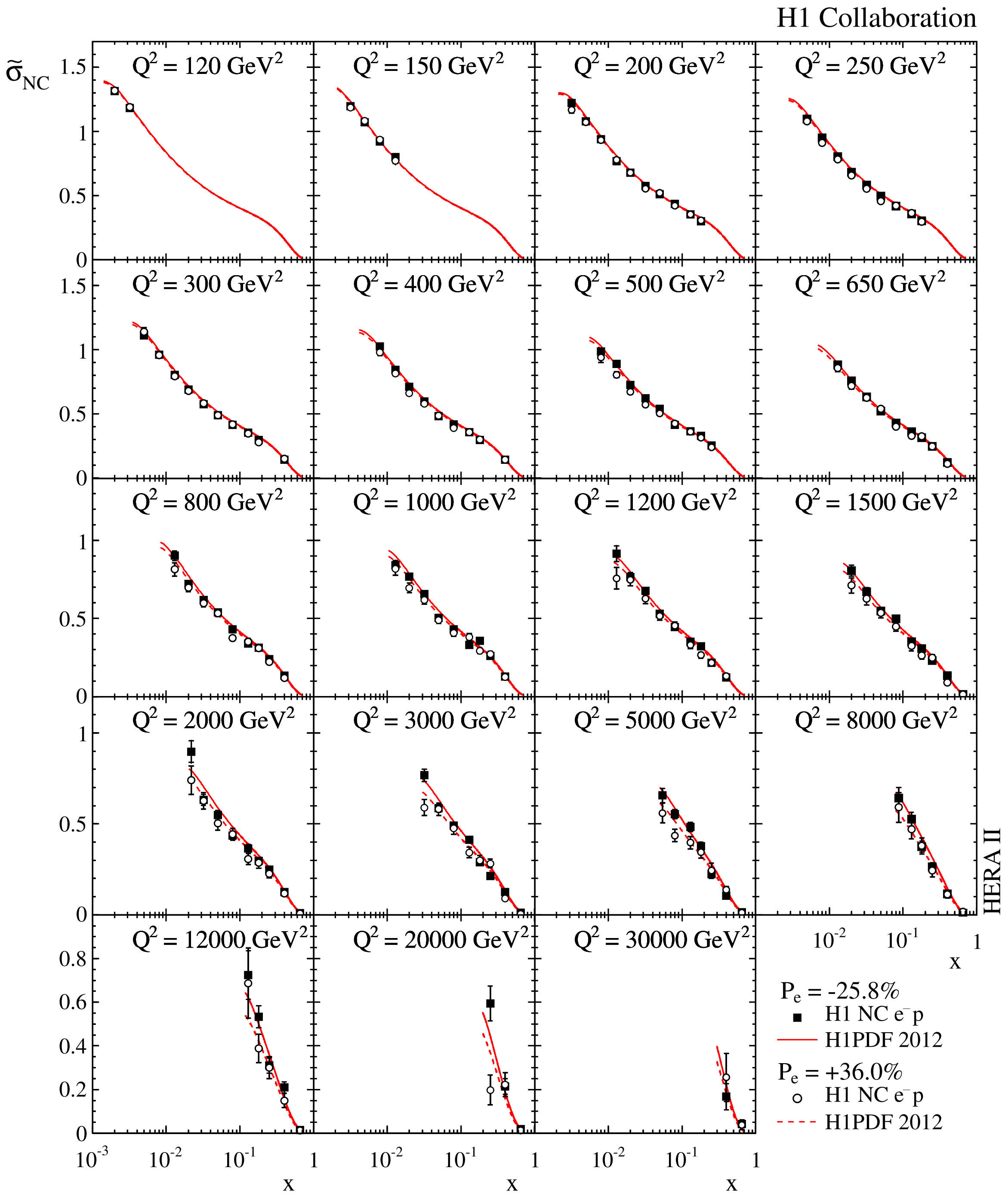

Figure 8: NC reduced cross sections $\tilde{\sigma}_{NC}$ for e^-p L (solid squares) and R (open circles) data sets shown for various fixed Q^2 as a function of x. The measurement at $Q^2 = 50\,000\,\mathrm{GeV}^2$ is not shown. The inner and outer error bars represent the statistical and total errors, respectively. The luminosity and polarisation uncertainties are not included in the error bars. The curves show the corresponding expectations from H1PDF 2012.

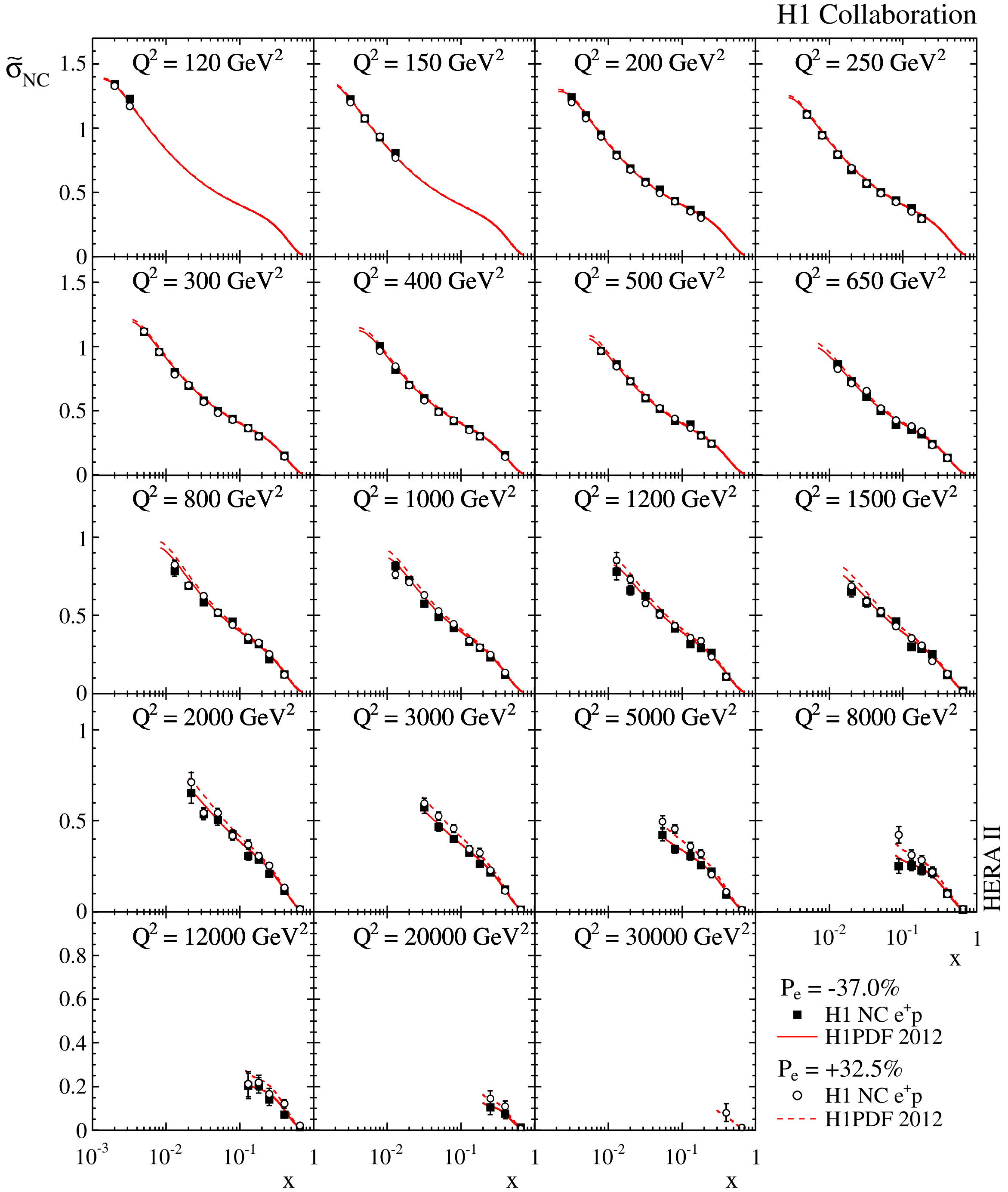

Figure 9: NC reduced cross sections $\tilde{\sigma}_{NC}$ for e^+p L (solid squares) and R (open circles) data sets shown for various fixed Q^2 as a function of x. The inner and outer error bars represent the statistical and total errors, respectively. The luminosity and polarisation uncertainties are not included in the error bars. The curves show the corresponding expectations from H1PDF 2012.

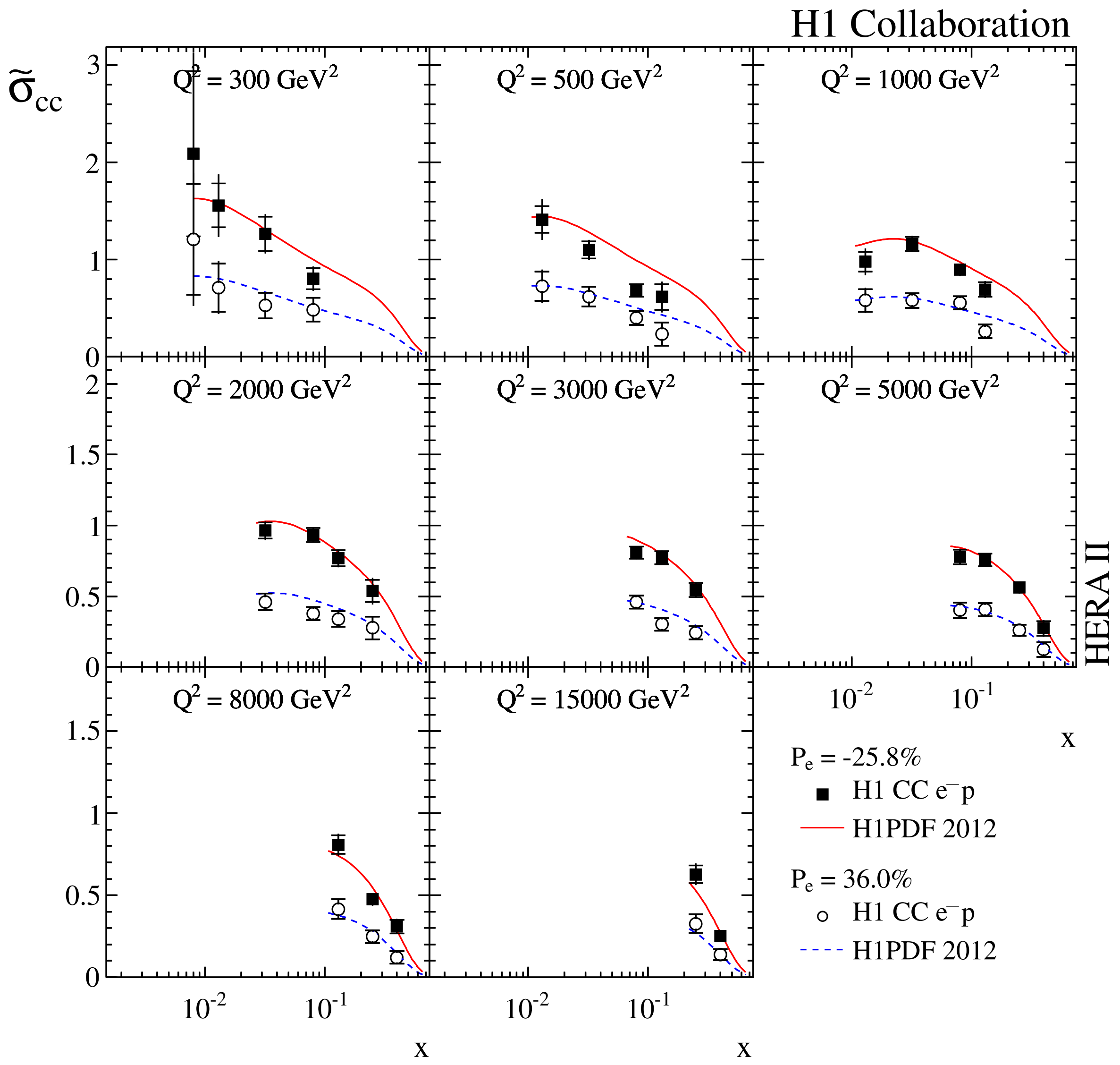

Figure 10: CC reduced cross sections $\tilde{\sigma}_{CC}$ for e^-p L (solid squares) and R (open circles) handed data sets shown for various fixed Q^2 as a function of x. The inner and outer error bars represent the statistical and total errors, respectively. The luminosity and polarisation uncertainties are not included in the error bars. The curves show the corresponding expectations from H1PDF 2012.

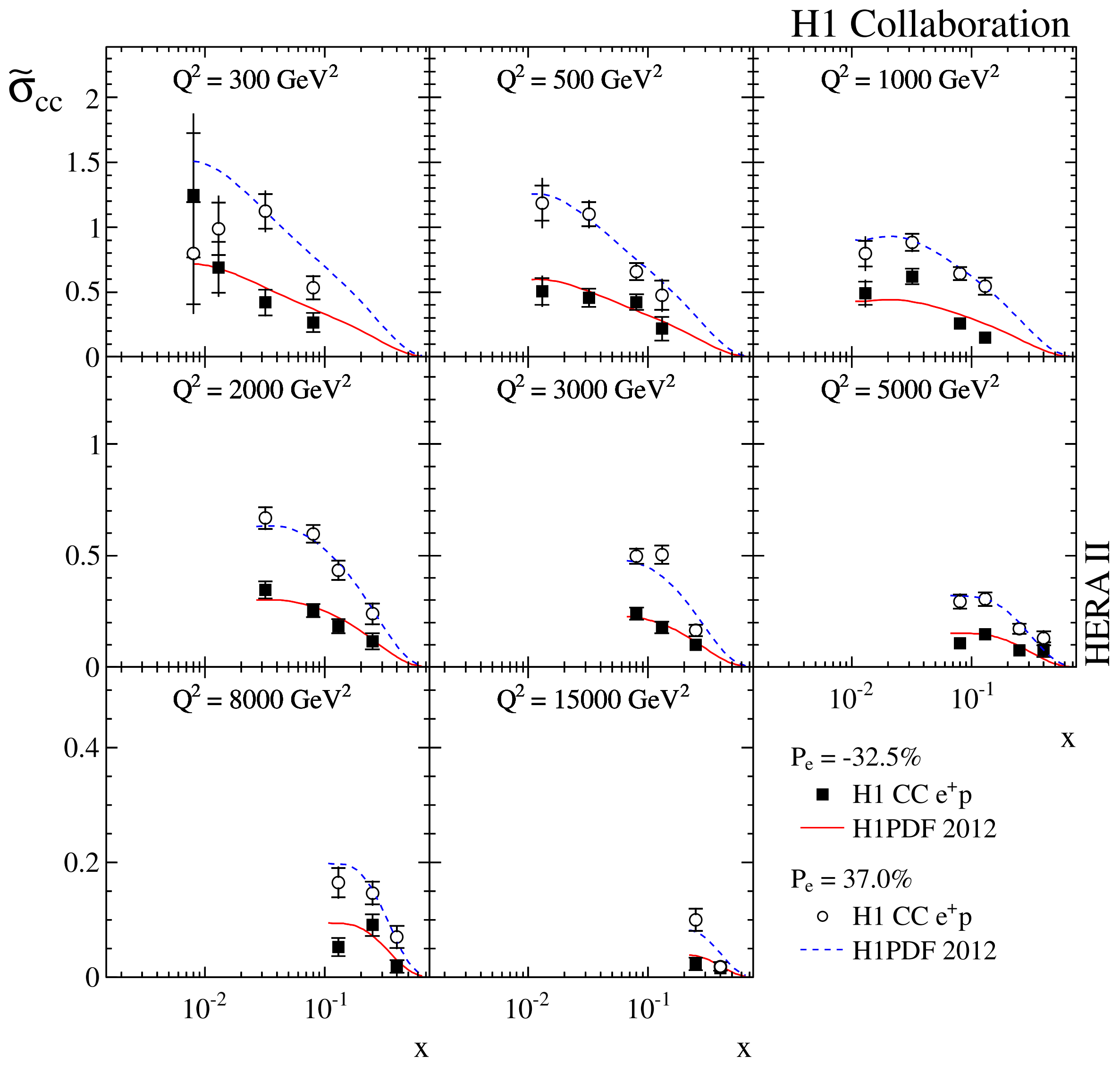

Figure 11: CC reduced cross sections $\tilde{\sigma}_{CC}$ for e^+p L (solid squares) and R (open circles) handed data sets shown for various fixed Q^2 as a function of x. The inner and outer error bars represent the statistical and total errors, respectively. The luminosity and polarisation uncertainties are not included in the error bars. The curves show the corresponding expectations from H1PDF 2012.

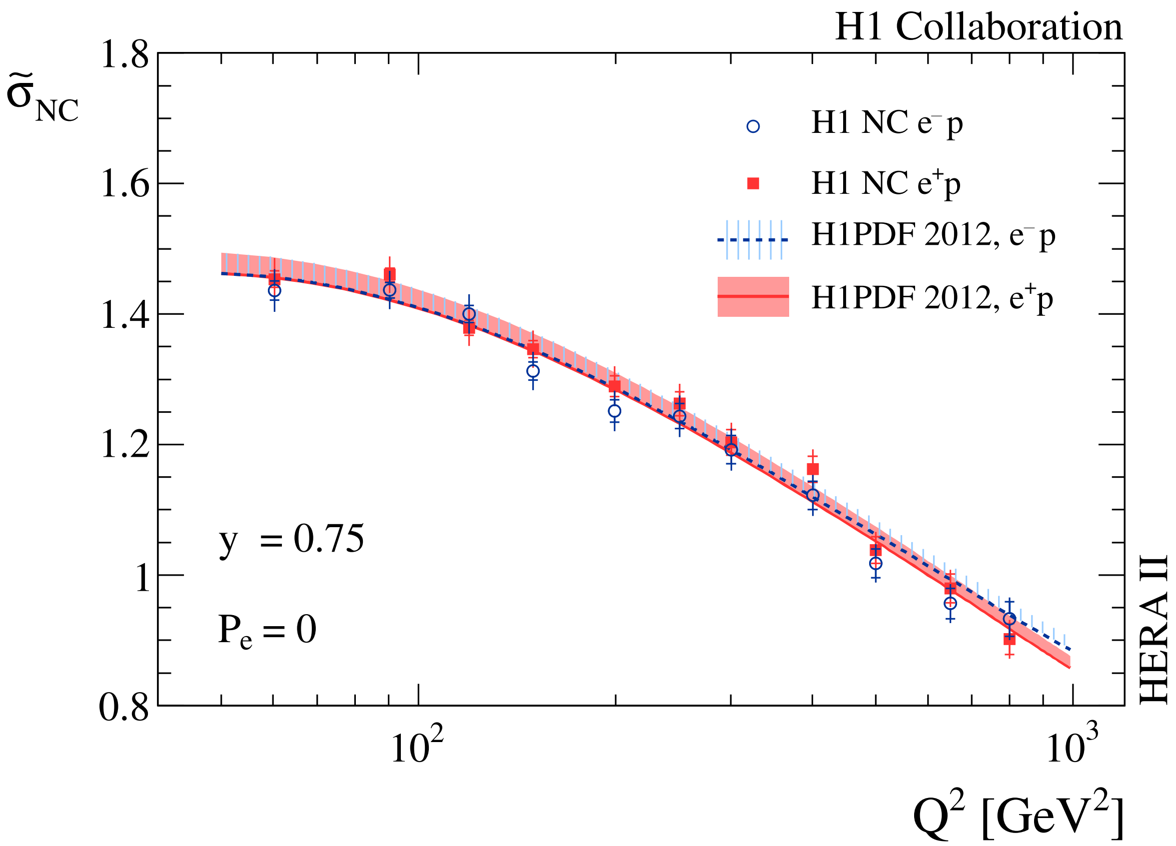

Figure 12: NC high y reduced cross sections $\tilde{\sigma}_{NC}$ for e^-p (open circles) and e^+p (solid squares) data shown as a function of Q^2. The inner and outer error bars represent the statistical and total errors, respectively. The luminosity and polarisation uncertainties are not included in the error bars. The error bands show the total uncertainty of the H1PDF 2012 fit.

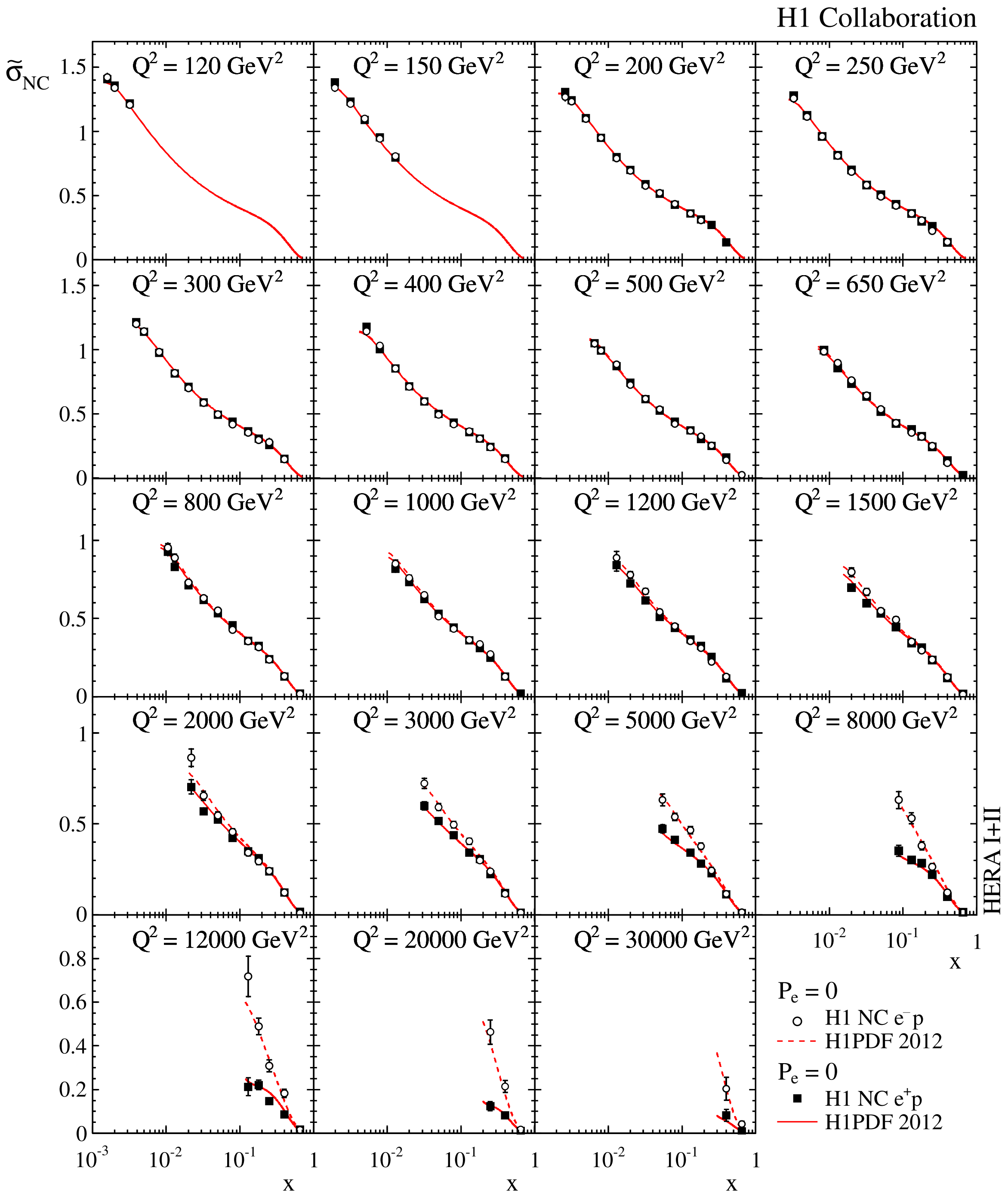

Figure 13: Combined HERA I+II unpolarised NC reduced cross sections $\tilde{\sigma}_{NC}$ for e^-p (open circles) and e^+p (solid squares) data shown for various fixed Q^2 as a function of x. Only the measurements at $\sqrt{s} = 319$ GeV in the range $120 \leq Q^2 \leq 30\,000\,\mathrm{GeV}^2$ are shown. The inner and outer error bars represent the statistical and total errors, respectively. The curves show the corresponding expectations from H1PDF 2012.

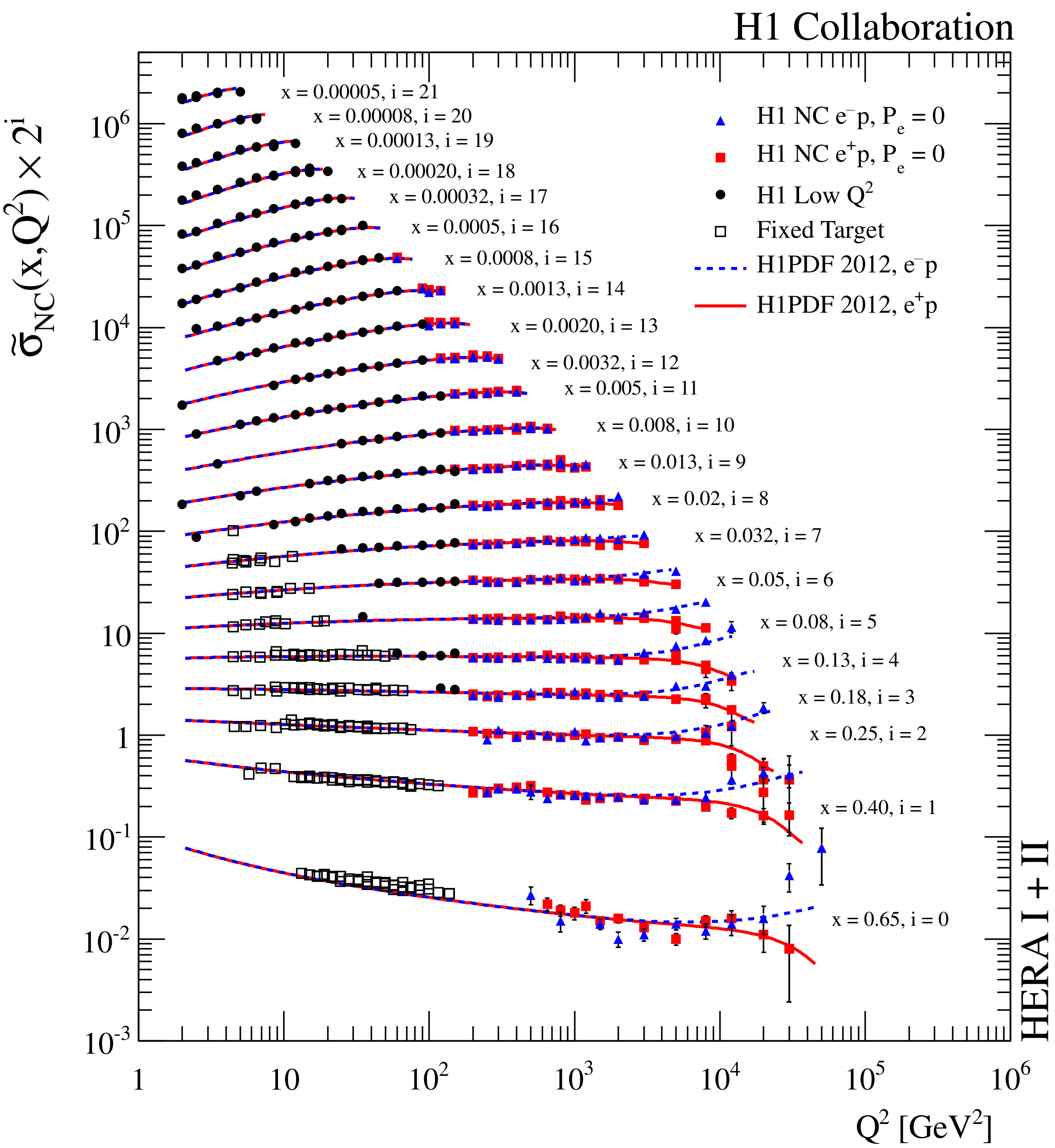

Figure 14: Combined HERA I+II unpolarised NC reduced cross sections $\tilde{\sigma}_{NC}$ for e^-p (solid triangles), e^+p (solid squares) and low Q^2 (solid points) data shown for various fixed x as a function of Q^2. The inner and outer error bars represent the statistical and total errors, respectively. The curves show the corresponding expectations from H1PDF 2012. Also shown in open squares are the fixed target data from BCDMS [95].

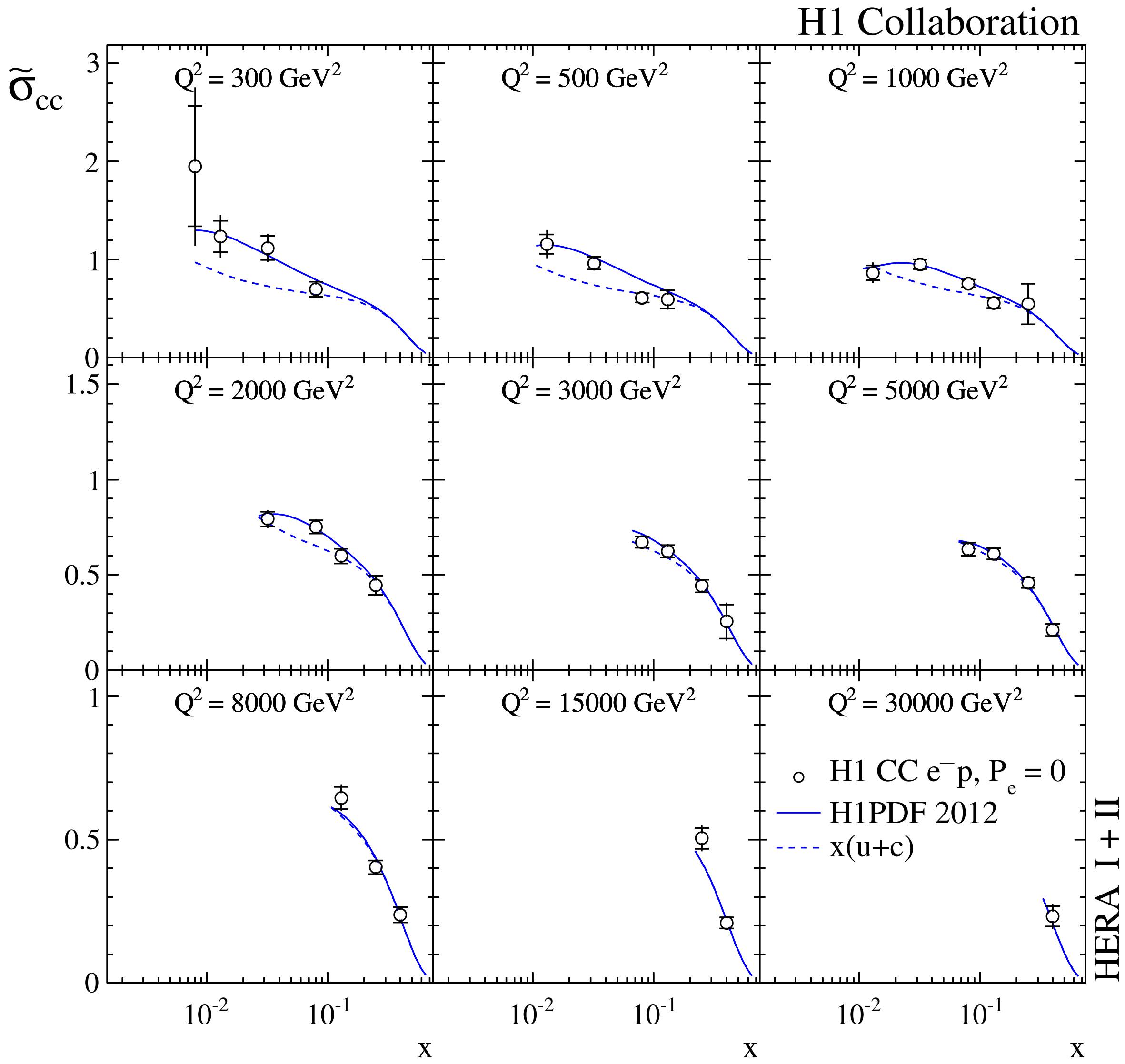

Figure 15: Combined HERA I+II unpolarised CC reduced cross sections $\tilde{\sigma}_{CC}$ for e^-p data shown for various fixed Q^2 as a function of x in comparison with the expectation from H1PDF 2012. The inner and outer error bars represent the statistical and total errors, respectively. The dominant contribution $x(u + c)$ is also shown.

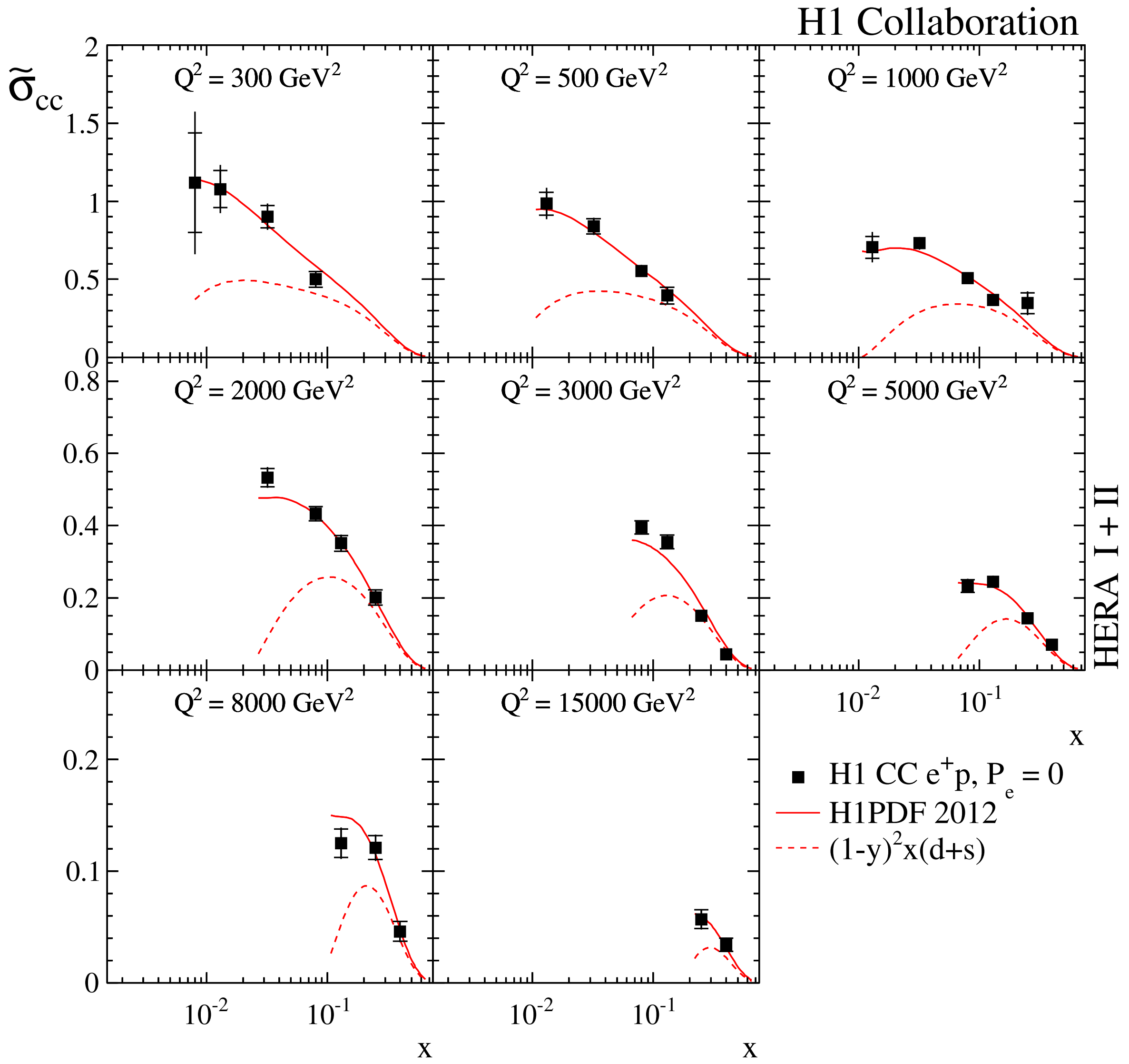

Figure 16: Combined HERA I+II unpolarised CC reduced cross sections $\tilde{\sigma}_{CC}$ for e^+p data shown for various fixed Q^2 as a function of x in comparison with the expectation from H1PDF 2012. The inner and outer error bars represent the statistical and total errors, respectively. The contribution $(1-y)^2x(d+s)$ is also shown.

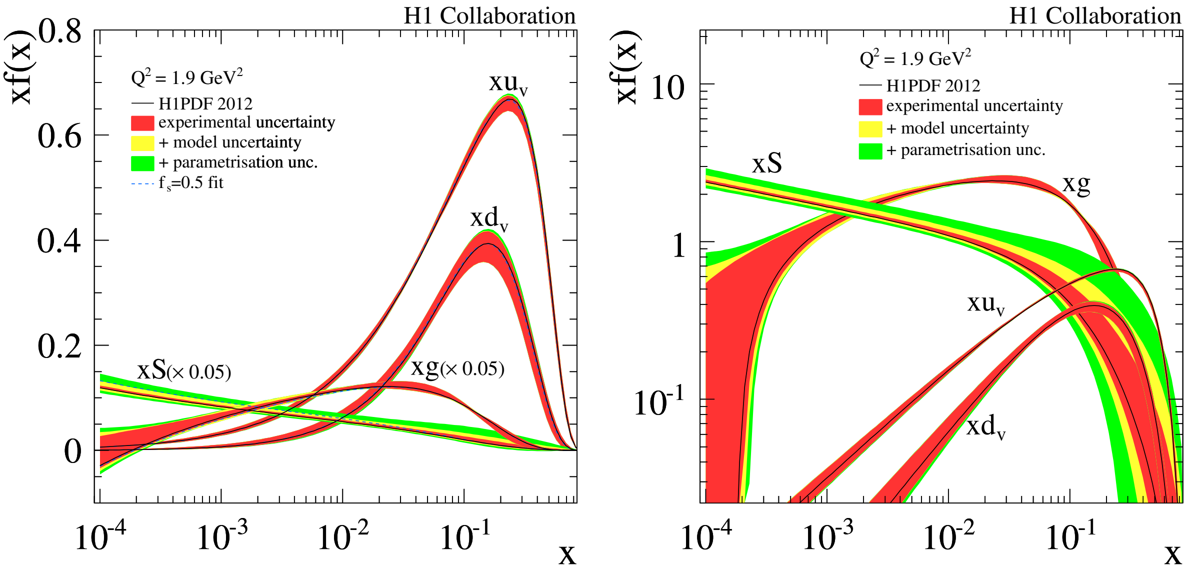

Figure 17: Parton distribution functions of H1PDF 2012 at the starting scale $Q^2 = 1.9\,\mathrm{GeV}^2$. The gluon and sea distributions in the linear scale plot (left) are scaled by a factor 0.05. The PDFs with $f_s = 0.5$ are also shown. The uncertainties include the experimental uncertainties (inner), the model uncertainties (middle) and the parametrisation variation (outer). All uncertainties are added in quadrature.

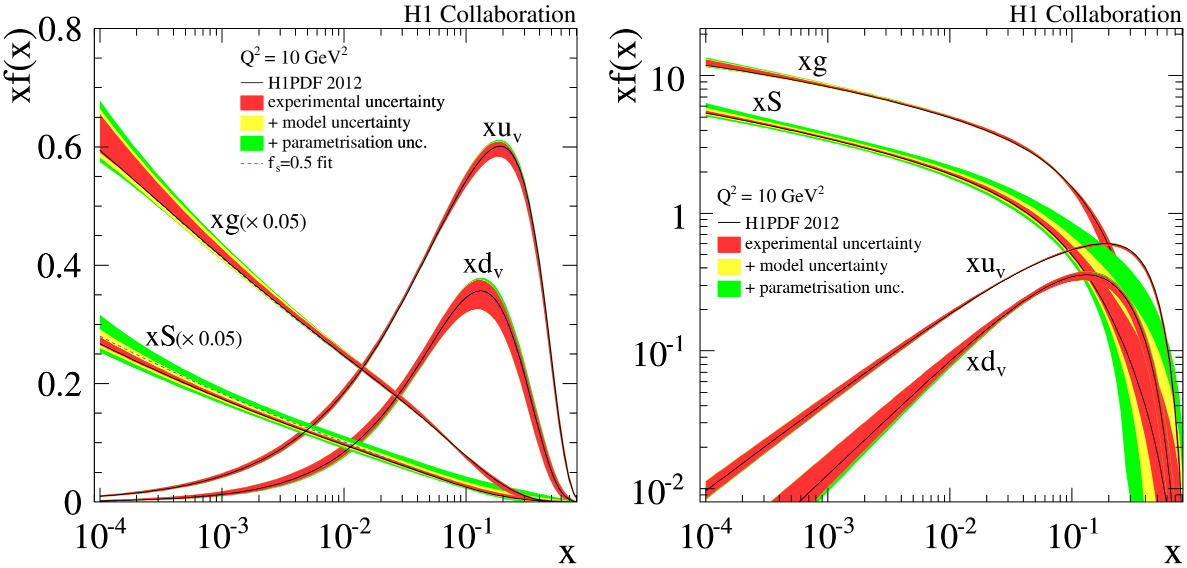

Figure 18: Parton distribution functions of H1PDF 2012 at the evolved scale of $10\,\mathrm{GeV}^2$. The gluon and sea distributions in the linear scale plot (left) are scaled by a factor 0.05. The PDFs with $f_s = 0.5$ are also shown. The uncertainties include the experimental uncertainties (inner), the model uncertainties (middle) and the parametrisation variation (outer). All uncertainties are added in quadrature.

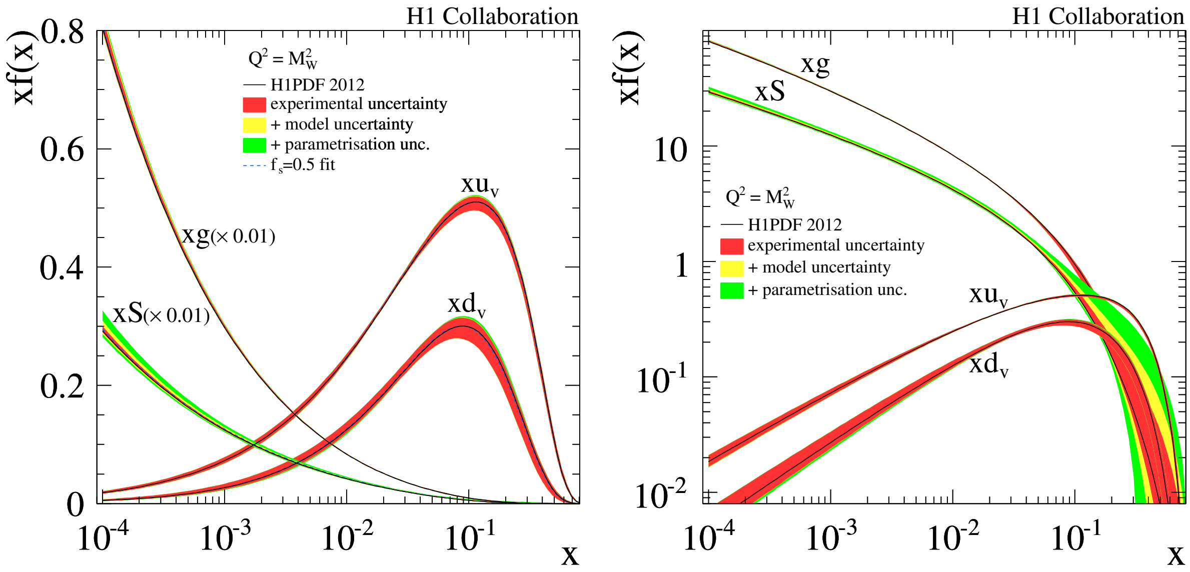

Figure 19: Parton distribution functions of H1PDF 2012 at the evolved scale of M_W^2. The gluon and sea distributions in the linear scale plot (left) are scaled by a factor 0.01. The PDFs with $f_s = 0.5$ are also shown. The uncertainties include the experimental uncertainties (inner), the model uncertainties (middle) and the parametrisation variation (outer). All uncertainties are added in quadrature.

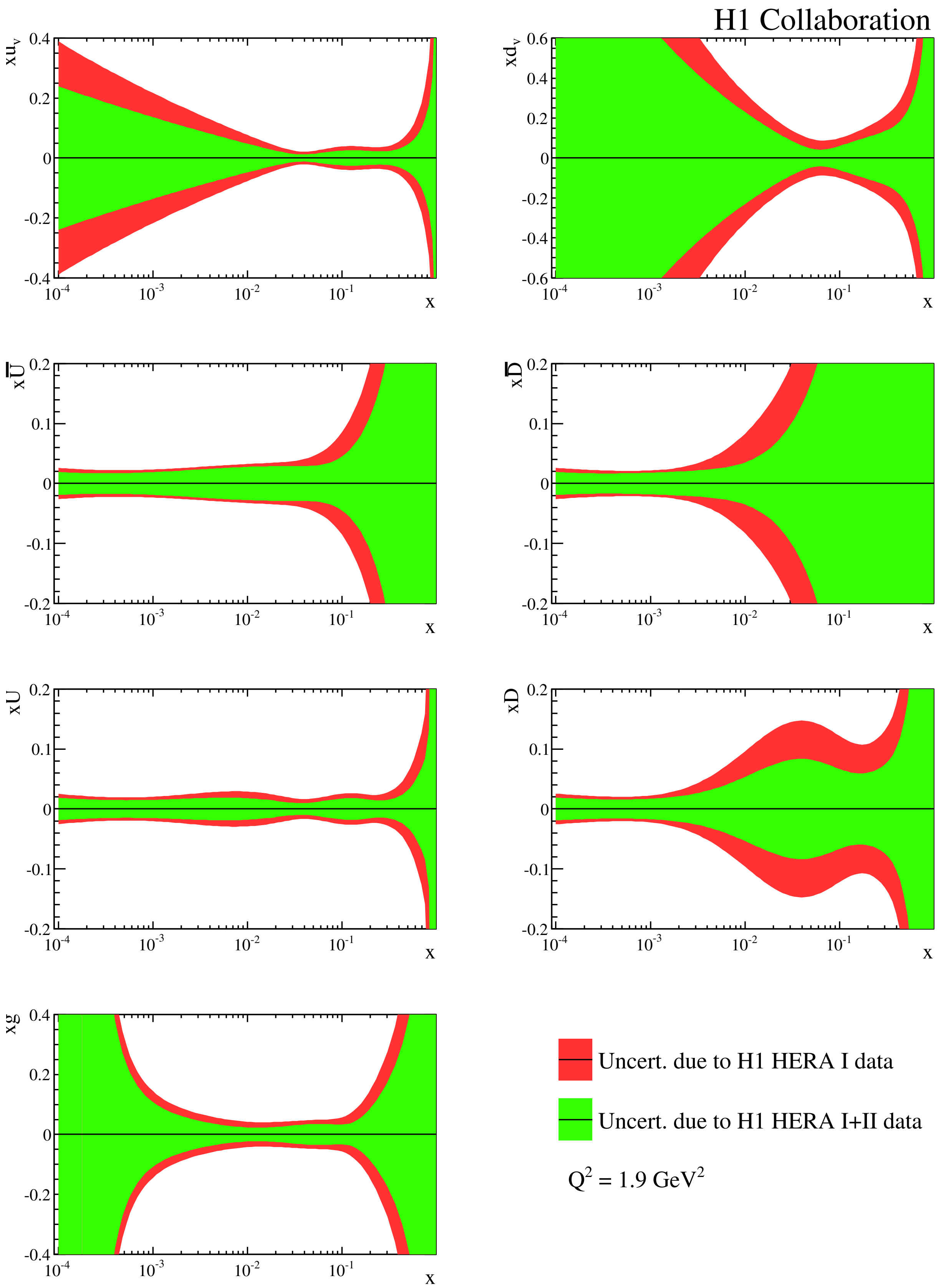

Figure 20: Comparison of relative experimental uncertainties of the PDFs extracted from HERA I (outer) vs HERA I+II (inner) data sets under the same fit conditions to better assess the effect of the new high Q^2 measurements.

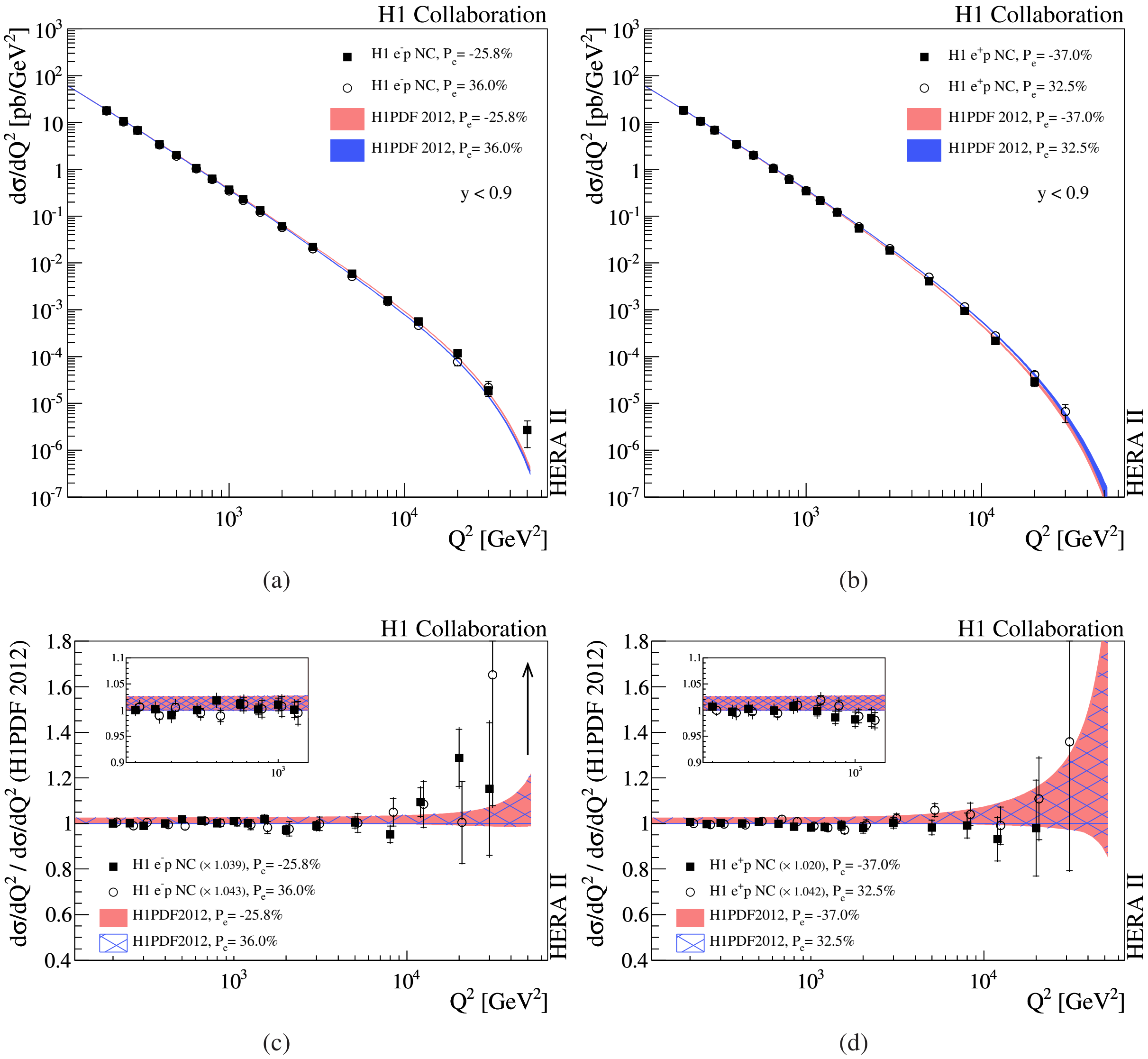

Figure 21: Q^2 dependence of the NC cross sections $\mathrm{d}\sigma/\mathrm{d}Q^2$ for the e^-p (a) and e^+p (b) L and R data sets. The ratios of the L and R cross sections to the corresponding Standard Model expectations are shown for the e^-p (c) and e^+p (d) data, where the normalisation shifts as determined from the QCD fit are applied to the data (see Table 10). The inner and outer error bars represent the statistical and total errors, respectively. The luminosity and polarisation uncertainties are not included in the error bars.

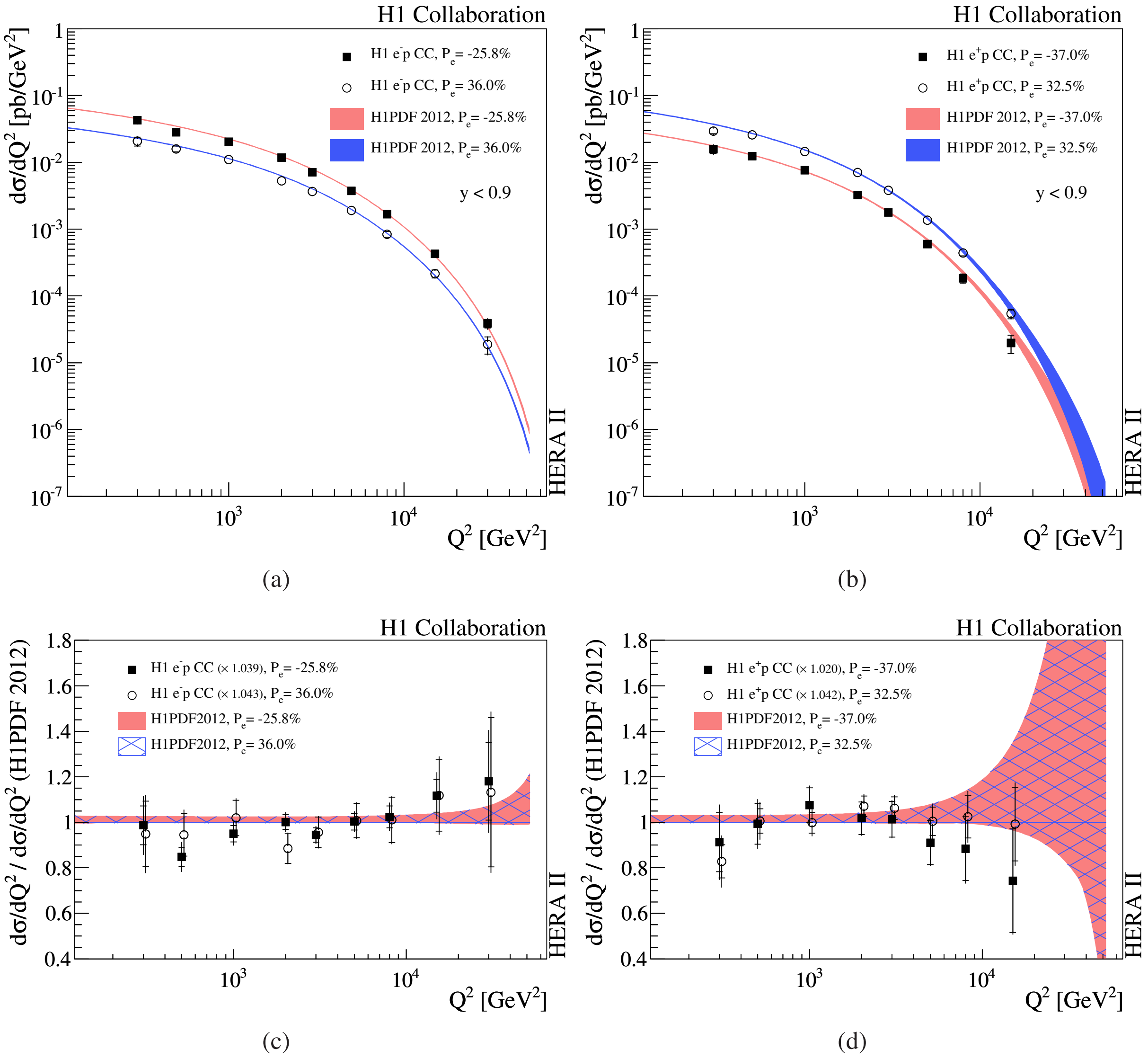

Figure 22: Q^2 dependence of the CC cross sections $\mathrm{d}\sigma/\mathrm{d}Q^2$ for the e^-p (a) and e^+p (b) L and R data sets. The ratios of the L and R cross sections to the corresponding Standard Model expectations are shown for the e^-p (c) and e^+p (d) data, where the normalisation shifts as determined from the QCD fit are applied to the data (see Table 10). The inner and outer error bars represent the statistical and total errors, respectively. The luminosity and polarisation uncertainties are not included in the error bars.

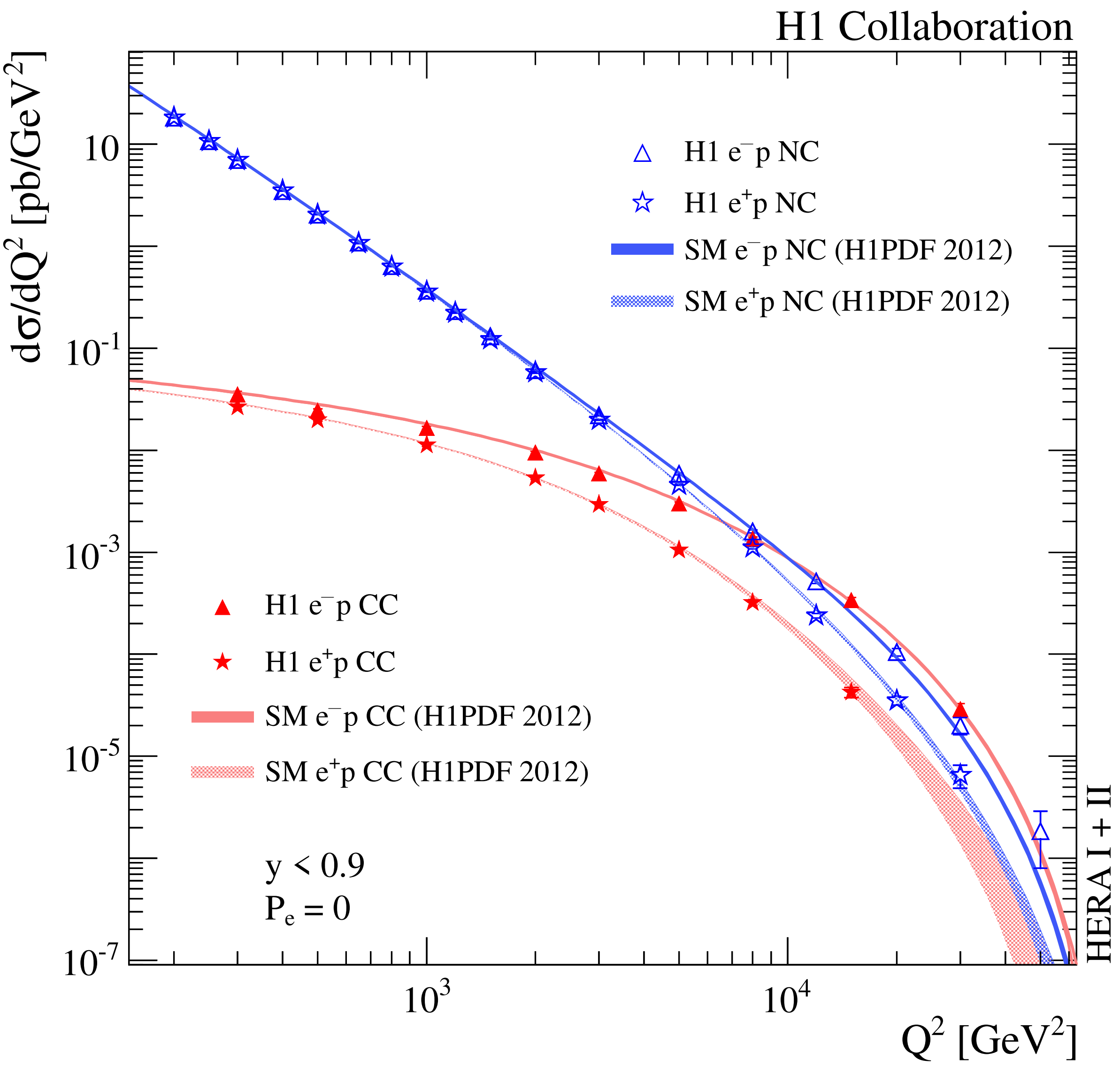

Figure 23: Q^2 dependence of the NC and CC cross sections $d\sigma/dQ^2$ for the combined HERA I+II unpolarised e^-p and e^+p data. The inner and outer error bars represent the statistical and total errors, respectively.

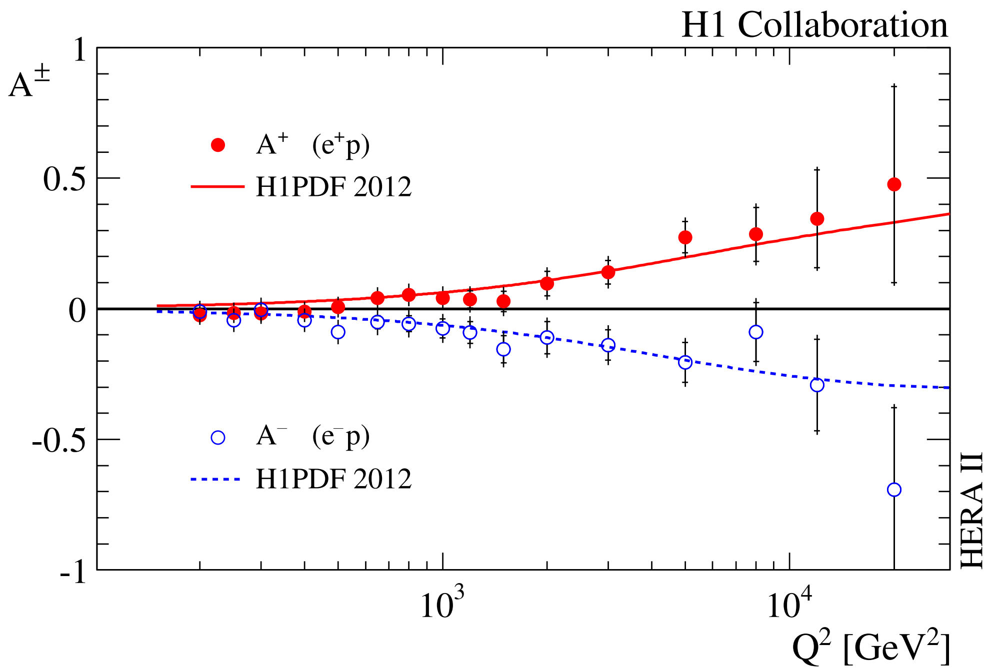

Figure 24: Q^2 dependence of the polarisation asymmetry $A^{\pm}$, for e^+p (solid points) and e^-p (open circles). The data are compared to the Standard Model expectation. The inner error bars represent the statistical uncertainties and the outer error bars represent the total errors. The normalisation uncertainty is not included in the error bars.

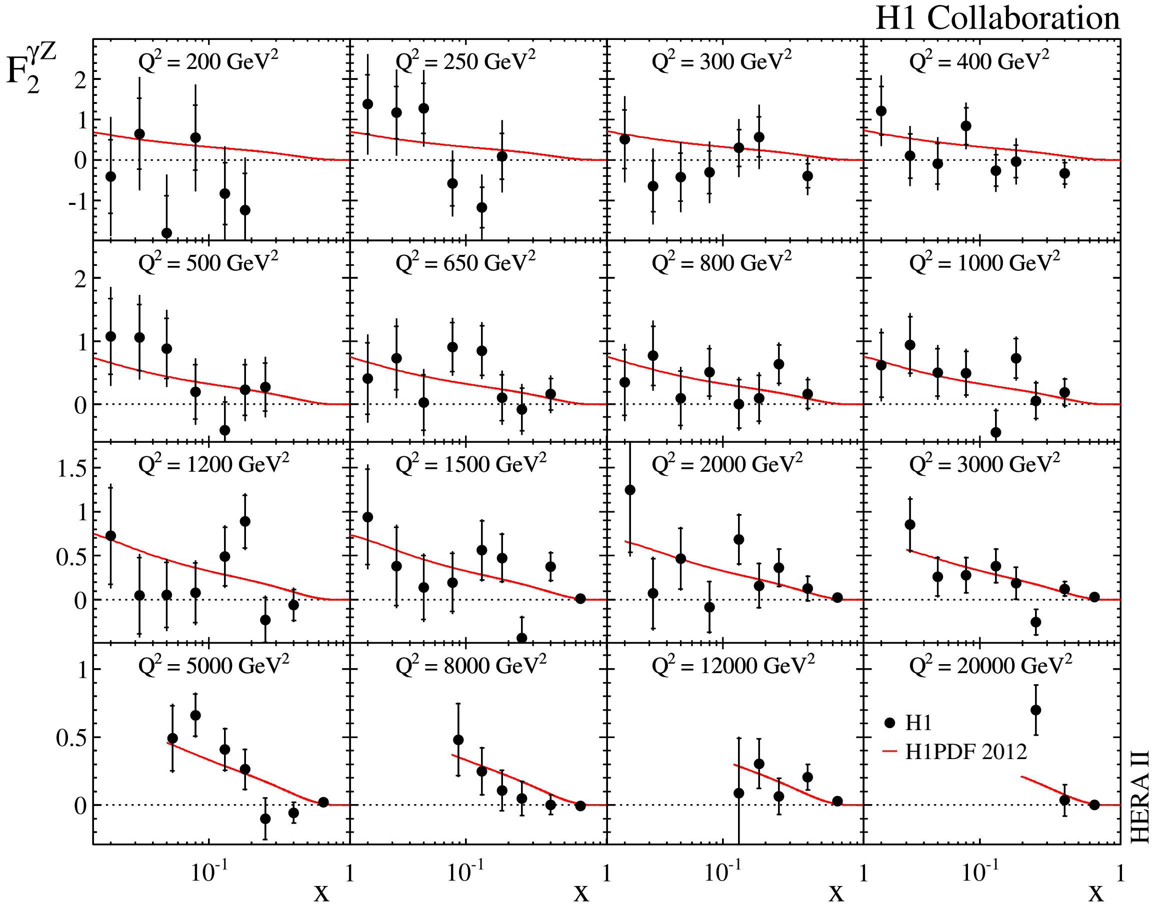

Figure 25: Structure function $F_2^{\gamma Z}$ for data (solid points) and the expectation from H1PDF 2012 (solid curve). The inner error bars represent the statistical uncertainties and the full error bar corresponds to the total measurement uncertainty.

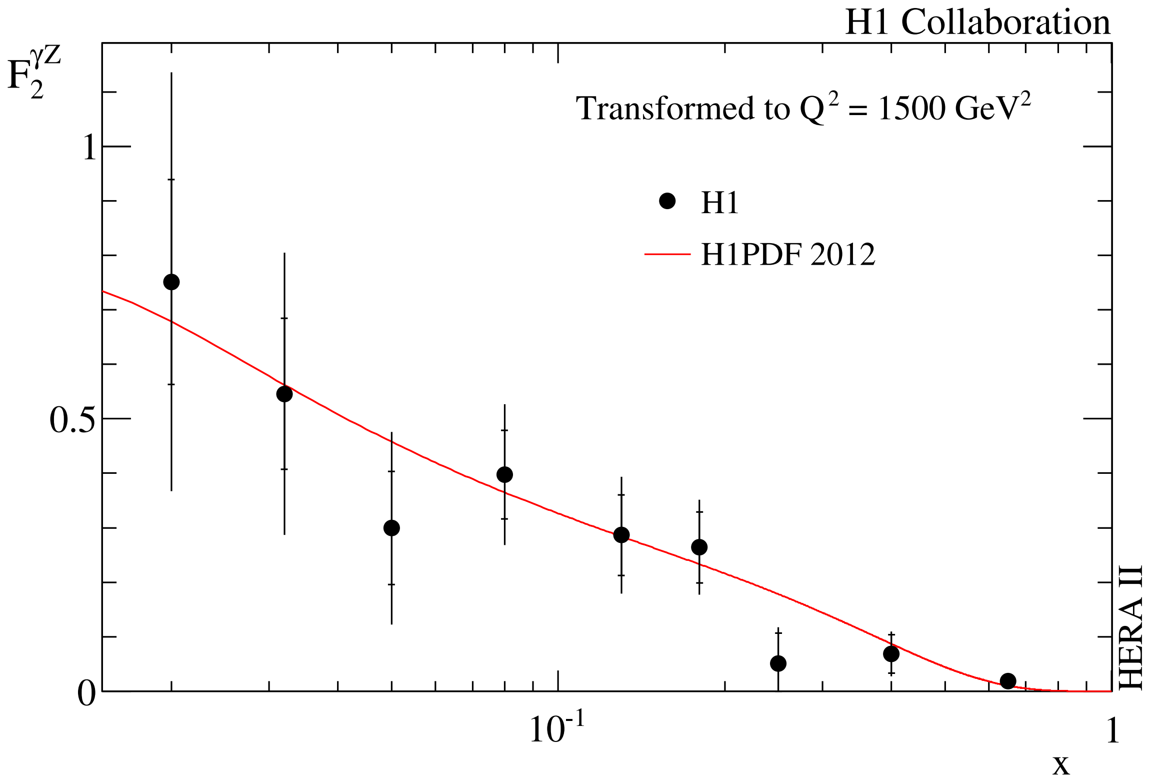

Figure 26: Structure function $F_2^{\gamma Z}$ transformed to $Q^2 = 1\,500\,\mathrm{GeV}^2$ for data (solid points) and the expectation from H1PDF 2012 (solid curve). The inner error bars represent the statistical uncertainties and the full error bar corresponds to the total measurement uncertainty.

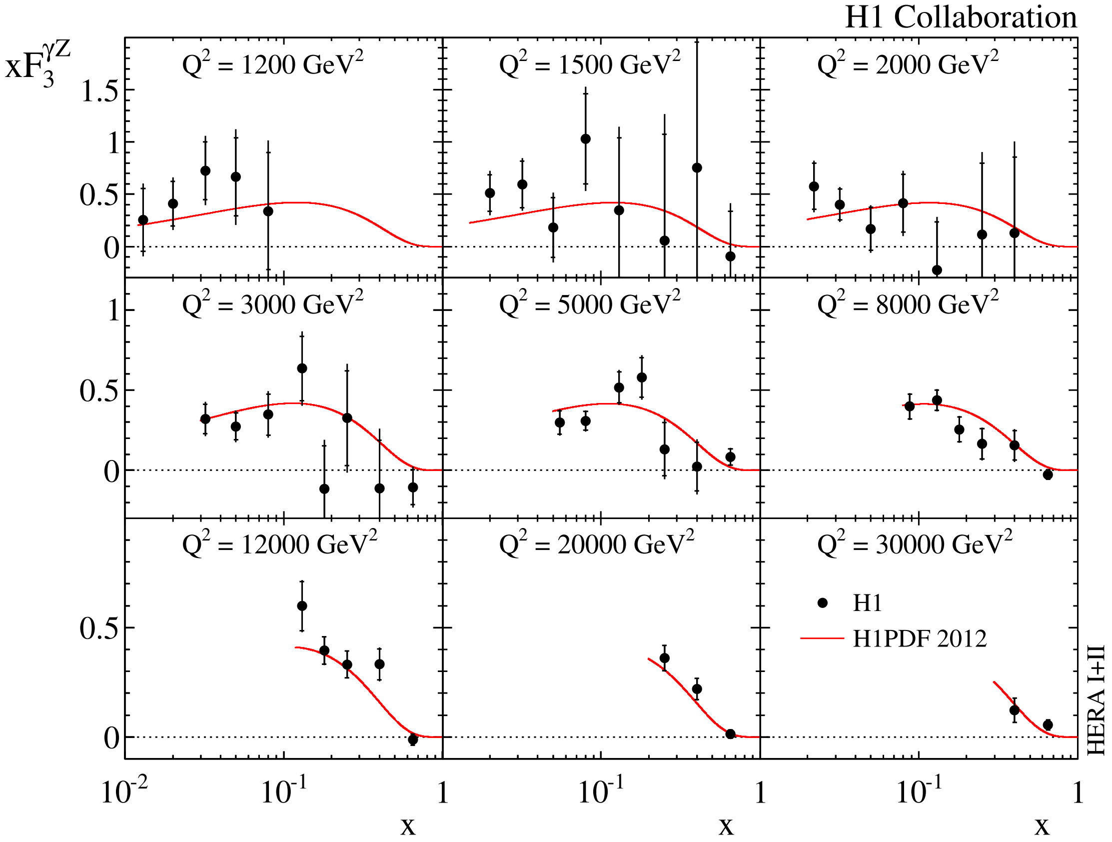

Figure 27: Structure function $xF_3^{\gamma Z}$ for the combined HERA I+II data (solid points) and the expectation from H1PDF 2012 (solid curve). The inner error bars represent the statistical uncertainties and the full error bar corresponds to the total measurement uncertainty.

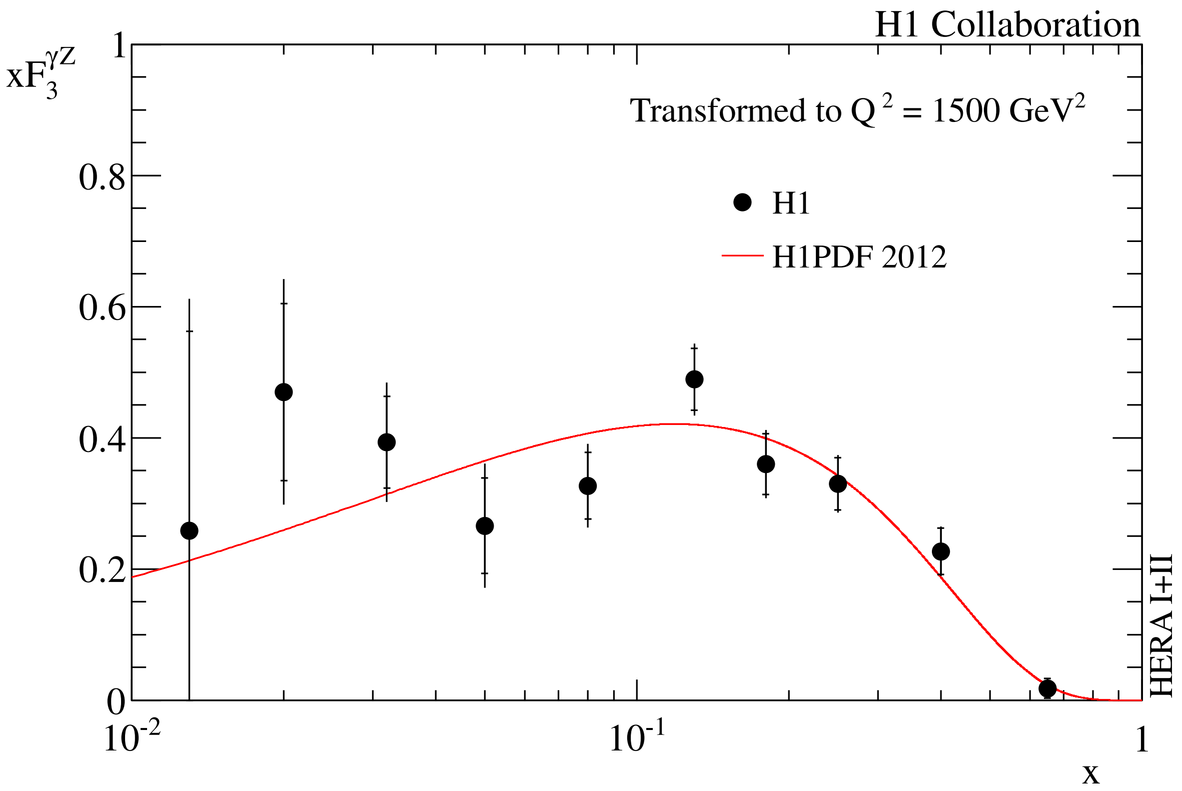

Figure 28: Structure function $xF_3^{\gamma Z}$ transformed to $Q^2 = 1\,500\,\mathrm{GeV}^2$ for data (solid points) and the expectation from H1PDF 2012 (solid curve). The inner error bars represent the statistical uncertainties and the full error bar corresponds to the total measurement uncertainty.

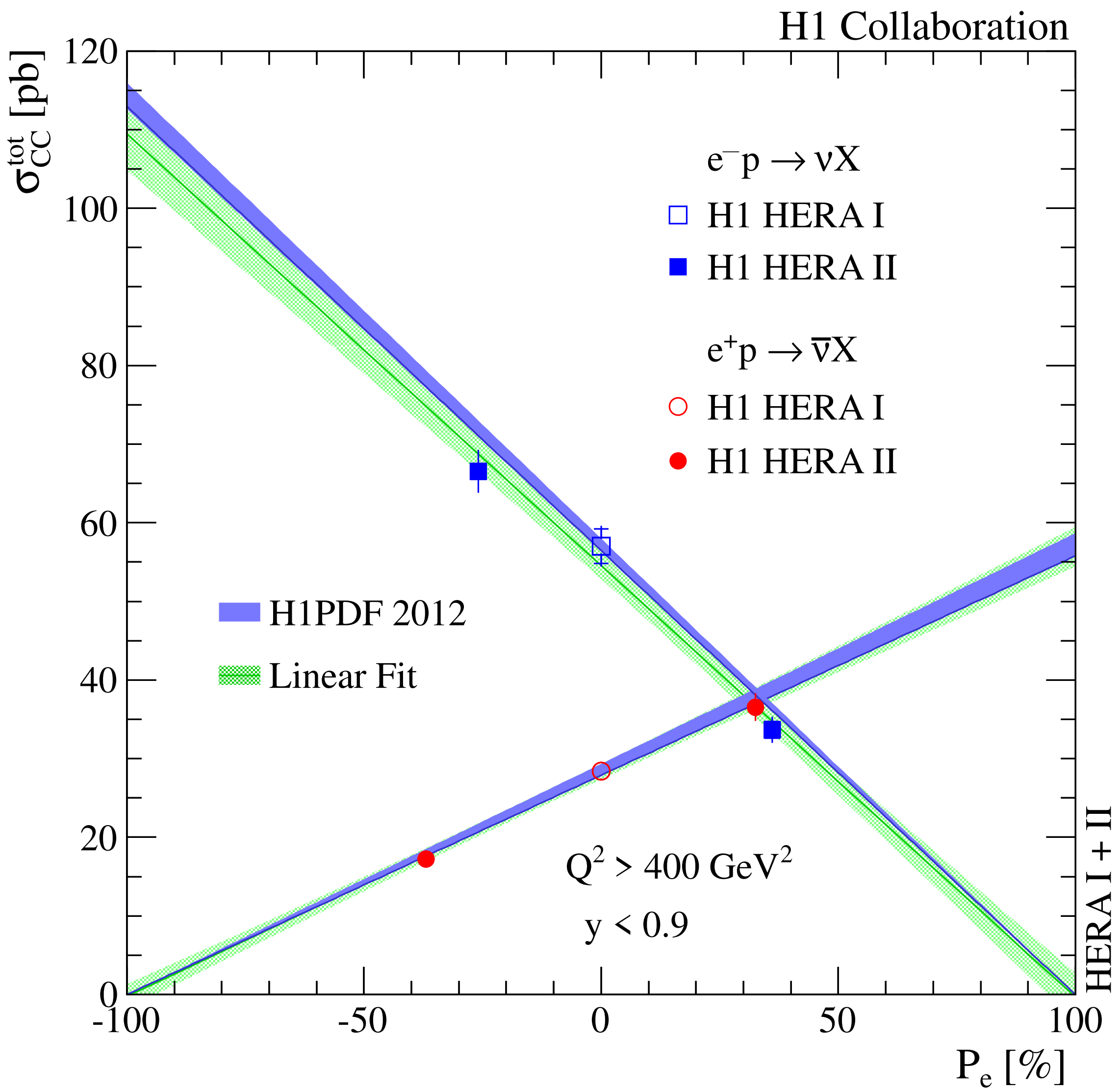

Figure 29: Dependence of the $e^{\pm}p$ CC cross sections on the longitudinal lepton beam polarisation P_e. The inner and outer error bars represent the statistical and total errors respectively. The uncertainties on the polarisation measurement are shown with horizontal error bars which are mostly smaller than the symbol size. The data are compared to the Standard Model expectation based on the H1PDF 2012 parametrisation (dark shaded band). The light shaded band corresponds to the resulting one standard deviation contour of a linear fit to the data shown as the central line.